SHEAR BEHAVIOR OF COLUMNS IN MASONRY INFILLED RC FRAMES UNDER LATERAL LOADS

by

Syed Humayun Basha

DEPARTMENT OF CIVIL ENGINEERING
INDIAN INSTITUTE OF TECHNOLOGY GUWAHATI
GUWAHATI – 781039, INDIA

January 2017

SHEAR BEHAVIOR OF COLUMNS IN MASONRY INFILLED RC FRAMES UNDER LATERAL LOADS

A Thesis Submitted
in Partial Fulfillment of the Requirements
for the Degree of

DOCTOR OF PHILOSOPHY

by

Syed Humayun Basha

DEPARTMENT OF CIVIL ENGINEERING
INDIAN INSTITUTE OF TECHNOLOGY GUWAHATI
GUWAHATI – 781039, INDIA

January 2017

CERTIFICATE

It is certified that the work contained in this thesis titled "*Shear Behavior of Columns in Masonry Infilled RC Frames under Lateral Loads*" by Mr. S*yed Humayun Basha* (11610410), has been carried out under my supervision, and this work has not submitted elsewhere for a degree.

Date: 05 January 2017

Place: IIT Guwahati

Dr. Hemant B. Kaushik
Associate Professor
Department of Civil Engineering
Indian Institute of Technology Guwahati
Guwahati-781039, Assam, India.

ABSTRACT

Reinforced concrete (RC) frame buildings with unreinforced masonry infills as exterior or partition walls are widely used in developing countries with high seismicity. Even though the presence of infills has a significant influence in enhancing the strength, stiffness and energy dissipation, these are frequently neglected in the seismic design calculations. A large number of research studies show that the presence of infilled panels drastically modify the lateral load behavior of RC frames depending on their mechanical characteristics, geometrical distribution and their interaction with the surrounding frame members. The increase in lateral stiffness of infilled frames leads to attraction of larger forces, and the confining columns should have sufficient capacity to resist the increase in shear demand near the contact zones with infill. This local adverse effect of infill is more pronounced in ground storey columns leading to collapse of the entire structure, especially where one-sided imbalanced contact exists between columns and infill. Some of the current earthquake standards have some recommendations to address the local adverse effect of infill, but their applicability has not been verified.

Therefore, the primary objective of the present study was to investigate the effect of infill on shear demand and failure of columns, and develop methodologies to prevent or delay the shear failure of columns due to the local adverse effect of infill. Prior to the development of methodologies, it is important to understand the modelling and design requirements of current earthquake standards concerning the design of masonry infilled RC frames. At the same time, the realistic evaluation of shear failure of columns requires suitable material and analytical models. To develop a nonlinear material model, a detailed material characterisation needs to be carried out, as most of the times the nonlinear properties of masonry significantly vary due to their composite nature and geographical dependancy. Some computationally intensive analytical tools to estimate the internal force distribution in columns due to the effect of infill are available, but a practical tool to predict the shear failure of columns is not available.

In the current study, the nonlinear material characteristics of fly ash brick masonry and its constituents were determined under different loading conditions (compression, tension and shear). It was found that the behavior of fly ash brick masonry under

compression was softer and weaker compared to the mortar. Simple empirical relations were proposed to estimate the strength and modulus of fly ash brick masonry under compression and shear. A preliminary experimental study was carried out to assess the recommendations of the current seismic standards on design of masonry infilled RC frames by investigating half-scale frames under in-plane slow cyclic loading. From the study, it was found that the columns were susceptible to shear failure even though the special detailing requirements of earthquake standards were followed. The existing analytical macromodel was improved by simulating the effect of infill along the contact length between column and infill. From the analytical study, it was perceived that the improved analytical model not only predicted the shear failure of columns but also captured the global response of infilled frames.

To prevent or delay the shear failure of columns, three methodologies (increasing the dimensions of the columns to consider the effect of infill, using weak and soft masonry to reduce the effect of infill on columns, and decreasing the frame-interaction using collector beams in infills) were adopted in the current study. It was found that the methodologies were feasible options in delaying the shear failure of columns without compromising the other functional requirements.

ACKNOWLEDGEMENT

I would like to express my deep and sincere gratitude to Dr. *Hemant B Kaushik*, who has inspired my academic and personal life with his guidance, encouragement, gracious support and care throughout my work. His valuable suggestions, effusive co-operation, co-ordination and encouraging interactions were a great driving force for me to carry out this research work. I express my sincere gratitude to my doctoral committee Professor *Uday Shanker Dixit*, Dr. *Kaustubh Dasgupta* and Dr. *Sandip Das* for their encouragement and valuable suggestions throughout the study. I would also to like to extend my gratitude to all my teachers for broadening and enriching my knowledge.

I am also thankful to all the technical and non-technical staff at Structural Engineering Laboratory, IIT Guwahati for their unconditional and most-willing support during the experiments. Financial assistance provided by the Ministry of Human Resource Development, Government of India, is greatly acknowledged.

I am grateful to all my friends, lab mates and well-wishers who made my stay at IIT Guwahati a memorable and pleasant experience. Finally I am thankful to my parents.

Syed Humayun Basha

This Page is Intentionally Left Blank

TABLE OF CONTENTS

LIST OF TABLES

LIST OF FIGURES

LIST OF SYMBOLS

A = constant depending upon state of masonry
A_c = area of the concrete section
A_g = gross area of the concrete section
A_i = cross-sectional area of the specimen parallel to bed joints
A_k = area of the confined core in the rectangular hoop
A_n = net area of masonry wallette
A_{nb} = net mortared area of infill parallel to bed joints
A_{sh} = area of shear reinforcement required as special confining reinforcement
A_{sl} = area of the tensile reinforcement
A_{sv} = total cross-sectional area of transverse reinforcement
A_w = piece-wise linear strut area
b = width of the cross section
B = constant depending upon mortar grade
b_c = width of gross cross section
b_i = distance between the consecutive engaged bars
b_o = width of confined core
C = empirical constant to indicate limit state of infill
COV = coefficient of variation
d = effective depth of the cross section
D = depth of the cross section in the direction of loading
DR_{80} = drift at 80% of maximum load in post peak
DR_f = drift at initiation of flexural cracks in columns
DR_i = drift at initiation of crack in infill (sliding/diagonal)
DR_s = drift at initiation of shear cracks in columns
DR_u = drift at ultimate deformation
E_b = modulus of elasticity of brick units
E_c = modulus of elasticity of concrete
E_{cycle} = energy dissipated per displacement cycle
ED = cumulative energy dissipation
E_j = modulus of elasticity of mortar cubes
E_m = modulus of elasticity of masonry prisms
E_s = modulus of elasticity of steel
F = shear force due to the effect of infill
F^- = peak lateral force in push direction
F^+ = peak lateral force in pull direction
f_a = compressive strength of infill considering out-of-plane failure
f_b = compressive strength of brick units
f_{bt} = split tensile strength of brick units

List of Symbols

f'_c = compressive strength of concrete cylinder
f_{ck} = compressive strength of concrete cube
f_{ct} = split tensile strength of concrete
f_{fb} = flexural or tension bond strength of masonry
f_{is} = initial shear strength
f_j = compressive strength of mortar cubes
f'_{jt} = tensile strength of mortar for diagonal cracking determination
f_{jt} = split tensile strength of mortar cylinder
f'_m = compressive masonry prism strength
F_u = maximum lateral load observed under lateral loading
f'_v = shear strength of masonry wallettes
f'_{vb} = bed joint shear strength
f_y = yield strength of reinforcement
f_{ys} = yield strength of the transverse reinforcement
g = gauge length of specimen in diagonal compression test
G_m = shear modulus of masonry wallettes
h = clear height of the column
h/l = aspect ratio
h_0 = depth of the confined core
h_c = longer dimension of rectangular confining core measured to its outer face
h_m = height of the infill wall
I_c = moment of inertia of column
IRA = initial rate of absorption of brick units
K_{eq} = effective stiffness
K_i = initial stiffness of infilled frame
K_{ult} = empirical constant determined from experimental crushing strength
l = centre to center distance between the columns
l_b = length of the brick unit
l_c = contact length between the infill and the column
l_d = diagonal length of infill wall
l_m = length of the infill wall
l_{mj} = length of the mortar joint
l_p = length of plastic hinge
L_v = shear span ratio
M/V = largest ratio of moment and shear under design loadings for column
M_{pb} = plastic moment capacity of beam
M_{pc} = plastic moment capacity of column
M_{pj} = minimum plastic moment capacity
M_r = residual moment capacity
M_u = ultimate moment capacity
M_{rd} = design moment capacity of the section

M_y = yield moment capacity
n = number of longitudinal bars laterally engaged by hoops or cross ties
P = axial compressive force on the column
P_f = failure load of Z-shaped specimen
P_{is} = peak shear strength reached during the initial shear strength test
q = behaviour factor accounting for energy dissipation capacity in structure
r = correlation coefficient
R^2 = coefficient of determination
R_c = diagonal compressive strength of infill
R_{cb} = diagonal compressive strength considering failure in infill-beam connection
R_{cc} = diagonal compressive strength considering failure in infill-column connection
R_{cr} = masonry infill crushing strength
R_{crb} = corner crushing strength of infills with failure in beams
R_{crc} = corner crushing strength of infills with failure in columns
R_{hor} = horizontal component of the strut force from linear equivalent strut frame analysis by applying a lateral displacement of 25 mm
R_n = nominal shear strength of the infill in accordance with MSJC (2013)
R_s = sliding shear strength of infill
R_t = diagonal cracking strength of infill
s = spacing of transverse reinforcement
t_{bar} = thickness of the bar in Z-shaped specimen
t_m = thickness of the infill wall
V = total shear resistance of the concrete section
V_c = contribution to shear resistance by concrete
V_{cr} = strength of infill based on corner crushing failure
V_{lim} = maximum limiting shear of a concrete section
V_s = contribution to shear resistance by transverse reinforcement
V_u = ultimate shear resistance
W = weight of the brick unit
WA = water absorption
w_b = width of the brick unit
w_s = equivalent width of the strut
x = height of the compressed zone
z = length of the internal lever arm
α = confinement effectiveness factor
α_c = normalized contact length of column-infill
β_{eq} = equivalent viscous damping
γ = shear strain in masonry wallette
γ_c = partial safety factor for concrete
γ_l = load factor for sliding shear strength
γ_{rd} = model uncertainty factor on value of resistances in the estimation of capacity design action effects, accounting for various sources of overstrength
δ = multiplication factor to design shear strength

List of Symbols

Δ^- = peak lateral displacements corresponding to peak lateral forces F^-
Δ^+ = peak lateral displacements corresponding to peak lateral forces F^+
δ_u = ultimate lateral displacement
ΔH = horizontal shortening of diagonal under diagonal compression test
ΔV = vertical elongation of diagonal under diagonal compression test
ΔV_{Rw} = total reduction in lateral resistance of infills in the concerned storey compared to the storey above
ε = compressive strain in masonry
ε_m = compressive strain corresponding to f'_m
ε_r = compressive strain corresponding to residual 0.5 f'_m in post peak regime
$\varepsilon_{sy,d}$ = design value of the tension steel strain at yield
ε_y = compressive strain corresponding to 0.3 f'_m
η = factor for increasing the design forces for weak or open storey columns
θ = angle between the horizontal and the panel diagonal
θ' = sloping angle of masonry diagonal strut at shear failure
θ_c = angle of the eccentric strut with respect to the horizontal
θ_r = rotation corresponding to residual moment capacity
θ_u = rotation corresponding to ultimate moment capacity
θ_y = rotation corresponding to yield moment capacity
λh = relative stiffness parameter
μ_Δ = ductility demand
μ_Δ^{pl} = plastic part of the ductility demand
μ_φ = curvature ductility factor
v = basic shear strength of bed joints of masonry
v_d = normalized design axial force
ρ_l = reinforcement ratio of longitudinal reinforcement
ρ_w = transverse reinforcement ratio
σ = standard error of estimate
σ_c = crushing strength of masonry infill panel
σ_{cp} = compressive stress in concrete from axial load
σ_m = compressive stress in masonry
ΣV_{Ed} = sum of the seismic shear forces acting on all columns of the storey concerned
τ_c = shear stress in concrete
τ_{cmax} = maximum shear stress in concrete with shear reinforcement
φ = curvature of concrete section
ω_{wd} = mechanical volumetric ratio of confining hoops within critical regions

This Page is Intentionally Left Blank

This Page is Intentionally Left Blank

Chapter 1
INTRODUCTION

CONTENTS

1.1 OVERVIEW

Masonry infilled reinforced concrete (RC) frame buildings are some of the most common building typologies found around the world, especially in developing countries, including India. The wide use of masonry infilled RC frame construction in the modern world derives from the wide availability of its constituents: reinforcing steel, concrete and masonry. Seismic design of masonry infilled RC frame buildings is generally carried out without accounting for the effect of infill irrespective of the fact that infills alter the lateral load carrying capacity, stiffness, and energy dissipation of the frame system. The main reason for not incorporating masonry infill in design, but rather considering it as non-structural element, lies in its intricate behavior under lateral loading and the uncertainty involved in evaluation of lateral load carrying capacity of masonry infilled RC frames.

Presence of infills alters the behavior of infilled frame systems both globally and locally due to their high compressive strength and stiffness. Referring to global response, it is generally observed and recommended that the symmetric and regular distribution of infills is beneficial to the building system. In addition to the global potential adverse effects of infills due to the irregular distribution of infill, there are local detrimental effects of infills due to presence of partial height infills, presence of stronger and stiffer infills compared to RC frames, etc. Such construction practices may cause short column

effect (captive columns), which tend to attract large shear forces compared to that for which they are designed, eventually leading to the failure of columns in shear.

The presence of infill panels increases the lateral stiffness of the frame significantly. Therefore, the infilled frames attract large lateral forces, which are transferred from the infill panel to the RC frame members. The RC frame members, especially the columns, should have sufficient capacity to resist the force exerted by the infill. This transfer of the force to the frame members due to infill-frame interaction takes place along the contact length of the frame members and infill. The stronger the infill, the larger the force exerted on the frame members, which increases the possibility of the failure of the columns in shear. This effect is further pronounced in ground storey columns, where the shear force demand is very high (Fig. 1.1). Such column failures are predominant where one sided-imbalanced contact exists between column and infill, especially in case of exterior ground storey frames.

Fig. 1.1. Local shear failure of columns due to infill-frame interaction (Cavaleri and Di Trapani 2015).

1.2 Major Concerns and Need of the Study

Performance of most of the masonry infilled RC frame buildings in the past earthquakes clearly shows the detrimental effect of infill. Several design standards (BIS 2002b; CEN 2004b; NBC 1994; ACI 2008) around the world provide recommendations to consider both the horizontal and vertical irregularities created due to the infills. At the same time, some of the past experimental and analytical studies (Fardis and Panagiotakos 1997; Crisafulli et al. 2000; Kaushik et al. 2009; Sahoo 2008) proposed design guidelines and strengthening techniques to consider and counteract the irregular distribution of infills.

Several past experimental studies (Mehrabi et al. 1996; Al-chaar et al. 2002; Blackard et al. 2009; Fardis 2009) reported shear failure of columns in frames not designed as per the current recommendations of prevalent seismic standards. Eurocode 8 (CEN 2004b), ASCE 41 (2013), MSJC (2013) provide certain design and detailing recommendations to consider the local adverse effect of infill while designing such frames. The Indian ductile detailing standard (BIS 1993) does not specifically mention about the local adverse effect of infill, but provide guidelines to improve the ductility of columns. The design and detailing guidelines of the current earthquake design standards need to be evaluated experimentally to assess their effectiveness in preventing the shear failure in columns of masonry infilled RC frames. If the current design provisions are found to be redundant in delaying the shear failure of column, methodologies need to be put forward and evaluated both analytically and experimentally.

In order to have a clear understanding on the behavior of infilled frames both experimentally and analytically, it is important to apprehend the performance of the infill and its influence on the surrounding frame members apriori. The performance of infill is generally defined by its strength, stiffness, failure mechanism, and stress-strain characteristics in case of nonlinear response. But due to the composite nature of masonry, geographic location and material dependencies lead to significant variation in strength and stiffness. In the recent times, availability of industrial by-products has led to the use of alternative building materials. Fly ash bricks are gaining prominence in building construction due to their energy efficient production process, preservation of cultivable land needed for the production of burnt clay bricks, and cutting down on greenhouse gases from firing of bricks. Apart from the social and environmental benefits, it is also essential that engineering properties of such by-products not be overlooked. Fly ash bricks have been employed in the current study. Nonlinear stress-strain characteristics of fly ash brick masonry under compression, shear and tension are not available in literature. To develop a nonlinear material model for proper analysis, a detailed experimental material characterisation needs to be carried out.

From the failure modes of infilled frames observed in the past earthquakes and experimental studies, it may be affirmed that the determination of the shear demand on the columns due to the local adverse effect of infill is of primary importance for proper design that should result in ductile flexural failure. Analytical modelling of RC frames

has been well established in the literature, but modelling the effect of frame-infill interaction has been a topic of research for some time due to the intricacies involved in behavior of infill under lateral loading. A lot of analytical models were proposed in the past ranging from the simplistic macromodelling technique using single-strut (Holmes 1961; Smith and Carter 1969; Mainstone 1971), multi-strut (Chrysostomou et al. 2002; El-Dakhakhni et al. 2003; Crisafulli and Carr 2007; Fiore et al. 2012) to more complicated micromodelling techniques (Mallick and Severn 1967; Mehrabi and Shing 1997; Ghosh and Amde 2002; Shing and Stavridis 2014). A comprehensive review of the various modelling techniques used in the past has also been presented in the literature (Asteris et al. 2011; Asteris et al. 2013; Di Trapani et al. 2015). The detailed behavior of the infilled frames under lateral loading may be captured by employing micromodelling approach but the major inefficacy of the micromodelling techniques is the high computational effort required for large building structures, which is unacceptable for practical engineering purposes.

Most of the past analytical studies resorted to macromodelling techniques, especially, modelling infill as equivalent diagonal strut because of the ease in idealizing the parameters involved in modelling. The global behavior of the infilled frames (lateral deformation or base shear) can be easily evaluated by performing the nonlinear static pushover analysis of the macromodel; and it has been proven to be successful in the past studies. But the major limitation of modelling the masonry as equivalent diagonal strut lies in its inability to evaluate the internal forces in columns and beams and to capture the local shear failure of the members near the joints. This may pose a serious threat to the safety of the frame members as the under-designed columns may fail in brittle shear mode due to their interaction with the masonry infill walls under lateral forces. In the recent years, more emphasis was given to upgrade the suitability of macromodels to capture the component failure. A few analytical studies by D'Ayala et al. (2009), Celarec and Dolšek (2012), Cavaleri and Di Trapani (2015), and Fiore et al. (2016) were carried out to evaluate the shear failure of columns by simplified modelling techniques. Due to the complications involved and computational difficulties in evaluating the parameters in the previous models, the existing simplified equivalent diagonal strut model needs to be improved in order to capture the component (shear) failure of the columns due to the effect of the infill. Once the numerical and analytical estimation of shear demand on the

column due to the effect of infill is carried out, it may be possible to design or propose methodologies to safeguard the columns against shear failure.

To counteract the adverse effect of infill, i.e., to prevent or delay the shear failure in columns three approaches or methodologies were adopted in the current study. In Methodology I, the effect of infill in the design of infilled RC frames was considered by increasing the dimensions of the columns to enhance the shear capacity of the column (Fig. 1.2). It may not be feasible every time to enhance the shear capacity of the column section as the designed sections may become unrealistic and uneconomical. Therefore, Methodology II was proposed where very weak and softer bricks were used as masonry infill to reduce the shear demand on the columns. However, sometimes it is difficult to find weaker and softer masonry, therefore Methodology III is also suggested where the infill-frame interaction was reduced by a providing sliding mechanism in infill along the predefined failure planes (Fig. 1.2).

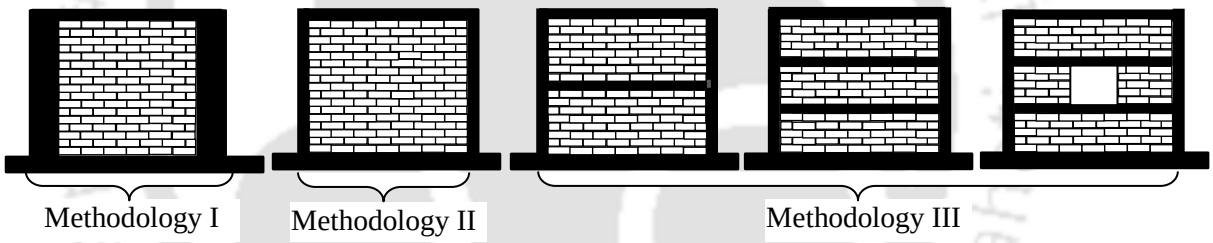

Methodology I: Enhancing Column Section; Methodology II: Using Low-strength and Soft Masonry; Methodology III: Adding Collector Beams in infills

Fig. 1.2. Methodologies to improve shear behavior of columns in masonry infilled RC frames.

Considering the gap areas in the literature as described above, the objectives of the current study are formulated as given below:

a) Experimental determination of material properties of fly ash brick masonry to model the nonlinear behavior of infill under lateral loading.
b) Experimental evaluation of effectiveness of the current codal recommendations in preventing the shear failure in columns of masonry infilled RC frames.
c) Numerical estimation and analytical prediction of the shear demand on the columns due to infill-frame interaction.
d) Development of methods to improve the shear behavior of columns of masonry infilled RC frames.

1 Introduction

The experimental investigation of the masonry infilled RC frames was carried out in two phases. In the first phase, effectiveness of the current codal recommendations was evaluated in preventing the shear failure in columns (Table 1.1). In the second phase, the developed methods to improve the shear behavior of columns were validated (Table 1.2). Displacement controlled slow-cyclic tests were conducted to evaluate the influencing parameters of all the tested frames: hysteretic load-deformation behavior, lateral strength and stiffness, energy dissipation potential, and the failure mechanisms.

Table 1.1. Details of test specimens (Phase I- preliminary study)

Specimen No	Type of Frame	Notations	Ductile Detailing	Type of Masonry
	Stage I			
1	Ductile bare frame*	DB	yes	no infill
2	Non-ductile bare frame	NDB	no	no infill
3	Ductile frame infilled with full-scale bricks	DFS	yes	full-scale bricks
4	Non-ductile frame infilled with full-scale bricks	NDFS	no	full-scale bricks
5	Ductile retrofitted frame infilled with full-scale bricks	DRFS	yes	full-scale bricks
6	Non-ductile retrofitted frame infilled with full-scale bricks	NDRFS	no	full-scale bricks
7	Ductile frame infilled with half-scale bricks	DHS	yes	half-scale bricks
8	Non-ductile frame infilled with half-scale bricks	NDHS	no	half-scale bricks
	Stage II: Ductile Infilled Frame			
9	Improved detailing along full column length	DISTL	yes	full-scale bricks
10	Improved detailing in critical regions	DISC	yes	full-scale bricks
11	Improved detailing in critical regions using high strength bars	DISCSB	yes	full-scale bricks

Key: D-ductile; ND-Non-ductile; B-Bare; FS-Full-scale bricks; HS-Half-scale bricks; R-Retrofitted; I-Improved; S-Shear capacity; Throughout Length-TL; C-Critical regions; SB-High strength bars.

*Specimens 1-6 were taken from Manchanda (2010) and Basha (2011).

Table 1.2. Details of test specimens (Phase II- improved methods)

Specimen No	Type of Frame	Notations	Ductile Detailing	Type of Masonry
	Methodology I			
12	Infilled frame with enhanced column section	IF-EC	yes	full-scale bricks
	Methodology II			
13	Infilled frame with class I clay bricks	IF-CC1	yes	full-scale bricks
14	Infilled frame with class III clay bricks	IF-CC2	yes	full-scale bricks
	Methodology III			
15	Bare frame with collector beam at lintel level	BF-CB	yes	no infill
16	Infilled frame with central collector beam	IF-CB1	yes	full-scale bricks
17	Infilled frame with two collector beams	IF-CB2	yes	full-scale bricks
18	Infilled frame with two collector beams with 10% opening	IF-CB3	yes	full-scale bricks

Key: IF-infilled frame; EC-enhanced column; CC-clay bricks; CB-collector beam.

1.3 ORGANIZATION OF THE THESIS WORK

The present study can be broadly divided into four parts, namely: (a) development of material stress-strain characteristics for fly ash brick masonry under compression, shear and tension; (b) experimental evaluation of the design and detailing requirements of the current earthquake standards for masonry infilled RC frames; (c) estimation of shear demand on the column due to the effect of infill numerically and analytically using improved nonlinear model for the infill; and (d) proposal of improved methodologies followed by their analytical and experimental validation to delay the brittle shear mode of failure.

Besides the introductory chapter, the current thesis is treasured into eight more chapters. A comprehensive review of the behavior of masonry infilled frames under lateral loading and the various factors influencing the behavior and failure mechanisms based on the past literature is presented in chapter 2. In addition, recommendations and limitations of the current codal provisions related to the design and adverse effects of masonry infill are also discussed. Chapter 3 presents a detailed experimental study to evaluate the nonlinear stress-strain properties of fly ash brick masonry for various mortar grades and its constituents (fly ash bricks and mortar) in compression, shear and tension. In addition, some important physical properties and chemical composition analysis of fly ash bricks was carried out.

Chapter 4 presents a detailed preliminary study on the behavior and failure mechanisms of half-scale RC frames infilled with fly ash brick masonry. From the experimental investigation, the shear failure of the columns due to the effect of infill is evaluated and the current codal recommendations are assessed. Chapter 5 presents the estimation of shear demand on the column due to the effect of infill both numerically and analytically. Further, the simple analytical macromodel which uses the equivalent diagonal struts for modeling masonry infill walls, is improved to capture the local shear failure of columns by accounting for the additional interaction effect of infill.

Methodologies to improve the shear behavior of columns due to the effect of infill are put forward in chapters 6 and 7. In chapter 6, the effectiveness of the two methodologies: increasing the dimensions of the columns considering the shear demand on the column due to the effect of infill, and influence of using weak and soft masonry to

decrease the effect of infill is evaluated analytically and experimentally. The third methodology in which the infill-frame interaction on the column is diffused by dividing the infill panel into sub-panels using collector beams is evaluated in chapter 7. In both the chapters, initially the parametric analysis is carried out to evaluate the effectiveness of both the methodologies, and the best performing models are verified experimentally. In chapter 8, experimental results of the three adopted methodologies are compared and the lateral load response of the tested specimens is analytically validated using the improved analytical model. Equivalent moment-curvature relationships for the tested specimens are also developed using the data obtained from the strain sensors. To demonstrate an application of the moment-curvature relationships developed, the obtained moment-curvature data is used to evaluate the lateral load response of the tested specimens.

The summary of the current study is presented in chapter 9 along with the conclusions drawn from the current study. In the end, recommendations for the possible future work are presented.

Chapter 2
REVIEW OF LITERATURE

CONTENTS

2.1 OVERVIEW

Masonry infilled reinforced concrete (RC) frame buildings are commonly constructed in several countries, including India, which are prone to earthquakes. The presence of masonry infills in framed structures significantly modifies the structural response to strong ground motion in terms of stiffness, strength, energy dissipation, and failure modes. A large number of analytical and experimental studies have been performed in the past on the behavior, modelling, analysis, and design of infilled frames; these investigations are reviewed in this chapter. Based on the available literature, the gap areas were identified and objectives of the present study were formulated.

2.2 BEHAVIOR OF MASONRY INFILLED FRAMES

The behavior of infilled frames is generally described in terms of strength, stiffness, and energy dissipation. The importance of infills and their significance in imparting strength, stiffness, and energy dissipation during earthquake excitations are discussed in following sections. Additionally, the failure modes are also discussed as the presence of infills majorly modifies the failure of infilled frames. Emphasis is given to reinforced concrete frames with masonry infills, although some test results related to steel frames are also included, especially when the frame material does not significantly alter the behavior of the parameter under consideration.

2.2.1 Lateral Strength

One of the most beneficial effects of infill on framed structures is the contribution to the lateral load resistance of the structure. It was observed from the past studies (Bertero and Brokken 1983; Moghaddam and Dowling 1987; Mehrabi et al. 1996; Al-chaar et al. 2002; Colangelo 2005; Kakaletsis and Karayannis 2008; Stylianidis 2012; Zovkic et al. 2013; Ravichandran and Klinger 2012; Mansouri et al. 2014; Cavaleri and Di Trapani 2014; Schwarz et al. 2015; Bose and Rai 2016, etc.,) that the increase in capacity of the infilled frame was found to be approximately 1.1 to 5 times that of the bare frame capacity. Moghaddam and Dowling (1987) divided the parameters on which the strength of the infilled frame is dependent on into two categories: the parameters, which are quantifiable; and the other, which are difficult to quantify. The parameters, which are quantifiable and easy to generalize, are: relative stiffness of frame and infill, aspect ratio, strength of infill, geometry of infill, type of infill, geometry of openings, amount of vertical loading, amount of infill reinforcement, etc. The parameters difficult to quantify include workmanship, interface bond condition, initial lack of fit between infill and frame, bond between mortar and bricks, etc. The parameters that are difficult to quantify and generalize may be of same importance and may altogether alter the behavior of the frame under seismic loading. The influence of various parameters on the strength of infilled frame with respect to past experimental and analytical studies has been discussed in the following.

Relative Stiffness Parameter (λh)

Smith (1966) related the strength and stiffness of infilled frame with the relative stiffness parameter (Eq. 2.1). It was observed that the relative stiffness parameter governs the failure of infill especially the corner crushing mode of failure. As the relative stiffness parameter is inversely related to the rigidity of the frame, with increase in rigidity of the frame the ultimate strength of the infilled frame increased as the corner crushing mode dominates the failure of infilled frame when compared to other modes (diagonal cracking mode) as observed by Moghaddam and Dowling (1987).

$$\lambda h = h\sqrt[4]{\frac{E_m t_m \sin 2\theta}{4E_c I_c h_m}} \tag{2.1}$$

where h represent the clear height of the column; E_c and E_m represent the modulus of elasticity of concrete and masonry infill, respectively; I_c represent the moment of inertia of column; l_m, h_m, t_m are the length, height and thickness of the infill wall, respectively; and θ is the angle between the horizontal and the panel diagonal. Mainstone (1971) reported that the influence of relative stiffness parameter was more significant for model infills rather than for full-scale infills.

Aspect Ratio

Variation of aspect ratio (h/l) has a significant influence on the behavior in terms of strength, stiffness and failure mechanisms (Stylianidis 2012). Low aspect ratio ($h/l < 1$) infilled frames observed higher lateral strength due to the higher compressive stresses near the column loaded corners. The influence of higher aspect ratio ($h/l > 1$) on strength and stiffness was found to be less significant (Moghaddam and Dowling 1987). From the investigation of two aspect ratios (0.48 and 0.67) under cyclic loading, Mehrabi et al. (1996) reported slight increase (16% and 9%) in lateral strength of infilled frame with decrease in aspect ratio. Schwarz et al. (2015) from their study on frames with two different aspect ratios ($h/l \approx 2/3$ and $h/l \approx 3/2$) infilled with AAC blocks reported that aspect ratio has less influence on the capacity of both integral and non-integral frames. However, Chiou and Hwang (2015) from their study on the frames infilled with strong bricks considering two aspect ratios (0.39 and 0.83), reported that aspect ratio and critical crack angle in infill has significant influence on lateral load behavior of infilled frames and failure mechanisms. It was reported that the infilled frames observed higher lateral strength, when the aspect ratio ($h/l \approx 0.83$) of infill is greater than the critical crack angle in infill. But the influence of aspect ratios ≥ 1 was not evaluated in their study.

Effect of Infill

As observed in all the past studies, the effect of infill type has a significant influence on the strength, which may be related to type of masonry units, strength of mortar, bond pattern, size of brick units and the reinforcement in infills employed in the construction of infilled frame. Most of the past experimental studies have incorporated various types of masonry materials due to the increased pace of construction. The infills include various sizes of solid bricks, hollow blocks, autoclaved aerated concrete blocks (AAC) manufactured using clay, adobe, fly ash, reinforced concrete, lime, pulverised ash, etc. It

was observed from the past studies (Mehrabi et al. 1996; Al-chaar et al. 2002; Zovkic et al. 2013; Cavaleri and Di Trapani 2014) that the strength of the infilled frames was higher for solid brick units compared to hollow units. This may be due to less disintegration observed in solid units compared to hollow units. Mehrabi et al. (1996) reported that the strength of both weak frames and strong frames infilled with solid infills under monotonic and cyclic loading was enhanced by approximately 1.5 to 2.3 times that of their corresponding infilled frames with weak (hollow) infills. Al-chaar et al. (2002) reported slight increase in the lateral strength of infilled frame when the frame was infilled with clay brick units when compared to concrete blocks as the variation in the strength of infill was very less.

In the recent times, AAC blocks (Ravichandran and Klingner 2012; Sucuoğlu and Siddiqui 2014; Schwarz et al. 2015; Bose and Rai 2016) as infill material are gaining prominence due to their lightweight and large-scale utilisation of industrial wastes (pulverised fuel ash). It was observed that the strength of the infilled frames with AAC blocks was found to be about 1.2 to 1.5 times that of their corresponding bare frame specimens. Three types of infills were employed in the tests carried out by Zovkic et al. (2013) on reinforced concrete frames under cyclic loading and reported that the strength of the frame infilled with strong infill (high strength perforated clay blocks) was found to be higher when compared to low strength lightweight AAC blocks.

According to CEB (1996), it was reported that the better quality mortar is expected to increase the cracking load of infill and ultimate lateral load resistance of the infilled frames. Use of better and high strength mortar leads to better bond characteristics between brick units and mortar joints and therefore to higher cracking load. This phenomenon holds true for certain limits; when the masonry becomes excessively strong with respect to the strength of the surrounding frame, premature failure of the frame elements may occur and therefore the strength of the whole system may be drastically reduced. Dawe and Young (1985) varied the strength of mortar from 24.4 MPa to 12.4 MPa and reported that there was a significant reduction in cracking load of infill and the lateral strength of the infilled frame. On the other hand, Stylianidis (2012) reported the influence of mortar strength on the lateral strength of the infilled frame is insignificant which may be due to the initiation of failure in frame elements prior to infill failure even for the low strength mortar infill (2.4 MPa). Chiou and Hwang (2015) reported that the

lateral strength of the infilled frames increased with increase in mortar strength which governs the failure of mortar joint in bed joint sliding and head joint splitting.

A very few studies have discussed the effect of bond pattern on the effect of lateral load behavior of infilled frame. Chiou and Hwang (2015) studied the failure pattern observed in case of English bond (alternate courses of stretcher and header) for two aspect ratios; and reported that the strength of the infilled frame was higher in case of English bond with higher aspect ratio (*h*/*l*) as the fracture path for infill has to be passed through vertical splitting of bricks in addition to bed joint sliding and cross joint splitting. Most of the past studies employed running bond pattern with single wythe infill walls.

Murty and Jain (2000) tested 1:2.7 scale frames infilled with full-scale and half-scale bricks and reported that the strength of the infilled frames with full-scale bricks found to be slightly higher compared to infilled frames with half-scale bricks. This condition may be valid in case of infilled frames with high brick strength compared to that of the mortar strength. Stavridis et al. (2012) reported that scaling of brick units and mortar joints was not important for scaled models (2/3rd scale) as the size of the units is relatively small with respect to the dimensions of a wall.

In the past research studies, one of the investigative parameters was the percentage of reinforcement in infills especially the horizontal reinforcement. Brokken and Bertero (1981) and Zarnic and Tomazevic (1985) (as referred in CEB 1996) reported that the experimental results did not show significant influence of the infill reinforcement on the lateral strength of the infilled frames. On the other hand, Jurina (1977) (as referred in CEB 1996) observed significant influence of reinforcement of the infill; and reported that the ratio of lateral strength of the plain infilled frame to the bare frame was about 4.0, whereas, the ratio was about 5.4 in case of infilled frame with reinforced infill. Murty and Jain (2000), owing to the adverse effect of larger thickness of mortar due to the presence of reinforcement reported no significant increase in strength of infilled frames with horizontal reinforcement compared to unreinforced infilled frames.

Effect of Vertical Load

From the past experimental studies, it was observed that the presence of vertical load modifies the behavior of infilled frames under lateral loading. Smith (1968) investigated

the influence of uniformly distributed load on single-bay infilled frame and observed a considerable increase in lateral strength of the structure. Valiasis and Stylianidis (1989) reported that the presence of compressive axial load on the columns considerably improved the lateral strength of the system investigated. Smith (1968) and Valiasis and Stylianidis (1989) did not consider the effects of vertical loads in postulating equivalent strut to the infill as the authors' considered the effect negligible or conservative. Cavaleri et al. (2004) reported that the effect of vertical load may be conservative for a single mesh just as the presence of the infill is in general conservative; but may not be conservative for a more complex framed structure with non-uniform distribution of infills. Cavaleri et al. (2004) also stressed that the exact lateral load behavior of infilled frames cannot be simulated if the non-negligible effect of vertical loads were not considered. It was also reported that the infilled frames with partial joints observed slightly lesser lateral strength when compared to infilled frame with continuous frame-infill joints. Schwarz et al. (2015) reported an increase in 50% capacity compared to the test specimens without prestressing force, but the infilled frame failed in shear mode, which is an undesirable mode of failure.

Effect of Openings

Effect of openings in infill walls lead to significant uncertainty in the assessment of the seismic behavior due to the variability of their size and location. In general, the presence of openings results in reduction of ultimate strength of the masonry wall. The influence of openings has been investigated by several researchers. The first study was carried out by Polyakov (1960) on eight steel infilled frames with openings of different sizes and observed the ultimate strength of the frames to be about 23% and 76% of the frame with the solid panel. Benjamin and Williams (1958) (as reported in CEB 1996) reported a 50% reduction in ultimate strength with central openings of dimensions one-third of the length and height of the infill panel. Kakaletsis and Karayannis (2008) investigated the influence of door and window openings on the hysteretic behavior of infilled frames, and reported that strength reduction was found to be 18.7% and 28.7% for window and door openings, respectively, with a width in range of 25-50% of the length of the infill panel. Tasnimi and Mohebkhah (2011), carried out an extensive experimental and analytical investigation on the behavior of brick infilled steel frames with central openings of

various dimensions, reported that the lateral strength for various opening configurations was found to be ranging from 0.57 to 0.83 times that of the fully infilled frame.

Summary

From the review of the past experimental investigations, it was found that the lateral strength of infilled frame depend on various parameters ranging from aspect ratio, type of infill, vertical load, reinforcement in infill, etc. The presence of infill offers strong contribution to lateral load resistance, especially in non-seismically designed frames. This the effect of infills become detrimental when the lateral force demand exceeds the lateral load resistance of the infills, as the infill walls fail suddenly, which may trigger collapse of the entire structure. This phenomenon is quite common in weak frame-strong infill configuration. From the past literature, it was also found that a clear distinction between the strong and weak frame with respect to strength of infill is not defined.

2.2.2 Lateral Stiffness

One of the remarkable effects of infills on the behavior of infilled frames is the increase in lateral stiffness and is repeatedly proved that the lateral stiffness of the infilled frames is many times higher than the stiffness of the bare frames. According to Moghaddam and Dowling (1987), masonry infilled frames are initially very stiff, and as soon as the interface cracking occur the initial tangential stiffness decreases and remains constant upto the formation of diagonal cracks, and then degrades quickly as the displacement increases further.

It was observed from the past studies (Bertero and Brokken 1983; Moghaddam and Dowling 1987; Mehrabi et al. 1996; Al-chaar et al. 2002; Colangelo 2005; Kakaletsis and Karayannis 2008; Stylianidis 2012; Zovkic et al. 2013; Ravichandran and Klinger 2012; Mansouri et al. 2014; Cavaleri and Di Trapani 2014; Schwarz et al. 2015, etc.,) that the increase in lateral stiffness of the infilled frame was approximately 7 to 15 times that of the bare frame stiffness. Similar to lateral strength of infilled frames, lateral stiffness is also dependent on various parameters which are quantifiable and non-quantifiable. Influence of various parameters on the lateral stiffness of infilled frames with respect to past studies is reviewed in the following sections.

Relative Stiffness Parameter (λh)

Smith (1966) related the strength and stiffness of infilled frame with the relative stiffness parameter (Eq. 2.1). It was observed that the relative stiffness parameter increases with increase in E_m and decrease with increase in I_c. It was also observed that the relative stiffness parameter is quite sensitive to masonry modulus (E_m) when compared to moment of inertia of column (I_c). From the past experimental results (Moghaddam and Dowling 1987), it was reported that the lateral stiffness does not seem to be an efficient measure of lateral stiffness of the entire infilled frame as the stiffness is approximately proportional to infill stiffness and insensitive to the frame stiffness.

Aspect Ratio

Based on the past experimental results, Moghaddam and Dowling (1987) concluded that aspect ratio significantly influences the lateral stiffness of the infilled frames if aspect ratio (h/l) is greater than 0.50 and the influence is negligible for lower aspect ratios (h/l < 0.50). Similar observation was made from the study carried out by Mehrabi et al. (1996) where variation in lateral stiffness was not significant in case of infilled frames for the two aspect ratios of 0.48 and 0.67 considered. Colangelo (2005) studied thirteen infilled frames, and reported that the stiffness of infilled frames with or without seismic detailing for two different aspect ratios ($h/l \approx 0.57$ and 0.75) found to be decreasing with increase in aspect ratio.

Effect of Infill

Past studies (Mehrabi et al. 1996; Al-chaar et al. 2002; Zovkic et al. 2013; Cavaleri and Di Trapani 2014) reported that the lateral stiffness of the infilled frames was found to be higher for solid brick units compared to hollow units. Mehrabi et al. (1996) from their study on infilled frames reported that the secant stiffness of both weak and strong frames infilled with solid infills under monotonic and cyclic loading has been enhanced by approximately 2 to 5 times that of their corresponding infilled frames with weak infills. Al-chaar et al. (2002) reported that the precracked stiffness of the infilled frames with concrete masonry and brick masonry was found to be about 24 and 18 times that of the corresponding bare frame. Zovkic et al. (2013) reported the initial stiffness of the infilled frames does not depend on the infill type but the stiffness degradation was found to be lower for AAC infills when compared to clay brick infill specimens.

Murty and Jain (2000) from their study on infilled frames with full-scale and half-scale bricks reported that the average initial stiffness of the infilled frames with full-scale bricks was approximately 1.7 times that of the infilled frames with reduced-scale bricks. This condition may be valid in case of infilled frames with high brick strength compared to that of the mortar strength. Benjamin and Williams (1958) (as referred in CEB 1996) reported that the stiffness of the infilled frames was reduced by approximately 25% when quarter scale model bricks were used in the construction of infill.

Zarnic and Tomazevic (1988) from their study on infilled frames with reinforced brick infills reported that the results did not show significant influence of the infill reinforcement on the lateral stiffness. On the other hand, Murty and Jain (2000) reported that the initial stiffness of the frames with horizontal reinforcement was reduced by about 20-40% when compared to frames infilled with full-scale bricks or reduced-scale bricks. This was mainly due to the adverse effect of larger thickness of mortar.

Effect of Vertical Load

Considerable increase in lateral stiffness was reported by Smith (1968) with vertical uniformly distributed load imposed on the beams. Similarly, Valiasis and Stylianidis (1989) reported that the presence of a compressive axial load on the columns improved the lateral stiffness of the system investigated. On the other hand, Mehrabi et al. (1996) reported that the distribution of vertical load between column and beam does not significantly affect the lateral stiffness of the infilled frames, unless the total vertical load is increased drastically (by more than 50% of design vertical loads) which may increase the stiffness by about 30%. Cavaleri et al. (2004) evaluated the influence of vertical loads and reported that the initial stiffness of the infilled frames with partial joints reduced to 50% when compared to infilled frame with continuous joints.

Effect of Openings

Benjamin and Williams (1958) (as reported in CEB 1996) from their study on brick infilled steel frames with central openings of dimensions one-third of the length and height of the infill panel reported that upto 50% of ultimate load, the openings slightly reduced the stiffness of the infilled frame, but as the load further increased the stiffness was sharply decreased in comparison with the frame infilled by a solid panel. Mallick and Garg (1971) reported that the lateral stiffness of infilled frames reduced by approximately

85% to 90% in case of openings located close to the loading corners when compared to infilled frames with solid panels. Liauw and Lee (1977) reported no significant influence of openings on the lateral stiffness of the infilled frames tested. Mosalam et al. (1997) reported that the presence of openings reduces the stiffness by about 40% for lateral loads below the cracking load level. Kakaletsis and Karayannis (2008) reported slight variation in lateral stiffness in case of window openings, whereas, the variation was found to be approximately about 40% in case of door openings for both strong and weak infills. Tasnimi and Mohebkhah (2011), reported that the initial stiffness of infilled frames with window openings was found to be slightly higher when compared to solid infilled frame which may be attributed to the presence of steel lintel beam, whereas, the lateral stiffness of infilled frame with door openings was found to be lesser than the corresponding solid infilled frame.

Effect of Gap between Infill and Frame

Moghaddam and Dowling (1987) from their experimental results on brick infilled steel frames reported a decrease of 40% for a 100 mm side gap. Further, the authors concluded that the provision of gap in the loaded corner lead to a considerable reduction of the stiffness of the system. Dawe and Seah (1989) studied the effect of the interface conditions between the top frame beam and the infill. Slight reduction in strength and stiffness was observed when a bond breaker (a polyethylene membrane) was adopted at the top interface. The authors also noted that a top gap of 20 mm which was about 0.8% of the height of the infill caused detrimental effects to the cracking pattern and ultimate capacity of the infilled frame system. Approximately 50% decrease in stiffness and 60% reduction in the strength was reported. Nazief (2014) investigated masonry infilled steel and RC frames having a full separation gap between the frame and the infill, as well as a top gap between the frame beam and the infill using finite element analysis. The sizes of the gaps considered were 5, 7, 10, and 15 mm. The author reported that the initial stiffness in case of infill steel frames experienced reduction of about 60% for 15 mm gap compared to infill walls in full contact with the surrounding frame.

Summary

From the review of past literature, it was observed that out of the various parameters, aspect ratio, strength of infill, openings and gap between the frame and infill have a

significant influence on the lateral stiffness of the infilled frame behavior. At the same time, it was also observed that various formulations were suggested to evaluate the initial stiffness of the infilled frames as the quantitative prediction of stiffness is quite difficult, since the stiffness of the infilled frame greatly depends on non-quantifiable parameters like workmanship. From the past literature, it was also observed that the strong and stiff infill improves the lateral load performance of the infilled frame system. But, under severe earthquake excitations, the brittle nature of the infill creates severe irregularities due to the variation in stiffness leading to the collapse of the entire building system.

2.2.3 Energy Dissipation

As it has been well understood that infills significantly modify the seismic response of the infilled frames, one of the effects of the presence of infill is the increased capability of the building to dissipate energy (Crisafulli et al. 2000). The infills dissipate energy by observing cracking, and by friction mechanism within the units as well along the column-wall and beam-wall interface. The most common feature observed of lateral loading systems can be observed from hysteresis loops produced from tests on infilled frames. Valiasis and Stylianidis (1989) pointed that the amount of energy absorbed by both frame and infill is higher than the energy absorbed by the bare RC frames. The reason is that in addition to the dissipative mechanism of plastic hinges in RC elements, some more mechanisms are mobilized in the presence of infill walls, namely: friction, relative displacements along the interfaces of RC elements with the infills, cracking, rotation and deformations of the infill itself. Zarnic and Tomazevic (1985) (as reported in CEB 1996) calculated damping ratios on the basis of hysteresis loops obtained from their quasi-static cyclic tests and reported that the hysteretic damping found to be increasing with increased imposed deformation. The authors also stated that the energy absorption is more important during the first cycle than during other cycle which was due to the reduced area after first cycle due to the pronounced pinching effect. The parameters on which energy dissipation of infilled frames is dependant is reviewed in the following sections.

Presence of Shear Connectors

Mallick and Severn (1967) (as reported in CEB 1996) carried out various tests to assess the dynamic characteristics of infilled frames. Two sets of steel infilled frames: one without shear connectors and other with shear connectors were investigated. Several

variations in the behavior of the two types of infilled frames were observed under lateral loading. The areas of the hysteresis loops are smaller in case of frames where shear connectors are provided leading lower hysteretic damping. More pronounced nonlinearity of the envelope curve was reported in case of frames without shear connectors which may be attributed to the friction between infill and frame. On the other hand, Liauw and Kwan (1992) reported that the infill walls which are connected to the bounding frame (integral frames) have linear and narrow hysteretic curves at small deflections (±5 mm), whereas, at the larger deflections (±10 mm) the hysteretic loops are wider which lead to tremendous energy dissipation, and it sustained for many cycles. The energy is dissipated through both material and interface damping. For non-integral frames, the lack of fit has pronounced effect after a few cycles, when the corners of the infills crush. The hysteretic curve has a noticeable pinching and is very narrow leading to a relatively small energy dissipation capacity.

Aspect Ratio

Stylianidis (2012) investigated the influence of two aspect ratios ($h/l \approx 1.0$ and 1.5), and reported that the energy dissipation capacity of the infilled frame with $h/l \approx 1.5$ increased by about 30% when compared to infilled frames with $h/l \approx 1.0$. Schwarz et al. (2015) from their study on frames with two different aspect ratios ($h/l \approx 2/3$ and $h/l \approx 3/2$) for both integral and non-integral infills reported that the narrow panel ($h/l \approx 2/3$) with integral infill possesses a substantially higher plastic area (energy absorbed) than a wide panel ($h/l \approx 3/2$) with non-integral infill.

Effect of Infill

Mehrabi et al. (1996) reported that the frames with strong infill panels exhibited higher energy dissipation than those with weak panels regardless of the frame design. Zovkic et al. (2013) from their study on reinforced concrete frames with various types of infills reported that the stronger infill had more energy dissipation capacity when compared to frame with weak infill. Similarly, Markulak et al. (2013) from their study on single bay steel frames with various types of masonry infills reported that the dissipation of hysteretic energy increases with increase in strength of infill. The amount of hysteretic energy dissipated in case of high strength clay block infilled frames and AAC block infilled frames was about 6.7 and 4.8 times that of the bare frames, respectively.

Kakaletsis and Karayannis (2008) reported slightly lower cumulative energy dissipation in case of frames with stronger infill when compared to frames with weak infill. At the same time, it was also reported that the effect of infill strength did not substantially influenced energy dissipation ratio especially in case of infilled frames with window openings. Misir et al. (2012) evaluated the performance of the reinforced concrete frames with two different types of masonry infills namely: standard and locked bricks. The authors reported that the cumulative energy dissipation of frames with both types of infills is higher than that of the bare frames which is mainly due to reaching higher levels of lateral forces. Another parameter called relative energy dissipation ratio was also used which is defined as the ratio of actual to ideal dissipated energy by a test specimen between the specified drift limits during the reversed cyclic response. The results showed that both types of bricks contributed to the energy dissipation capacity at drift ranges between 0.5% and 1%. Stylianidis (2012) reported that use of strong mortar leads to slight increase in the energy dissipation capacity of the infilled frames.

Zarnic and Tomazevic (1988) reported that significant influence of the infill reinforcement on the behavior of specimens was observed only in the case of infilled frames with openings. Murty and Jain (2000) reported that energy dissipation of infilled frames without horizontal reinforcement was about 22% higher than the reinforced infilled frames, which was because of the localization of sliding along the few mortar bed joints along which reinforcements were placed.

Effect of Openings

Kakaletsis and Karayannis (2008) reported that the total energy dissipation of infilled frame with openings was about 1.02 to 1.43 times the capacity of the corresponding bare frame. Further it was reported that the energy dissipation capacity of infilled frame with window openings was not substantially influenced, whereas, the energy dissipation capacity of the infilled frames found to be decreasing in case of door openings.

Effect of Vertical Load

Stylianidis (2012) reported that the presence of axial load on the columns increased the energy dissipation capacity of the infilled frames where the system dissipates energy through friction across the relatively small width infill cracks. It must be pointed out that higher values of the dissipation ratio appear in case of strong frames, i.e., when there is an

external axial compression load on the columns or an increased reinforcement ratio. This result can be attributed to the fact that when the frame is stronger the confinement of the infill is better. The ratio of energy dissipation capacity of the infilled frames to the bare frames is about 3 to 5 times at distortions of 2% and about 1.3 to 1.5 at distortions of 30%.

Summary

From the review of the past literature, it may be summarized that the energy dissipation of frame systems can be significantly enhanced by the presence of infills in addition of the formation of plastic hinges in columns by observing damage in infill by friction mechanism. Even though major importance has been given to the energy dissipation capacity as a structural parameter to understand the cyclic response of infilled frames, the evaluation of energy dissipation was only useful from a qualitative view point.

2.2.4 Modes of Failures of Infilled Frames

The failure of infilled frames are difficult to predict as it depends upon various parameters involving relative stiffness of frame and infill, strength of frame and infill, and aspect ratio of the frame. Further, the failure of infilled frame is a combination of one or more failure modes, which occur both in infill as well in frame elements. Asteris et al. (2011) based on the past studies (Wood 1978; Mehrabi and Shing 1997; El-Dakhakhni 2003; Ghosh and Amde 2002) categorised the failure of infilled frames in to five distinct modes (Fig. 2.1). The failure modes are corner crushing (CC), diagonal compression (DC), sliding shear (SS), diagonal cracking (DK), and frame failure (FF). Crisafulli (1997) distinguished the failure of infilled frames into failure of masonry panel and frame elements as shown in Fig. 2.2. Asteris et al. (2011) also described the sequential failure of infill under lateral loading as cracking along the compression diagonal followed by crushing near one of the loaded corners or by crushing alone and will lead to collapse if the infill is made of concrete; or else if the infill is made of brick masonry, an alternative possibility of shearing failure along the mortar planes may arise as shown in [Fig. 2.1(b)].

Based on extensive investigations (Wood 1978; Mainstone 1971; Paulay and Priestley 1992; Saneinejad and Hobbs 1995; Flanagan and Bennett 1999; Al-Chaar et al. 2002; Haldar et al. 2013; MSJC 2013; ASCE 2013) in the last decades, several models

have been proposed to evaluate the strength of infill frames under different failure modes. Description of the failure modes along with their analytical relations with respect to the strength of infill are reviewed in this section.

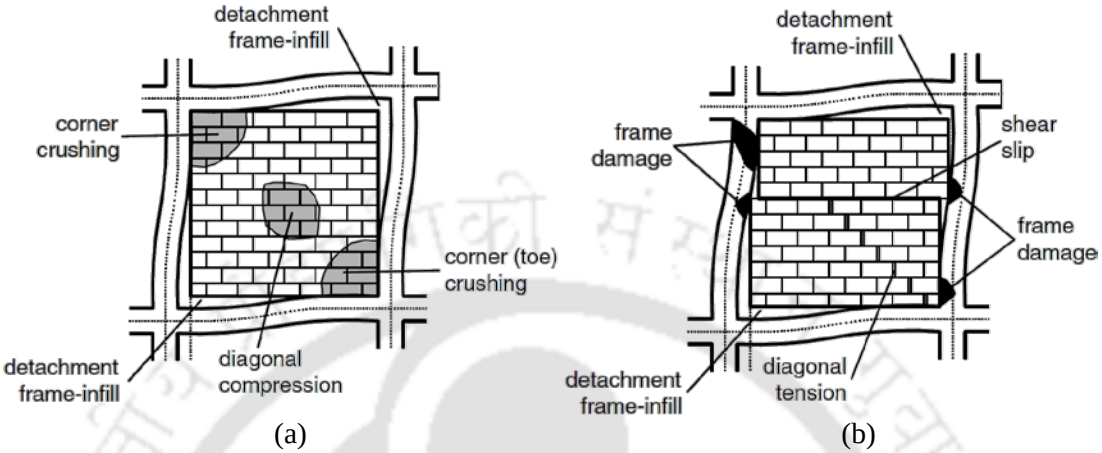

Fig. 2.1. Different failure modes of masonry infilled frames: (a) corner crushing (CC) mode and diagonal compression (DC) mode; (b) sliding shear (SS) mode, frame failure (FF) mode, and diagonal cracking (DK) mode (Asteris et al. 2011).

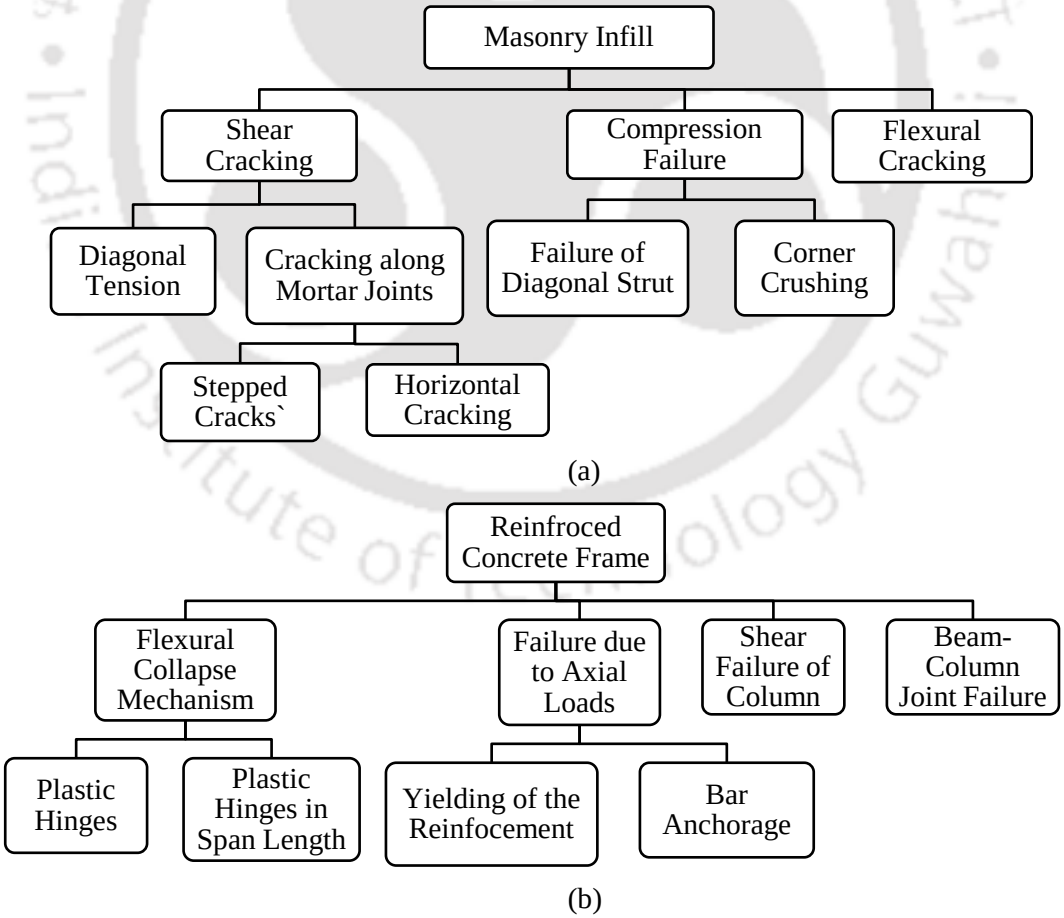

Fig. 2.2. Modes of failures in: (a) Masonry infill panel; and (b) reinforced concrete frame (Crisafulli 1997).

Corner Crushing (CC) Mode

Crushing of infill is observed near the corners under lateral loading as shown in Fig. 2.1(a). Crushing of infill is generally associated with the infilled frames with weak masonry infill panel surrounded by a frame with weak joints and strong members. According to Crisafulli (1997), crushing mode of failure of masonry is observed due to the compression where bi-axial compression stress state develops in case of a very flexible frame which cause reduction of contact length and increase the compressive stresses near the corners. Mainstone (1971) evaluated the nominal diagonal crushing strength (R_{cr}) of unreinforced masonry infills with the relative stiffness parameter (λh) given in Eqs. (2.2) and (2.3).

$$R_{cr} = 0.17(\lambda h)^{-0.4} f'_m d_m t_m \sin 2\theta \text{, for } 4 \le \lambda h \le 5 \tag{2.2}$$

$$R_{cr} = 0.15(\lambda h)^{-0.3} f'_m d_m t_m \sin 2\theta \text{, for } \lambda h > 5 \tag{2.3}$$

where f'_m represents the compressive strength of masonry infill, and l_d represent the diagonal length of the infill. Based on the finite element analysis of infilled frames, Liauw and Kwan (1985) identified two different corner crushing modes of infills considering the plastic moments of beams and columns. A simplified version of corner crushing strength of infills with failure in beams (R_{crb}) and columns (R_{crc}) as reported in Haldar et al. (2013) is given in Eqs. (2.4) and (2.5), respectively.

$$R_{crb} = \frac{\sigma_c t_m h_m}{\cos\theta} \sqrt{\frac{2(M_{pj} + M_{pc})}{\sigma_c t_m h_m^2}} \tag{2.4}$$

$$R_{crc} = \frac{1}{\sin\theta} \left[\sqrt{\frac{2(M_{pj} + M_{pc})}{\sigma_c t_m h_m^2} \sigma_c t_m h_m} \right] \tag{2.5}$$

where σ_c is the crushing strength of masonry infill panel; M_{pj} is the minimum plastic moment capacity of beam (M_{pb}) and column (M_{pc}). Flanagan and Bennett (1999) proposed simple analytical relationship to determine the corner crushing (R_{cr}) strength of the diagonal strut based on the large scale structural clay tile tests on steel frames and is given in Eq. (2.6) as

$$R_{cr} = \frac{K_{ult} t_m f'_m}{\cos\theta} \tag{2.6}$$

where the empirical constant, K_{ult} was determined from the experimental results.

Diagonal Compression (DC) Mode

According to Crisafulli (1997), diagonal cracks occur when the normal stress dominate the shear stress in infill in case of medium to high aspect ratio infilled frames. Generally, the cracks initiate in the central zone of the panel, where the tensile principal stresses are higher and then propagate towards the corners. Similarly, Asteris et al. (2011) reported that the diagonal compression mode of failure is associated with a relatively slender infill, in which failure results from out-of-plane buckling of infill, with the crushing of infill within its central region [Fig. 2.1(a)]. According to Priestley and Calvi (1991), diagonal tension cracking of infill should be considered as the failure of the structure, because of the out-of-plane fall-out of infill when cracks propagate along both the diagonals. Smith (1967) developed expressions to evaluate the diagonal compressive strength (R_c) of infill panel for equivalent diagonal strut, which were later adopted by Smith and Carter (1969) and is given in Eq. (2.7) as

$$R_c = l_c t_m f'_m \sec\theta \tag{2.7}$$

where $l_c = \frac{\pi}{2\lambda}$ is the contact length between the frame and infill. Haldar et al. (2013) reported simplified expressions proposed by Liauw and Kwan (1985) for the evaluation of diagonal compressive strength of infills, considering "failure in infill-beam connections" (R_{cb}) and "failure in infill-column connections" (R_{cc}), as given in Eqs. (2.8) and (2.9), respectively,

$$R_{cb} = \frac{1}{\cos\theta}\left(\frac{4M_{pj}}{h_m} + \frac{\sigma_c t_m h_m}{6}\right) \tag{2.8}$$

$$R_{cc} = \frac{1}{\cos\theta}\left(\frac{4M_{pj}}{h_m} + \frac{\sigma_c t_m h_m}{6\tan^2\theta}\right) \tag{2.9}$$

Paulay and Priestley (1992) proposed the expressions to evaluate the capacity of the infill in diagonal compression failure mode (R_c), as a function of vertical contact length (l_c) is given in Eq. (2.10). Based on the compressive strength of infill (f_a)

considering out-of-plane failure in its central region, Saneinejad and Hobbs (1995) proposed Eq. (2.11) to evaluate the diagonal compressive strength of the slender infill.

$$R_c = \frac{2}{3} l_c t_m f'_m \sec\theta \tag{2.10}$$

$$R_c = 0.5 h_m t_m f_a \sec\theta \tag{2.11}$$

Sliding Shear (SS) Mode

According to Asteris et al. (2011), sliding shear type of failure is by cracking through bed joints of a masonry infill and is generally associated with weak mortar joints or weak infill and strong frame [Fig. 2.1(b)]. Crisafulli (1997) reported that sliding shear failure as cracking in infill initiated few layers below the loaded corner and propagates towards centre of the panel, after which the crack propagates horizontally (Fig. 2.3).

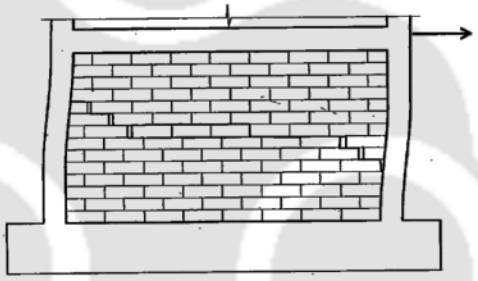

Fig. 2.3. Failure of infilled panel by sliding (Crisafulli 2000).

The shear strength (R_s) of the infilled panel considering horizontal crack along the length of the infill proposed by Saneinejad and Hobbs (1995) is expressed in Eq. (2.12) as

$$R_s = \frac{\gamma_l v t_m l_m}{(1 - 0.45\tan\theta')\cos\theta} \leq \frac{0.83\gamma_l}{\cos\theta} \tag{2.12}$$

where γ_l is the load factor for sliding shear strength; v is the basic shear strength of bed joints of masonry; θ' the sloping angle of masonry diagonal strut at shear failure, $tan\theta' = (1-\alpha_c)h_m/l_m$, and α_c is the normalized contact length of column–infill (i.e., contact length/length of member). The in-plane shear strength of infill panel (R_s) as per ASCE 41 (2013) was estimated as the bed joint shear strength (f'_{vb}) times the net mortared area of infill (A_{nb}) as shown in Eq. (2.13). The equation proposed by Al-chaar (2002) was similar

to the one recommended in ASCE 41 (2013) considering reduction factors for openings and for any existing infill damage.

$$R_s = A_{nb} f'_{vb} \sec\theta \tag{2.13}$$

Diagonal Cracking (DK) Mode

Diagonal cracking mode of failure considered as the most common type of failure of infill as it has been widely observed in laboratory tests, as well in infilled frame buildings. In this type of failure, failure takes place in the form of crack propagation along the compressed diagonal and which often takes place with simultaneous initiation of the SS mode [Fig. 2.1(b)]. This mode of the failure is associated with weak frame or a frame with weak joints and strong members with a rather strong infill (Mehrabi et al. 1996). Generally, diagonal cracking occurs when the bond strength of the head joints is less either due to shrinkage or due to no proper filling of head joints, and the bed joint shear strength is very weak. Smith (1967) proposed expressions to calculate the diagonal cracking strength (R_t) based on the tensile strength of mortar (f'_{jt}) given in Eq. (2.14) as

$$R_t = f'_{jt} h t_m \tag{2.14}$$

The equation was proposed assuming the tensile strength of mortar found to be weaker compared to brick units. Mainstone (1971) evaluated the nominal diagonal cracking strength (R_t) of infills with the relative stiffness parameter (λh) and proposed the expressions to estimate the diagonal cracking strength as given in Eq. (2.15) and Eq. (2.16). Saneinejad and Hobbs (1995) recommended the diagonal tensile strength of infill strut (R_t) at infill cracking and is given in Eq. (2.17).

$$R_t = 0.56(\lambda h)^{-0.875} f'_m d_m t_m \sin 2\theta \text{ , for } 4 \le \lambda h \le 5 \tag{2.15}$$

$$R_t = 0.52(\lambda h)^{-0.8} f'_m d_m t_m \sin 2\theta \text{ , for } \lambda h > 5 \tag{2.16}$$

$$R_t = 2\sqrt{2} t_m h_m f'_t \cos\theta \tag{2.17}$$

Frame Failure (FF) Mode

Crisafulli (1997) categorised the failure of frame elements into various categories based on the characteristics of the frame members and on the effects resulting from frame-infill

interaction as shown in Fig. 2.2(b). The damage of frame elements usually occurs from flexural plastic hinges, shear failure, yielding under axial forces, compression failure or a combination of all. Evaluation of the strength of the reinforced concrete members especially in flexure, axial compression, tension has been standardised as most of the design codes have consensus pertaining to their evaluation. Much emphasis is given to the evaluation of shear strength as most of the past studies reported premature failure of frame elements, and shear strength estimation observed slight variations in the various design standards.

Flexural Failure

Flexure failure of columns was developed by observing plastic hinges at ends of the columns [Fig. 2.4(a)] unlike the shear failure, which is brittle in nature. In case of masonry infilled RC frames, the flexural failure of beams was a rare phenomenon. In some cases, plastic hinges in columns were formed at mid-height of the columns due to shear-sliding failure in infills leading to high shear demand [Fig. 2.4(b)]. Therefore, higher shear forces need to be resisted when flexural hinges were formed at the mid-height of the column.

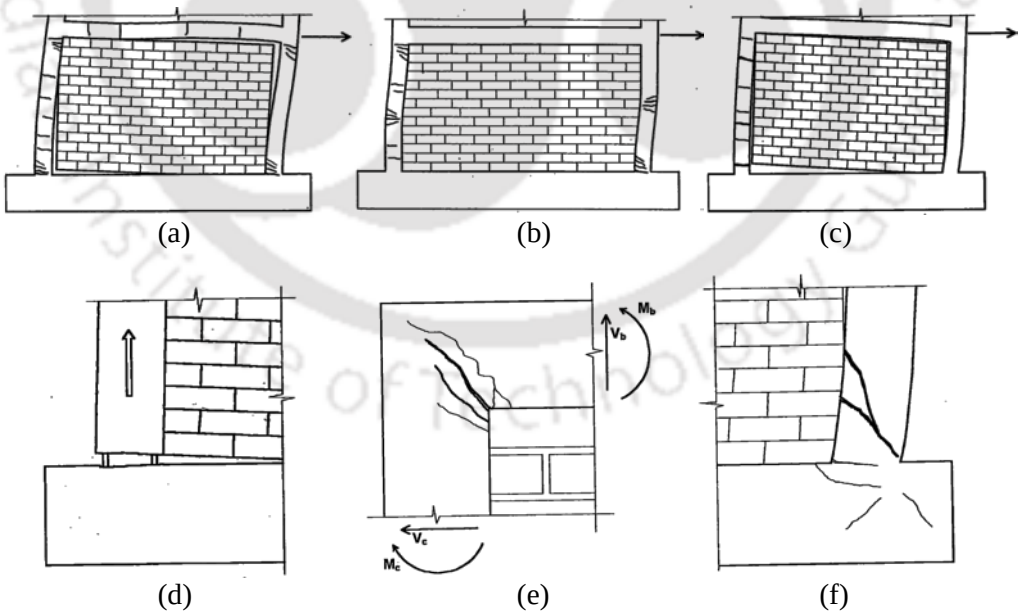

Fig. 2.4. Failure in frame members: (a) and (b) flexural hinges at member ends and span length, respectively; (c) tension failure; (d) bar anchorage failure; (e) beam-column joint failure; and (f) shear failure of columns (Crisafulli 1997).

Failure due to Axial Loads

Cracking of reinforced concrete members were observed due to tensile axial forces, and cracking and yielding of members may be observed under increased lateral loading. Generally two types of modes of failure due to axial load are reported (Crisafulli 1997): tensile failure due to yielding of longitudinal reinforcement [Fig. 2.4(c)] and bar anchorage failure [Fig. 2.4(d)]. Due to the yielding of reinforcement, elongation of columns was observed leading to the decrease in frame-infill interaction due to the significant variation in deformation of both infill and frame members. Bar anchorage failure is generally associated with the slip of the longitudinal reinforcement of the tension column and can be avoided by providing adequate development length for the longitudinal bars.

Failure of Beam-Column Joints

The behavior of beam-column joints in shear under lateral loading is a complex phenomenon, as a number of parameters affect the strength of joints. According to Crisafulli (1997), high normal and tangential stresses develop along the contact lengths in the zones near to the loaded corners, resulting in large shear forces and bending moments in the loaded corners. The stress-state induced in the beam-column joints may cause the formation of wide diagonal cracks running across the joint from interior to exterior corner [Fig. 2.4(e)]. Vast numerical studies were carried out in the past to evaluate the shear strength of beam-column joints and several models (CEN 2004b; ACI 2012; ASCE 2013) were proposed for interior and exterior joints.

Shear Failure of Columns

The most adverse effects of infills in the infill-frame systems are the alteration of failure of column members from flexure mode to shear mode (Mehrabi et al. 1996; Al-chaar et al. 2002; Fardis 2009) due to the interaction between the frame and infill [Fig. 2.4(f)]. It was observed that the shear failure of columns may be either due to: (i) the interaction of columns with strong and stiff infills which may shear-off weak columns in ground storey where contact is only on one-side, or (ii) the column is in contact with infill over a partial height creating captive column effect by decreasing the effective length of the column that has to resist the entire inter-storey drift. According to Moghaddam and Dowling (1987), shear failure in windward column occurs due to the combined shear and tensile

forces acting on the reinforced concrete section adjacent to the compressive corner of the frame. In order to evaluate the shear failure of columns of infilled frames, estimation of shear strength of reinforced concrete columns is a pre-requisite. The shear strength of RC members is considered to have distinct contributions from concrete and transverse reinforcement. Contribution of concrete in shear strength determination is complex and is influenced by several parameters (Sezen and Moehle 2004), such as, compressive force, column dimensions, ductility demand, etc. Design standards (BIS 2000; ACI 2008; CEN 2004b; ASCE 2013; CEN 2005b) provide various equations for the evaluation of shear strength of RC members. A brief overview of the some of the standards employed in the current study is presented in Table 2.1. The design standards IS 456 (BIS 2000), ACI 318 (2008), and Eurocode 2 (CEN 2004a) evaluate the shear strength of the RC members without considering the effect of cyclic loading. Whereas, ASCE 41 (2013) and Eurocode 8 (CEN 2005b) consider the effect of reversed cyclic deterioration of shear capacity.

Table 2.1. Shear strength models based on various standards

Standard	V_c*	V_s
IS 456 (2000)	$V_c = \delta \tau_c b d$	$V_s = \dfrac{f_{ys} A_s d}{s}$
ACI 318 (2008)	$V_c = 0.17\left(1+\dfrac{P}{14A_g}\right)\sqrt{f_c'}A_g$	$V_s = \dfrac{f_{ys} A_s d}{s} \le 0.66\sqrt{f_c'}A_g$
Eurocode 2 (2004a)	$V_c = \left[\dfrac{0.18}{\gamma_c} K\left(100\rho_l f_{ck}\right)^{1/3} + 0.15\sigma_{cp}\right] bd$	$V_s = \dfrac{f_{ys} A_s z d \cot\theta}{s}$
ASCE 41 (2013)	$V_c = \lambda k \left(\dfrac{0.5\sqrt{f_c'}}{M/Vd}\sqrt{1+\dfrac{P}{0.5\sqrt{f_c'}A_g}}\right)0.8A_g$	$V_s = k\left(\dfrac{A_s f_{ys} d}{s}\right)$
Eurocode 8 (2005b)	$V = 1/\gamma_{el}\left[\dfrac{D-x}{2L_v}\min\left(P;0.55A_c f_c'\right)+\left(1-0.05\min\left(5;\mu_\Delta^{pl}\right)\right)\right.$ $\left.\cdot\left[0.16\max\left(0.5;100\rho_l\right)\left(1-0.16\min\left(5;\dfrac{Lv}{D}\right)\right)\sqrt{f_c'}A_c+\rho_w b z f_{ys}\right]\right]$	

*V_c , V_s and V represent the shear resistance by concrete, shear reinforcement and total shear resistance of concrete section; $\delta = 1+\dfrac{3P}{A_g f_{ck}} \le 1.5$; δ multiplication factor to design shear strength; P is the axial compressive force on the column; A_g is the gross area of the concrete section; f_{ck} is the compressive strength of concrete cube; τ_c is the shear stress in concrete; b, d are the width and effective depth of the cross section; f_{ys} the yield strength of the transverse reinforcement; A_{sv} is the total cross-sectional area of transverse reinforcement within a spacing s;

f_c' is the compressive strength of concrete cylinder; γ_c is the partial safety factor for concrete; $K = 1 + \sqrt{\frac{200}{d}} \leq 2.0$; $\rho_l = \frac{A_{sl}}{bd} \leq 0.02$; ρ_l is the reinforcement ratio of longitudinal reinforcement; A_{sl} is the area of the tensile reinforcement; $\sigma_{cp} = \frac{P}{A_c} < 0.2 f_{ck}$; σ_{cp} is the compressive stress in concrete from axial load; A_c is the area of the concrete section; z is the length of the internal lever arm; M/V is the largest ratio of moment and shear under design loadings for column; λ = 0.75 for lightweight aggregates and 1.0 for normal weight aggregates; k = 1.0 in regions where ductility demand is less than or equal to 2, 0.7 in regions where displacement ductility is greater than or equal to 6, and varies linearly for displacement ductility between 2 and 6; γ_{el} is assumed to be equal to 1.15 for primary seismic elements; D is the depth of the cross section in the direction of loading, x is the height of the compressed zone; L_v is the shear span ratio; μ_Δ^{pl} is the plastic part of the ductility demand calculated as $\mu_\Delta^{pl} = \mu_\Delta - 1$; and ρ_w is the transverse reinforcement ratio.

Summary

Of the various failure modes in infill and frame members, especially in columns, it was noted that the corner crushing and sliding shear mode of failure in infill and shear failure of columns were prominent. Even though infill observed diagonal cracking along the tension and compression side, the ultimate failure of infill was reported in corner crushing or sliding shear mode of failure. In case of column members, the major potential adverse effect of infill is shear failure of columns near the loaded corners. Most of the past experimental studies reported shear failure of columns in frames not designed as per the recommendations of prevalent seismic standards. But a realistic estimation of shear demand on the column and the design methods to counteract the adverse effect of infill has not been put forward.

2.3 MODELLING OF INFILLED FRAMES

Large number of experimental and numerical investigations was carried out on infilled frames, and analytical modelling of RC frames has been well established in the literature. A lot of models were proposed and few were improved to overcome the known deficiencies. Generally, masonry infills have been modelled as equivalent diagonal struts, based on the idea of Polyakov (1960) who advocated that infill act as bracing members. Later the idea was put forward by various studies leading to the development of single strut models (Holmes 1961; Smith and Carter 1969; Mainstone 1971) and multiple strut models (El-Dakhakhni et al. 2003; Crisafulli and Carr 2007; Fiore et al. 2012).

Alternatively, infills may be modelled by means of detailed finite element micromodelling. Two ways of modelling infills were observed in the literature: either by simplistic macromodelling approach or by the more complicated micromodelling approach. A brief review of the different analytical models pertaining to the current study and their limitations are reviewed in this section.

2.3.1 Macromodels

Macromodelling is based on the concept of understanding the behavior of an infill panel as a whole under lateral loading. In some cases, a single element simulates entire infill panel, and in some macromodels, multiple struts are used for each infill panel. Most of the past analytical studies resorted to macromodelling techniques, especially, modelling infill as equivalent diagonal strut because of the ease in idealizing the parameters involved in modelling.

2.3.1.1 Single-strut Models

Based on the idea of compressive behavior of infill under lateral loading in infilled frames, Holmes (1961) replaced infill with an equivalent pin jointed diagonal strut with the same material and an equivalent width (w_s) as $l_d/3$ where, l_d is the diagonal length of the infill wall. Later, based on large experimental studies, Smith and Carter (1969) related the width of the strut as a function of relative stiffness as described in the previous section (2.1). Using the relative stiffness parameter (λh), Mainstone (1974) upgraded the expression of equivalent diagonal strut as given in Eq. (2.18).

$$\frac{w_s}{d_m} = 0.175\lambda h^{-0.4} \tag{2.18}$$

The equation proposed to evaluate the width of the strut by Mainstone (1974) was accepted by many researchers and is included in ASCE 41 (2013). Klingner and Bertero (1976) proposed the first hysteretic diagonal strut which was able to simulate the stiffness degradation due to cyclic loading in the two directions. Inspite of the originality, the proposed model was not able to simulate the experimental results accurately. Liauw and Kwan (1984) proposed a semi-empirical relation (Eq. 2.19) for calculating the width of the strut, for various values of θ. Paulay and Priestley (1992) proposed the equivalent diagonal strut (w_s) as one fourth of the diagonal length of the infill wall for design of

masonry infilled RC frames. Based on large experimental study on full-scale infilled steel frames tested under lateral loading, Flanagan and Bennett (1999) proposed a piecewise linear strut area (A_w) as shown in Eq. (2.20).

$$\frac{w_s}{d_m} = \frac{0.95 \sin 2\theta}{2\sqrt{\lambda h}} \tag{2.19}$$

$$A_w = \frac{\pi t_m}{C\lambda \cos\theta} \tag{2.20}$$

where C is an empirical constant which varied with the in-plane drift displacement and is an indicator of the limit state of infill. Puglisi et al. (2009) proposed a new modified diagonal strut model based on the theory of plasticity (plastic concentrator) to overcome the drawback of equivalent strut model under cyclic or earthquake loadings. The modified model considers a concentrator (plastic/elastic) linked between the two diagonal strut bars, which transfer the effects from one strut to other. From the analysis, it was found that the conventional strut models need to be modified by considering coupling between the bars in order to observe the more realistic behavior under lateral loading. To study the nonlinear hysteretic behavior of masonry infill in RC frames, Rodrigues et al. (2010) upgraded the equivalent diagonal compression strut model to consider the interaction of masonry in both directions (Fig. 2.5).

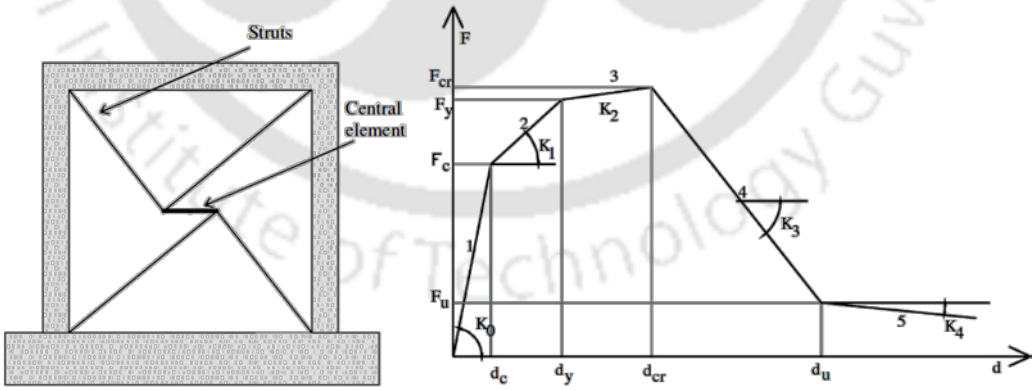

Fig. 2.5. Macromodel for the simulation of infill and force displacement monotonic curve (Rodrigues et al. 2010).

The masonry panel hysteretic procedure considers rules for loading, reloading, unloading and also degradation of stiffness and strength along with pinching effect. It was reported that the proposed model was able to represent the response in terms of

displacements, global shear-drift at each storey, and cumulative dissipated energy. Among the various parameters influencing the behavior of equivalent strut, the effect of vertical load acting on the frames is well recognized as discussed in the previous sections (2.2, 2.3, and 2.4) but not quantified. Addressing this effect, Campione et al. (2015) modified the equivalent strut taking into account the stiffening effect produced by the vertical loads on the infill in the initial state. A family of curves to modify the width of the strut was proposed for different vertical loads and for different Poisson's ratio by imposing the equivalence between the frame containing the infill and the frame containing the diagonal strut. Along the same lines, Asteris et al. (2016) modified the equivalent pin-jointed diagonal compressive strut by a stiffness reduction factor which considers the effects of both openings and vertical loads. The effect of vertical loads on the stiffness of the dimensionless strut width is prominent in case of fully infilled frames and negligible for panels with larger openings. From the study, it was also concluded that the proposed mathematical macromodel may be used as a reliable and useful tool for the determination of the equivalent compressive strut width, since it accounts for a large number of parameters, which are not generally accounted by the available models.

2.3.1.2 Multiple-strut Models

To overcome the limitations of single-strut models, multiple-strut models were proposed to simulate the effect of infill under lateral loading more accurately. In this regard, Thiruvengadam (1985), proposed multiple-strut model to evaluate the realistic natural frequencies and modes of vibration using several diagonal and vertical struts in each direction. The model has been adopted by various researchers as the model accounts effect of openings (Singh and Das 2006; FEMA 2000).

Chrysostomou et al. (2002) considering infill hysteretic stiffness and strength degradation simulated the response of infilled frames using six struts with three struts in each diagonal direction [Fig. 2.6(a)]. Only three struts were activated at any time of analysis, whenever tensile force exists the struts are switched to other loading direction. The infill model allows the interaction between infill and the frame, and takes into account the strength and stiffness degradation of the infill. El-Dakhakhni et al. (2003) simulated the effect of infill by three diagonal struts in each direction to estimate the stiffness and the lateral load capacity of concrete masonry infilled frames. The masonry

model was developed based on the orthotropic properties of masonry infill. It was observed that the method can be easily implemented in finite element models and design of three dimensional masonry infilled concrete frames.

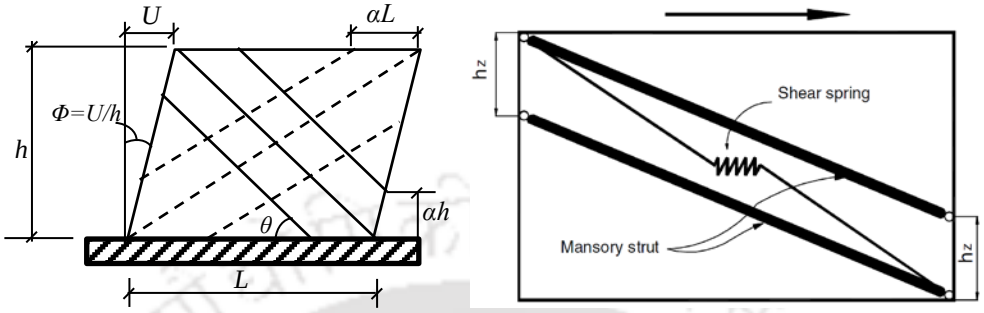

Fig. 2.6. Multiple-strut models: (a) six-strut idealization of infill wall (Chrysostomou et al. 2002); and (b) double strut model with shear spring for infill panel (Crisafulli and Carr 2007).

To appropriately, simulate the response of infilled frame in terms of lateral stiffness and strength a new macromodel consisting of two parallel struts with a shear spring [Fig. 2.6(b)] was proposed by Crisafulli and Carr (2007). The major inefficacy was the model not able to predict the distribution bending moment and shear forces in the frame elements. Uva et al. (2012) performed sensitivity analysis varying width of the strut (w_s), the constitutive force-displacement law of the panel and number of struts adopted. The equivalent strut with larger width (w_s) has shown higher capacity but exhibited brittle behavior, whereas, vice-versa behavior observed for lower values of w_s. The constitutive force-displacement relation of the masonry panel has a significant dependence on the type of failure mechanisms of the panel. The authors reported that only the multi-strut model can represent the brittle failure mechanism occurring at the nodes due to the presence of the masonry infill.

2.3.1.3 Improved Macromodels to Capture Local Shear Failure of Columns

It has been already discussed in the previous section that the single strut models were not be able to reproduce the realistic shear forces and bending moments in the surrounding frame elements. Under-estimation of shear demand on the columns may lead to their brittle shear failure which is not desirable. In the recent years, the basic strut macromodels were improved to predict the shear distribution in frame critical sections. D'Ayala et al. (2009) analysed single storey infilled RC frames to evaluate the shear

capacity of the columns due to the detrimental effect of infill using two finite element programmes and validated the results with similar experiments (Al-chaar et al. 2002). Even though the analytical model predicted the shear failure of columns, the applicability of the model in practical engineering problems is limited and computationally intensive as the contact elements were found to be difficult to calibrate.

Celarec and Dolšek (2013) carried out an iterative pushover based procedure involving model adaptation by modifying the moment-rotation and force-displacement relationships of the columns and diagonal strut, respectively. Their procedure was found to be approximate due to several limitations and simplifications, especially, the limitations concerning the shear strength model and the proportion of force transferred from infill to column. Cavaleri and Di Trapani (2015) proposed a predictive tool, to estimate the shear forces at the ends of the beam and column as a fraction of axial load experienced by the equivalent diagonal strut. Fiore et al. (2016) tried to predict the brittle shear collapse mechanism of columns due to the infill-frame interaction using the double-strut model (Fig. 2.7) proposed previously by Fiore et al. (2012). However, the major difficulty of the double-strut model is the placement of the equivalent non-parallel struts and the shear force and bending moment distribution due to the application of the concentrated force near the stress resultants.

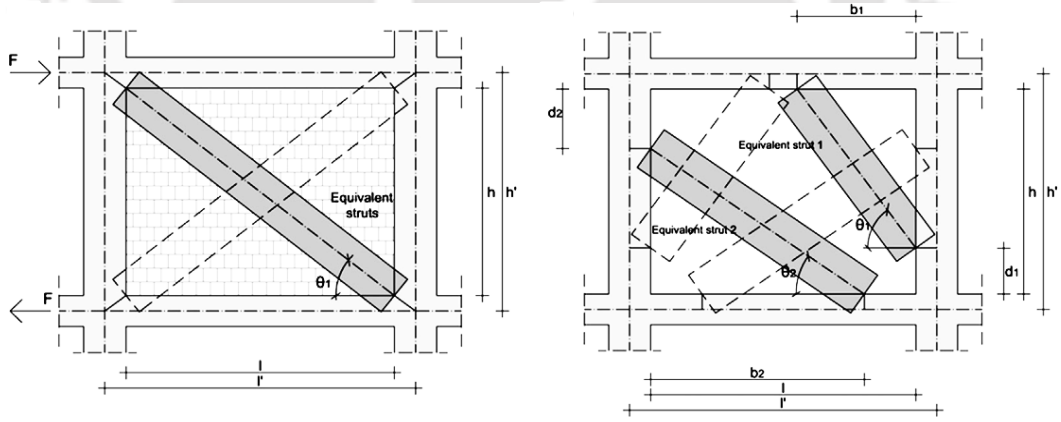

(a) (b)

Fig. 2.7. Macromodels of infill panels: (a) single-strut model; and (b) double-strut model (Fiore et al. 2016).

2.3.2 Micromodelling

Micromodelling (finite element) methods generally adopt three kinds of elements to characterize: the frame, the infill, and their interaction. The simulation of frame elements

and infills has been well established in the literature (Mallick and Severn 1967; Mehrabi and Shing 1997; Stavridis and Shing 2010; Ellul and D'Ayala 2012; Asteris et al. 2013), while most of the attention has been focused on the development of appropriate contact elements. The frame elements and the infill panel were modelled by shell elements or beam elements and planar shell finite elements, respectively (Di Trapani et al. 2015). The interface contact elements were defined to simulate the frictional and frame-infill detachment in contact regions. This type of modelling approach is able to provide detailed structural response in terms of local effects, in addition to global force distribution. The major difficulty in carrying out analysis using micromodelling technique is the sensitivity of the model to the material constitutive laws, definition of the interface connections and their calibration. In addition, analyses of the large buildings require high computational effort which found to be unacceptable for practical engineering purposes.

2.3.3 Summary

From the available literature, it was observed that the single-strut models are able to capture the global response of the infilled frames but are inadequate for accurately estimating the force distribution in surrounding frame members. Models with multiple-struts were proposed to overcome the limitations of the single-strut models. The models with multiple-struts were able to capture the frame-infill interaction but with a considerable increase in modelling complexity. From the available literature, it can be said that the available macromodels does not possess the capability and necessary simplicity to be used in everyday engineering practice and to be implemented in finite element models. Therefore, it may be observed that there is a need to improve the simplistic mathematical equivalent diagonal strut modelling technique, so as to capture the shear failure of columns due to the detrimental effect of infill.

2.4 Design of Masonry Infilled RC Frames using Codal Approaches

Masonry infill is used extensively in RC buildings in several countries worldwide and has significant effect on their behavior during earthquakes. It is important to know how national codes of various countries control behavior and design of masonry infilled RC frames. A comprehensive review of the design of masonry infilled RC frames by various earthquake standards was presented in the state-of-the-art report by Kaushik et al. (2006).

It was showed that generally two types of approaches were considered in the standards: whether to or not to consider infill in the design. Some design standards recommend isolation of masonry infill from the frame system, such that the masonry does not affect the stiffness of the structure. On the other hand, some national standards provide guidelines on analytical modelling to consider adverse effects of infill. Generally, two kinds of effects, i.e., global and local adverse effects were created in the RC frames due to the presence of infills. Global adverse effects deal with the overall distribution of infill in plan and elevation. The detrimental effect is created due to the irregular distribution leading to the catastrophic damage of the whole structure. Local adverse effects are related to the damage of the individual members due to the presence of infills, which will ultimately lead to the overall failure of the structure. Recommendations of the various earthquake standards related to both global and local adverse effects of infills are discussed in the following sections.

2.4.1 Global Adverse Effects of Infills

According to Eurocode 8 (CEN 2004b), non-structural masonry infills act as second line of defence and a cost-effective source of significant overstrength. Eurocode 8 does not decrease seismic action effects for which the structure is designed due to the beneficial effect of infill in imparting lateral strength, stiffness to the structure (Fardis 2009). If the contribution of infill to the lateral strength and stiffness is very large compared to the frame members, the infills may override the seismic design by spreading inelasticity throughout the system.

The major potential adverse effects of infills are the irregular distribution of infills in plan and elevation, and creation of soft-storey due the loss of integrity of infills in the ground floors. To address the global adverse effects, Eurocode 8 recommends consider modelling of infill when their contribution significantly affects the lateral load behavior of the system in terms of strength and stiffness. According to Eurocode 8, when the infills are not regularly distributed in plan, the irregularity may be taken into account by increasing the accidental eccentricity by a factor of 2. The code also states to include infill walls in models by performing a sensitivity analysis regarding their position and their properties. In case of vertical irregularity, Eurocode 8 recommends to increase the seismic

action effects of the vertical elements (columns) of the respective storeys shall be increased by a factor η as shown in Eq. (2.21)

$$\eta = 1 + \frac{\Delta V_{Rw}}{\sum V_{Ed}} \leq q \tag{2.21}$$

where ΔV_{Rw} is the total reduction in lateral resistance of infills in the concerned storey compared to the storey above, and ΣV_{Ed} is the sum of the seismic shear forces acting on all columns of the storey concerned. Behavior factor q, which accounts for energy dissipation capacity in structure, varies from a minimum value of 1.5 to 4.68 depending upon building systems, ductility classes, and plan regularity in buildings. The standard also recommends that there is no need for magnification if factor η is less than 1.1.

IS 1893 (BIS 2002b) does not exclusively deal with the plan irregularity but provide guidelines about the torsional irregularity in buildings. In case of vertical irregularity specifically in buildings with soft-storey, dynamic analysis has to be carried out including the mass, stiffness of infills. Further, the inelastic deformations in the members, particularly, those in the soft-storey need to be considered and the frame members designed accordingly. Alternatively, IS 1893 recommends the frame members to be designed for 2.5 times the seismic storey shears and moments without modelling the effect of infill in any storey. The other alternative was to provide the symmetric shear walls designed for 1.5 times the design storey shear force in both directions of the building.

Nepal code (NBC 1994), provide certain guidelines to control the plan and vertical irregularities arising in buildings due to unsymmetrical placement of infills. According to the standard, the ratio of lumped mass of each storey to the sum of thicknesses of walls including plaster finish in the storey shall not be more than 125% of the same ratio for any higher storey except at the roof level. Additionally, the standard also limits the eccentricity to 10% of the building dimension between center of mass and center of rigidity along the considered principal direction.

2.4.2 Local Adverse Effects of Infills

In addition to the potential adverse effects of infills on global response, there may be local effects of infills on the structural elements especially columns of infilled frames. Among

these firstly the presence of strong and stiff infills which may shear-off weak columns, especially the imbalanced contact, i.e., when the infills are present only one side of the columns. Secondly, the captive column effect where infill is in contact over a fraction of full height of the column. Under lateral loading, failure or heavy damage of the strong and stiff infill panel may dislodge part of it, exerting a concentrated force on the infill (Fardis 2009). The stronger the infill, larger is the magnitude of this force and higher the likelihood of the column shear failure. This type of failure is more pronounced in ground storeys as the shear force demand is largest. Captive columns in buildings are provided for purely architectural reasons; with openings between the beam soffit and the sill level. Failure of captive columns is very common in earthquakes, especially if the column is weak and fails before it crushes the adjoining infill over the contact area. To address the first local adverse effect of strong and stiff infill, Eurocode 8 recommends the length of the column against which the diagonal strut acts should be verified for the smallest of the following design forces: (a) The horizontal component of the strut force of the infill, taken equal to the horizontal shear strength of the panel calculated from the shear strength of the bed joints. (b) The shear force computed assuming the overstrength flexural capacity of the column developed at both ends of the contact length (l_c). Additionally, Eurocode 8 also imposes special detailing and confinement requirements for columns over the full height of the ground storey, and also recommends the columns that are in contact with infills on only one side to help withstand local overloading due to the dislodgement of the infill at any point along their height.

To address the captive column effect, Eurocode 8 recommends calculating the design shear force accordance with (b) with length of the column (l_c) was taken equal to its free length not in contact with the infill (i.e., the clear height of the opening). The presumption behind the calculation is the lateral restraint of the captive column by the infill is sufficient to induce a column plastic hinge at the sill level of the opening, rather than at the column bottom. Eurocode 8 also imposes the special detailing rules on captive columns by placing the required transverse reinforcement not just over the free length of the column and also along the column in contact with infill for a distance equal to the depth of the column. The code also recommends applying special detailing and confining requirements for column critical regions over the full height of the column in the storey. If the clear height of the opening is short, the calculated design shear force may be very

large and it may be difficult to verify the column for it, especially if the column fails in shear compression failure and cannot be increased further through transverse reinforcement.

Alternatively, Eurocode 8 recommends placing diagonal reinforcement along the clear length of the column within the plane of the infill. Eurocode 8 recommends modelling of infill in structural analysis only for buildings with severely irregular layout of infills in plan and requires more accurate estimation of strut width taking into account the elastic properties and geometry of the infill and column, otherwise the strut width may be assumed to be fraction of the diagonal length of the masonry wall. No reference models as a guide to designers for practical applications were provided by the standard.

Indian ductile detailing standard IS 13920 (BIS 1993) recommends special confining reinforcement in columns, only if significant variation in stiffness is observed along the column length or when the calculated point of contra-flexure is not within the middle half of the member clear height.

Nepal code NBC 201 (1994) recommends estimating the axial forces in the frame members by pin-jointed frame and representing masonry infill by compression diagonal struts without specifying their cross-sectional properties. The results are superimposed on vertical loads and moments on the columns determined for seismic forces. The design shear force in column in contact with a lateral load resisting wall was taken as half of the shear force in the wall.

ASCE 41 (2013) also recommends checking the shear strength of the column members adjacent to the infill panels for higher of: (a) horizontal component of the strut force at the column using the shear strength of the column with zero axial load; and (b) the shear force obtained from development of column flexural strengths at top and bottom. These two recommendations of ASCE 41 are in line with the recommendations of Eurocode 8.

MSJC (2013) provides a basic set of provisions for the design of masonry infilled RC frames based on the experimental research and the anecdotal performance. The provisions addresses both non-participating infills which are structurally isolated from the lateral force resisting system, as well as participating infills which are designed to resist

in-plane forces. The standard recommends not considering the effect of partial height infills and infills with openings in lateral force resisting system due to the detrimental effect in causing premature failure of the columns. Infills need to be considered in the design when the specified gap between the bounding beams or slab at the top of the infill is less than 9.5 mm. The bounding columns in contact with infill shall be designed for shear and moment for 1.1 times the results obtained from equivalent strut frame analysis. Additionally, the design shear capacity of section is increased by the horizontal component of the equivalent strut force.

2.4.3 Summary

From the review of the codal approaches, it was clearly observed that most of the national standards provide guidelines to counteract the global adverse effect of infill, while, some of the standards provide recommendations to safeguard the frame against the local adverse effect of infill, e.g., shear failure of columns. It was observed that the effectiveness of the design and detailing requirements of the current design standards pertaining to shear design of columns are not verified experimentally.

2.5 Summary and Gap Areas

From the review of the past literature, it is observed that the masonry infills contribute to strength, stiffness and energy dissipation and act as a second line of defence against lateral loads. But the columns of masonry infilled RC frames are prone to shear failure due to the detrimental effect of infill, if they do not possess sufficient capacity to resist the forces exerted by the infill. This effect is more catastrophic in ground storey columns, where the shear force demand is very high. Even though some of the popular national standards consider the detrimental effect of infills, they do not define a proper modelling technique to consider the frame-infill interaction. Therefore, the effectiveness and the applicability of the current technical standard recommendations pertaining to design, detailing and modelling of masonry infilled RC frames have to be evaluated both experimentally and analytically.

Performance of masonry infill and its influence on the surrounding frame members need to be understood for proper interpretation of the behavior of infilled frames under lateral loading. Therefore, the nonlinear material characteristics of masonry

have to be evaluated for modelling of infill especially when new engineering materials, like fly ash bricks, are adopted. A lot of analytical modelling techniques have been proposed in the literature but a simplified macromodel to capture the shear failure of columns for practical engineering purposes is not available. If the current design provisions are found to be redundant in delaying the shear failure of columns, strategies need to be proposed to prevent the shear failure of columns in masonry infilled frames. These adopted strategies need to be investigated analytically and experimentally. As discussed in chapter 1, these gap areas form the objectives of the current study.

Various types of masonry (solid clay bricks, autoclaved aerated concrete blocks, hollow clay blocks, reinforced concrete, etc.) were used as infills in RC frames in the past studies. Recently, use of alternative building materials, e.g., fly ash bricks, are gaining importance in building construction due to the large-scale utilisation of industrial wastes (pulverised fuel ash) in their manufacturing. In the current study, fly ash bricks were used to examine their suitability as infill material. A detailed study on the evaluation of the nonlinear stress-strain characteristics of fly ash brick masonry is not available in literature. Therefore the next chapter contains details of the material characterisation of fly ash brick masonry under compression, shear and tension.

This Page is Intentionally Left Blank

Chapter 3
MATERIAL CHARACTERISATION OF BRICK MASONRY

CONTENTS

3.1 OVERVIEW

Masonry walls are generally used as load bearing walls, external claddings, partitions, etc., due to easy availability of their constituent materials and simple method of construction. Most of the times, masonry is constructed using locally available materials and due to this reason, their behavior in terms of strength and stiffness varies from region to region. Kaushik et al. (2007) reported average compressive strength of bricks of northern India to be varied from 16.1 MPa to 28.9 MPa, whereas, Sarangapani et al. (2005) reported that the compressive strength varied from 3.2 MPa to 11 MPa for the burnt clay bricks found in southern India. Not only the compressive strength, but also the stiffness of the bricks govern the behavior of structures especially during seismic excitations. Keeping this in view, significant research was dedicated during the last three decades to evaluate the non-linear behavior of clay brick masonry (Atkinson and Noland

1983; McNary and Abrams 1985, Drysdale et al. 1994; Sarangapani et al. 2005; Kaushik et al. 2007; Singhal and Rai 2014).

In the current scenario, availability of industrial by-products leads to the use of alternative building materials. Recently, bricks manufactured using fly ash are gaining importance due to their easy mode of manufacturing by utilizing the industrial by-product, fly ash, from thermal industries, and at the same time decreasing the emission of greenhouse gases produced during firing of brick (fly ash bricks are sun dried). Few studies, such as, Malaviya et al. (1999), Kumar (2002), Turgut (2010, 2012), Christy and Tensing (2011), and Christy et al. (2013), are available in the literature that discuss manufacturing of fly ash bricks and their physical properties. However, a detailed study to evaluate the nonlinear stress-strain characteristics of fly ash brick masonry is not available in literature. During seismic excitations, in-plane masonry wall is subjected to various failure modes (flexure and shear controlled) as reported in the literature (Magenes and Calvi 1997; Mahmood and Ingham 2011; Dizhur and Ingham 2013). A lot of research was carried out to evaluate shear strength of burnt clay brick masonry wallettes, and techniques were suggested to strengthen the shear deficient masonry wallettes (Ismail et al. 2011; Mahmood and Ingham 2011; Borri et al. 2011). The behaviour of fly ash brick masonry under diagonal compression is also required to be evaluated experimentally.

At the same time, one of the major objectives of the current study was to evaluate failure mechanism of frames infilled with fly ash brick masonry under lateral loads analytically. To model the non-linear behavior of the infill, stress-strain characteristics are required which are not available in the literature, and therefore, needs to be evaluated. The current study attempts at investigating the nonlinear stress-strain characteristics and failure mechanisms of fly ash brick masonry and its constituents (fly ash brick units and mortar) under compression, shear and tension. Based on the experimental results, simple relations were proposed to evaluate the modulus of elasticity of fly ash brick masonry prisms in terms of compressive strength of masonry prisms. Shear strength and shear modulus of masonry was evaluated by testing two different size masonry wallettes. A parametric study was also carried out to evaluate the effect of different strengths of brick units, mortar cubes and masonry prisms on shear strength of masonry wallettes. Nonlinear stress-strain characteristics of locally available burnt clay brick masonry under compression and shear were also evaluated in the current study, as the burnt clay bricks

were used as infill material in evaluating the methodologies to improve the shear behavior of infilled frames under lateral loading.

In the current study, locally available sun dried fly ash bricks were used. The binder-aggregate ratio used in the manufacturing of fly ash bricks was about 1:4. The raw materials used in fly ash bricks were PPC (Portland Pozzolona cement, 7%), hydrated lime (3%), fine aggregate consists of fly ash (60%) and stone dust (40%), and a small quantity of gypsum (1-2%). Fly ash bricks were manufactured by mixing the raw materials in pan mixer with required proportion of water to make it a homogenous mixture and then fed into a brick machine for the bricks to be moulded automatically. Later the bricks were transported to open area for drying under sun for 1-2 days and water cured for 15-21 days.

3.2 EXPERIMENTAL PROGRAM AND TEST SETUP

The properties of fly ash bricks include the physical (water absorption *WA* and initial rate of absorption *IRA*), and engineering characteristics (nonlinear compressive stress-strain curves and split tensile strength) were evaluated in the current study (Table 3.1). The properties of mortar include the compressive stress-strain characteristics of three different grades of 50 mm mortar cubes, and split tensile strength of mortar. Stack bonded masonry prisms constructed with three different grades of mortar were subjected to monotonic compressive loads to obtain the stress-strain properties of masonry prisms. Tension bond strength of fly ash brick masonry for the three grades of mortar was evaluated based on the new test method proposed by Khalaf (2005). The initial shear strength of masonry was determined by testing masonry triplets and masonry wallettes under diagonal compression to evaluate shear behaviour of fly ash brick masonry (Table 3.1). Average size of the fly ash brick unit was 230×110×75 mm and the average height of the five brick prism was about 420 mm, with thickness of mortar joint varying from 10-12 mm.

Uniaxial monotonic compressive (displacement controlled) loading was applied using servo controlled hydraulic actuator of 250 kN capacity (resolution 0.003 kN) with a stroke length of ±125 mm. Displacement rates were determined following the relevant Indian and ASTM standards. In order to record the non-linear behaviour of materials, displacement controlled tests were carried out at a very slow rate (arrived at by conducting some trial tests) ranging from about 0.11-0.16 mm/sec in case of compression

tests and about 0.05 mm/sec for masonry wallettes in case of diagonal compression tests. Brick units, mortar cubes and masonry prism specimens were instrumented with contact and non-contact extensometer to record the deformations during the tests (Fig. 3.1). Epsilon contact extensometers with varying gauge lengths (25 mm and 200 mm) depending on the specimen size were used in the current study. The displacement capacity of the contact extensometer was ±2.5 mm in case of 25 mm gauge length and ±12.5 mm for 200 mm gauge length. In addition, a laser extensometer was also used as a non-contact extensometer to record the deformations (Fig. 3.2).

Table 3.1. Types of tests for the determination of masonry properties

Unit Properties		
Physical Properties	Mechanical Properties of Bricks	Mechanical Properties of Mortar
Water absorption (*WA*) Initial rate of absorption (*IRA*)	Compressive strength and modulus of elasticity of bricks 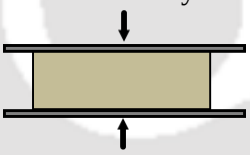	Compressive and modulus of elasticity strength of mortar cubes 
	Split Tensile Strength 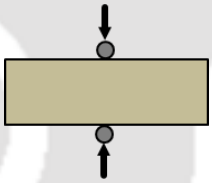	Flexural Strength 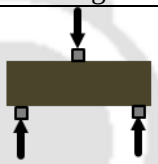
		Split Cylinder Strength 
Masonry Properties		
Compressive Strength and Modulus of Elasticity 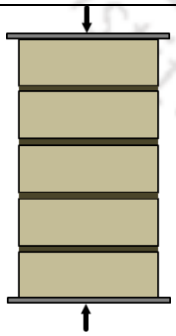 Masonry Prism	Tension Bond Strength 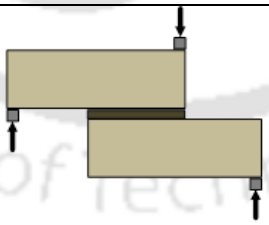 Z-shaped Specimen Initial Shear Strength 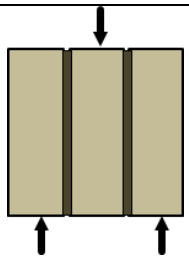 Masonry Triplet	Shear Strength and Shear Modulus Diagonal Compression Test 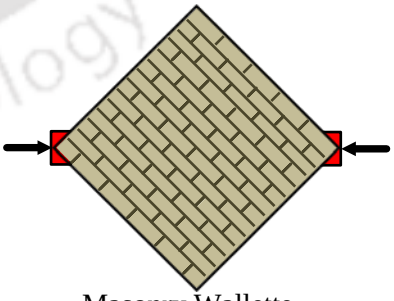 Masonry Wallette

The resolution of both the contact and non-contact extensometer was approximately 1 micron. As the thickness of the fly ash brick unit was 75 mm and that of mortar cubes was 50 mm, the gauge length of both contact and non-contact extensometers was adjusted to 25 mm (Fig. 3.2). The gauge length was maintained at 200 mm with a displacement capacity of ±12.5 mm in case of masonry prisms for both types of extensometers. Applied loads and deformations at various locations were recorded using a computer based data acquisition system.

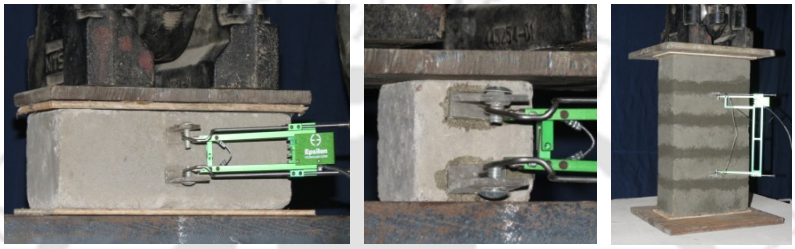

(a) (b) (c)

Fig. 3.1. Experimental setup of: (a) fly ash brick units; (b) mortar cubes; (c) masonry prisms.

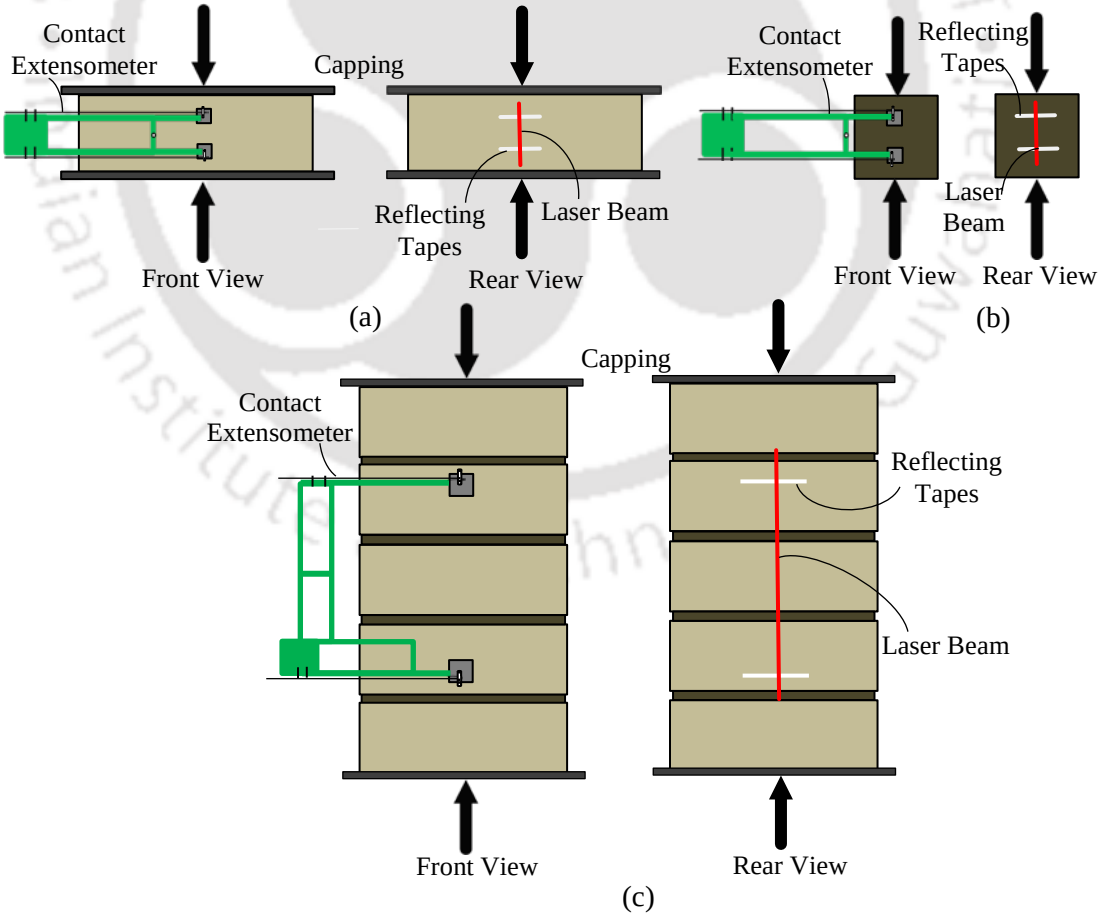

Fig. 3.2. Instrumentation of extensometers: (a) fly ash brick unit; (b) mortar cube; and (c) masonry prism.

Stress-strain curves reported in the study are arrived at by double averaging method, i.e., the averaged strain values are plotted on the abscissa against the predetermined stress values on the ordinate, which are also averaged across different specimens (Kaushik et al. 2007). The highest and lowest values in a set of data are considered as outliers and not used while averaging that particular set of data. The modulus of elasticity was calculated as the slope of the secant connecting 5%-33% of the maximum compressive strength of the specimens (MSJC 2013). A similar type of testing methodology was adopted in previous studies (Sarangapani et al. 2002; Gumaste et al. 2007; Kaushik et al. 2007; Singhal and Rai 2014) to evaluate the stress-strain characteristics and modulus of elasticity of masonry and its constituents.

3.3 PROPERTIES OF BRICK UNITS

Brick units are the major constituent materials of masonry. Physical and engineering properties form the basis in the selection of brick units and in-turn helps in determination of strength of brick masonry. Determination of *WA*, *IRA* and nonlinear compressive stress-strain curves, and split tensile strength of fly ash brick units are discussed in the following sections.

3.3.1 Determination of WA and IRA of Fly Ash Brick Units

The total *WA* of the bricks was determined in accordance with IS 3495 (BIS 1992b) and ASTM C67-13 (ASTM 2013a) standards. The *IRA* was measured by immersing the brick in 3-mm-deep water bath with an area of 300 in^2 for 1 minute in accordance with ASTM C67-13 (ASTM 2013a) standard. *WA* and *IRA* tests were carried out on ten brick specimens. The *WA* ranges from 17.5 to 19% with an average of 18.3% [with a coefficient of variation (COV) of 0.04]. This satisfies the current maximum limits of 20% specified in IS 12894 (BIS 2002a). The water absorption capacity of fly ash brick units is highly variable and location–dependent, as observed in several past studies where *WA* was found to vary from 12.5 to 37% (Malaviya et al. 1999; Christy and Tensing 2011; Kumar 2002). Turgut (2010) reported that *WA* varied from 13 to 19% when the amount of fly ash used in the bricks varied from 10 to 30%. The *IRA* for fly ash brick units used in the current study was found to vary from 3 to 7 $kg/m^2/min$ with an average of 5.1 $kg/m^2/min$ [COV of 0.19]. According to Drysdale et al. (1994), *IRA* values ranging from 0.25 to 1.5 $kg/m^2/min$ provide good bond strength. If *IRA* is higher than 1.5 $kg/m^2/min$,

brick units are highly absorptive and should be wetted prior to laying to achieve better bond strength. These *IRA* limits were derived based on the tests carried out on clay bricks. However, fly ash bricks are a newly emerging engineering material and are highly water-absorbant; the limits proposed for clay bricks may not be applicable to fly ash bricks.

3.3.2 Compressive Stress-Strain Characteristics of Fly ash Brick Units

The compressive strength of fly ash brick units (f_b) is determined by testing ten brick units under direct compression in accordance with ASTM C67-13 (ASTM 2013a) and IS 3495 (BIS 1992a). Fly ash brick units were tested by placing the specimen with frog-filled face towards the loading surface between two plywood sheets (soft capping) under uniaxial monotonic compressive loading at a displacement rate of 0.16 mm/s. The brick units were found to behave linearly up to approximately half of the ultimate failure load after which the behavior was highly non-linear. Fig. 3.3(a) shows the average stress-strain curve for all the brick units used in the study. The compressive strength of brick units was found to vary from 4.3 to 6.9 MPa with an average of 5.7 MPa [COV of 0.15] as shown in Table 3.2.

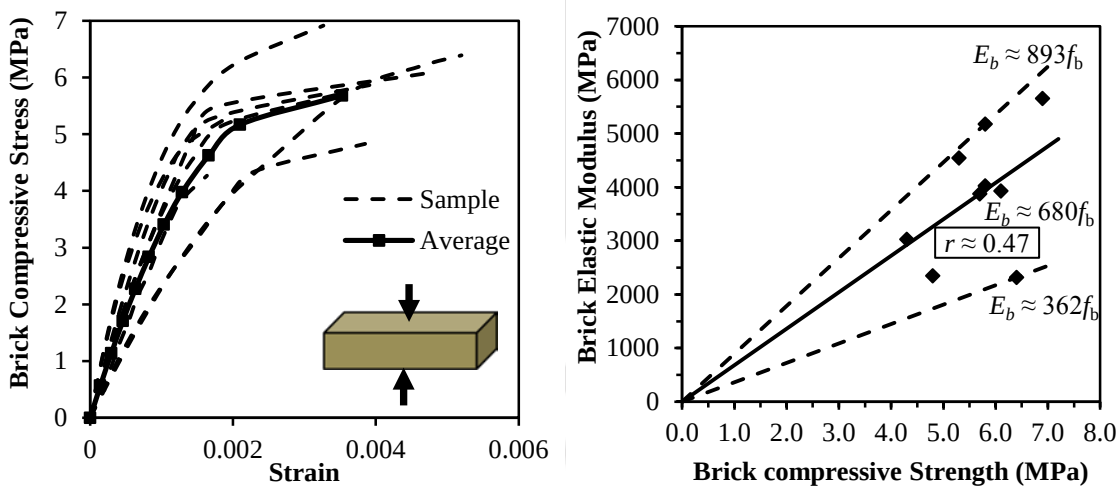

(a) (b)

Fig. 3.3. Compressive properties of fly ash brick units: (a) stress-strain curves; and (b) variation of modulus of elasticity.

In most of the specimens, the contact and non-contact extensometers were detached from the specimens at the maximum compressive strength level due to the crushing failure of brick units. A sudden decrease in load was observed after the peak load was reached; therefore, the strain corresponding to the peak load was considered the

failure strain. Failure strain was found to vary from 0.0016 to 0.0052 with an average of 0.0035 [COV of 0.35]. The compressive strength of the brick specimens was found to be in good agreement with studies carried out by Kumar (2002) and Malaviya et al. (1999) in which the compressive strength was reported to vary from 5 to 8 MPa.

Table 3.2. Properties of fly ash brick units and mortar cubes

Material	Compressive Strength (MPa)	Strain Corresponding to Compressive Strength	Failure Strain	Elastic Modulus (MPa)
Fly ash brick (10 specimens)	5.7 [0.15]*	0.0035 [0.35]	0.0035 [0.35]	3878 [0.32]
Strong Mortar (1:3) (10 specimens)	21.6 [0.07]	0.0085 [0.14]	0.0184 [0.28]	7591 [0.26]
Intermediate mortar (1:4) (10 specimens)	17.3 [0.16]	0.0061 [0.24]	0.0111 [0.11]	7403[0.28]
Weak mortar (1:6) (10 specimens)	6.9 [0.07]	0.0037 [0.47]	0.0055 [0.31]	4361 [0.31]

*Figures in [ ] brackets indicate coefficient of variation.

Fig. 3.3(b) shows the variation of modulus of elasticity (E_b) of the fly ash brick units with compressive strength. Modulus of elasticity was found to vary from 362 to 893 times the brick compressive strength with an average value of approximately 680 times the average compressive strength of the bricks. A *correlation coefficient* (r) of 0.47 was calculated from the experimentally determined elastic modulus and linearly predicted values from Eq. (3.1). The large variation in correlation is primarily due to the poor workmanship involved in the manufacture of the bricks and, in some cases, due to uneven contact between the bearing plates and surfaces of specimens.

$$E_b \approx 680\, f_b \quad \text{[COV 0.15]} \tag{3.1}$$

Although care was taken during the testing by providing soft capping between the specimens and the steel plates, the state of stress in squat specimens may still be influenced by the confining effects of the steel plates. Therefore, the reported compressive behavior may not truly represent the pure uniaxial behavior under compression. Clearly, the bricks used in the current study were very soft and weak compared to burnt clay brick units, as reported by Kaushik et al. (2007). During the compression test of the fly ash brick units, vertical splitting cracks originated at the edges of the bricks [Fig. 3.4(a)], and, subsequently, additional cracks developed at the center before the bricks failed in crushing [Fig. 3.4(b)].

The tensile strength of the fly ash bricks (f_{bt}) was determined using the split tensile test as per ASTM C1006-07 (ASTM 2007). The test involved applying a compressive line load by means of bearing rods, which produces a tensile stress along the height and split length of the masonry unit [Fig. 3.4(c)]. Tests were carried out on 10 specimens in flat position, and the splitting tensile strength of the fly ash brick units was found to be approximately 0.5 MPa [COV of 0.18], which is approximately 9% of the average compressive strength of the bricks.

(a) (b) (c)

Fig. 3.4. Failure mechanism in fly ash brick units: (a) initiation of vertical cracks along depth; (c) crushing of fly ash brick units under compression; and (c) split tensile failure.

3.4 Properties of Mortar Units

The compressive strength of mortar cubes (f_j) was determined using 50-mm cube specimens in accordance with ASTM C109/C109M-13 (ASTM 2013b) and IS 2250 (BIS 1981) as shown in Fig. 3.1(b). In the current study, three different grades of mortar were used: 1:3 (strong), 1:4 (intermediate), and 1:6 (weak), where the numbers indicate the ratio of cement to sand by volume. For each grade, tests were carried out on 10 specimens, and the water-cement ratio was maintained as 0.6-0.7 to obtain a workable mix. The surfaces of the mortar cubes and bearing plates of the hydraulic actuator were wiped clean to remove any loose material.

The mortar cube was placed centrally such that the load was applied to the opposite faces. Both the Indian and ASTM standards, recommend no capping material be used for mortar cubes while testing under uniaxial monotonic compressive loading, and this recommendation was followed in this study. The rate of displacement adopted for mortar cubes was about 0.11 mm/s. The stress-strain curves were found to behave linearly up to approximately one third of their maximum strength, followed by the nonlinear behavior [Fig. 3.5(a)]. The post peak reduction in the compressive strength for strong

mortar (1:3) was gentle in comparison with that of intermediate (1:4) and weak (1:6) mortar grades. This can also be verified from strains corresponding to maximum strength and failure load (Table 3.2). Strong mortar was found to be more deformable compared to intermediate and weak mortar. The difference in strain corresponding to failure load and f_j was about 0.0099 for strong mortar, and 0.0050 and 0.0018 for intermediate and weak mortar, respectively. The average value of the compressive strength of strong mortar was 21.6 MPa [COV of 0.07], whereas it was 17.3 MPa [COV of 0.16] and 6.9 MPa [COV of 0.07] for intermediate and weak mortar, respectively.

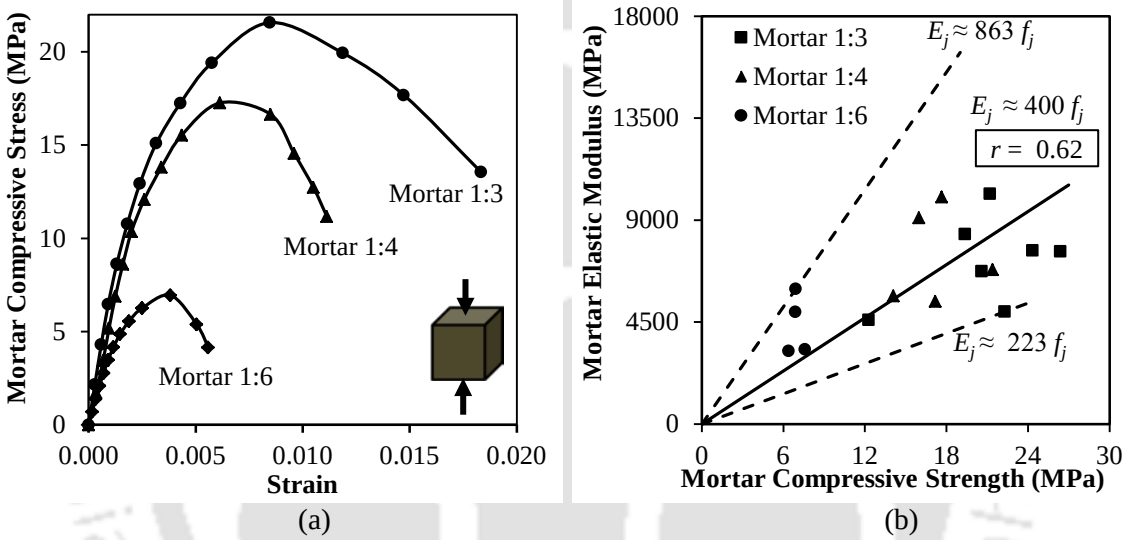

Fig. 3.5. Compressive properties of mortar cubes: (a) stress-strain curves; and (b) variation of modulus of elasticity.

The average modulus of elasticity of mortar cubes (E_j) was calculated as 7,591 MPa [COV of 0.26] for strong mortar, followed by 7,403 MPa [COV of 0.26] and 4,361 MPa [COV of 0.31] for intermediate and weak mortars, respectively. The E_j for similar mortar cubes tested by Kaushik et al. (2007) was found to be significantly less (3,750-545 MPa). This may be due to the different cement and aggregates used in the two studies. The E_j in this study varied from 223 to 863 times f_j, as shown in Fig. 3.5(b); the average E_j may be determined using Eq. (3.2), which gives a *correlation coefficient* (r) of 0.62.

$$E_j \approx 400\ f_j\ ;\ \text{[COV 0.4]} \qquad (3.2)$$

Failure in mortar cubes was found to initiate by vertical cracks along the loading direction [Fig. 3.6(a)], leading to formation of the pyramidal shape [Fig. 3.6(b)]. Due to

non-uniform loading, bending was observed in few specimens and cracks formed in the perpendicular direction of loading [Fig. 3.6(c)]. The tensile strength of mortar (f_{jt}) was determined by split cylinder tests in accordance with IS 5816 (BIS 1999) and ASTM C496/C496M (ASTM 2011). The test was carried out by applying compressive line load on its side by bearing rods along the diametrical plane which produces tensile stress along the diameter and split the cylinder along the loaded plane [Fig. 3.6(d)]. The tensile strength of 1:4 mortar cylinders was found to be about 1.2 MPa [0.1] which is approximately 7% of the average compressive strength of mortar.

(a) (b) (c) (d)

Fig. 3.6. Failure mechanism in mortar cubes and cylinder: (b) initiation of vertical cracks; (c) pyramidal shape failure; (d) tension break failure of mortar cubes; and (e) split tensile failure of mortar cylinder.

3.5 Behavior of Masonry in Compression

Masonry is a non-homogenous, anisotropic material composed of two different materials with distinctive elastic properties. Generally, masonry is composed of stiffer and stronger bricks and relatively weaker and softer mortar. It is a well-understood concept that under compressive loads on masonry prisms, lateral strain in mortar tends to be greater than that of bricks due to its lower elastic modulus and higher Poisson's ratio. However, lateral deformation in mortar is inhibited by the stiffer bricks due to friction and bond at the brick-mortar interface [Fig. 3.7(b)]. Therefore, brick and mortar are subjected tri-axial stress state in which brick is under uniaxial compression and biaxial tension, and mortar is under tri-axial compression.

Few studies observed contradictory behavior (Sarangapani et al. 2005, Gumaste et al. 2007) in which modulus of elasticity of brick was found to be significantly less than that of mortar. Therefore, under compressive loads on masonry prisms, tri-axial compression develops in brick along with biaxial tension and axial compression in mortar joints Fig. 3.7(c). In the current study, the average f_b and E_b of fly ash brick units was

found to be 5.7 MPa and 3878 MPa, respectively, whereas the average f_j and E_j of mortar cubes ranged from 20.6 to 6.9 MPa and 7,591 to 4,361 MPa, respectively, for different grades of mortar. Clearly, the fly ash bricks were significantly weaker and softer than the mortar used. To further understand the effect of such bricks on compressive load behavior of masonry, the stress-strain characteristics of fly ash brick masonry were determined by testing thirty stack bonded five-brick-high prisms under monotonic compressive loading.

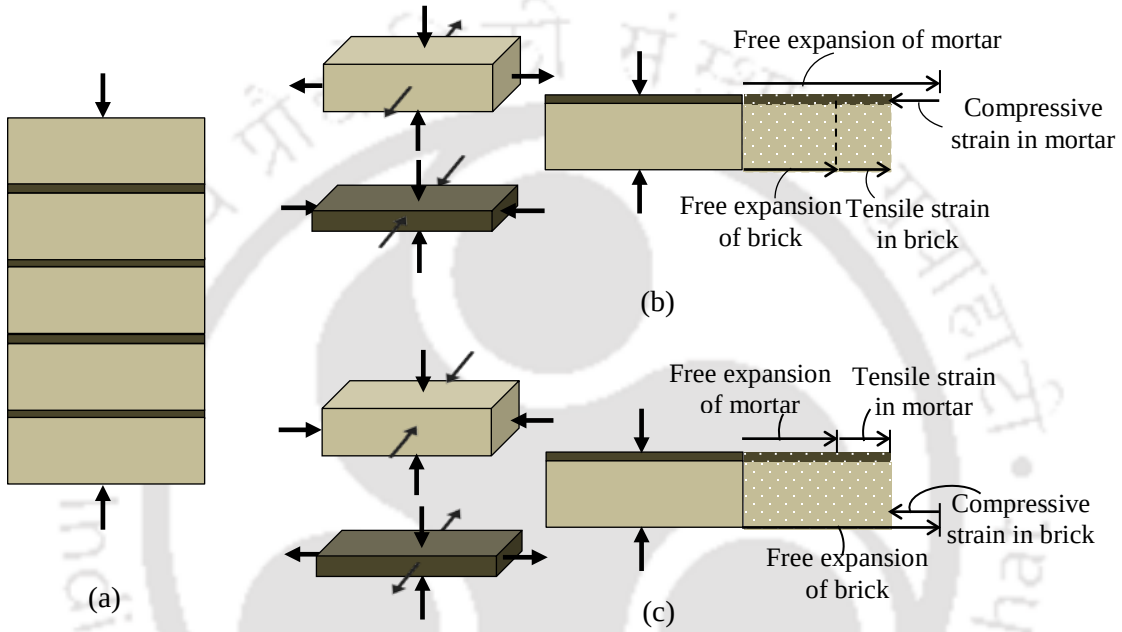

Fig. 3.7. (a) Masonry prism under compression; (b) state of stress for *stiff brick-soft mortar* combination; and (c) state of stress for *stiff mortar-soft brick* combination.

3.5.1 Compressive Behavior of Fly Ash Brick Masonry Prisms

Masonry prisms were constructed using three mortar grades (strong, intermediate, and weak). The compressive strength of masonry increases with the bond strength between bricks and mortar, as it is also a function of water-cement ratio in mortar; the ratio was required to be maintained as 0.6-0.7 to obtain a workable mix. The compressive strength of the fly ash brick masonry prisms was determined after 28 days of curing in accordance with ASTM C1314-12 (ASTM 2012) and IS 1905 (BIS 1987) as shown in Fig. 3.1(c). Masonry prisms were tested with their faces cleaned for any loose material and placed between two plywood sheets (soft capping). The specimen was placed centrally between the loading plates and tested under monotonic uniaxial compressive loading at a displacement rate of 0.16 mm/s.

Fig. 3.8 shows the stress-strain curves obtained for masonry prisms for three mortar grades. The stress-strain curves were found to behave linearly until approximately one-third of the prism strength followed by nonlinear behavior. Table 3.3 summarizes the average compressive strength and corresponding strain, failure strain and modulus of elasticity of the prisms. The average prism strength (f'_m) for strong, intermediate, and weak mortar grades was found to be 4.6 MPa [COV of 0.22], 3.9 MPa [COV of 0.13], and 3.1 MPa [COV of 0.13], respectively.

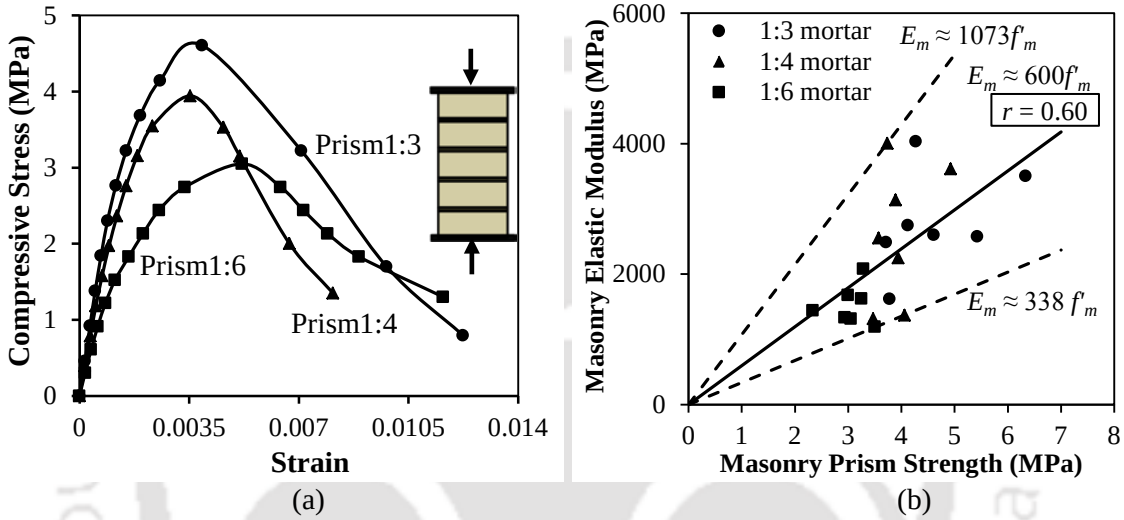

Fig. 3.8. Compressive stress-strain curves for fly ash masonry prisms.

Table 3.3. Test results for fly ash masonry prisms

Mortar Type used in Prisms	Compressive Strength, f'_m (MPa)	Strain Corresponding to f'_m	Failure Strain	Masonry Elastic Modulus, E_m (MPa)
Strong Mortar (1:3) (10 specimens)	4.6 [0.22]	0.0039 [0.12]	0.0122 [0.5]	2830 [0.29]
Intermediate Mortar (1:4) (10 specimens)	3.9 [0.13]	0.0036 [0.29]	0.0081 [0.5]	2667 [0.42]
Weak Mortar (1:6) (10 specimens)	3.1 [0.13]	0.0052 [0.33]	0.0116 [0.37]	1457 [0.14]

The strain in the masonry prisms corresponding to prism strength for the strong (0.0039; COV of 0.12) and intermediate (0.0036; COV of 0.29) mortar cases was found to be almost the same, whereas it was 0.0052 [COV of 0.33] for weak mortar. The failure strain was reported at which the masonry prisms were found to damage irreparably during testing. This was found to correspond to approximately 80% drop in prism strength for

strong mortar case (0.0122; COV of 0.5), 60% drop for the intermediate mortar case (0.0081; COV of 0.5), and 50% for the weak mortar case (0.0116; COV of 0.37). Although the strength degradation was lowest for the masonry prisms with weak mortar, it showed significant deformability compared to that showed by the intermediate and strong masonry prisms.

The average elastic modulus (E_m) of prisms with strong mortar (2830 MPa; COV of 0.29) and with intermediate mortar (2667 MPa; COV of 0.42) was found to be similar. However, E_m was comparatively quite low for prisms with weaker mortar (1457 MPa; COV of 0.14). This is analogous to the elastic modulus observed for three mortar grades. The elastic modulus of masonry prisms was found to vary from 338 to 1,073 times as shown in Fig. 3.8(b). A reasonably good prediction of E_m can be made using Eq. (3.3), which gives a COV of 0.23 and a *correlation coefficient* (r) of 0.60 between the experimentally determined and linearly predicted values.

$$E_m \approx 600\ f'_m\ ;\ [\text{COV } 0.23] \tag{3.3}$$

Failure in masonry prisms with strong mortar started with the formation of vertical splitting cracks, followed by crushing of bricks [Fig. 3.9(a)]. Diagonal shear cracking and vertical splitting [Figs. 3.9(b and c)] are the predominant failure modes observed in the case of prisms with intermediate and weak mortar.

(a) (b) (c)

Fig. 3.9. Failure mechanisms of fly ash brick masonry prisms: (a) vertical splitting cracks (1:3 strong mortar); (b) vertical splitting and crushing of bricks (1:4 intermediate mortar); and (c) initiation of vertical splitting and crushing of mortar joint (1:6 weak mortar).

Bond failure was not observed during the tests, and both brick and mortar joint were intact until the end of the test for strong and intermediate mortar prisms, whereas, crushing of the joint and joint separation was observed for the weak mortar prism [Fig. 3.7(c)]. This observation is analogous to a past study (Sarangapani et al. 2005), where it was reported that the failure of brick was postponed due to the induced lateral compression, which will be higher if the bond strength is high. It was also reported that the bond strength increases with the strength of mortar.

Fig. 3.10 compares the stress-strain curves obtained for the masonry prisms, brick units, and mortar cubes. The compressive strength of brick units was found to be significantly less than that of all three grades of mortar. The behavior of masonry prisms in terms of strength, stiffness and failure strain falls below that of the mortar and brick units. Therefore, the go-between compressive behavior of masonry prisms may not be applicable for all cases, especially for low-strength bricks. The nature of stresses in masonry depends on the bond strength and elastic properties of both brick units and mortar. Fig. 3.10 shows that the mortar cubes are stiffer than the brick units, thus representing stiff mortar-soft brick combination.

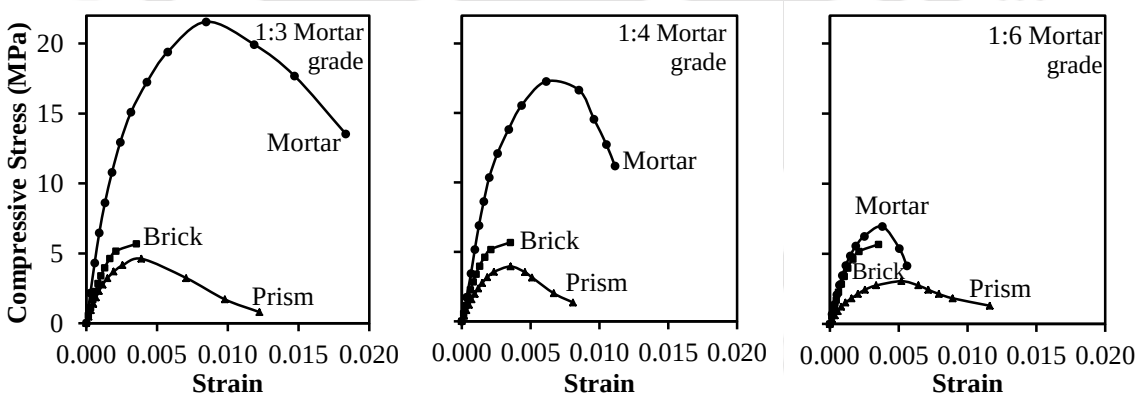

Fig. 3.10. Comparison of stress-strain curves obtained for brick units, mortar cubes and masonry prisms for different grades of mortar: (a) strong (1:3); (b) intermediate (1:4); and (c) weak (1:6).

Therefore, as previously discussed, bricks are subjected to tri-axial compression in which horizontal confining compression is the result of stiffer mortar pulling it inwards for strain compatibility, and mortar joints are under bilateral tension and uniaxial compression. The prism strength of masonry was found to increase with mortar strength;

but it was always less than the compressive strength of the brick units, even when strong mortar was used. Further, when mortar strength increased by approximately 213% from a weak to a strong grade, the corresponding increase in prism strength was only approximately 48%. This shows that the prism strength of masonry depends more on the compressive strength of bricks (even though the bricks are softer and weaker than mortar).

Fig. 3.11 shows the comparison of the nonlinear stress-strain characteristics of fly ash brick masonry prisms with that obtained for burnt clay brick masonry prisms from previous study (Kaushik et al. 2007). The compressive strength and stiffness of fly ash brick masonry prisms was found to be significantly lower compared to that of burnt clay brick masonry prisms (Fig. 3.11). The average compressive strength of clay brick masonry prisms constructed with strong and weak mortar was found to be about 1.6 times (7.5 MPa) and 1.3 times more (4.1 MPa), than that of the corresponding fly ash brick masonry prisms. Modulus of elasticity of strong and weak burnt clay brick masonry prisms was found to be about 1.5 times (4200 MPa) and 1.6 times (2300 MPa) that of fly ash brick prisms. But the post-peak reduction in strength in case of fly ash brick prisms was more gradual due to their soft nature.

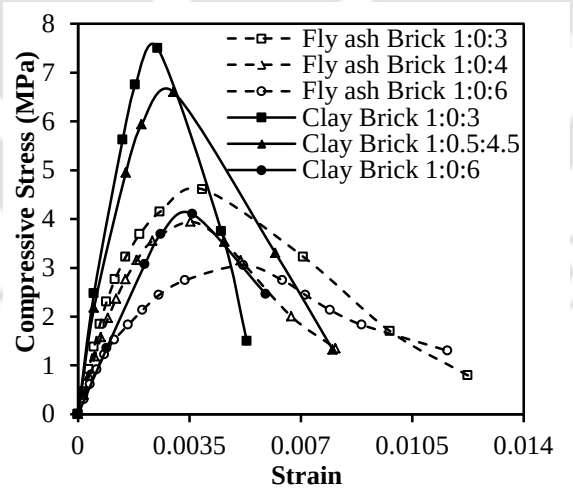

Fig. 3.11. Comparison of nonlinear stress-strain curves of masonry prisms.

The strain corresponding to the prism strength was about 0.0039 and 0.0052 for strong and weak fly ash brick masonry prisms, whereas, the corresponding strain was about 0.0025 and 0.0036 for strong and weak burnt clay brick prisms, respectively. Failure strain in case of fly ash brick prisms, considered as the strain at which the

specimen was found to be damaged irreparably during testing, was approximately 0.0122 (for 80% drop in strength) for strong mortar prisms, and 0.0116 (for 50% drop in strength) for weak mortar. Kaushik et al. (2007) reported that the failure strain for burnt clay brick prisms was about 0.0053 (for 80% drop in strength) for strong mortar prisms, and 0.0059 (for 50% drop in strength) for weak mortar prisms. Clearly, the fly ash brick masonry prisms exhibited significantly more deformable behavior (failure strain was about twice) when compared to burnt clay brick masonry, highlighting the gradual dropdown in strength after peak.

3.5.2 Analytical Estimation of Masonry Prism Strength

Masonry prism strength has been estimated analytically by researchers in the past by relating it with brick and mortar compressive strength. A number of empirical relations (Dayaratnam 1987; CEN 2005a; Bennet et al. 1997; MSJC 2013; Kaushik et al. 2007) have been proposed for clay brick masonry in which generally stiffer and stronger bricks were used in comparison with mortar. Few past studies (Gumaste et al. 2007; Christy et al. 2013) were dedicated to the evaluation of the masonry prism strength for soft brick–stiff mortar combination. Unconstrained linear regression analysis was carried out using the least-square fit method on the results obtained in the current experimental study, and Eq. (3.4) was proposed to estimate masonry prism strength for soft brick–stiff mortar combination. In the regression analysis, the average compressive strength of fly ash bricks (constant value of 5.7 MPa), and the average compressive strength of three grades of mortar were used to estimate the masonry prism strength. Eq. (3.4) gives *coefficient of determination* (R^2) of 0.93 and *standard error of estimate* (σ) of 0.67 MPa.

$$f'_m = 1.34\, f_b^{0.1}\, f_j^{0.33};\ [R^2 = 0.93;\ \sigma = 0.67 \text{ MPa}] \qquad (3.4)$$

To validate Eq. (3.4), a comparative study was carried out in which experimentally obtained f'_m values were predicted using Eq. (3.4) and using empirical equations available in literature. As shown in Table 3.4, prism strength of masonry can be very well predicted using Eq. (3.4) for low strength bricks ($f_b \leq 7.2$ MPa), and high strength mortar ($f_j \leq 22$ MPa), whose $E_j/E_b < 2.5$. The E_j/E_b ratio is emphasized because the prism strength of masonry depends not only on the strength but also on the stiffness of brick and mortar joints, especially when weaker and softer bricks are used in masonry.

Table 3.4. Comparison of experimental prism strengths with their predicted values

Past Studies	Experimental Values				Predicted f'_m using Different Empirical Relations						
	f_b	f_j	f'_m	E_j/E_b	C[1]	G	K	D	E	B	M
	(MPa)				(MPa)						
Sarangapani et al. (2005)	3.2	7.3	0.6	11.9	2.9 {383}[+]	1.1 {83}	2.1 {250}	1.3 {117}	2.3 {283}	1.0 {67}	3.4 {467}
Christy et al. (2013)	3.3	12.7	1.9	3.5	3.5 {84}	1.3 {46}	2.6 {37}	1.8 {6}	2.7 {42}	1.0 {90}	3.4 {79}
Christy et al. (2013)	3.3	8.5	1.7	5.0	3.1 {82}	1.2 {42}	2.2 {29}	1.5 {13}	2.4 {41}	1.0 {70}	3.4 {100}
Christy et al. (2013)	3.3	5.5	1.7	11.7	2.6 {53}	1.1 {55}	1.9 {12}	1.2 {42}	2.1 {24}	1.0 {70}	3.4 {100}
Sarangapani et al. (2005)	4.3	7.3	1.1	12.3	3.0 {173}	1.5 {36}	2.4 {118}	1.5 {36}	2.8 {155}	1.3 {18}	3.6 {227}
Gumaste et al. (2007)	5.7	0.9	1.7	0.2	1.5 {13}	1.4 {21}	1.4 {21}	0.6 {183}	1.8 {6}	1.7 {0}	3.9 {129}
Current study	5.7	6.9	3.1	1.1	3.0 {3}	1.9 {63}	2.7 {15}	1.7 {82}	3.3 {6}	1.7 {82}	3.9 {26}
Gumaste et al. (2007)	5.7	1.8	1.6	1.5	1.9 {19}	1.6 {0}	1.8 {13}	0.9 {78}	2.2 {38}	1.7 {6}	3.9 {144}
Current study	5.7	17.3	3.9	1.9	4.1 {5}	2.1 {86}	3.7 {5}	2.7 {44}	4.4 {13}	1.7 {129}	3.9 {0}
Current study	5.7	21.6	4.6	2.0	4.4 {5}	2.2 {109}	4 {15}	3.1 {48}	4.7 {2}	1.7 {171}	3.9 {18}
Gumaste et al. (2007)	5.7	6.6	1.3	8.8	3.0 {140}	1.8 {44}	2.7 {116}	1.7 {36}	3.3 {154}	1.7 {36}	3.9 {212}
Keshava et al. (2010)	5.8	8.0	1.6	3.6	3.2 {100}	1.9 {19}	2.9 {81}	1.9 {19}	3.5 {119}	1.7 {6}	3.9 {144}
Christy et al. (2013)	7.2	12.7	2.7	1.7	3.8 {41}	2.5 {8}	3.7 {37}	2.6 {4}	4.7 {74}	2.2 {23}	4.2 {56}
Christy et al. (2013)	7.2	8.5	3.0	2.4	3.3 {10}	2.3 {30}	3.3 {10}	2.2 {36}	4.2 {40}	2.2 {36}	4.2 {40}
Keshava et al. (2010)	10.6	8.0	3.9	1.0	3.4 {15}	3.2 {22}	3.9 {0}	2.5 {56}	5.4 {38}	3.2 {22}	4.9 {26}
Kaushik et al. (2007)	20.8	15.2	6.6	0.5	4.5 {47}	6.3 {5}	6.7 {2}	4.9 {35}	10.4 {58}	6.2 {6}	6.9 {5}
Kaushik et al. (2007)	20.8	20.6	7.5	0.6	4.9 {53}	6.6 {14}	7.3 {3}	5.7 {32}	11.4 {52}	6.2 {21}	6.9 {9}
Gumaste et al. (2007)	23.0	12.2	10.0	2.1	4.2 {138}	6.7 {49}	6.5 {54}	4.6 {117}	10.5 {5}	6.9 {45}	7.4 {35}
Gumaste et al. (2007)	23.0	6.6	6.7	2.5	3.4 {97}	6.2 {8}	5.4 {24}	3.4 {97}	8.7 {30}	6.9 {3}	7.4 {10}

[1]C: Current study $f'_m = 1.34\, f_b^{0.1} f_j^{0.33}$; G: Gumaste et al. (2007) $f'_m = 0.317\, f_b^{0.8665} f_j^{0.134}$; K: Kaushik et al. (2007) $f'_m = 0.63\, f_b^{0.49} f_j^{0.32}$; D: Dayaratnam (1987) $f'_m = 0.275\, f_b^{0.5} f_j^{0.5}$; E: Eurocode 6 (CEN 2005a) $f'_m = 0.55\, f_b^{0.7} f_j^{0.3}$; B: Bennett et al. (1997) $f'_m = 0.3\, f_b$; M: MSJC (2013) $f'_m = A\,(400 + B\, f_b)$ (psi) and $A = 1.0$ for inspected masonry and $B = 0.2$.

Note: [+]Figures in {} brackets indicate the percent error between experimental and predicted values.

The error between the predicted and the experimental values was found to be higher if the proposed equation was used for higher E_j/E_b ratios. The equation proposed

by Kaushik et al. (2007) and Eurocode 6 (CEN 2005a) was found to be useful in predicting masonry prism strength up to 20 MPa for an E_j/E_b ratio ≤ 5. Dayaratnam's (1987) equation predicts the prism strength fairly good if f_b and f_j are nearly the same irrespective of the E_j/E_b ratio, as the equation gives equal weight to f_b and f_j. Gumaste et al. (2007) considered bricks with a compressive strength of 5.7 MPa and 23 MPa and different combinations of mortar (0.86-12.21 MPa) with an E_j/E_b ratio ≤ 8.8; their prediction of f'_m was reasonably good up to 23 MPa with different E_j/E_b ratios.

The Bennet et al. (1997) and MSJC (2013) equations were found to be not suitable to predict the masonry strength for lower strength bricks as the equations were developed principally considering only the compressive strength of brick. The f'_m values obtained experimentally by Keshava et al. (2010) matched quite well with their analytical prediction for E_j/E_b=1.0, even though the prisms were constructed with similar strength brick units (f_b = 10.6 MPa) and mortar (f_j = 8.0 MPa); this highlights the importance of considering E_j/E_b ratio in predicting prism strength of soft brick–stiff mortar combination. The error between the experimentally obtained f'_m values and analytically predicted f'_m values was large in the case of the study conducted by Sarangapani et al. (2005) study due to high E_j/E_b ratios (11.9 and 12.3) encountered in the study.

3.6 TENSION BOND STRENGTH

The flexural bond (tension) strength of masonry was determined by following the test procedure proposed by Khalaf (2005). The specimens were constructed with two bricks bonded together in two courses by 10-12 mm thick mortar joint in staggered arrangement (Z-shaped configuration) similar to construction of masonry wall [Fig. 3.12(a)]. Seven specimens for each (1:3; 1:4; 1:6) mortar grade were constructed and cured for 28 days. The specimens were tested to failure by bending under three point loading. The bond strength derivation was based on the assumption that the brick-mortar bond remains intact upto the point of failure, when hinge occurs at the right side of the mortar joint under the applied load [Fig. 3.12(b)]. Khalaf (2005) assumed two types of bond stress distributions at the brick-mortar interface under bending: linear stress distribution and parabolic distribution. Parabolic stress distribution found to be more realistic and reported that it

provided a conservative estimate of the bond strength as compared to the linear stress distribution [Fig. 3.12(c)].

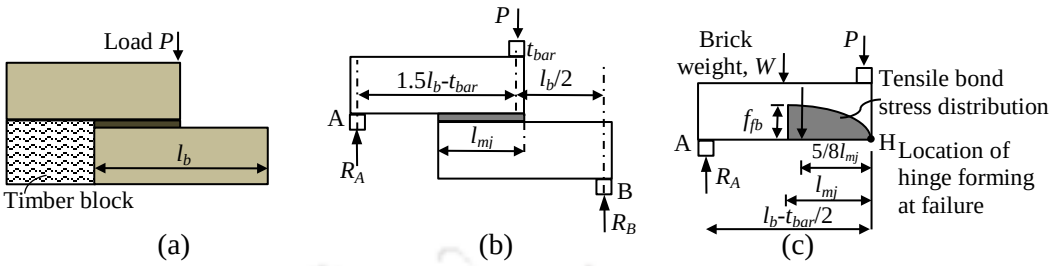

Fig. 3.12. Typical experimental set up of Z-shaped specimen: (a) construction; (b) free body diagram of brick forces; and (c) free body diagram of top brick and parabolic distribution of stress.

The flexural bond strength (f_{fb}) considering parabolic distribution is determined using Eq. (3.5)

$$f_{fb} = \frac{\left(0.5l_b^2 - l_b t_{bar} + 0.5t_{bar}^2\right)P_f + \left(0.75l_b^2 - 1.25l_b + 0.5t_{bar}^2\right)W}{\left(0.42l_{mj}^2 w_b\right)\left(1.5l_b - t_{bar}\right)} \quad (3.5)$$

where l_b, w_b, and l_{mj} represent the length of the brick, width of the brick and length of the mortar joints, respectively; P_f represent the failure load; W is the weight of the brick unit; and t_{bar} represent the thickness of the bar. The tension bond strength of the fly ash brick with 1:4 mortar (0.07 MPa; COV of 0.37) found to be slightly higher when compared to fly ash bricks with 1:4 mortar (0.05 MPa; COV of 0.27) and 1:6 mortar grade (0.04 MPa; COV of 0.3). It is inferred that the flexural bond strength increased with increase in strength of mortar, but the strength was found to be smaller when compared to tension bond strength of clay bricks (0.18 MPa; COV of 0.14) tested in the previous study (Singhal and Rai 2014). Low tension bond strength of fly ash brick masonry may be due to the smooth surfaces of the fly ash brick units which might have led to weak interface bond. Khalaf (2005) also reported that the tension bond strength of the calcium silicate bricks tested for different grades mortar found to be smaller (0.1-0.14 MPa) than the clay bricks (0.43-0.35 MPa) due to the smoothness of the surfaces of the calcium silicate bricks. The tension bond strength values may be used with caution as the data found to be scattering (large values of coefficient of variation).

The failure of Z-shaped specimens observed failure both on the upper face of the joint as well on the lower face of the joint [Figs. 3.13(a and b)], whereas, Khalaf (2005)

and Singhal and Rai (2014) reported most of the specimens observed failure on the upper face of the joint due to the lower face of the mortar-bed joint was in more favourable condition for developing good bond due to the presence of frog and also the position of the lower brick during laying and curing than the upper brick. Additionally, gravitational forces tend to assist the flow of mortar into both small pores and larger pores on the lower face, while the same forces act against the mortar on the top brick bottom face. In the current study, fly ash brick was highly absorptive and both the top and bottom surfaces of the bricks were smooth which might have led to the failure of joint at the upper and lower face.

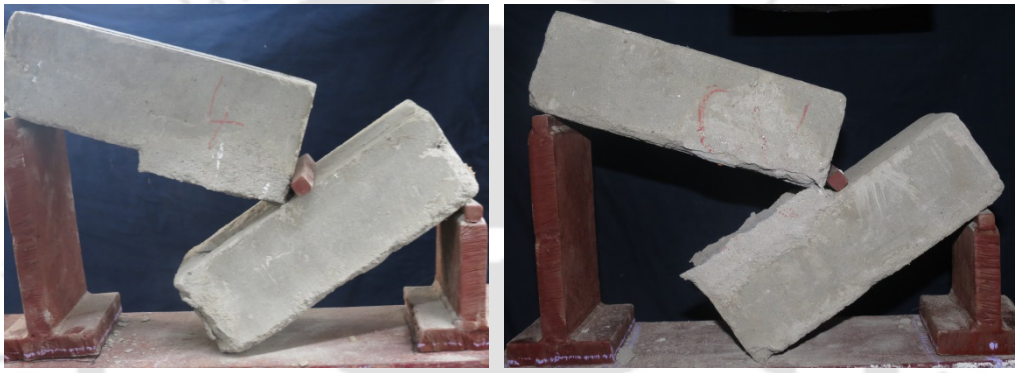

(a) (b)

Fig. 3.13. Tension bond failure in Z-shaped specimens at: (a) top brick and mortar joint; and (b) mortar joint and bottom brick.

3.7 BEHAVIOR OF MASONRY IN SHEAR

Shear strength is required for the design of masonry panels when they are subjected to lateral loads. The stress state in masonry is more complex and general failure criteria are required to evaluate the strength of masonry (Crisafulli 1997). The failure mechanism of infill walls may fail in out-of-plane or in-plane. Of the two failure mechanisms out-plane was critical and many a times is inhibited by addition of wall diaphragm connections. The in-plane failure mode depends on wall aspect ratio, wall boundary, the size and geometry of wall penetrations, the magnitude of axial compressive force and the wall constituent material properties (Magenes and Calvi 1997). During seismic excitations, the in-plane masonry wall is subjected to various failure modes (flexural-controlled or shear-controlled). The flexural controlled failure mode was characterized by rocking with associated masonry crushing, while the shear failure mode of wall components was identified by two mechanisms: horizontal bed joint sliding and diagonal shear (tension)

cracking (Crisafulli 1997, Magenes and Calvi 1997, Dizhur and Ingham 2013). Sliding and rocking failure modes exhibit considerable ductility, whereas, diagonal shear is a brittle failure mode where crack initiates at peak lateral force followed by rapid degradation of strength. In the current study, both the initial shear strength (bed joint sliding strength) and the diagonal tension strength were evaluated and discussed in detail in the following sections.

3.7.1 Initial Shear Strength of Fly Ash Brick Masonry

Eurocode 6 (CEN 2005a), suggests determining the initial shear strength of masonry from horizontal bed joint shear strength following Eurocode 1052 (CEN 2002). Generally, the bed joint sliding was observed due to the formation of tensile horizontal crack in the bed joints and it is calculated as the amount of force required for the movement of masonry unit. Masonry triplets were constructed for three grades of mortar and cured for 28 days by applying a pre-compressive stress of 3.3×10^{-3} MPa, so as to achieve better bond strength. The specimens were placed in the testing apparatus and were loaded to failure without lateral pre-compressive loads [Figs. 3.14(a and b)].

Fig. 3.14. Initial bed joint shear test setup (a and b); and failure mechanism in fly ash brick masonry triplet (c and d).

The initial shear strength f_{is} of masonry triplets was determined using Eq. (3.6) as

$$f_{is} = \frac{P_{is}}{2A_i} \tag{3.6}$$

where P_{is} is the peak shear strength reached during the test and A_i is the cross-sectional area of the specimen parallel to the bed joints. A total of twenty one specimens were

tested for the three mortar grades. The shear strength was found to be about 0.15 MPa [COV of 0.32], 0.04 MPa [COV of 0.03] and 0.03 MPa [COV of 0.36] for fly ash bricks with 1:3, 1:4 and 1:6 mortar grades, respectively. It was clearly observed that the initial shear strength was dependant on the grade of mortar and found to be increasing with increase in strength of mortar. The strength of the fly ash brick masonry triplets found to be lower compared to the burnt clay brick triplets tested in the previous study by Singhal and Rai 2014 (0.43 MPa; COV of 0.23) and Alecci et al. 2013 (0.531MPa). The reason for the fly ash brick triplets to observe low strength even for high strength mortar may be due to the smooth surfaces of fly ash bricks which might have decreased the bond strength of mortar. Figs. 3.14(c and d) shows the typical failure mechanism observed in masonry triplets where it was observed that failure was observed on either side of the central brick and bed joint interface.

3.7.2 Shear Strength of Fly Ash Brick Masonry

Eurocode 8 (CEN 2005b) suggests determining the shear strength from diagonal compression tests following ASTM E519/E519M-10 (ASTM 2010). Different sizes of specimens have been employed in the past studies to determine the shear strength of masonry wallettes following the specifications of ASTM (2010) and RILEM (1994) codes. According to ASTM (2010), specified size of masonry wallette is 1,200×1,200 mm; however, the code does not address the effect of specimen size on the evaluation of the shear strength of masonry wallettes due to a lack of experimental data. According to RILEM (1994), the finished specimen should be as square as possible and should be a minimum of four brick units wide. A summary of different diagonal compression tests has been reported by Mahmood and Ingham (2011).

In order to evaluate the effect of specimen size on diagonal tensile strength of masonry, two different size wallettes were tested in the current study. Twenty running-bond single-wythe masonry wallettes of sizes 1,200×1,200×110 mm (full-scale: ten specimens) and 600×600×110 mm (half scale: ten specimens) were constructed using 1:4 (cement:sand) mortar with a water-cement ratio of 0.7. In the current study, displacement-controlled loading was applied along the diagonal in the horizontal direction slightly different from the standard test set up (ASTM 2010). Steel loading shoes designed as per ASTM (2010) were fabricated to apply the displacement-controlled loading on the

specimens. One of the loading shoes was fixed to the loading end, and the other to a rigid reaction frame. Masonry wallettes were placed between the loading shoes and instrumented with two LVDTS to measure the deformation (shortening ΔH and elongation ΔV) along both the diagonals. The gauge length (g) of LVDTs was maintained at 430 mm and 1,000 mm for 600 mm and 1,200 mm size specimens, respectively (Fig 3.15). The specimen was supported vertically at the base during installation between the loading shoes. The specimen was not supported at the bottom during the testing by providing a small gap between the specimen and the bottom support in order to avoid possible freefall of the specimen after failure. The tests were carried out in the horizontal direction due to laboratory constraints, especially for full-scale specimens.

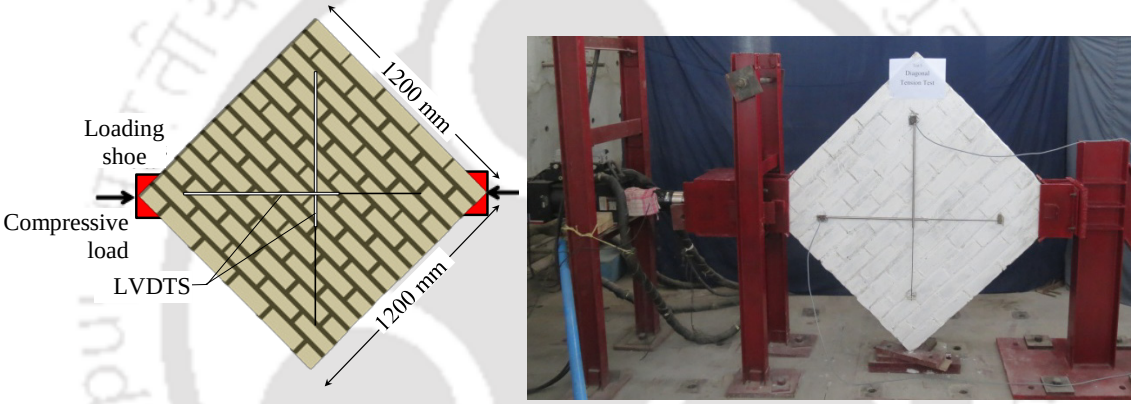

Fig. 3.15. Diagonal compression test up for full-scale masonry wallettes (1200×1200 mm).

Two different loading configurations were mainly adopted in the literature: one involving the rotation of masonry wallette by 45^o and loading applied in the vertical direction along the diagonal (ASTM 2010), and the other by applying the load at 45^o to the horizontal for in-situ and masonry wallettes with weak bond strength (Mahmood and Ingham 2011; Ismail et al. 2011; Dizhur and Ingham 2013). In the current study, the steel shoes designed for both full-scale panels (1,200 mm wide) were used for the scaled panels (600 mm wide). However, care was taken in the case of the scaled specimens to reduce the contact area through which the compressive loads were applied on the specimens through which the compressive loads were applied on the specimens. Steel plates 70 mm long (one-eighth the length of the specimen) were used as packing material inside the steel shoes to decrease the length of the bearing area for the application of compressive load at the two opposite corners. In the case of masonry wallettes, the displacement rate was adjusted to 0.05 mm/s to capture the nonlinear behavior. Various

interpretations (ASTM 2010; RILEM 1994; Brignola et al. 2009) are available in the literature to evaluate the masonry shear strength from diagonal compression tests. The standard interpretation of the test assumes that the state of stress at the center of the panel is of pure shear and that the shear stress is equal to the maximum principal tensile strength under diagonal compression.

Following the standard interpretation, ASTM (2010) proposed Eqs. (3.7) and (3.8) to determine the shear strength (f_v') and shear strain (γ), respectively, for masonry wallettes. On the other hand RILEM (1994) assumes non-uniform stress state at the center of the square panel under diagonal compression, and the masonry shear strength was equated to ultimate principal tensile stress (Eq. 3.9). Similarly, using finite element analysis Brignola et al. (2009) proved the stress state at the center of panel was not pure shear and proposed similar equation (Eq. 3.9), with constant being replaced by a coefficient which is dependent on masonry typology.

$$f_v' = \frac{0.707P}{A_n} \tag{3.7}$$

$$\gamma = \frac{\Delta V + \Delta H}{g} \tag{3.8}$$

$$f_v' = \frac{0.5P}{A_n} \tag{3.9}$$

where A_n is the net area calculated as the average of the width and height of the specimen times its thickness. Fig. 3.16(a) shows the average shear stress-shear strain curves obtained for full-scale and half-scale masonry wallettes. As given in Table 3.5, the maximum shear stress using Eq. (3.7) carried by full-scale specimen was 0.14 MPa [COV of 0.44], whereas it was 0.46 MPa [COV of 0.2] for half-scale specimen corresponding to a shear (diagonal) force of 27 kN and 43 kN, respectively. The shear modulus of masonry wallettes (G_m) is calculated as the slope of the secant connecting 5-33% of maximum shear stress. The average shear modulus of full-scale masonry wallettes was computed as 728 MPa [COV of 0.07], whereas it was 2,943 MPa [COV of 0.29] for half-scale wallettes. The shear modulus was found to vary from 3,348 to 9,639 times the average shear stress [Fig. 3.16(b)]. Based on the experimental results, Eq. (3.10) is suggested to estimate average shear modulus for masonry wallettes.

$$G_m = 6226\, f_v' \quad [r = 0.83;\ \text{COV} = 0.49] \tag{3.10}$$

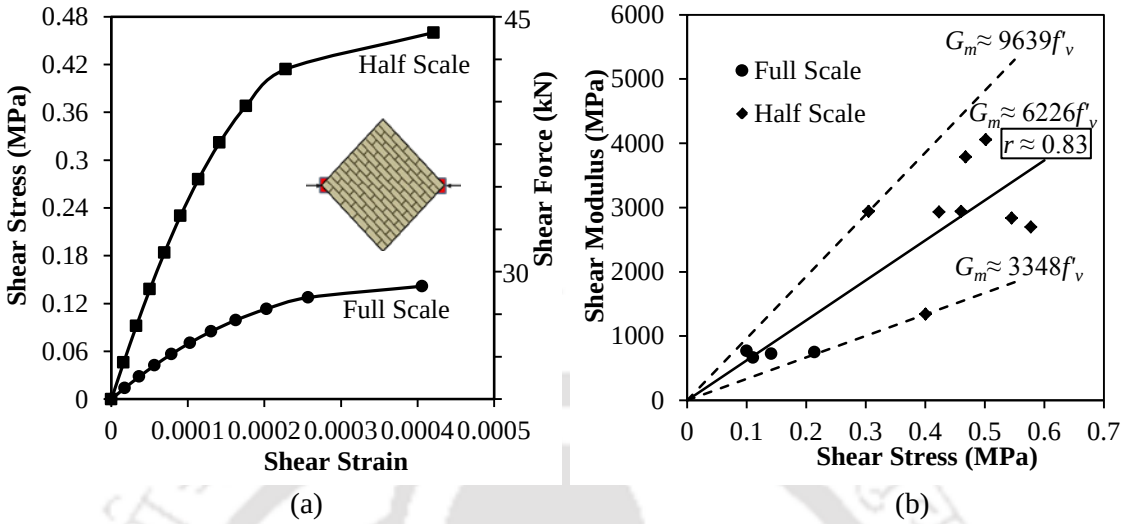

(a) (b)

Fig. 3.16. Shear stress-shear strain curves for full-scale and half-scale masonry wallettes.

Table 3.5. Test results for masonry wallets (diagonal tension tests)

Specimen	Size (mm)	Shear Force, P (kN)	Shear Strength, f_v' (MPa)	Shear Strain Corresponding to f_v'	Shear Modulus, G_m (MPa)
Full Scale	1200×1200×110	27 [0.44]	0.14 [0.44]	0.00041 [0.41]	728 [0.07]
Half Scale	600×600×110	43 [0.2]	0.46 [0.2]	0.00042 [0.27]	2943 [0.3]

It has been a common practice in past literature (CEN 2005a; Magenes et al. 2010; ASCE 2013) to relate elastic modulus with shear modulus; an attempt was made in the current study to find a relation between the two moduli based on the experimental results for fly ash brick masonry. According to Eurocode 6 (CEN 2005a) and ASCE 41 (2013), G_m may be computed as 40% of the elastic modulus (E_m) of masonry. In the current study, the average shear modulus for full-scale wallettes (728 MPa) was found to be approximately 27% of the elastic modulus for intermediate mortar fly ash masonry prisms (Table 3.2). Therefore, it appears that the ratio G_m/E_m reduces significantly when weaker and softer bricks (compared to mortar) are used in masonry.

The primary failure mechanisms observed in the masonry wallettes were diagonal shear cracking, bed joint sliding, and a combination of both. Both type of failure mechanisms were brittle in nature; as soon as the cracks initiated the peak strength of the specimens reached and the specimens broke suddenly into two pieces. In diagonal shear failure, cracking was initiated along the loading direction passing through bed joints, head

joints, and bricks [Figs. 3.17(a and b)]. This may be attributed to the principal tensile stress, which exceeds the tensile strength of brick and mortar joints. Mohammed and Hughes (2011), Dizhur and Ingham (2013), and Alecci et al. (2013) reported similar type of failure mechanisms in which the cracks initiated at the centre of the panel and propagate along the diagonal length of the wall.

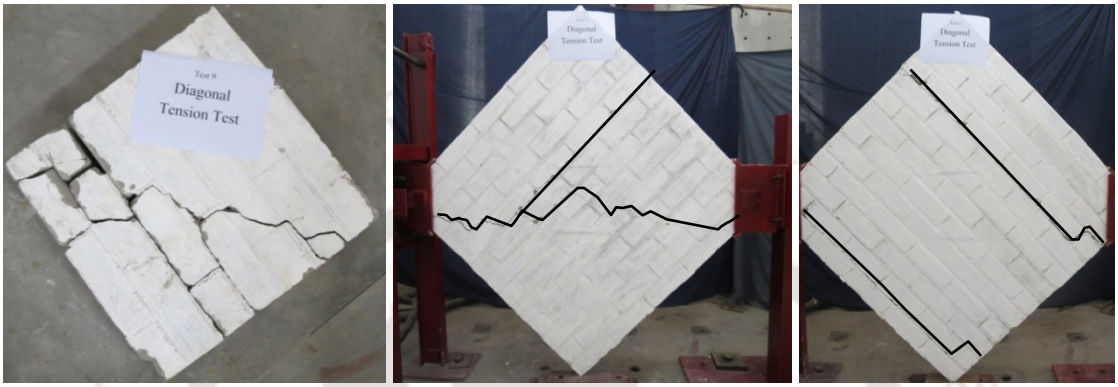

(a) (b) (c)

Fig. 3.17. Failure mechanisms in masonry wallettes: (a) diagonal shear cracking and sliding of bed joint (half-scale specimen); (b) diagonal shear cracking and sliding of bed joint (full-scale specimen); and (c) sliding of bed joint (full-scale specimen).

Bed joint sliding, shown in Fig. 3.17(c), which is also sometimes referred to as shear slip failure, was observed in the case of full-scale specimens in those cases where the bond between bricks and mortar joints was weaker compared to the tensile strength of bricks. El-Dakhakhni et al. (2006) and Dehghani et al. (2015) reported similar types of failure mechanisms for unretrofitted masonry assemblages. In the current study, it was observed that the bed joint sliding cracks initiated away from the mid height of the panel [Fig. 3.17(c)]. This may be due to the non-uniform loading from the inclined confining plates of the loading shoe that might have exerted load along the off-diagonal bed joint leading to failure of the first bed joint of the masonry wallette.

A parametric study was carried out to evaluate the influence of the compressive strength of brick, mortar, and masonry prism on shear strength of masonry wallettes (Table 3.6). It was observed that fairly high strength bricks (f_b >17 MPa) and low strength mortars (1.1 MPa < f_j < 13.9 MPa) were used in past studies. However, low strength bricks (f_b = 5.7 MPa) and high strength mortar (f_j = 17.3 MPa) were used in the current study. In past studies, masonry prism strength (f'_m) varied from 3.9 to 23.0 MPa– the

lowest being in the current study–whereas the shear strength (f_v') varied from 0.09 to 1.15 MPa. Table 3.6 provides a moderately fair correlation ($r \approx 0.53$) between f_b and f_v' and no significant correlation ($r \approx -0.13$) between f_j and f_v'. However, it has been reported in the literature that diagonal tensile strength (shear) increases with mortar strength for both single leaf masonry panels (Alecci et al. 2013), and double leaf masonry wallettes (Dizhur and Ingham 2013). It was also observed that f_m' and f_v' are well correlated ($r \approx 0.64$). Therefore, shear strength (f_v') appears to be more directly related to brick compressive strength (f_b) rather than mortar strength (f_j).

Table 3.6. Relationship between compressive and shear strength of masonry

Past Studies	Masonry Properties			Details of Tests Conducted on Masonry						
	Material	Size of Brick Unit	Size of Wallette	f_b	f_j	f_m'	f_v'	$\frac{f_v'}{f_b}$	$\frac{f_v'}{f_j}$	$\frac{f_v'}{f_m'}$
		Length×Width×Thickness (mm)		(MPa)						
Marshall et al. (2000)	*CMU*	406×203×203	1220×1220×203	-	9.1	16.3	1.15	-	0.126	0.070
Alecci et al. (2013)	*C*	250×120×55	1200×1200×120	17.0	2.8	-	0.58	0.034	0.211	-
Singhal & Rai (2014)	*C*	229×110×72	1200×1200×110	21.9	8.5	5.3	0.43	0.020	0.051	0.081
Current Study	*FA*	230×110×75	1200×1200×110	5.7	17.3	3.9	0.14	0.025	0.008	0.036
Bosiljkov (2006)	*C*	250×120×65	800×800×120	17.4	13.9	15.0	0.42	0.024	0.030	0.028
Bosiljkov (2006)	*C*	250×120×65	800×800×120	17.4	9.5	12.5	0.38	0.022	0.040	0.030
Bosiljkov (2006)	*C*	250×120×65	800×800×120	17.4	1.1	6.9	0.10	0.006	0.088	0.014
Borri et al. (2011)	*SB*	250×125×55	515×510×125	21.0	10.8	-	0.54	0.026	0.050	-
Borri et al. (2011)	*SB*	250×125×55	515×510×125	21.0	2.6	-	0.09	0.004	0.037	-
M & H (2011) [a]	*C*	215×103×65	940×905×103	29.2	3.9	9.2	0.91	0.031	0.232	0.099
M & H (2011)	*C*	97×46×29	423×404×46	30.6	4.0	11.0	0.76	0.025	0.192	0.069
M & H (2011)	*C*	54×26×16	236×223×26	41.9	4.5	23.0	0.96	0.023	0.215	0.042
M & H (2011)	*C*	36×17×11	157×153×17	47.4	4.1	20.3	0.63	0.013	0.155	0.031
Dehghani et al. (2015)	*C*	225×105×40	450×450×105	47.5	6.3	18.5	0.74	0.016	0.117	0.040
Dehghani et al. (2015)	*C*	225×105×40	450×450×105	47.5	6.3	18.5	0.63	0.013	0.100	0.034
Singhal & Rai (2015)	*C*	120×61×38	600×600×61	40.0	4.5	5.2	0.20	0.005	0.044	0.038
Current Study	*FA*	230×110×75	600×600×110	5.7	17.3	3.9	0.46	0.081	0.027	0.118
Correlation coefficient (r) between f_b, f_j, and f_m' with f_v'				0.53	-0.13	0.64				

Note: *CMU*-Concrete Masonry Unit; *C*-Clay; *FA*-Fly ash; *SB*-Sand blasted.

[a]Represents Mohammed and Hughes (2011) study.

In addition, the relation between other parameters, e.g., tensile strength of brick units and mortar and their bond strength needs to be established with shear strength. No limits or correction factors have been reported in the literature for shear strength assessment based on slenderness (h/t) ratio of wallettes. Interestingly, a large variation was observed across the experimental results reported in past studies. Shear strength normalized with respect to f_b varies from 0.004 to 0.034, except in the case of the current

study for half scale specimens, where f_v'/f_b was 0.081 because of use of weaker bricks. Similarly, f_v'/f_j varies from 0.008 to 0.23, the lowest value observed in the current study, where higher-strength mortar was used. The value of f_v'/f_m' was found to vary from 0.014 to 0.128. Clearly, it is difficult to develop a generalized model for shear strength estimation of masonry.

3.8 CHEMICAL COMPOSITION OF FLY ASH AND BURNT CLAY BRICKS

From the results of compressive behavior of fly ash brick units and fly ash masonry prisms, it was observed that fly ash brick units exhibit very weak and soft nature in comparison with burnt clay brick units. To find out the exact nature of fly ash brick units in comparison with the burnt clay brick units, mineralogical and chemical composition analysis was carried out. Three different techniques were employed in the current study to determine the chemical and mineralogical composition of burnt clay and fly ash bricks. Initially, major elements present in the brick samples were identified and semi quantified using X-Ray Fluorescence (XRF) analysis. Subsequently, the microstructure that shows the spatial distribution of specific chemical elements on a sub-micron scale and chemical spectra were identified using Scanning Electron Microscope associated with Energy Dispersive Spectrometer (SEM-EDS). Finally the compounds formed in the samples were ascertained and identified using powder X-Ray Diffraction *(*XRD) technique.

Clay used in brick production is a mixture of plastic (phyllo-silicates like montmorillonite, vermuculite, chlorite, illite, and kaolinite), and non-plastic minerals (feldspars, quartz, and carbonates), and few impurities usually made of iron oxy-hydroxides. When molded clay is fired at high temperatures (850-1000 ^{o}C), quartz remains constant, feldspars evolves to sanidine, and decomposition of phyllosilicates leads to the formation of hematite (Cultrone et al. 2005). From XRF analysis (Table 3.7), it was observed that the burnt clay brick sample consists of large amount of quartz (SiO_2), alumina (Al_2O_3), and ferric oxide (Fe_2O_3), and small percentage of manganese oxide (MgO), magnesium oxide (MnO), calcium oxide (CaO), sodium oxide (Na_2O), and titanium oxide (TiO_2). When fired at higher temperatures, calcite present in the calcium rich clays decomposes into calcium oxide by releasing carbon dioxide leading to more porous structure (Cultrone et al. 2005). As the percentage of calcium oxide in burnt clay

bricks was very low, it can be ascertained that calcium poor clays were used in brick production and the same was confirmed from SEM image and EDS spectrum (Fig. 3.18). From the SEM image [Fig. 3.18(a)] it was observed that the layers of burnt clay brick were bonded together very strongly making the clay body impervious and representing very high mechanical resistance.

Table 3.7. Mineralogical composition of bricks using *XRF* (in % weight)

Sample	SiO_2	Al_2O_3	Fe_2O_3	MnO	MgO	CaO	Na_2O	K_2O	TiO_2	P_2O_5
Clay Brick	66.68	15.34	7.08	0.131	0.28	1.04	2.23	3.84	1.05	0.146
Fly ash Brick	53.98	14.51	3.85	0.058	0.81	12.34	2.75	1.5	1.3	0.121

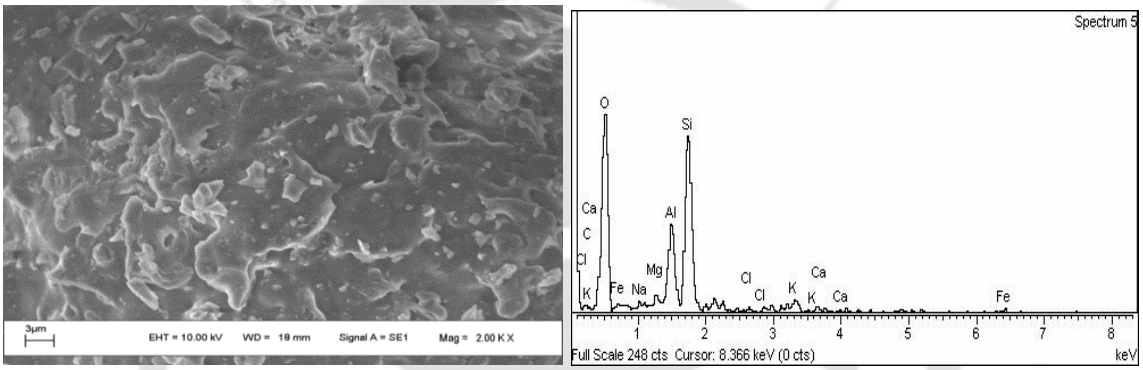

(a) (b)

Fig. 3.18. Microstructure of burnt clay brick: (a) *SEM* image; and (b) *EDS* spectrum.

XRD analysis results (Fig. 3.19) show that hematite was present in the microstructure of burnt clay bricks; therefore, it appears that the clay bricks must have been subjected to high firing temperature (> 850 ^{o}C). Quartz, feldspar, and hematite are the major minerals identified from XRD patterns, and absence of calcite confirmed that calcium poor clays were employed in the brick manufacture. More than 60% of silica [Table 3.7; Fig. 3.18(b)] was present in the burnt clay brick sample, which proves that burnt clay bricks to be of good quality (Rai and Dhanapal 2013).Finally it can be established that due to the presence of high amount of silica, use of calcite poor clay (less porosity), and presence of hematite (molded clay fired at higher temperature) are the primary reasons for significantly better compressive behavior of burnt clay bricks.

On the other hand, from XRF analysis of fly ash brick sample, it was observed that major constituents of fly ash bricks were quartz, alumina, and calcium oxide, with minor percentages of oxides of iron, sodium, potassium and magnesium (Table 3.7). The

glassy (siliceous) materials of fly ash and alumina react with the calcium hydroxides to form the cementitious CSH (calcium silicate hydrate) gel and CAH (calcium alumino hydrate) (Turgut 2012). It is a well-established philosophy (Mehta and Monteiro 2006) that volume of solids in a completely hydrated cement paste contains about 50 to 60% of CSH gel, 20 to 25% of CH (calcium hydroxide), 15 to 20% CAH and minor percentage of unhydrated residue. Therefore, it can be ascertained that CSH, CAH and CH are the main compounds responsible for imparting compressive strength to fly ash bricks.

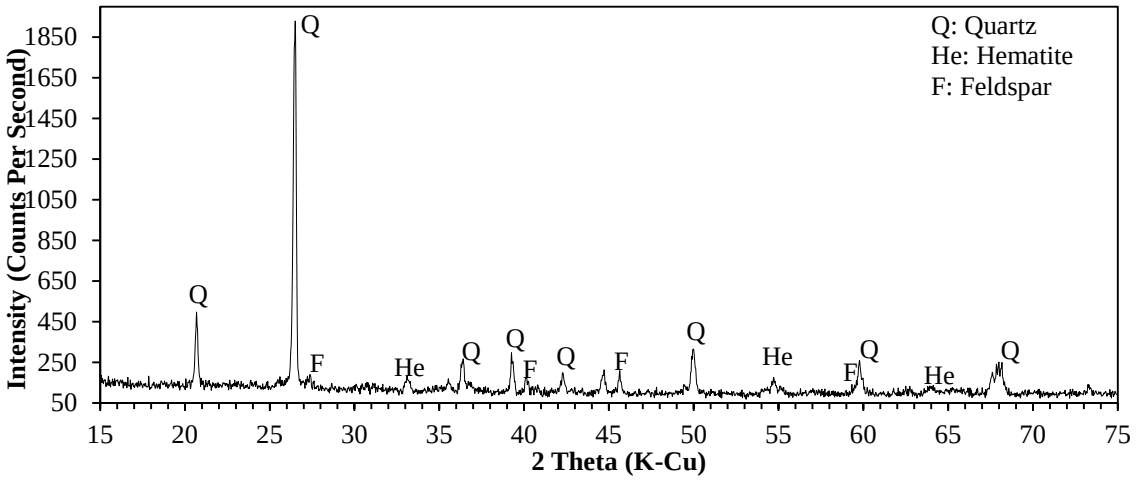

Fig. 3.19. *XRD* pattern of burnt clay brick sample.

The elemental composition of fly ash bricks obtained from XRF analysis was confirmed from SEM-EDS analysis. From the SEM image [Fig. 3.20(a)], it was observed that large amount of unreacted glassy siliceous compounds were present in fly ash brick sample, highlighting incomplete pozzolanic reaction that resulted in porous matrix (and hence softer bricks). The compounds formed in hydrated fly ash brick sample were confirmed using XRD technique as shown in Fig. 3.21, where it was observed that the width of the peaks of CSH, CAH, CASH (Calcium alumino silicate hydrate) were very small signifying very low percentages of hydrated compounds. Presence of CH (Portlandite) shows incomplete pozzolanic reaction which lead to porous matrix and is responsible for lower strength of fly ash bricks.

The incomplete pozzolanic reaction may be attributed to the low reactivity of fly ash. Chemical activation is frequently recommended for increasing the reactivity of fly ash due to advantages in terms of low cost, attaining high strength in early as well later stages, and simple production process (Aimin and Sarkar 1991; Shi 1998; and Lee et al.

2003). It is carried out by adding activators, such as, sulphate activators (gypsum $CaSO_4.2H_2O$, sodium sulphate Na_2SO_4, calcium chloride $CaCl_2$), and alkali activators (sodium hydroxide NaOH, calcium hydroxide $Ca(OH)_2$) to fly ash. Therefore, chemical activation technique may be used during manufacturing of bricks in order to assist in completing the pozzolanic reaction, and hence to improve the compressive behavior of fly ash bricks, in case it is required.

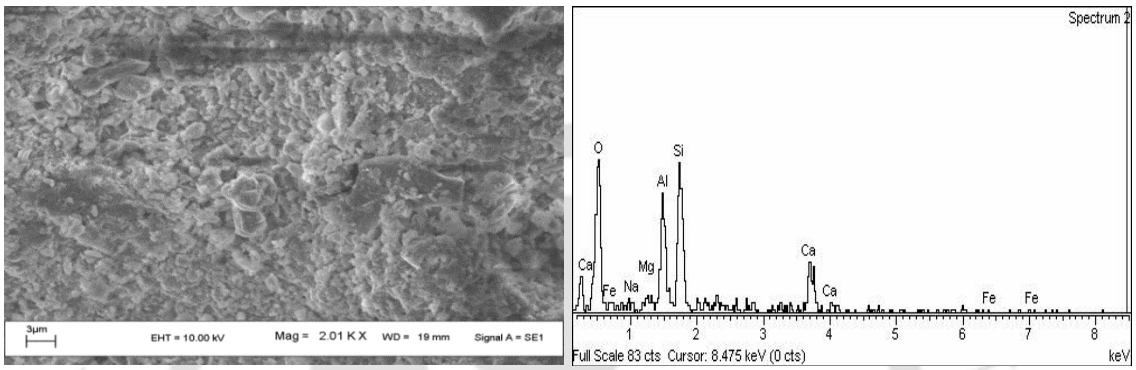

(a) (b)

Fig. 3.20. Microstructure of fly ash brick: (a) *SEM* image; and (b) *EDS* spectrum.

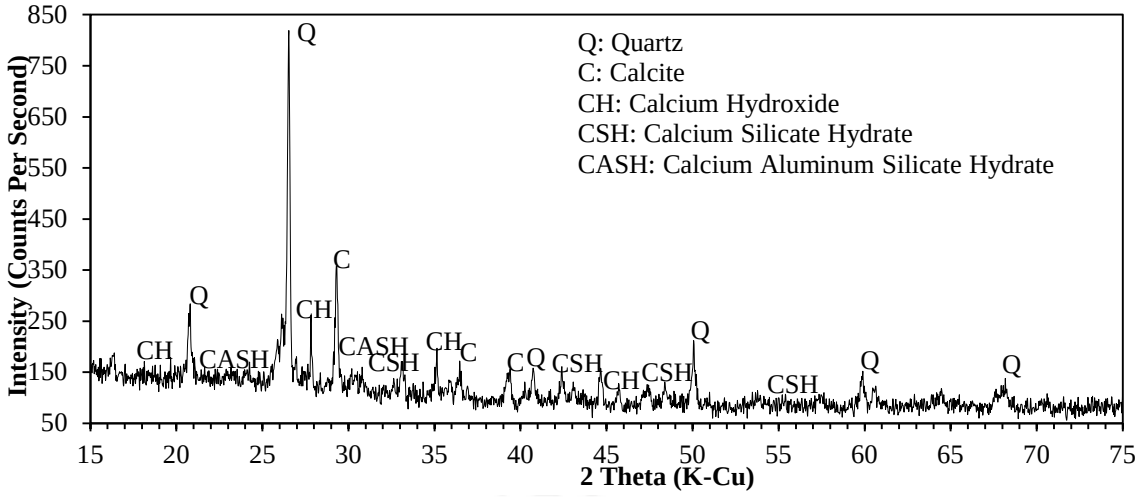

Fig. 3.21. *XRD* pattern of fly ash brick sample.

3.9 DETERMINATION OF PROPERTIES OF CLAY BRICK MASONRY

To demonstrate the influence of strength and stiffness of masonry on the behavior of infilled frames, a methodology in chapter 6 was designed by considering masonry of two different grades: class-I burnt clay brick masonry with 1:4 mortar grade and class-III burnt clay brick masonry with 1:8 mortar grade. The two different grades of masonry

represent high and low strength with relatively stiff and soft masonry, respectively. The main reason behind choosing low strength and soft masonry was to ensure weak and ductile mechanism which may induce large deformation mechanism and energy dissipation for ordinary unreinforced masonry walls. In order to understand the non-linear behavior initially material characterisation was carried out by testing clay brick masonry and its constituents under compression and shear.

The tests include *WA* (ASTM 2013a, BIS 1992b), *IRA* (ASTM 2013a), nonlinear compressive stress-strain behavior (ASTM 2013a, BIS 1992a), split-tensile strength (ASTM 2007) of class-I and class-III burnt clay bricks; nonlinear compressive stress-strain (ASTM 2013b, BIS 1981) and tensile characteristics (ASTM 2011, BIS 1999) of 1:4 and 1:8 mortar. The nonlinear compressive stress-strain characteristics of 1:4 and 1:8 burnt clay brick masonry was determined by testing five brick high stack bonded masonry prisms (BIS 1987, ASTM 2012). To determine the shear strength, diagonal compression tests (ASTM 2010) were carried out on 1200×1200×110 mm masonry wallettes constructed with their respective 1:4 and 1:8 mortar grades. Servo controlled hydraulic actuator was used to apply the displacement controlled monotonic loading on all specimens. The specimens were instrumented with epsilon contact extensometer to capture the strain accumulation under compressive loading. The summary of results of class-I and class-III burnt brick masonry along with their constituent properties are given in Table 3.8 and shown in Fig 3.22.

Table 3.8. Properties of burnt clay brick masonry

Material	Compressive Strength (MPa)	Strain Corresponding to Compressive Strength	Failure Strain	Elastic Modulus (MPa)
		Clay Brick-Class I		
Brick unit	19.2 [0.20]	0.0163 [0.06]	0.0163 [0.06]	2061 [0.26]
Mortar (1:4)	17.3 [0.16]	0.0061 [0.24]	0.0111 [0.11]	7403 [0.28]
Prism (1:4)	4.4 [0.37]	0.0047 [0.19]	0.0088 [0.22]	1744 [0.18]
		Clay Brick-Class III		
Brick unit	6.3 [0.28]	0.0231 [0.49]	0.0231 [0.49]	516 [0.26]
Mortar (1:8)	3.2 [0.19]	0.0052	0.0052	3795 [0.27]
Prism (1:8)	1.5 [0.29]	0.0045 [0.29]	0.0123 [0.45]	608 [0.36]

*Figures in [ ] brackets indicate coefficient of variation.

The total water absorption (*WA*) and initial rate of absorption (*IRA*) was determined by carrying out tests on ten brick units for each test. *WA* was found to be approximately 20% [COV of 0.038] and 25% [0.02] for class-I and class-III burnt clay

bricks, respectively, and *IRA* was found to be 3 kg/m^2/min [COV of 0.11] and 2 kg/m^2/min [COV of 0.23] for class-I and class-III bricks, respectively. Based on *IRA* limits (0.25 to 1.5 kg/m^2/min), it can be understood that both class-I and class-III burnt clay bricks needs to be wetted before laying to achieve better bond strength.

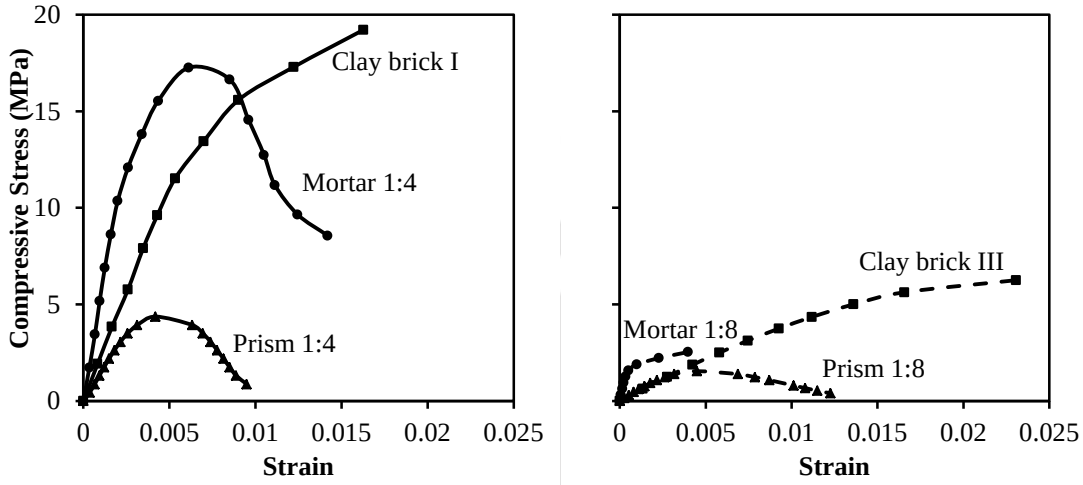

Fig. 3.22. Comparison of stress-strain curves obtained for burnt clay brick units, mortar cubes and masonry prisms obtained for different grades of mortar: (a) 1:4 mortar grade; and (b) 1:8 mortar grade.

Fig. 3.22 shows the average compressive stress-strain curves for class-I and class-III burnt clay brick units. The bricks observed linear behavior until one third of their maximum strength, later the behavior found to be nonlinear. The average compressive strength of class-I and class-III burnt clay brick units was found to be approximately 19.2 MPa [COV of 0.20] and 6.3 MPa [COV of 0.28], respectively. The average strain corresponding to maximum strength in case of class-III bricks was found to be slightly higher when compared to class-I bricks.

Modulus of elasticity calculated as the secant connecting 5% to 33% of maximum strength was found to be approximately 2,061 MPa [COV of 0.26] and 516 MPa [COV of 0.26] for class-I and class-III bricks, respectively. From the modulus of elasticity it is inferred that the class-III burnt clay bricks were softer when compared to class-I burnt clay bricks. The same can be interpreted from the failure mechanism observed in brick units where full crushing of class-III brick units under compressive loading was observed and brittle failure with popping sound was witnessed in case of class-I burnt clay bricks

(Fig. 3.23).The split tensile strength of class-I and class-III clay brick units was found to be approximately 1.03 MPa [COV of 0.37] and 0.44 MPa [COV of 0.29], respectively. Sudden split failure of class-I burnt clay brick was observed, whereas, the failure of class-III burnt clay bricks was significantly gradual compared to class-I burnt clay brick units [Figs. 3.23(c and d)].

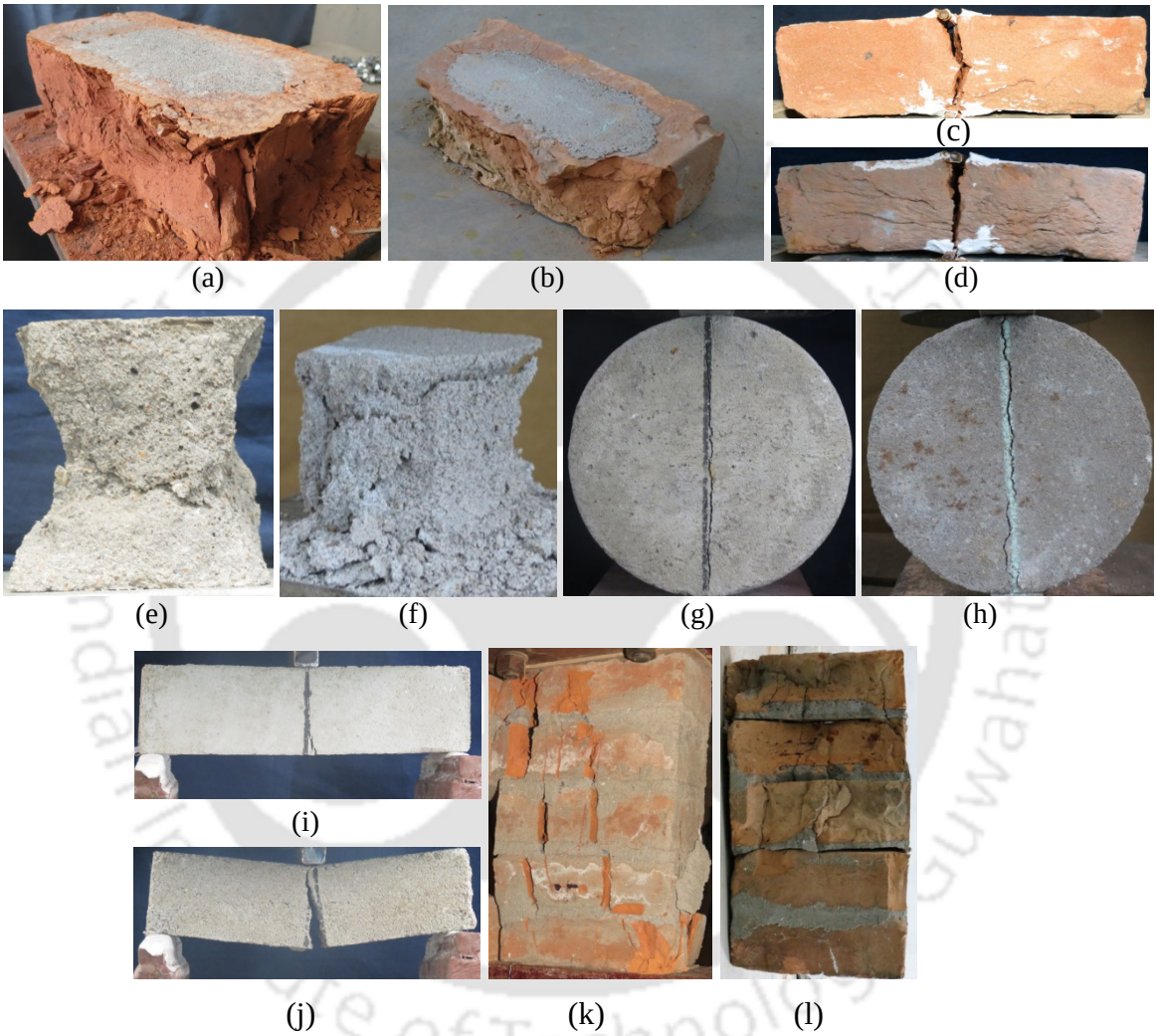

Fig. 3.23. Failure mechanisms in burnt clay brick masonry and its constituents: (a) and (b) crushing failure; (c) and (d) split-tensile failure of class-I and class-III burnt clay bricks; (e) and (f) pyramidal shape and crushing failure of 1:4 and 1:8 mortar cubes; (g) and (h) split-tensile failure of 1:4 and 1:8 mortar cylinders; (i) and (j) flexure failure of 1:4 and 1:8 mortar prisms; (k) vertical splitting and crushing failure of class-I burnt clay brick masonry prism; and (l) crushing of bricks and joint failure of class-III burnt clay brick masonry prisms.

Two different grades of mortar were used to construct the masonry prisms and 50 mm mortar cubes were tested under compressive loading to evaluate the nonlinear stress-strain characteristics of mortar joints. The behavior of mortar cubes was found to be

linear until one third of and 80% of their respective maximum strengths in case of 1:4 and 1:8 mortar grades, respectively (Fig. 3.22). The average compressive strength was found to be approximately 17.3 MPa [COV of 0.16] and 3.2 MPa [COV of 0.19] for 1:4 and 1:8 mortar cubes, respectively. In most of the specimens of 1:8 mortar grade, strain measuring instruments were disconnected before the strength was reached, and the post-peak behavior was not captured. The amount of strain recorded corresponding to the maximum strength was found to be almost similar in case of both 1:4 mortar (0.0061) and 1:8 mortar grade (0.0052) specimens. It was observed that 1:8 mortar found to be weaker (f_j = 3.2 MPa) and softer (E_j = 3795 MPa) when compared to 1:4 mortar cubes (f_j = 17.3 MPa; E_j = 7403 MPa). Under compressive loading, 1:4 mortar cubes observed pyramidal shape failure, whereas, full crushing of mortar cubes was observed in case of 1:8 mortar grade [Figs. 3.23(e and f)]. The split tensile strength of 1:4 and 1:8 mortar cylinders following IS 5816 (BIS 1999) and ASTM C496 (ASTM 2010) was found to be approximately 1.2 MPa [COV of 0.08] and 0.4 MPa [COV of 0.34], respectively. The modulus of rupture of 1:4 and 1:8 mortar grade prisms (160×40×40 mm^3) determined following EN 1015 (2007) and ASTM C348 (2008) was found to be approximately 4.26 MPa [COV of 0.16] and 2.6 MPa [COV of 0.1]. It was observed that the modulus of rupture of mortar was found to be proportional to square root of the mortar compressive strength.

The average compressive strength of class-III clay brick masonry prisms (1.5 MPa, 0.29) was found to be smaller than class-I clay brick masonry prisms (4.4 MPa, 0.37). The strain corresponding to maximum strength of both clay brick masonry prisms was found to be similar, whereas, the ultimate failure strain was found to be higher in case of class-III clay masonry prisms (Fig. 3.22). It can be attributed that due to the inherent softness of class-III burnt clay bricks and 1:8 mortar joint, the modulus of elasticity (E_m) of class-III burnt clay brick masonry prisms was found to be significantly smaller (608 MPa, COV of 0.36) than class-I clay brick masonry prisms (1744 MPa, COV of 0.18). Both class-I and class-III burnt clay brick prisms observed vertical splitting of brick units followed by crushing, and in case of class-I prisms the mortar joint was found to be intact, whereas, joint failure was observed in case of class-III burnt clay brick prisms as shown in Figs. 3.23(k and l).

Shear strength of class-I and class-III burnt clay brick masonry was determined from diagonal compression tests by constructing masonry wallettes of size 1200×1200×110 mm constructed using 1:4 and 1:8 mortar grades. The test was carried out by applying displacement-controlled loading using servo-controlled hydraulic actuator of 250 kN capacity along the diagonal. The shear strength was determined using the equations proposed by ASTM (2010) and it was found to be about 0.18 MPa [COV of 0.18] and 0.08 MPa [COV of 0.17], for class-I and class-III brick masonry wallettes, respectively.

The failure mechanisms observed in clay brick masonry wallettes were diagonal shear cracking, sliding of bed joint and a combination of both (Fig. 3.24). In case of class-I clay brick masonry the major failure mechanism was diagonal shear cracking with cracks passing through mortar bed joints and bricks along the loaded diagonal. In a few specimens, diagonal shear cracking along with bed joint sliding was also observed [Fig. 3.24(b)]. In case of class-III burnt clay brick masonry wallettes, the major failure mechanism was bed joint sliding and a combination of bed joint sliding and diagonal shear cracking due to the weak 1:8 mortar bed joint [Figs. 3.24(c and d)].

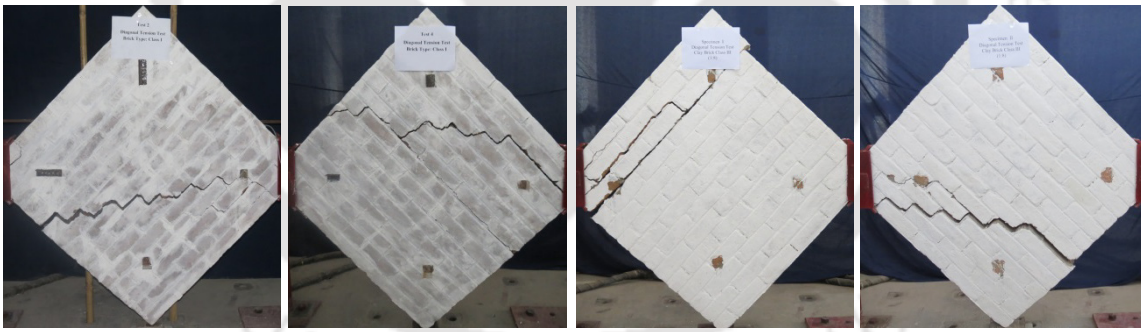

(a) (b) (c) (d)

Fig. 3.24. Failure mechanisms in masonry wallettes: (a) diagonal shear cracking and (b) combination of diagonal shear cracking and sliding of bed joint in class-I clay brick masonry; (c) bed joint sliding and (d) combination of diagonal shear cracking and sliding of bed joint in class-III clay brick masonry.

3.10 SUMMARY

To obtain the material characteristics of fly ash brick masonry and burnt clay brick masonry, an extensive experimental study was undertaken by testing masonry and its constituents under various loading conditions (compression, shear and tension). *WA* and

IRA tests were also carried out on fly ash brick units in order to compare the relative porosity. It was observed that average *WA* (18.3%) for fly ash brick units was higher than that of burnt clay bricks. The average *IRA* (5.1 kg/m^2/min) of fly ash brick units was found to be exceeding the limits proposed for burnt clay brick units (0.5 kg/m^2/min - 1.5 kg/m^2/min) for their structural use. The strength and stiffness of mortar used in the current study was higher than that of fly ash bricks and masonry prisms. For different mortar grades, the increase in compressive strength of mortar was about three-fold, but increase in corresponding masonry strength was not even twice; this shows that masonry prism strength does not depend too much on the compressive of the strength of mortar due to the use of weaker and softer bricks in the current study. Failure modes in masonry prisms showed that good bond can be achieved using higher grade mortar.

From the diagonal compression tests, it was found that the shear strength of full scale specimen was about 0.31 times the strength of half scale specimen. The average shear modulus of full scale fly ash brick masonry wallette was found to be 27% of the elastic modulus. From parametric study, it was observed that a fairly good correlation exists between brick compressive strength and masonry prism strength, whereas the correlation between mortar strength with shear strength was very weak. The effect of other parameters, such as, tensile strength of both brick units and mortar, and their bond strength need to be assessed which will give more insight into the shear strength. High water absorption and smooth surfaces were found to be the major factors for low tensile bond strength of fly ash bricks. The weak and soft nature exhibited by the fly ash bricks in comparison with the burnt clay bricks was attributed to the incomplete pozzolanic reaction in fly ash bricks. Using the nonlinear material characteristics of fly ash brick and clay brick masonry obtained in the current chapter, the capacity of infill and its influence on the behavior infilled frames designed using the current codal recommendations are assessed in the next chapters.

Chapter 4
PRELIMINARY STUDY ON LATERAL LOAD BEHAVIOR OF MASONRY INFILLED RC FRAMES

CONTENTS

4.1 OVERVIEW

Masonry walls are generally used as infills in reinforced concrete (RC) frames without accounting for their resistance to lateral loads under strong ground motions. RC frames are designed to exhibit flexural behavior under seismic actions, and when infills are introduced, though the lateral strength, stiffness and energy dissipation capacity of the frames are improved, the lateral load resistance is mostly dominated by shear behavior of columns. A comprehensive review (Moghaddam and Dowling 1987; CEB 1996; Kaushik et al. 2006; Asteris and Cotsovos 2012; Asteris et al. 2013) of past research showed that when the strength and stiffness of infill is sufficiently large, local detrimental effect of infill may cause shear failure of columns. Most of the past experimental studies (Mehrabi et al. 1966; Al-chaar et al. 2002; Blackard et al. 2009; Fardis 2009) reported shear failure of columns in frames not designed as per the recommendations of prevalent seismic standards. From the past studies (Fardis 2009; Asteris et al. 2011; Markulak et al. 2013;

Uva et al. 2012; Anil and Altin 2007; Schwarz et al. 2015), it was observed that several factors have significant influence on failure mechanism of masonry infilled RC frames, which include aspect ratio, openings in the infill panels, column to beam stiffness ratio, axial load ratio on columns, type of infill and the construction methodology, number of stories and bays, etc. Based on the classification of failure modes of infilled frames Asteris et al. (2011), also reported that the frame failure mode, associated with weak frame-strong infill configuration, was particularly important. To address this problem, Eurocode 8 (CEN 2004b), ASCE 41 (2013), MSJC (2013), and Moretti et al. (2014) recommended methods to evaluate the shear demand on columns taking into account the effect of infill. From the recommendations of the past studies, it is understood that infilled frames need to be designed to resist the excessive shear force from infill.

In order to evaluate the effectiveness of these recommendations, and to understand the failure mechanisms of such frames, an experimental study was undertaken in which half-scale RC frames designed using the current seismic standards were tested. It was also observed that several past studies (Moretti et al. 2014; Tasnimi and Mohebkhah 2011; Kakaletsis and Karayannis 2008; Zovkic et al. 2013; Cavaleri and Di Trapani 2014) used solid clay or fly ash bricks, hollow blocks or concrete bricks/blocks as infills. The chapter mainly focuses on evaluating the effectiveness of the design recommendations of infilled frames in some commonly used earthquake standards. Further, effect of T-beam action provided by RC slab on behavior of RC beams was assessed, as most of the past studies did not consider stiffening effect of slab and reported failure of beams and beam-column joints.

4.2 Description of RC Frames Studied

Most of the building stock in developing countries, including India, consists of medium rise masonry infilled RC frame buildings (2-5 storey). From the report of housing encyclopaedia (Jaiswal et al. 2002) it was noted that approximately 10% of all urban constructions in India consisted of RC frame structures. In the current study, half-scale models of an exterior ground-story frame of a two-storey office building in Assam, which is one of the most seismic-prone regions in India, have been studied. The effect of RC slab on behavior of the specimens was observed by providing slab over the beam and extending it over a width of 400 mm on both sides of the frame (Fig. 4.1). Columns of the

specimens were constructed on a RC beam of size 400×350 mm to provide fixity at the base. Columns were supported laterally using roller bearing steel frames on either side to prevent out-of-plane movement of the specimens during in-plane lateral loading. Vertical load applied to the specimens was calculated based on the tributary area above the frame in the storey above it. The total vertical load was applied by placing RC plates on the RC slab, corresponding to an axial load ratio ($P/f_{ck}A_g$) of about 1% on each column of the frame, where P, f_{ck} and A_g represent the axial compressive load, compressive strength of concrete cubes at 28 days, and gross area of concrete section, respectively. Due to the laboratory constraints, no vertical load was applied on the columns and it is not a major deviation from the prototype loading distribution as the vertical load acting on the columns due to upper storey was quite low. The stiffening action provided by the RC beam-slab was quite high, and moreover, infill wall was constructed after the casting of the frame. At the same time, this type of construction practice apparently leaves a gap between the soffit of the beam and the infill wall. Therefore, it was unlikely that the vertical loads applied over the slab were transferred to the infill wall below.

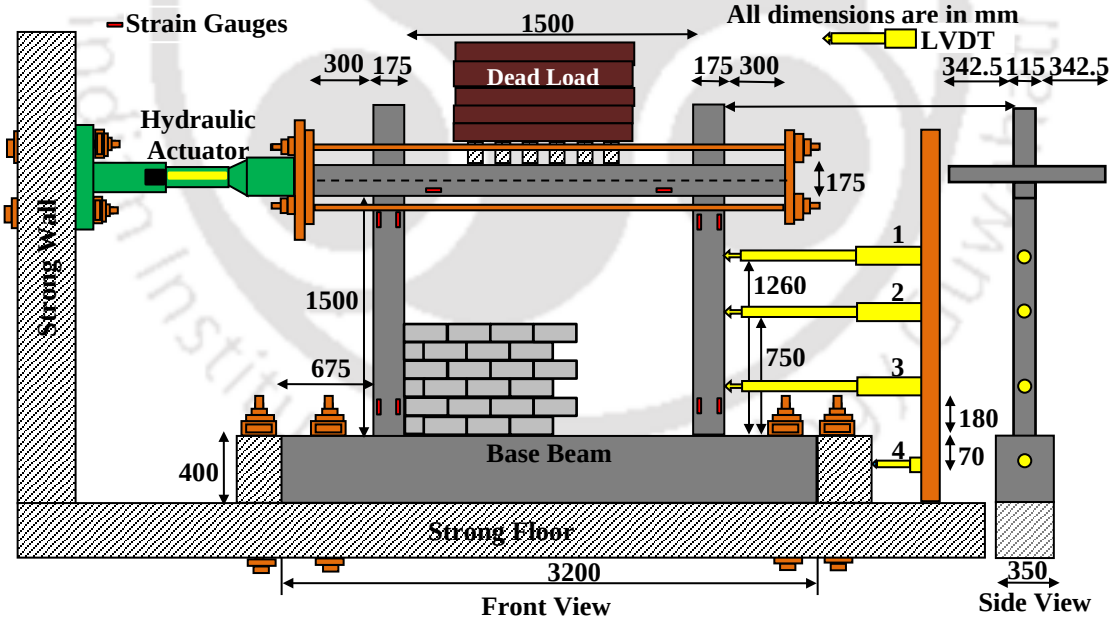

Fig. 4.1. Details of experimental set up and instrumentation.

Currently, three Indian standards deal with the design (BIS 2000; BIS 2002b) and detailing (BIS 1993) of reinforced concrete members of which IS 456 (BIS 2000) deals with the general design considerations of RC members, IS 1893 (BIS 2002b) with the calculation of earthquake forces, and IS 13920 (BIS 1993) with the ductile detailing of

RC structures subjected to seismic forces. The prototype structure considered in the study was designed for the lateral forces corresponding to the highest seismic zone in India but not detailed as per the ductile detailing guidelines (BIS 1993) (design lateral shear was about 15% of the seismic weight). In order to evaluate the effectiveness of ductile detailing, two types of frames (ductile and non-ductile) were designed in the current study. Reinforcement in RC beam and columns of the non-ductile bare frame specimen was not detailed to exhibit ductility. The design of non-ductile bare frame was similar to that of the ordinary moment frames designed in accordance with ACI 318 (2008) and also to the frame designed according to Eurocode 8 (CEN 2004b) without following the detailing requirements for local ductility. The ductile detailing code of India (IS 13920) requires providing special confining reinforcement in the expected plastic hinge locations in beams and columns. However, in ductile bare frame the reinforcement was detailed in accordance with IS 13920 but without provision of special confining reinforcement. Design of ductile bare frame corresponds to special moment resisting frame as per ACI 318 (2008) without considering the effect of discontinued stiff members, and it also corresponds to the frame designed for high ductility class in accordance with Eurocode 8 (CEN 2004b), without considering the local effects due to masonry infill. Table 4.1 gives the details of the test specimens and reinforcement detailing of ductile and non-ductile frame is shown in Fig. 4.2.

Table 4.1. Details of test specimens (Phase I- preliminary study)

Specimen No	Type of Frame	Notations	Ductile Detailing	Type of Masonry
	Stage I			
1	Ductile bare frame*	DB	yes	no infill
2	Non-ductile bare frame	NDB	no	no infill
3	Ductile frame infilled with full-scale bricks	DFS	yes	full-scale bricks
4	Non-ductile frame infilled with full-scale bricks	NDFS	no	full-scale bricks
5	Ductile retrofitted frame infilled with full-scale bricks	DRFS	yes	full-scale bricks
6	Non-ductile retrofitted frame infilled with full-scale bricks	NDRFS	no	full-scale bricks
7	Ductile frame infilled with half-scale bricks	DHS	yes	half-scale bricks
8	Non-ductile frame infilled with half-scale bricks	NDHS	no	half-scale bricks
	Stage II: Ductile Infilled Frame			
9	Improved detailing along full column length	DISTL	yes	full-scale bricks
10	Improved detailing in critical regions	DISC	yes	full-scale bricks
11	Improved detailing in critical regions using high strength bars	DISCSB	yes	full-scale bricks

Key: D-ductile; ND-Non-ductile; B-Bare; FS-Full-scale bricks; HS-Half-scale bricks; R-Retrofitted; I-Improved; S-Shear capacity; Throughout Length-TL; C-Critical regions; SB-High strength bars.

*Specimens 1-6 were taken from Manchanda (2010) and Basha (2011).

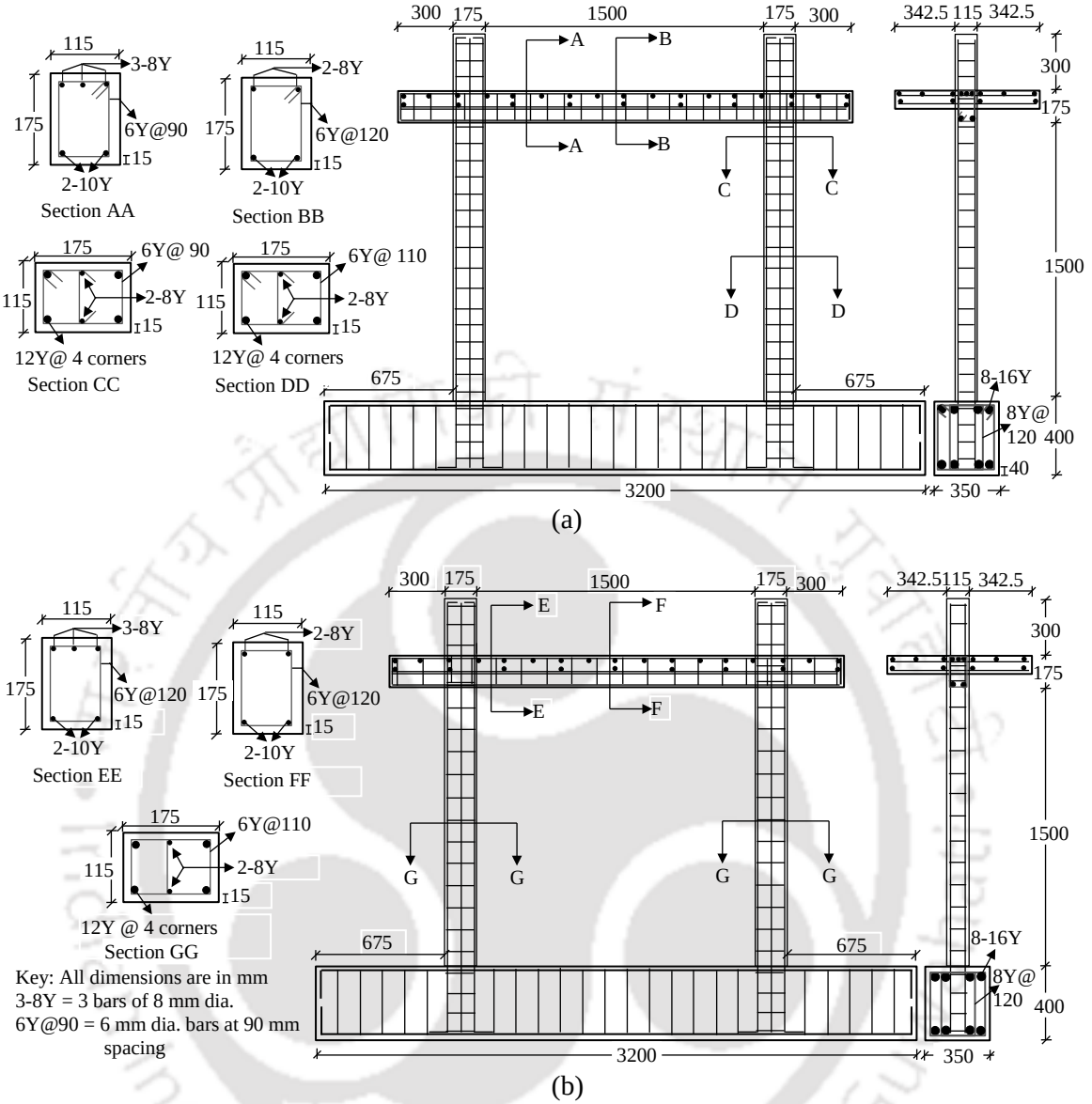

Fig. 4.2. Reinforcement detailing of: (a) ductile frame; and (b) non-ductile frame model.

Major distinctions between ductile and non-ductile frames were: spacing of shear reinforcement, bending of hooks, and embedment of ends of shear reinforcement into the core concrete. The longitudinal reinforcement remained same in both ductile and non-ductile frames and the members framing into joints were detailed as continuous members. In case of non-ductile frames, shear reinforcement in columns at critical locations (upto 500 mm from the face of top and bottom beams) consisted of 3-legged, 6 mm diameter bars with 90^{o} hooks at 110 mm spacing [Fig. 4.2(b)]. Whereas, in case of ductile frames, similar shear reinforcement in columns was placed with 135^{o} hooks at 90 mm spacing, and embedment length of 10 times bar diameter [Fig. 4.2(a)]. The experimental study was

carried out in two stages: eight specimens were tested in the first stage considering different reinforcement detailing in RC members and using different size bricks for masonry. Three specimens were tested in the second stage to study the influence of providing special confining reinforcement required as per IS 13920 (BIS 1993). Two different size of fly ash bricks: full-scale (230×110×75 mm) and half-scale (115×55×38 mm) were used as infill constructed using 1:4 (cement:sand) mix mortar with a water cement ratio of 0.6. A few past studies (Murty and Jain 2000; Stavridis et al. 2012) have reported that the lateral load behavior of RC frame infilled either with full or half scale bricks doesnot differ significantly. Stavridis et al. (2012) also reported that scaling of bricks and mortar joints was not important for a scaled model (2/3rd scale) as the size of the units is relatively small with respect to the dimensions of the wall. Moreover procurement of half-scale bricks is quite difficult as they are not commercially manufactured, and cutting the cutting the full-scale bricks into half (all dimensions) is not advisable as the surface of the bricks becomes smooth in the cutting process. Therefore full-scale bricks were used in the half-scale specimens. Infill wall was constructed by laying bricks in two different patterns: Stretcher bond (running bond) in case of full-scale bricks and English bond in case of half-scale bricks in order to maintain similar thickness of infill in both full-scale and half-scale brick specimens. An aspect ratio (h/l) of 1.0 was considered keeping in view the general room sizes in apartment-type buildings (3 m × 3 m with 3 m high floors). Further, in order to study the effectiveness of a commonly adopted retrofitting method, damaged ductile and non-ductile infilled frames (Specimens 3 and 4) were retrofitted by replacing the damaged concrete after welding additional reinforcement in the region where bars had yielded (Specimens 5 and 6). A comparative performance assessment of all the specimens is carried out in the following sections.

4.3 MATERIAL PROPERTIES

Material properties were evaluated using relevant standards by conducting tests on masonry and its constituents, concrete, and reinforcing bars (Table 4.2). The average compressive cube strength of concrete (f_{ck}) was 22.4 MPa with modulus of elasticity E_c of about 23700 MPa. Average compressive strength of fly ash brick units (f_b) and mortar cubes (f_j) was about 5.7 MPa and 17.3 MPa, respectively, with modulus of elasticity as 3900 MPa (E_b) and 7400 MPa (E_j), respectively. The compressive masonry prism strength (f'_m) was about 3.9 MPa with modulus of elasticity E_m as 2700 MPa.

Table 4.2. Material properties of specimens

Material	Characteristics	Units	Full-scale Bricks	Half-scale Bricks
Brick	Dimensions	mm	230×110×75	110×55×38
	Compressive strength	MPa	f_b = 5.7, E_b = 3900	f_b = 7.3, E_b = 4960
	Split tensile strength	MPa	f_{bt} = 0.54	f_{bt} = 1.0
Mortar	Compressive strength	MPa	f_j = 17.3, E_j = 7400	f_j = 17.3, E_j = 7400
	Flexural strength	MPa	3.78	3.78
	Split tensile strength	MPa	f_{jt} = 1.2	f_{jt} = 1.2
Masonry prism	Compressive strength	MPa	f'_m = 3.9, E_m = 2700	f'_m = 4.6, E_m = 2800
Masonry wallette	Shear strength	MPa	f'_v = 0.14, G_m = 730	f'_v = 0.14, G_m = 730
Concrete	Compressive strength	MPa	f_{ck} = 22.4, E_c = 23700	
Longitudinal steel	Tensile strength	MPa	f_y = 460/365/530*, E_s = 2×10^5	
6Y Stirrups	Tensile strength	MPa	f_y = 265/520, E_s = 2×10^5	
8Y Stirrups	Tensile strength	MPa	f_y = 460, E_s = 2×10^5	

*Three types of reinforcing bars were used

The average shear strength of masonry wallettes (f'_v) was found to be 0.14 MPa with shear modulus G_m as 730 MPa. Failure of both fly ash brick masonry prisms and fly ash brick masonry wallettes is shown in Fig. 4.3. Further details on the material characterisation can be found in chapter 3. In line with the current construction practice in India, three different grades of reinforcing bars were used in the current study (Table 4.2). In the first stage (Specimens 1-8), the most common reinforcing bars with yield stress f_y as 460 MPa were used as longitudinal bars, and mild steel bars (6 mm diameter) with f_y as 265 MPa were used as shear reinforcement.

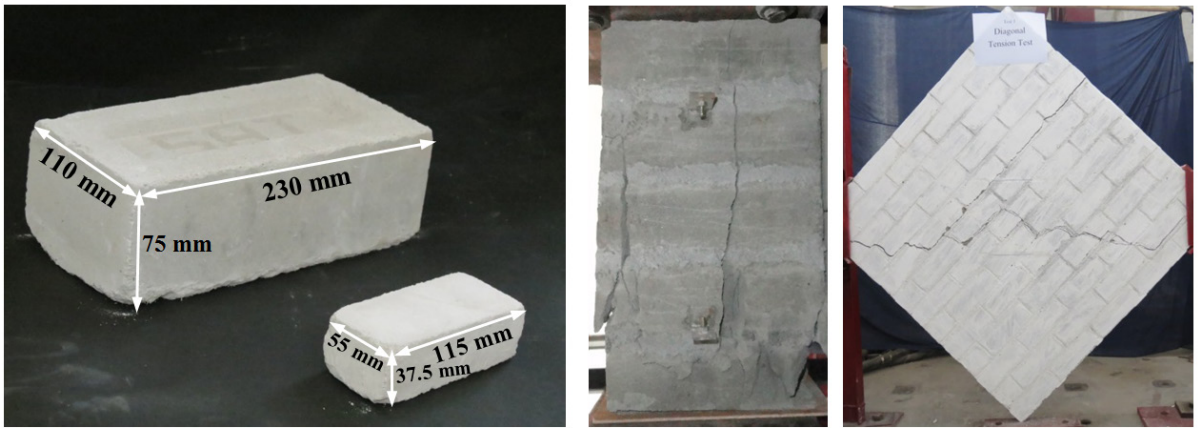

(a) (b) (c)

Fig. 4.3. (a) Description of full-scale and half-scale bricks; failure of: (b) masonry prism; and (c) masonry wallette.

In the second stage, low strength brittle bars with f_y as 365 MPa were used in specimens 9 and 10 as longitudinal reinforcement, and shear reinforcement consisted of 8 mm diameter bars with f_y as 460 MPa. High strength ductile bars with f_y as 520-530 MPa were used in specimen 11 as both longitudinal and shear (6 mm bars) reinforcement. In the past studies, a distinction between strong and weak frame with respect to infill strength was not clearly defined. Zovkic et al. (2013) and Mehrabi et al. (1996) qualitatively reported that strong frames are those designed for seismic actions in which columns and beams had heavier reinforcement near critical regions and expected to behave in ductile mode. Kakaletsis and Karayannis (2008), Asteris et al. (2011) and Mansouri et al. (2014) quantitatively reported frame-infill configuration based on lateral strength of frame and infill, but did not define a range to differentiate the same. Based on these studies, the ratio of frame to infill strength was quantitatively established in the current study. The infill strength was calculated as the shear strength of the panel (f_v') times the net-mortared area of the infill (A_n). Lateral strength of the frame was calculated assuming plastic hinges formed at both ends of columns, as $4M_{pc}/(h\text{-}l_p)$, where M_{pc} is the plastic moment capacity of the column, h is the height of the column and l_p is the length of plastic hinge (taken as half the depth of the column). The lateral strength of frame and infill was found to be about 40 kN and 23 kN, respectively, and the ratio was about 1.7.

Similarly, ASCE 41 (2013) does not explicitly state the type of frame-infill configurations, but defined three ratios of frame to infill strength (< 0.7, between 0.7 to 1.3, and ≥ 1.3) while defining limits on in-plane lateral drifts. The ratio of frame to infill strength is calculated in ASCE 41 considering the expected story shear strengths of frame (considering bare frame) and infill. The first ratio (< 0.7) corresponds to weak frame-strong infill configuration, and the last (≥ 1.3) to strong frame-weak infill configuration. Therefore, considering both qualitative and quantitative estimation, the current system may be termed as strong frame-weak infill configuration (since the ratio is more than 1.3).

4.4 TESTING PROCEDURE AND INSTRUMENTATION

The frame specimens were tested under slow-cyclic displacement loading (Fig. 4.4) applied at the slab level using servo-controlled hydraulic actuator of 250 kN load capacity and a stroke length of ± 125 mm (Fig. 4.1). Experimental results were recorded continuously using load cell and displacement transducer located in the actuator arm,

external *LVDT*s (linear varying displacement transducers), and strain gauges. Three cycles of each displacement level were applied and the response was recorded using a data acquisition system.

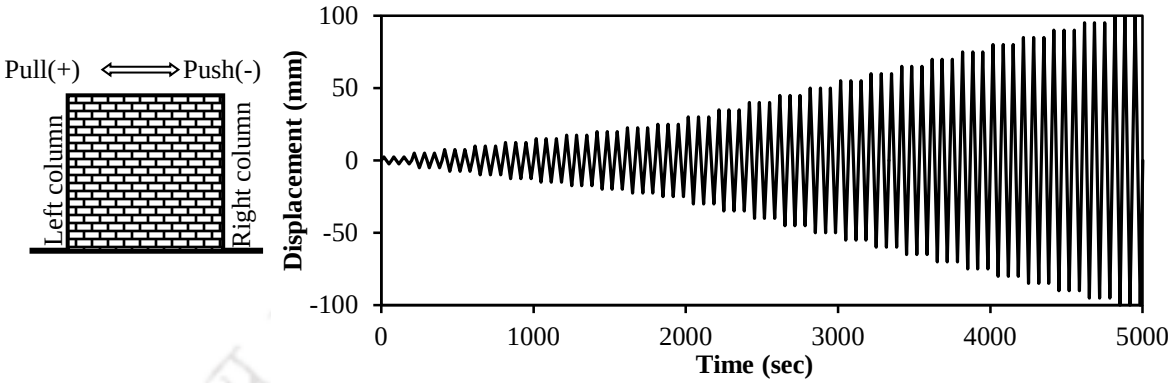

Fig. 4.4. Push and pull directions, and displacement cycles of the actuator for slow-cyclic test.

*LVDT*s were used at different locations on the columns and base beam to record the lateral displacements. Base beam was restricted from sliding by bolting it to the strong floor. Quarter-bridge, four wired, linear strain gauges (*HBM* made) were used to record the strains in the reinforcement. Strain gauges were bonded to the longitudinal reinforcement at the most likely locations of formation of plastic hinges from the face of beam and columns (Fig. 4.1). Maximum lateral load resistance of the specimens is reported in both push (-) and pull (+) directions. In the current study, tests were terminated when the capacity of the specimen reduced to about 75% of its maximum or when the failure was imminent.

4.5 Hysteretic Response of Specimens

The lateral load behavior of the specimens during slow-cyclic loading in the form of hysteretic response (actuator load-lateral deformation) for first cycle of every lateral displacement level is shown in Fig. 4.5. In ductile and non-ductile bare frames, hysteretic loops were evenly spaced before and after reaching the lateral load capacity. The non-ductile bare frame exhibited higher amount of pinching when compared to the ductile frame, and therefore, dissipated lesser amount of energy. In case of infilled frames, initially the loops were closely spaced until the lateral load carrying capacity was reached. As the infill wall cracked and gaps developed along the frame-infill interface, hysteretic loops were found to be unevenly spaced (i.e., slight uneven variation in the lateral load

resistance and pinching was observed due to reorganization of infill after infill failure). Pinching in hysteresis loops of infilled frames (Specimens 3 to 8) was more pronouncing at higher displacement levels. This shows that the resistance provided by the infill decreased after significant damage in the infill. The beneficial effect of ductile detailing was evident in infilled frames only after the frame reached its maximum capacity. The dropdown in load carrying capacity was gradual in case of ductile infilled frames when compared to corresponding non-ductile frames (full- or half-scale bricks).

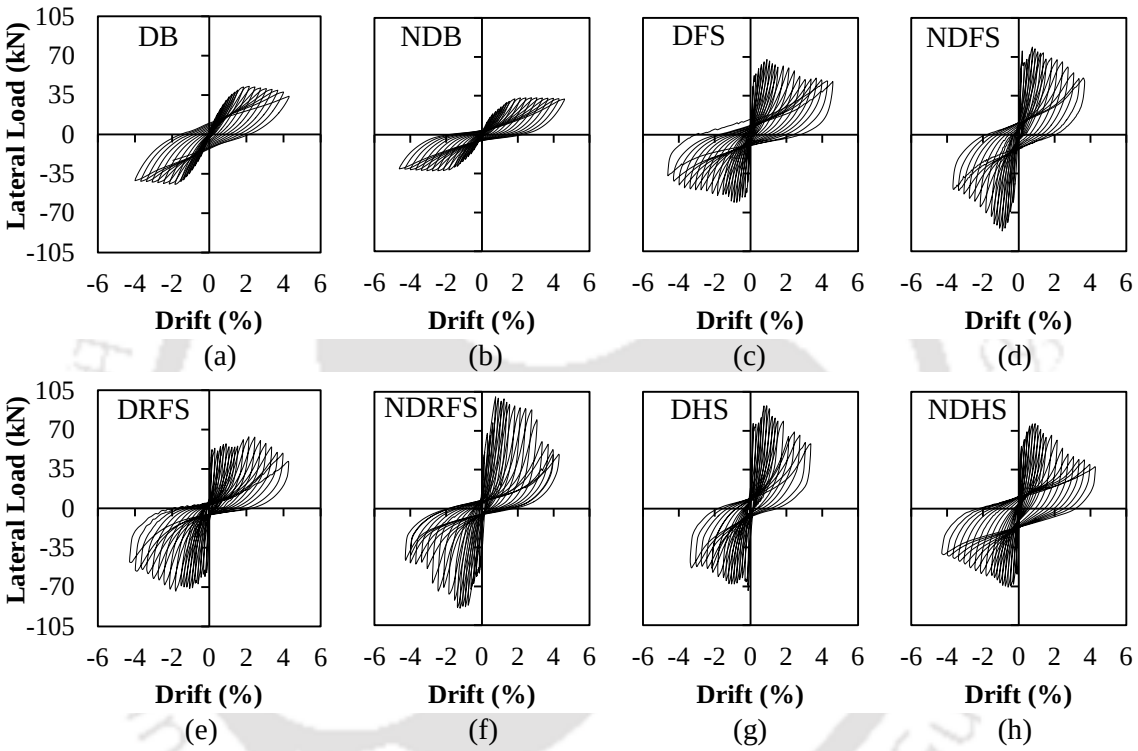

Fig. 4.5. Hysteretic response of specimens 1-8: (a) ductile bare frame; (b) non-ductile bare frame; (c) ductile frame infilled with full-scale bricks; (d) non-ductile frame infilled with full-scale bricks; (e) ductile retrofitted frame infilled with full-scale bricks; (f) non-ductile retrofitted frame infilled with full-scale bricks; (g) ductile frame infilled with half-scale bricks; and (h) non-ductile frame infilled with half-scale bricks.

4.6 Evaluation of Influencing Parameters

The parameters influencing the behavior of test specimens were quantified in terms of lateral strength, lateral stiffness, and energy dissipation. Initial stiffness was calculated as the slope of the secant connecting 5% to 33% of the lateral load corresponding to the first hysteretic loop (first drift level). It was observed that initial stiffness of the infilled frames was about 7 to 10 times that of the corresponding bare frames [Table 4.3 and Fig. 4.6(a)]. Frames infilled with half-scale bricks (Specimens 7 and 8) observed marginally higher

initial stiffness (3% for non-ductile and 8% for ductile) when compared to specimens 3 and 4. The reason for the frames to observe slightly higher initial stiffness may be due to the fact that the frames resisted slightly higher lateral load in the initial drift level (0.15%). English bond used in case of half-scale brick specimens (Specimens 7 and 8) appears to have provided higher lateral load resistance in the initial drift level when compared to lateral load resistance provided by the stretcher (running) bond in case of full-scale brick specimens (Specimens 3 and 4). The lateral strength of specimen 3 and 4 was about 1.6 (ductile) and 2.5 (non-ductile) times that of their corresponding bare frames. Frames infilled with half-scale bricks resisted a lateral strength of about 1.9 (ductile) and 2.2 (non-ductile) times that of the corresponding bare frames. As discussed earlier, the difference in the brick bond pattern possibly resulted in slightly higher lateral strength of frames infilled with half-scale bricks compared to frames infilled with full-scale bricks.

Table 4.3. Influencing parameters of tested specimens

S. No	Type of Frame	K_i	ED	F_u	δ_u	DR_i	DR_f	DR_s	DR_{80}	DR_u
		(kN/mm)	(kNmm)	(kN)	(mm)			(%)		
1	Ductile bare frame	4.0	43,900	-44, +43	70	-	0.62	1.38	-	4.31
2	Non-ductile bare frame	3.2	32,100	-33, +33	75	-	0.46	0.77	-	4.62
3	Ductile frame infilled with full-scale bricks	28.6	64,300	-68, +73	75	0.31	0.77	0.77	-3.3, +2.9	4.62
4	Non-ductile frame infilled with full-scale bricks	29.2	51,900	-87, +79	60	0.31	1.08	0.46	-1.9, +2.6	3.69
5	Ductile retrofitted frame infilled with full-scale bricks	30.5	48,300	-73, +63	70	0.15	0.92	0.46	-3.2, +3.8	4.31
6	Non-ductile retrofitted frame infilled with full-scale bricks	31.2	56,900	-90, +101	70	0.15	0.77	0.62	-2.6, +3.1	4.31
7	Ductile frame infilled with half-scale bricks	31.0	40,200	-74, +93	55	0.15	1.23	0.46	-1.9, +1.9	3.38
8	Non-ductile frame infilled with half-scale bricks	30.1	74,500	-71, +76	70	0.15	0.77	0.62	-2.2, +2.1	4.31
9	Ductile infilled frame with improved shear capacity throughout the length of the column	30.3	64,300	-46, +55	80	0.31	0.92	0.92	-2.6, +3.8	4.92
10	Ductile infilled frame with improved shear capacity in critical regions only,	30.5	62,400	-45, +60	80	0.31	0.77	0.92	-3.6, +3.9	4.92
11	Ductile infilled frame with improved shear capacity in critical regions using high strength bars	35.7	78,200	-105, +107	95	0.46	0.92	0.77	-2.7, +2.0	5.85

Note: K_i is the initial stiffness, ED is the cumulative energy dissipation, F_u is the maximum lateral load, δ_u is the ultimate lateral displacement, DR_i, DR_f, DR_s, DR_{80}, and DR_u represents the drift at initiation of crack in infill (sliding/diagonal), initiation of flexural cracks in columns, initiation of shear cracks in columns, 80% of maximum load, and ultimate deformation, respectively.

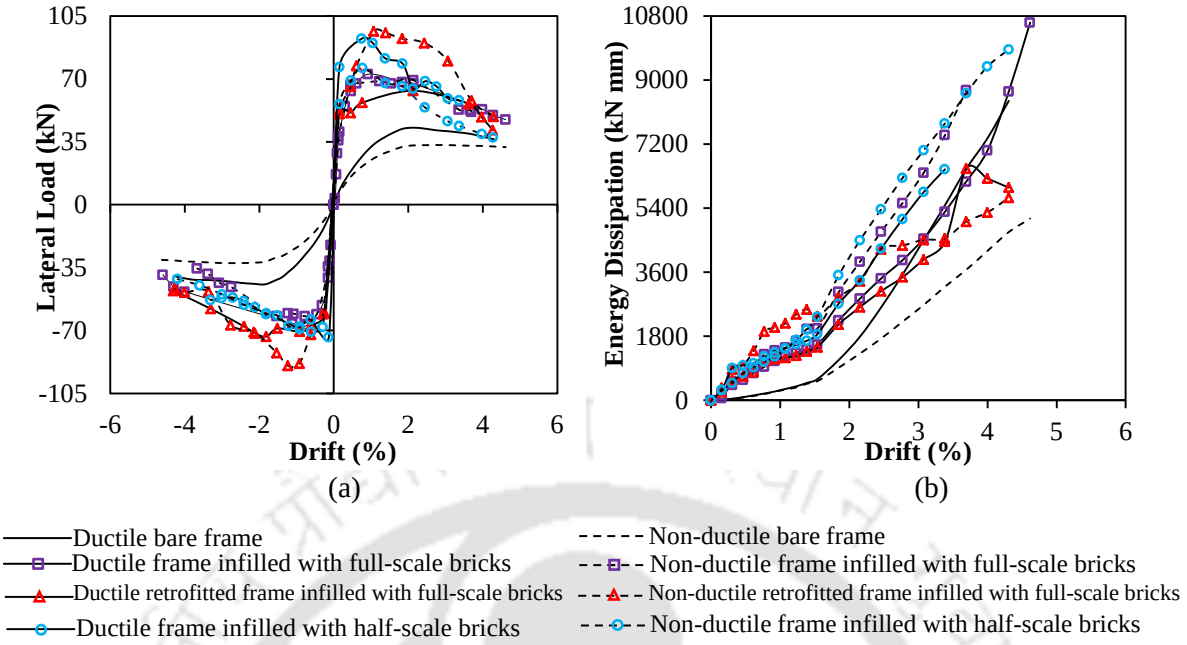

Fig. 4.6. Lateral load behavior of specimens 1-8: (a) envelope curves showing force vs. drift at actuator level; and (b) energy dissipation at different drift levels.

The crack propagation in infill in case of full-scale bricks was easier as the bricks were laid in stretcher (running) bond, whereas, in the case of half-scale bricks the crack propagation was difficult due to the presence of alternate courses of headers and stretchers. Further, Chiou and Hwang (2015) reported that the compressive strength of mortar is also one of the factors that influence the lateral strength of the infilled frames. Mortar used in the current study was stronger and stiffer than the bricks (Table 4.2), and the number of mortar layers provided in half-scale brick specimens (Specimens 7 and 8) was higher (almost double). Further, compressive and tensile strength of half-scale bricks and masonry prism strength for half-scale specimens is higher than that of the full-scale brick specimens. These factors further resulted in higher lateral load resistance of the half-scale brick specimens. The lateral strength of retrofitted frames (Specimens 5 and 6) was approximately equal to that of the original infilled frames (Specimens 3 and 4), highlighting the effectiveness of the retrofitting technique in restoring the original capacity of the structure.

Energy dissipation per displacement level was computed as the area enclosed under the hysteresis loops (3 loops per displacement level), and the cumulative energy dissipation is calculated by summing the individual areas of each displacement level (Table 4.3). Energy dissipation during the initial stages was due to the contribution of

frame and infill. After significant damage in infill, dissipation was primarily due to the formation of plastic hinges in columns of the frame. Energy dissipation can be quantified based on the lateral strength, displacement sustained, and the effect of pinching as described earlier. The amount of energy dissipated by the frames infilled with full-scale bricks was about 1.5 (ductile) and 1.6 (non-ductile) times that of the corresponding bare frames [Table 4.3 and Fig. 4.6(b)]. As expected, the energy dissipated by the ductile frame infilled with full-scale bricks was higher (about 20% more) when compared to the non-ductile frame. This is because in ductile frame, the degradation of strength was gradual, ultimate displacement levels were larger (75 mm), and lesser pinching was observed in hysteretic behavior (Fig. 4.5).

Frames infilled with half-scale bricks showed an energy dissipation of about the same (in case of ductile frame) and about 2.3 times (in case of non-ductile frame) that of their respective bare frames. Non-ductile frame infilled with half-scale bricks dissipated highest energy due to the lesser amount of pinching [Fig. 4.5(h)]. Compared to other infilled frames, non-ductile frame infilled with half-scale bricks (Specimen 8) developed high friction mechanism between brick layers due to intense sliding cracks along bed and head mortar joints, and vertical splitting cracks in bricks. However, in case of ductile frame infilled with half-scale bricks (Specimen 7) only bed joint sliding of brick layers and minimal vertical splitting cracks in bricks was observed [Fig. 4.7(g)]. Under lateral loading, more cracks were formed in infill in non-ductile half-scale specimen due to more number of mortar joints in alternate courses of headers and stretchers, and it was also observed that cracking in infill in case of ductile frame infilled with half-scale bricks was limited to a few brick layers [Fig. 4.7(h)].

Stylianidis (2012) reported that at higher drift levels the contribution of infill to energy dissipation was negligible as infill degrades rapidly. On the contrary, in non-ductile frame infilled with half-scale bricks, infill was found to remain intact with the bounding frame even at higher drift levels, and therefore, contributed to higher energy dissipation due to the friction mechanism as compared to other infilled frames (Specimen 3-7). Energy dissipated by the retrofitted frames was about 0.8 (ductile) and 1.1 (non-ductile) times that of the original specimens (3 and 4). This is due to the fact that the ductile retrofitted frame (Specimen 5) underwent lesser ultimate lateral displacement and higher pinching when compared to other infilled frames.

Drift ratio (ratio of lateral displacement to storey height) was calculated corresponding to major events such as formation of infill cracks (sliding and diagonal cracking), initiation of shear cracks and flexure cracks in columns, peak load and 80% of peak load in post peak regime. Slight variations in quantification of influencing parameters is expected due to poor quality of bricks available in the region, variable workmanship, variable thickness of mortar joints, and improper bond and interface connections between infill and frame. From the current study, it may be inferred that since the masonry infilled RC frames are quite stiffer systems than the bare frames, it may not be practical to compare the lateral strength and stiffness of ductile and non-ductile specimens because the initial behaviour depends primarily on the infill properties.

4.7 Crack Pattern and Failure Mechanisms

Crack patterns observed in various members provide an insight into the lateral load resistance path, damage pattern, and mode of failure, which depends on the relative strength of frame and infill. The crack pattern observed in all the specimens and resulting failure mechanisms are discussed below.

4.7.1 Ductile and Non-Ductile Bare Frame (Specimens 1 and 2)

The crack pattern observed in both ductile and non-ductile bare frames was similar, but the amount of cracks developed in non-ductile frame was higher in which cracks initiated at 0.46% drift (lateral load of 15 kN). In ductile bare frame, flexural cracks initiated at a drift of 0.62% and lateral load of 24 kN near left beam-column joint [Figs. 4.7(a and b)]. With increase in lateral drift, minor diagonal shear cracks developed in non-ductile columns at a drift of 0.77% (21 kN), whereas, in ductile columns shear cracks developed at 1.38% drift (40 kN). Few cracks were observed in beams in both the bare frames emphasizing the T-beam action due to the presence of RC slab. Finally, it was ascertained that though significant shear cracks developed in columns of non-ductile frame, both ductile and non-ductile bare frames failed due to flexural mechanism in columns.

4.7.2 Ductile and Non-Ductile Infilled Frames (Specimens 3 to 8)

In case of infilled frames, both ductile and non-ductile, cracks formed initially in infill, and with increasing lateral drift, cracks propagated into frame members. The drift levels corresponding to the initiation of major events in infilled frames are shown in Table 4.3.

It was observed that the initiation of cracks in frame elements depends on the location of cracks in infills. Cracks in infill panels originated mainly from two locations: one near the mid-height of the infill panel and the other slightly below the soffit of the top beam or slightly above the bottom beam. Specimens 3, 6, and 8 observed bed joint sliding cracks in infill near mid-height at a drift level of 0.31% (56 kN), 0.15% (57 kN), and 0.15% (59 kN), respectively. In case of ductile frame infilled with full-scale bricks (Specimen 3), bed joint sliding cracks near the mid-height of the panel were connected by diagonal stepped cracks (cracks in both bed and mortar head joints and vertical splitting cracks in bricks) originated from the column ends. Later the cracks propagated to the opposite column ends by similar diagonal stepped cracks. Whereas, in case of specimens 6 and 8, the bed joint sliding cracks in the middle of the panel were connected by vertical interface cracking between infill and column in upper middle panel and propagated to the opposite ends by diagonal stepped cracking in the lower middle infill panel.

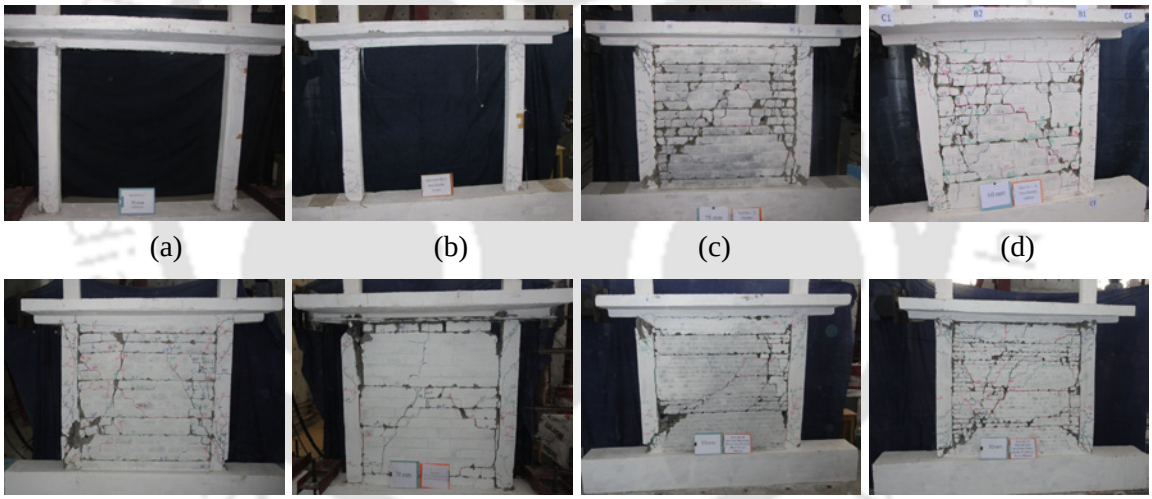

Fig. 4.7. Failure mechanisms observed in specimens 1-8: (a) ductile bare frame; (b) non-ductile bare frame; (c) ductile frame infilled with full-scale bricks; (d) non-ductile frame infilled with full-scale bricks; (e) ductile retrofitted frame infilled with full-scale bricks; (f) non-ductile retrofitted frame infilled with full-scale bricks; (g) ductile frame infilled with half-scale bricks; and (h) non-ductile frame infilled with half-scale bricks.

On the other hand, in specimens 4, 5, and 7 bed joint sliding cracks formed slightly away from the mid-height of the infill panel (i.e., below top beam soffit and above the bottom beam) at a drift level of 0.31% (-61 kN, +75 kN), 0.15% (57 kN), and 0.15% (77 kN), respectively. In case of specimen 4, cracks in infill commenced at a drift level of 0.31% (-61 kN, +75 kN), 3 courses above and below the mid-height of the panel

and later these bed joint sliding cracks were joined by diagonal stepped cracks. Bed joint sliding cracks in ductile retrofitted frame (Specimen 5) were initiated away from the mid-height of the infill panel at 0.15% (57 kN) drift level two courses below the soffit of the beam. Similar sliding cracks were formed away from mid height of the panel four courses above the bottom beam at next drift level of 0.32% (60 kN), with vertical cracks along the column-wall interface. In case of specimen 7, bed joint sliding cracks in infill initiated four courses below the soffit of the top beam at a lateral load of 77 kN (0.15% drift). Later similar cracks were formed nine courses above the top of the bottom beam away from the mid-height of the infill panel in the subsequent 0.31% drift (-66 kN, +76 kN) in addition to cracks along the column-wall interface [Fig. 4.7(g)].

Formation of bed joint sliding cracks away from the mid-height weakened the interface connection between infill and column, and decreased the effective length of column in contact with infill (thus creating captive column effect). This resulted in concentration of the entire inter-storey drift within the column free length, thereby increasing the chord rotation demand at both ends of the columns. Since the shear span (moment to shear ratio) for captive columns is short, diagonal shear cracks (diagonal tensile cracks) developed/initiated along the free length of the columns at a smaller drift level. Similar behavior of masonry infilled RC frames is also reported in past literature (Fardis 2009). Due to the formation of bed joint sliding cracks away from the mid-height of infill panel in specimens 4, 5, and 7, diagonal shear cracks initiated in columns at a smaller drift level of 0.46% (69 kN), 0.46% (61 kN), and 0.46% (77 kN). With increase in drift levels, bed joint sliding cracks in specimens 3, 6, and 8 also started forming away from the mid-height of the panel leading to diagonal shear cracks (diagonal tensile cracks) at a drift level of 0.77% (70 kN), 0.62% (77 kN), and 0.62% (74 kN), respectively. Interestingly, the first crack formed in columns was diagonal shear crack (diagonal tensile cracks) in most of the infilled specimens.

As the drift levels increased, flexural cracks initiated along the length of the columns. In specimens 3, 6, and 8 flexural cracks initiated almost simultaneously along with diagonal shear cracks (Table 4.3), whereas the flexural cracks in specimens 4, 5, and 7 were delayed as most of the cracks formed in infill. In all the infilled frame specimens, very few cracks formed in the beams due to the strong T-beam action provided by the slab. Subsequent widening of shear cracks, spalling of cover concrete and buckling of

longitudinal reinforcement was observed in case of ductile frames infilled with full-scale and half-scale bricks (Specimens 3 and 7). In case of non-ductile infilled frames, opening of 90^{o} hook along with widening of shear cracks and buckling of longitudinal reinforcement was observed. Damage to infills in both the retrofitted frames (Specimens 5 and 6) was lesser compared to the original frames (Specimens 3 and 4).

From the available strain gauge data, photographic study, and from visual inspection, it was observed that the shear cracks in the columns were formed much earlier than the first yielding of the column reinforcing bars. Further, widening (opening) of shear cracks in columns also occurred before the yielding/buckling of reinforcing bars in columns. In specimen 3 (ductile frame), widening of shear cracks and subsequent spalling of concrete was observed at a drift level of 4.3% followed by buckling of longitudinal reinforcement near the column ends at a drift level of 4.62%. Whereas, specimen 4 (non-ductile frame) observed widening of diagonal shear cracks at a lower drift level (2.46%) with subsequent buckling of longitudinal reinforcement at 3.38% drift level. In case of retrofitted frames, widening of shear cracks was observed at a drift level of 3.38% and 2.15% for specimens 5 and 6, respectively. From the analysis of strain data, it was observed that yielding/buckling of longitudinal reinforcement occurred at 4% (Specimen 5) and 2.76% drift level (Specimen 6). Specimens 7 and 8 observed widening of shear cracks at 2.76% and 2.46% drift, respectively, and yielding/buckling of longitudinal reinforcement at about 3.38% drift level.

The tests were terminated when the capacity of the specimen reduced to about 75% of its maximum or when the failure was evident. Most of the cracks developed near the column ends in infilled frames were primarily diagonal in nature (45^{o} to the direction of loading) due to the diagonal strut effect of infill along the contact length of column. With increase in drift level, widening of the diagonal shear cracks followed by spalling of concrete between the widened cracks was observed. This resulted in opening of hooks of shear reinforcement followed by yielding/buckling of longitudinal reinforcement in the spalled concrete region. A few flexural cracks were also formed in the columns of some specimens parallel to the direction of loading; these cracks propagated towards the shear cracks with increasing drift. This observed behavior of infilled frames was completely different than the bare frame, which exhibited flexural mode of failure. Based on these observations, the failure mechanism in case of infilled frames was termed as shear failure

of columns. Similar failure mechanisms were also reported in the past experimental studies (Mehrabi et al. 1996; Al-chaar et al. 2002; Blackard et al. 2009). The test was terminated at a drift level of 4.62% (-39 kN, 47 kN) and 3.69% (-35 kN, 52 kN) in ductile and non-ductile infilled frames (Specimens 3 and 4), respectively, when crushing or spalling of concrete along the diagonal shear cracks and buckling of longitudinal reinforcement was observed in both the columns [Figs. 4.7(c and d)].

In case of retrofitted frames (Specimens 5 and 6), the tests were terminated when both the columns failed in shear and crushing or spalling of concrete between the widened shear cracks was observed at lateral drift level of 4.31% and lateral load level 48 kN for both specimens [Figs. 4.7(e and f)]. Specimens 7 and 8 with half-scale bricks were tested till a drift level of 3.38% (58 kN), and 4.31% (41 kN), respectively, when shear failure in column and out-of-plane movement of infill wall was observed [Figs. 4.7(g and h)]. In the current study, frames with a moderately higher aspect ratio ($h/l \approx 1$) were tested, and it was observed that all the infilled frames failed due to shear failure of columns. Therefore, it becomes important to find out methods for improvement of lateral load behavior of masonry infilled RC frames such that shear failure of columns can be prevented.

4.8 Improving Shear Capacity of Masonry Infilled RC Frames

The frames considered in the current study were designed to exhibit flexural behavior. However, columns of the frames failed in shear failure mode when infill walls were introduced. This is primarily due to excessive shear demand on columns from infills for which the columns were not designed. Past literature (Mehrabi et al. 1996; El-Dakhakhni et al. 2003; Kakaletsis et al. 2011) reported that columns do not fail in shear in case of strong frame-weak infill configuration. But in the current study, though strong frame-weak infill configuration was used, all the columns of infilled frames failed in shear mode irrespective of the reinforcement detailing in RC members (ductile or non-ductile) and size of bricks used (full-scale or half-scale).

In order to prevent/delay the shear failure in columns, shear design of columns was upgraded following the guidelines of IS 13920 (1993) and Eurocode 8 (CEN 2004b). IS 13920 recommends special confining reinforcement in columns, only if significant variation in stiffness is observed along the column length. Area of shear reinforcement required as special confining reinforcement (A_{sh}) can be calculated using Eq. (4.1).

$$A_{sh} = 0.18 s h_c \frac{f_{ck}}{f_y}\left(\frac{A_g}{A_k} - 1\right) \tag{4.1}$$

where A_{sh} is the area of the bar, s is the spacing of transverse reinforcement, h_c is the longer dimension of the rectangular confining core measured to its outer face, A_g is the gross area of the concrete section, and A_k is the area of the confined core in the rectangular hoop measured to its outside dimensions. In the current study, special confining reinforcement in critical regions works out to be 3 legged, 8 mm diameter bars at a spacing of 90 mm.

Similarly, according to Eurocode 8 (CEN 2004b), the amount of transverse reinforcement required to be provided in critical regions of column sections especially at column base should satisfy Eq. (4.2). The required volumetric ratio (ω_{wd}) works out to be about 0.65 in the present study, whereas, in case of special confining reinforcement using Eq. (4.1), it was found to be 0.71.

$$\alpha\omega_{wd} \geq 30\mu_\varphi \nu_d \varepsilon_{sy,d} \frac{b_c}{b_0} - 0.035 \tag{4.2}$$

$$\alpha_n = 1 - \sum_n \frac{b_i^2}{6 b_0 h_0}, \quad \alpha_s = \left(1 - \frac{s}{2b_0}\right)\left(1 - \frac{s}{2h_0}\right) \tag{4.3}$$

where α is confinement effectiveness factor ($=\alpha_n\alpha_s$), ω_{wd} is mechanical volumetric ratio of confining hoops within the critical regions, μ_φ is curvature ductility factor, ν_d is normalized design axial force, $\varepsilon_{sy,d}$ is design value of the tension steel strain at yield, b_c and b_o represent the width of gross cross section and confined core, respectively, n is number of longitudinal bars laterally engaged by hoops or cross ties, s is the spacing of the transverse reinforcement, b_i is the distance between the consecutive engaged bars, and h_0 is the depth of the confined core. Since IS 13920 requirements were found to be more stringent, columns were provided with 3 legged stirrups of 8 mm diameter bars at 90 mm spacing. Both IS 13920 and Eurocode 8 recommend the length of critical region (from the face of the joint), in which closely spaced shear reinforcement is required to be provided, as larger of: largest dimension of member, 1/6 of the clear span, and 450 mm. In the current study, the critical length comes out to be 450 mm.

To verify the effectiveness of these detailing provisions in earthquake standards in preventing or delaying shear failure in RC columns of infilled frames, three ductile frames infilled with full-scale bricks with different shear reinforcement in columns were tested in the second stage. In the first infilled frame with improved shear capacity throughout the length of the column (Specimen 9), 8 mm diameter bars (f_y = 460 MPa) with 3-legged stirrups were provided at 90 mm spacing throughout the length of the column. In the second infilled frame with improved shear capacity in critical regions only (Specimen 10), 8 mm diameter bars (f_y = 460 MPa), 3-legged stirrups were provided at 90 mm spacing only in critical regions (about 500 mm from the face of top and bottom beam), and a spacing of 110 mm was maintained in the remaining length. In case of specimen 11, high strength deformed bars were used in both longitudinal (f_y = 530 MPa) and transverse reinforcement (f_y = 520 MPa). The shear reinforcement consisted of 3-legged, 6 mm diameter bars at a spacing of 90 mm in critical regions only.

4.8.1 Lateral Load Response of Frames with Improved Shear Capacity

In the second stage, slow cyclic lateral load tests were carried out on three specimens in which shear capacity of columns was enhanced and the results are reported in Table 4.3 and Fig. 4.8. It can be observed that the hysteresis loops were closely spaced in the initial drift levels until infill reached its capacity, and later the loops were unevenly spaced as observed in the previous specimens. Fig. 4.9 compares the lateral load-drift envelope and energy dissipation curves obtained for frames infilled with improved shear capacity with that obtained for original infilled frames.

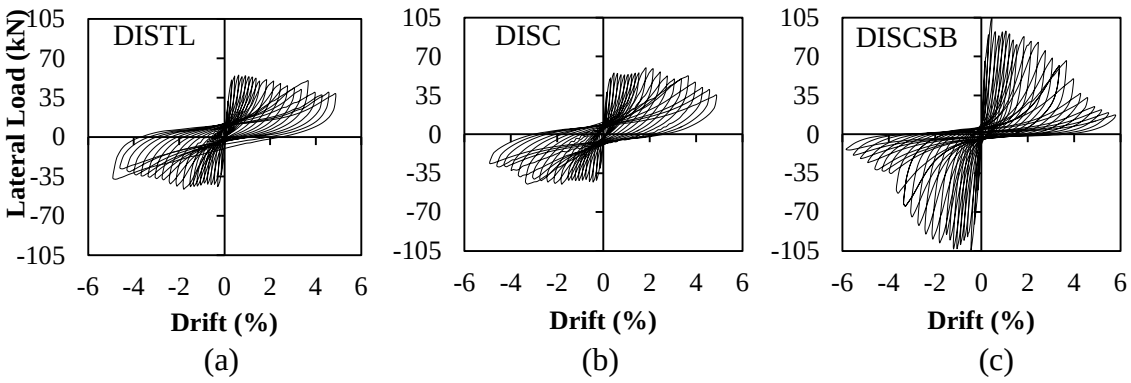

Fig. 4.8. Hysteretic response of ductile infilled frame (Specimens 9-11) with: (a) improved shear capacity throughout the length of column; (b) improved shear capacity in critical regions only; (c) improved shear capacity in critical regions using high strength bars.

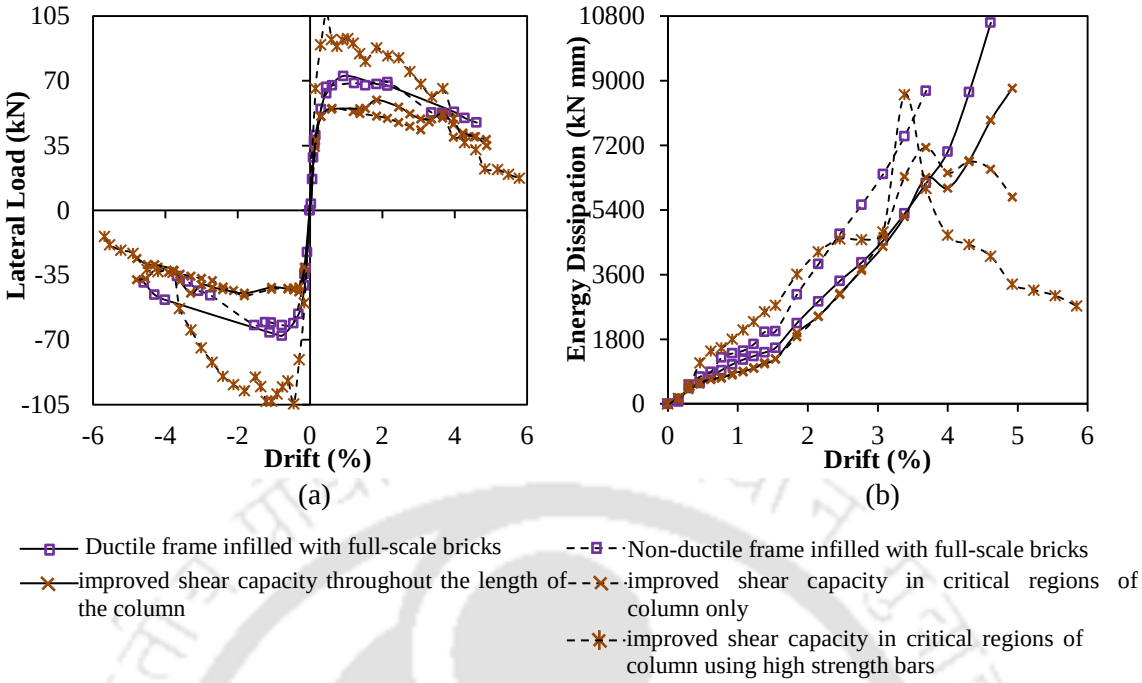

Fig. 4.9. Comparison of lateral load behavior of specimens 3, 4, 9, 10 and 11: (a) envelope curves showing force vs. drift at actuator level; and (b) energy dissipation.

Though the initial stiffness of frames with improved shear capacity throughout length of the column and in critical regions was similar to that of the original infilled frame specimens (Table 4.3), ductile frame with improved shear capacity using high strength bars exhibited about 15% more lateral stiffness. Lateral load carrying capacity of shear capacity improved frames (Specimens 9 and 10) was slightly lower than that of ductile frame infilled with full-scale bricks due to the use of weaker and brittle reinforcing bars. Degradation of lateral load carrying capacity was found to be gradual in case of improved frames (Specimens 9 and 10), whereas, sudden dropdown was observed in case of previously tested infilled frame specimens [Fig. 4.6(a)].

Frame with improved shear capacity using high strength bars (Specimen 11) exhibited highest lateral load carrying capacity (about 1.5 times that of original ductile infilled frame) at a very low drift level (0.46%). Nevertheless, the subsequent sudden dropdown was observed in strength similar to that observed in the original infilled frame specimens (Specimens 3 and 4). Energy dissipated by frame with improved shear capacity throughout the length of the column and in critical regions was similar to that dissipated by the previously tested infilled frames [Table 4.3 and Fig. 4.9(b)], whereas, energy dissipation by frame with improved shear capacity using high strength bars was

significantly higher. Experimental results showed that using special confining reinforcement is beneficial in enhancing the lateral load behavior of infilled frames, especially in improving the post-peak load behavior, energy dissipation, and ultimate deformation capacity.

Effectiveness of using regular and spiral rectangular shear reinforcement in columns of one third-scale infilled RC frames was investigated by Kakaletsis et al. (2011) under two cycles of reversible loading. It was reported that the average lateral strength and energy dissipation of the weak infilled frame was about 1.84 and 1.64 times that of the bare frame, respectively. In the current study, the lateral load carrying capacity and energy dissipation capacity of the improved frames was found to be about 1.2 to 2.4 and 1.42 to 1.78 times that of the bare frame, respectively, for three cycles of lateral loading.

As observed in original infilled frame specimens (Specimens 3 and 4), first major crack in case of frames with improved shear capacity throughout the length of the column and in critical regions only (Specimens 9 and 10) was observed along the column-wall interface and bed joints at a drift level of 0.31% (51 kN) (Fig. 4.10). In case of frame with improved shear capacity in critical regions using high strength bars (Specimen 11), cracks appeared in infill as diagonal stepped cracks with bed joint sliding cracks near the mid-height of infill panel at a drift level of 0.46% (107 kN). Till 0.62% drift level most of the cracks were concentrated in infill.

(a) (b) (c)

Fig. 4.10. Failure mechanisms observed in specimens 9-11: (a) ductile infilled frame with improved shear capacity throughout the length of column; (b) ductile infilled frame with improved shear capacity in critical regions; and (c) ductile infilled frame with improved shear capacity in critical regions using high strength bars.

At a drift level of 0.77%, flexural cracks along the length of the column and diagonal shear cracks near the ends of columns developed in specimens 10 and 11,

respectively, whereas in case of frame with improved shear capacity throughout the length of column (Specimen 9), flexural cracks and diagonal shear cracks in columns developed at a higher drift 0.92% (54 kN). Interestingly, shear cracks initiated at a lower drift level of 0.46% (Specimens 4, 5, 7) to 0.77% (Specimen 3) in original ductile and non-ductile infilled frame specimens (Table 4.3). Therefore, providing special confining reinforcement in columns may help in delaying the initiation of shear cracks in columns. With increase in drift level, further sliding of brick layers and formation of flexural cracks along the length of the columns was observed.

The frame with improved shear capacity using high strength deformed bars (Specimen 11) enhanced the lateral load carrying capacity and stiffness but the amount of shear cracks in columns was significantly more compared to specimens 9 and 10. Clearly, use of lower yield strength reinforcing bars in columns did not result in improved performance due to buckling of longitudinal reinforcement. But even before buckling of longitudinal steel in column, significant damage occurred in column due to the formation of shear cracks. In case of specimens 9, 10, and 11 widening of shear cracks was observed at a drift level of 4%, 3.69%, and 2.46%, respectively. Subsequently, spalling or crushing of concrete was observed between the widened shear cracks at a drift level of 4.6%, 4.3%, and 3.69% respectively. The tests were terminated when out-of-plane fall out of infill, buckling of longitudinal reinforcement was observed in the spalled concrete region at a drift level of 4.92% (Specimens 9 and 10) and 5.85% (Specimen 11).Figure 10 represent the failure pattern observed at the termination of tests, where it appears that failure was by flexural hinging in columns near the column ends, but it was observed during testing, that spalling of concrete and buckling of reinforcement occurred due to the widening of shear cracks. Therefore, the failure mode was termed as shear failure in columns. Though infilled frames with improved shear capacity showed better behavior compared to all other infilled frames in terms of delaying shear failure, it fell short of expectations, as the desired behavior (flexural failure of columns instead of shear failure) could not be achieved.

4.9 IDEALIZATION OF LOAD-DISPLACEMENT RELATIONSHIP FOR INFILLED FRAMES

The drift levels corresponding to onset of major damage in masonry infilled RC frames, as also discussed by other investigators (Mehrabi et al. 1996; Al-chaar et al. 2002), can serve as a guideline for design of similar infilled frames for a particular performance level. Using the lateral drift levels obtained in the current study (Table 4.3), an idealized load-displacement relationship is proposed (Fig. 4.11) by considering the average points corresponding to the onset of major events (infill cracks, shear cracks, flexure cracks, peak load, and 80% post peak load). The lateral load on primary y-axis of Fig. 4.11 is normalized with the average lateral load carrying capacity, and the secondary y-axis shows the base shear ratio (lateral load normalized with seismic weight). Large deviations in a set of values is not considered while averaging particular set of data and the considered values are clubbed into a set of packets (dotted line boxes in Fig. 4.11).

The first major event observed was initiation of cracks (diagonal and sliding) in infill. Infilled frames behaved linearly till an average drift level of 0.23% [coefficient of variation, COV of 0.36] corresponding to a load level of about 78% of lateral load capacity [COV of 0.17]. Similarly, Mehrabi et al. (1996) tested half-scale RC frames infilled with strong and weak masonry under monotonic and cyclic loading and defined serviceability limit state as the drift corresponding to the initiation of damage in infills. Subsequently, RC columns start behaving non-linearly as shear cracks and flexural cracks are initiated at a drift level of 0.58% [COV of 0.22] and 0.88% [COV of 0.17], respectively, corresponding to a lateral load of about 95% [COV of 0.05] and 100% [COV of 0.09], respectively, of the peak load. It can be observed that lateral strength of most of the specimens reached at a drift level corresponding to the initiation of flexure cracks in columns. The post-peak drift corresponding to 80% [COV of 0.14] of the lateral strength of the infilled frame was in the range of 1.9% to 3.8%, with an average value of 2.6% [COV of 0.24]; this can be regarded as ultimate limit state. The design drift level (0.4%) of the frame based on IS 1893 (BIS 2002b) was reached before the initiation of any major cracks in the frame elements at about 80% of the lateral strength of the infilled frame. Lateral drift values reported by Mehrabi et al. (1996) for RC frames infilled with weak masonry were 0.17% to 0.36% for serviceability limit state, 1.02% to 1.88% for ultimate limit state, and 1.7% to 2.6% considering ultimate deformation. The lateral drift

observed in the current study was significantly higher when compared to previous studies, due to the strong frame-weak infill configuration.

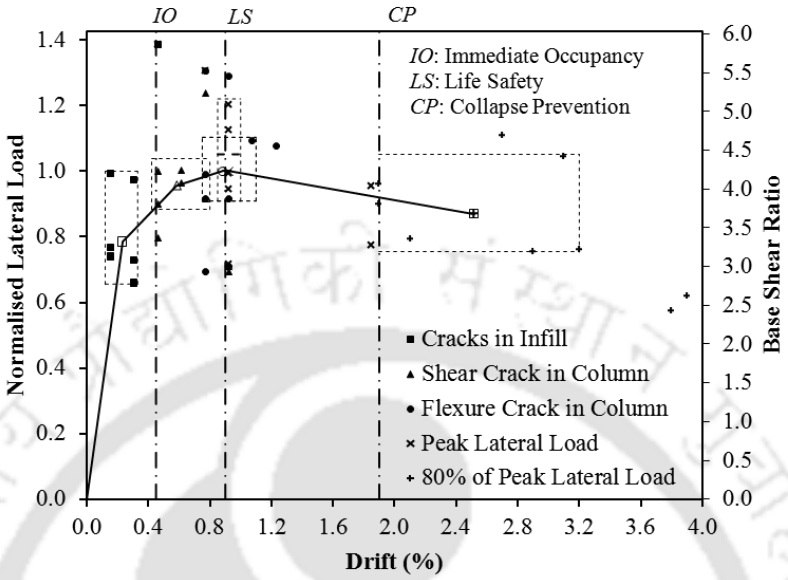

Fig. 4.11. Idealized load-displacement relationship for masonry infilled RC frames.

Based on these observations, three performance levels - *IO* (Immediate Occupancy), *LS* (Life Safety), and *CP* (Collapse Prevention) are suggested for the tested infilled RC frames. The performance level *IO* may be defined at a drift level of 0.45% before the onset of any major cracks (shear or flexure) in RC columns (infills may crack). According to ASCE 41, *IO* refers to minor cracking of both masonry infills and RC members followed by minor spalling of concrete cover. *LS* performance level may be defined at a drift level of 0.90% where significant shear cracks developed in columns and flexural cracks were initiated; at this level the lateral strength of the system was attained. ASCE 41 recommends *LS* level corresponding to extensive cracking and damage in infills and beams, and shear cracking in ductile columns. In the current study, *LS* is limited to cracking in infills and shear cracking in columns as no significant damage was observed in beams due to T-beam action. Since the lateral load behavior of infilled frames is quite brittle, *CP* performance level may be fixed at a drift level of 1.9% corresponding to initiation of significant drop in capacity (80% of lateral strength). According to ASCE 41, *CP* refers to extensive cracking and hinge formation in RC members. The idealized load-displacement curve proposed in the study is developed based on the limited study involving many uncertainties and the results need to be employed cautiously.

4.10 SUMMARY

Seismic design codes of many countries neglect the contribution of masonry infills in lateral load resistance and design RC frames as bare frames. On the other hand, a few national codes (IS 13920, Eurocode 8, and ASCE 41) have specific provisions for design and detailing of columns in such buildings. Effectiveness of such provisions in improving the lateral load behavior of infilled frames was assessed by carrying out an experimental study using full-scale and half-scale fly ash bricks for two types of detailing in two stages. From the experimental results of the first stage, it was found that infilled frames (using both full-scale and half-scale bricks) were significantly stiffer and stronger, and dissipated more energy than the corresponding bare frames. Though mortar to brick thickness was quite high in case of half-scale brick specimens, their lateral load behavior was quite similar to that of the specimens with full-scale bricks. The beneficial effect of ductile detailing in RC members was observed in the post peak regime of load-displacement curves in the form of gradual drop-down in capacity. Even though the influencing parameters were significantly enhanced, it was observed that columns of infilled frames failed in shear mode.

To prevent or delay shear failure of RC columns, shear capacity of columns was enhanced in the second stage by following special confining recommendations of IS 13920, and Eurocode 8. From the results, it was ascertained that using special confining reinforcement is beneficial in enhancing the lateral load behavior of infilled frames and delaying the initiation of shear cracks; however, shear failure of columns could not be prevented. The detailing provisions in current codes of practice do not seem to prevent the shear failure in RC columns. The shear demand on the column due to the detrimental effect of infill needs to be estimated so as to propose methodologies to counteract the adverse effect of infill. In the next chapter the shear demand on the column due to the local adverse effect of infill is estimated both numerically and analytically using capacity of infill obtained in the previous chapter for the considered infilled frame specimens in the current chapter.

Chapter 5
ASSESSMENT OF SHEAR FAILURE IN COLUMNS OF MASONRY INFILLED RC FRAMES

CONTENTS

5.1 OVERVIEW

From the preliminary experimental evaluation and past experimental studies, it was clearly understood that the masonry infilled reinforced concrete (RC) frames are known to have high seismic vulnerability under strong ground motions due to the detrimental effect of infill. From the past studies (Mehrabi et al. 1996; Al-chaar et al. 2002; Fardis 2009), it was understood that stronger the infill, the larger the force exerted by them on the frame members, which increases the possibility of the failure of the columns in shear. Therefore, determination of shear demand on columns due to the detrimental effect of infill, both numerically and analytically, is of primary importance for proper design that results in ductile flexural failure.

To understand the phenomenon of local interaction effects of infills, large number of studies were carried out both analytically and experimentally and recommendations were incorporated in the national technical standards of various countries. A comprehensive review of the clauses on design of masonry infilled RC frames in various earthquake codes showed that generally two types of approaches were considered in the standards: whether to or not to consider infill in the design (Kaushik et al. 2006). Some design standards recommend isolating masonry infill from the frame system, such that the

masonry does not affect the lateral stiffness of the structure. On the other hand, some provide guidelines on analytical modelling to consider the local adverse effects of infill, but there is no clear understanding on their applicability. Therefore, an attempt has been made in the current study to understand the modelling recommendations that consider the local effects of infill in the analysis of masonry infilled RC frames.

A comprehensive review of the various modelling techniques for masonry infilled RC frames has been amalgamated in the literature (Asteris et al. 2011; Asteris et al. 2013; Di Trapani et al. 2015). Most of the past analytical studies resorted to macromodelling techniques, especially modelling infill as equivalent diagonal strut, due to the simplicity involved in modelling. The major drawback of equivalent diagonal strut model lies in its inability to estimate the realistic shear forces and bending moments in the frame members further leading to its inability to capture the local shear failure of the members. As discussed in chapter 2, in the recent years some emphasis was laid to improve the models to capture the component shear failure (D'Ayala et al. 2009; Celarec and Dolšek 2013; Cavaleri and Di Trapani 2015; Fiore et al. 2016). Due to the complications involved and the computational difficulties in evaluating the parameters, there is a need to improve the simplistic macromodelling technique, especially the equivalent diagonal strut model, for practical engineering purpose in order to capture the global as well as the local behavior of the frames.

In the current chapter, applicability of the technical standard recommendations to estimate the shear demand on the columns is discussed, and improvement is suggested in simplified macromodelling technique to capture the component shear failure of columns due to the local adverse effect of infill. Initially, the shear demand on the columns was estimated numerically based on the recommendations of the seismic technical standards. Later, the effectiveness of the existing macromodels in predicting the lateral load behavior was evaluated, followed by a proposal for the improvement in the single-strut macromodel. The improved analytical macromodelling technique was also verified using the results of past experimental studies.

5.2 Estimation of Shear Demand on Columns

The shear demand on the columns due to the local adverse effect of infill was evaluated numerically and analytically following the codal recommendations and analytical

macromodelling, respectively. Three half-scale specimens (BF, IF-FB1 and IF-FB2) from the preliminary experimental study were considered to evaluate the local adverse effects of infills and to understand the recommendations of the current seismic standards. For convenience sake, the notations of specimen 3 (DFS) and specimen 9 (DISCSB) from preliminary experimental study were modified to IF-FB1 and IF-FB2, respectively. The results of bare frame (BF) using high strength bars were considered from the study carried out by Surendran (2012). The major difference between the two infilled frame specimens was that the shear capacity of the column sections in case of IF-FB2 was enhanced by approximately two times compared to that of IF-FB1 by using high strength bars. Additionally, masonry infilled frames constructed in different regions using three different types of infills from the past experimental studies were also considered: IF-CT (weak frame infilled with solid concrete bricks, Mehrabi et al. 1996); IF-CM1 (non-ductile frame infilled with clay bricks, Al-chaar et al. 2002); and IF-CM2 (infilled frame with clay bricks; Cavaleri and Di Trapani 2014) as shown in Table 5.1. The specimens were single-storey, single-bay, half-scale frames constructed with different strength infills. The specimens represented the ground-storey frame of older framed structures designed using the non-seismic design provisions. Experimental results of these studies showed shear mode of failure of columns under in-plane lateral loads.

Table 5.1. Details of infilled frame specimens

	IF-CT	IF-CM1	IF-CM2
Frame Properties (mm)			
Bay width	2134	2032	1600
Bay height	1422	1524	1600
Column depth	178	203	200
Column width	178	127	200
Beam depth	229	197	400
Beam width	153	127	200
Column longitudinal reinforcement	8-12.7Y*	4-10Y	4-10Y
Column ties	6.35Y at 63.5 c/c	4.88Y at 152 c/c	6Y at 100 c/c
Beam longitudinal reinforcement	4-15.87Y	4-10Y (top) 2-10Y (bottom)	6-10Y
Beam ties	6.35Y at 76.2 c/c	4.88Y at 76 c/c	6Y at 80 c/c
Material Properties (MPa)			
Concrete compressive strength	20.8	38.4	25.0
Elastic modulus of concrete	18,052	29,992	25,500
Brick compressive strength	15.6	80.9	37.7
Mortar compressive strength	17.6	10.6	9.2
Masonry prism strength	13.8	26.7	8.2
Yield strength of reinforcing bars	420.3	338.5	450

*8-12.7Y represent 8 number of 12.7 mm diameter bars.

Masonry infill was modelled as equivalent diagonal strut to consider its influence in structural analysis as per the recommendations of some earthquake standards (Eurocode 8; ASCE 41; MSJC). Eurocode 8 (CEN 2004b) does not suggest a specific model to evaluate the effect of infill, but requires verifying the columns for the shear forces acting on the contact length over which the diagonal strut force is applied. MSJC (2013) specifies participating infills to be modelled as equivalent diagonal compression strut and suggests equations to evaluate the parameters of strut, whose applicability needs to be verified. In general, various parameters that govern the equivalent diagonal strut modelling are the geometrical properties and strength of the strut. Therefore, to estimate the shear demand on the column, estimation of shear capacity of the columns, definition of parameters, such as strength of the infill, width of the strut, contact length of the column is of significance to obtain a realistic response. Detailed calculation of the mentioned parameters is discussed in the following sections.

5.2.1 Calculation of Shear Capacity of Column Sections

Prior to the evaluation of shear demand, realistic shear capacity of the column sections was evaluated following various design standards: IS 456 (BIS 2000), ACI 318 (2008), Eurocode 2 (CEN 2004a), ASCE 41 (2013), and Eurocode 8 (CEN 2005b). The equations to evaluate the shear capacity of the column sections are presented in chapter 2. The shear capacity calculation for the considered infilled frame specimens is shown in Table 5.2. From the table it can be observed that the shear capacity calculated following IS 456, Eurocode 2 and ACI 318 was found to be almost same with the variation in the calculation of shear resistance of concrete as discussed in chapter 2. The shear capacity evaluated following ASCE 41 (2013) and Eurocode 8 (CEN 2004b) was found to be lesser than the other design standards due to the consideration of cyclic degradation.

Table 5.2. Calculation of shear capacity of columns

Type of Frame	IS 456 (BIS 2000)			ACI 318 (2008)			Eurocode 2 (CEN 2004a)			ASCE 41 (2013)			Eurocode 8 (CEN 2005b)		
	V_C*	V_S	V	V_C	V_S	V	V_C	V_S	V	V_C	V_S	V	V_C	V_S	V
IF-FB1	22.6	36.1	59	12.7	36.1	49	16.9	36.1	53	7.5	25.3	33	12.8	19.1	32
IF-FB2	22.7	72.5	95	13.7	72.5	86	17.6	72.5	90	7.9	50.8	59	13.6	38.4	52
IF-CT	46.2	53.5	100	26.9	53.5	80	37.9	53.5	91	17.6	37.4	55	36.5	20.2	57
IF-CM1	20.4	15.3	36	24.1	15.3	39	19.9	15.3	35	12.2	10.7	23	8.7	11.0	20
IF-CM2	37.2	43.0	80	34.9	43.0	78	41.8	43.0	85	22.5	30.1	53	30.4	22.1	52

*V_c, V_s, and V represent the contribution to shear resistance by concrete and shear reinforcement, and total shear resistance of the concrete section, respectively.

5.2.2 Evaluation of Masonry Infill Parameters

Various formulations were proposed in the literature to evaluate the geometric properties of the equivalent diagonal struts. In the present study, the effective width of strut (w_s) was calculated as a fraction of diagonal length of infill (l_d) using the equations proposed in the past studies and is shown in Fig. 5.1. Most of the experimental investigations and some technical standards (*e.g.*, ASCE 41) recommend the equation proposed by Mainstone (1971) to estimate the width of the strut as it provides lower bound estimate for the width of the strut, and has been implemented by many researchers. Other equations proposed by Liauw and Kwan (1984), Decanini and Fantin (1987), Paulay and Priestley (1992) and Hendry (1998) overestimated the width of the strut. The width of the strut calculated based on MSJC (2013) was found to be quite smaller when compared to that calculated using Mainstone's equation.

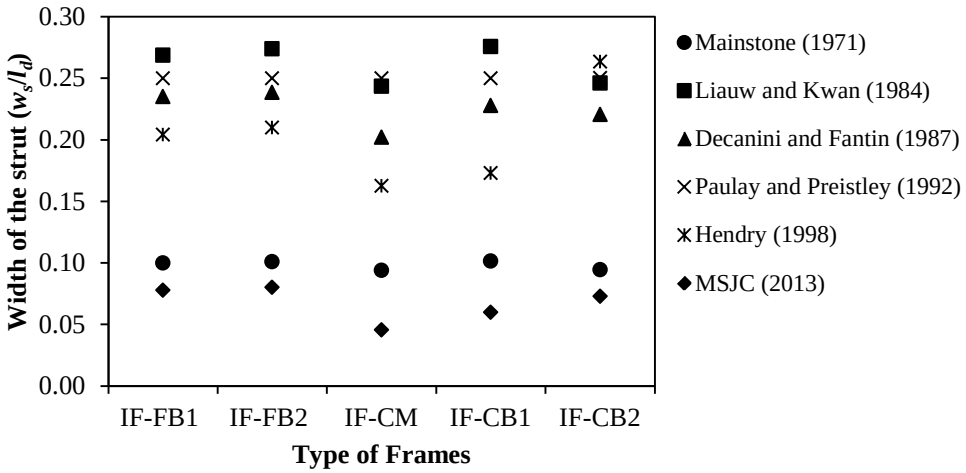

Fig. 5.1. Calculation of width of strut using various formulations.

The other significantly important geometric parameter in the masonry infill modelling is the contact length (l_c) between the infill and the column, to simulate the frame-infill interaction under lateral loading. Smith (1966) formulated the contact length for columns and beams on the basis of behavior of beams on elastic foundation. In the current study, the contact length was calculated based on geometric calculations as well as empirical relationships. In case of geometric calculation, the contact length is calculated by assuming full width of the strut forming along the length of the column (width of the strut was placed eccentrically) as specified in Eurocode 8 (CEN 2004b). The contact length (l_c) along the column length was calculated using Eq. (5.1).

$$l_c = \frac{w_s}{\cos\theta_c}, \tan\theta_c = \frac{[h-(w_s/\cos\theta_c)]}{l} \quad (5.1)$$

where h represent the clear height of the column; l represent the centre to center distance between the columns; θ_c is the angle of the eccentric strut with respect to the horizontal. The empirical equation proposed by Smith (1966) was considered to calculate the contact length (l_c) of the column as given in Eq. (5.2).

$$l_c = \frac{\pi}{2}\left[\frac{4E_c I_c h_m}{E_m t_m \sin 2\theta}\right]^{\frac{1}{4}} \quad (5.2)$$

where E_c and E_m represent the modulus of elasticity of concrete and masonry, respectively; I_c represent the moment of inertia of column; l_m, h_m, t_m are the length, height and thickness of the infill wall, respectively; and θ is the angle between the horizontal and the panel diagonal. The contact length calculated using Eq. (5.1) was found to be realistic where the whole width of the equivalent diagonal strut was considered to act on the column rather than on the beam. From Table 5.3, it is observed that the contact length of the column calculated based on empirical relation was very high when compared to geometric calculations. Moreover, l_c estimated using Eq. (5.2) was found to be quite high compared to experimental observations. Therefore, for further analysis the contact length calculated based on geometric relationships (Eq. 5.1) has been considered.

Table 5.3. Calculation of contact length of column

Type of Frame	Eq. 5.1 (mm)	Eq. 5.2 (mm)
IF-FB1	274	612
IF-FB2	279	629
IF-CT	309	512
IF-CM1	292	571
IF-CM2	278	609

From the past studies, it was observed that the calculation of the masonry infill parameters mainly depend on the failure mode of the infill. Based on the past experimental and analytical studies, Asteris et al. (2011) categorised the failure of infilled frames into five distinct modes as discussed in detailed in chapter 2. The failure modes were: *corner crushing mode* observed as crushing of infill near the loaded corners;

diagonal compression mode as crushing of slender infill in the central panel; *sliding shear mode* observed as bed joint sliding cracks associated with weak mortar joints; *diagonal cracking mode* represented as cracks passing through the compressed diagonal; and *frame failure mode* with the formation of plastic hinges in frame members. In the present study, the effect of infill was evaluated based on the failure modes observed in the preliminary tests on infilled frame specimens. The infill wall was constructed in running bond pattern and failed due to the formation of bed joint sliding cracks, corner crushing, and diagonal cracking. Based on the experimental observations two infill failure modes were finalized: *crushing* and *shear*. The masonry infill crushing strength (R_{cr}) is the compressive load that the equivalent masonry strut (f'_m) can carry before crushing of masonry and was calculated using Eq. (5.3).

$$R_{cr} = f'_m w_s t_m \tag{5.3}$$

The capacity of masonry under shear forces was evaluated from the diagonal compression strength (f'_v) of masonry wallettes, which is a representative of the shear strength of the masonry panel. Shear strength (R_s) was calculated using Eq. (5.4).

$$R_s = f'_v l_m t_m \tag{5.4}$$

5.2.3 Local Effects of Infill Based on Codal Approaches

Eurocode 8 (CEN 2004b) addresses the local adverse effect of infill due to frame-infill interaction by verifying the length of the column against which diagonal strut bears in shear for the smallest of the two shear forces: the horizontal component of the strut force of the infill taken equal to the horizontal shear strength of the infill panel; and the shear force computed assuming the overstrength flexural capacity of the column developed at both ends of the contact length (l_c). According to Eurocode 8, the effect of infill was calculated as the horizontal component of bed joint force, assuming bed joint sliding is the observed failure mechanism of the infill under lateral loading.

In the present study, the failure of infill panel was calculated based on two different failure modes (crushing failure and shear failure of infill) using Eqs. (5.3) and (5.4). The shear force demand on each column due to the formation of flexural hinges

was calculated by considering design moment capacity (M_{rd}) of the section was reached at both ends of the contact length of the column (l_c) as $\gamma_{rd}(2M_{rd})/l_c$, where γ_{rd} represent the model uncertainty factor on value of resistances in the estimation of capacity design action effects, accounting for various sources of overstrength, and is taken as 1.3 for high ductility class. Table 5.4 shows the calculation of shear demand on columns due to the effect of infill and due to the formation of flexural hinges. The shear demand calculated considering the formation of flexural hinges was found to be critical in case of infilled frame with low strength bars (IF-FB1) and infilled frame with high strength bars (IF-FB2) due to strong frame-weak infill configuration. Whereas, in case of IF-CT, IF-CM1, and IF-CM2, the shear demand due to the effect of infill was found to be dominating. This may be due to the weak frame-strong infill configuration.

Table 5.4. Calculation of shear demand based on codal recommendations

Type of Frame	Column Shear Capacity	Eurocode 8 (CEN 2004b)			MSJC (2013)		
		Effect of Infill		Flexural Hinge	Capacity of Infill		
		R_{cr}	R_s	$\gamma_{rd}(2M_{rd})/l_c$	R_{cr}	$R_n/1.5$	R_{hor}
	kN	kN	kN	kN	kN	kN	kN
IF-FB1	58.6	90.8	23.1	138.2	64.4	68.6	258.3
IF-FB2	95.2	91.8	23.1	159.3	64.4	68.6	265.0
IF-CT	99.7	307.4	-*	182.2	191.1	82.0	587.3
IF-CM1	35.6	353.2	97.4	151.4	231.4	44.0	742.8
IF-CM2	80.2	107.1	128.8	226.1	195.8	110.2	778.5

*Data not available.

Besides, ASCE 41 (2013) also recommends that the shear strength of column members adjacent to an infill panel shall be higher of: horizontal component of the expected infill strut force using the shear strength of the column with zero axial load; and the shear force resulting from the development of expected column flexural strengths at the top and bottom of the column. In this case, a reduced column height equal to the distance between the flexural hinges shall be considered. Moreover, ASCE 41 recommends that the requirements to be waived off if the shear strength of the masonry is less than 0.13 MPa.

MSJC (2013) recommends designing the bounding columns in contact with infill for 1.1 times the shear and moment obtained from the equivalent strut frame analysis. Additionally, the standard requires increasing the design shear at each end of the column by the horizontal component of the equivalent strut force acting on that end under design

loads. Therefore, MSJC recommends increasing the shear capacity of the column by the horizontal component of the equivalent strut force to counteract the detrimental effect of infill on columns. In the current study, the shear demand on the column due to the effect of infill was taken as the capacity of the infill. Based on the experimental investigations of Flanagan and Bennet (1999, 2001), MSJC (2013) recommends evaluating the capacity of the infill based on three modes: corner crushing; bed joint shear failure; and horizontal component of the force in the equivalent strut at a horizontal displacement of 25 mm (Table 5.4). The strength of infill (R_{cr}) based on corner crushing failure mode was calculated using Eq. (5.5). Bed joint shear strength (R_n/1.5) was calculated based on the nominal shear strength (R_n) of the infill in accordance with MSJC. The horizontal component of the strut force (R_{hor}) was calculated from linear equivalent strut frame analysis by applying a lateral displacement of 25 mm.

$$R_{cr} = 150 t_m f'_m \tag{5.5}$$

It can be observed from Table 5.4 that the component of the horizontal racking force is significantly higher in all the considered test specimens when compared to the strength corresponding to the other two failure modes. This is because of the estimation of the strut force at a displacement level of 25 mm, which is unreasonably high. Flanagan and Bennet (1999) reported that the capacity of the infill reaches at a displacement level of 25 mm based on the results of approximately 2.4 m high to 7.3 m high infill tests. But in case of scaled specimens (considered in the present study), the height of the specimens was less than 2.5 m, and at the same time the strength of the infill was reached at a displacement level ranging from 7.5 mm to 15 mm. Based on these observations, it is recommended that the horizontal component of the strut force may be evaluated by applying a lateral displacement corresponding to the capacity of the infilled frame instead of finding out the strut force at 25 mm displacement. Similarly, the calculation of the corner crushing mode may be improved by replacing 150 in Eq. (5.5) with the width of the strut, i.e., $R_{cr} = f'_m w_s t_m$, which is more realistic. From the numerical study based on codal recommendations, the frames considered in study were found to be shear deficient under lateral loading. The shear demand on the column due to the effect of infill was found to be very high, and therefore, it becomes essential to predict the shear failure of

columns analytically so as to propose some methodologies to prevent the shear failure of columns.

5.3 Analytical Prediction of Shear Failure of Columns

Analytical study of the masonry infilled RC frames was carried out using the equivalent diagonal strut macromodelling approach (Fig. 5.2). Response of the infilled frame under lateral loading was evaluated by carrying out nonlinear static pushover analysis. Nonlinear behavior was modelled in different members by assigning appropriate load deformation material properties at predefined potential plastic hinge locations and the analysis was carried out using SAP 2000 (CSI 2015). The characterisation of the modelling parameters for the pushover analysis is discussed in the following sections.

5.3.1 Modelling Parameters of RC Members

Columns and beams of the frame were modelled using 2-noded frame elements with column ends fixed at the bottom. The dimensions of beams and columns are 115 mm × 175 mm, respectively. No damage was observed in the monolithic beam-slab during the experimental stage due to the T-beam stiffening action. Hence, linear elastic shell elements were used to model the RC slab. Nonlinearity in frame elements was modelled using lumped plasticity approach at specified hinge locations. Plastic hinge length (l_p) and location was determined based on the damage pattern observed during the experiments. It was observed that the hinges in columns were formed at a distance 90 mm from the top face of the bottom beam and bottom face of the top beam, respectively. Plastic hinge length was found to be approximately half of the depth of the column.

The nonlinear flexural hinge properties in columns were defined using axial force-bending moment interaction (P-M) as the failure envelope, and bending moment-rotation (M-θ) was used as the corresponding load deformation relation for defining flexural hinge properties in beams and columns [Fig. 5.2(c)]. Mander confined concrete model (Mander et al. 1988) and nonlinear model for rebars from the uniaxial stress-strain curves obtained from tension tests were used to define the flexural hinges. Force controlled shear hinge (V-Δ) properties involve specification of shear capacity of the sections [Fig. 5.2(d)]. This ensures that the shear hinges fail in a brittle manner as soon as the shear capacity of the section is reached. The shear capacity of the force controlled shear hinge was

calculated using the shear strength provided by the concrete and the steel reinforcement (BIS 2000) as shown in Table 5.2.

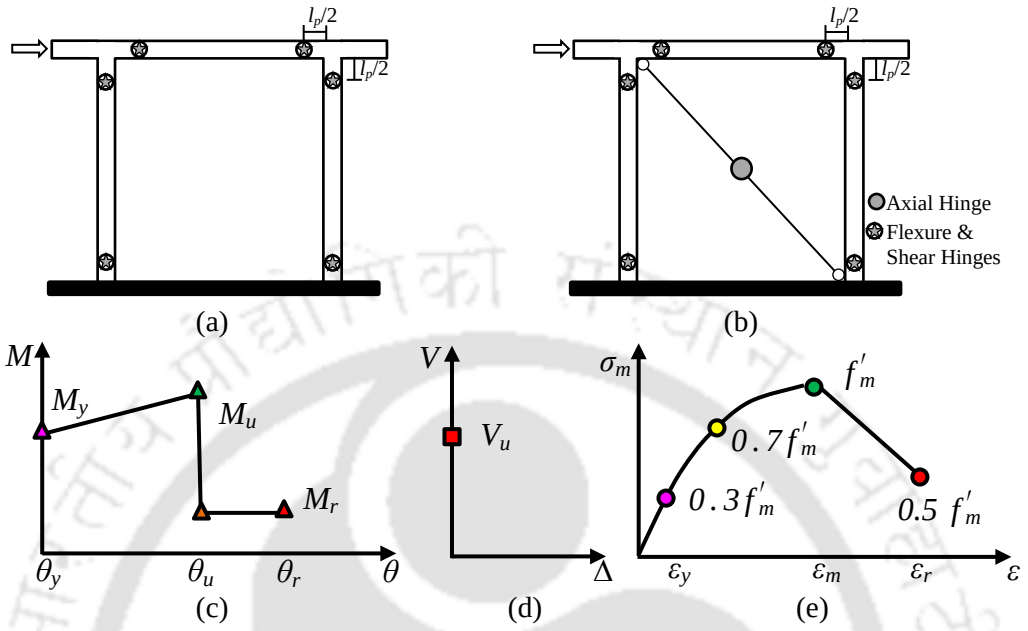

Fig. 5.2. Schematic representation of plastic hinge locations and definitions: (a) bare frame; (b) single strut model representing infilled frame; (c) M-θ relation for RC members; (d) V-Δ relation for RC members; and (e) σ_m-ε relation for masonry.

5.3.2 Masonry Infill Modelling Parameters

Masonry infill was idealised as equivalent diagonal strut [Fig. 5.2(b)] and the parameter that influences the behavior of the strut is its equivalent width, which depends on the relative infill-frame properties. Width of the equivalent diagonal strut was calculated using Mainstone's equation and was found to be about one-tenth of the diagonal length of the infill panel (Fig. 5.1). The equivalent strut was modelled as a compression element and moment releases were provided at both ends of the diagonal strut to prevent transfer of moment from beam and column to the strut. Since the equivalent strut was modelled as compression only elements, axial hinge was assumed to develop in the masonry infill at the mid-point of the strut. As suggested by the past studies (Kaushik et al. 2009; Bose and Rai 2016), nonlinear compressive stress-strain (σ_m-ε relation) curves were assigned to model the hinge properties of masonry infill as shown in Fig. 5.2(e). The average nonlinear stress-strain curve for 1:4 fly ash brick masonry with control points is shown in Fig. 5.3. More details on the nonlinear behavior of the fly ash brick masonry are given in chapter 3.

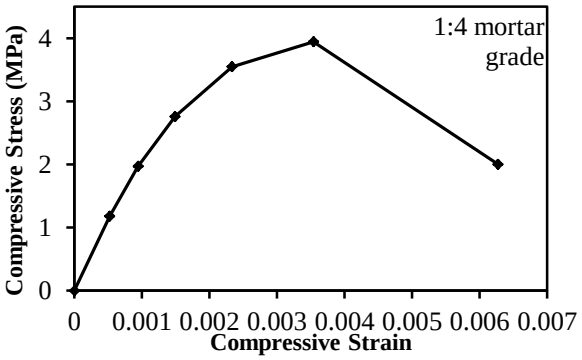

Fig. 5.3. Average compressive stress-strain curve for 1:4 fly ash brick masonry prism.

5.3.3 Analytical Results of Bare Frame and Infilled Frames

The analytical model of the bare frame was first calibrated with the experimental results and it can be observed from Fig. 5.4 that the analytical response in terms of initial stiffness and the lateral load capacity matched very well with the experimental results. In the experimental study, it was noted that the bare frame failed by forming flexural plastic hinges in columns and no damage occurred in the beam due to the stiffening action provided by the slab.

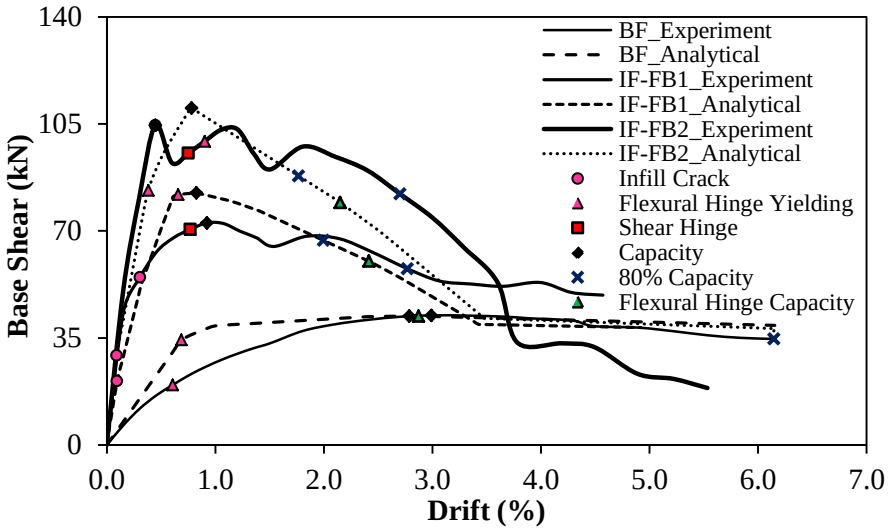

Fig. 5.4. Comparison of analytical and experimental results for bare frame (BF) and infilled frames (IF-FB1 and IF-FB2).

In the analytical bare frame model also, flexural plastic hinges were formed in columns only and no hinges were formed in beams (Fig. 5.5). Initially, flexural yielding (stage I) was observed near the bottom portion of left and right columns. Later, as the monitored drift increased, similar yielding of flexural hinges was observed near the top of

the columns (Stage II). After the lateral load capacity of the frame was attained, flexural hinge capacity was reached near the bottom (Stage III) and the top (Stage IV) of the columns. From Fig. 5.4 it can be observed that the post peak lateral load response of the bare frame was appropriately simulated by the analytical model. Therefore, it can be ascertained that global response of the bare frame can be evaluated analytically by modelling the frame elements as 2-noded elements and modelling the non-linear deformational properties by lumped plasticity approach.

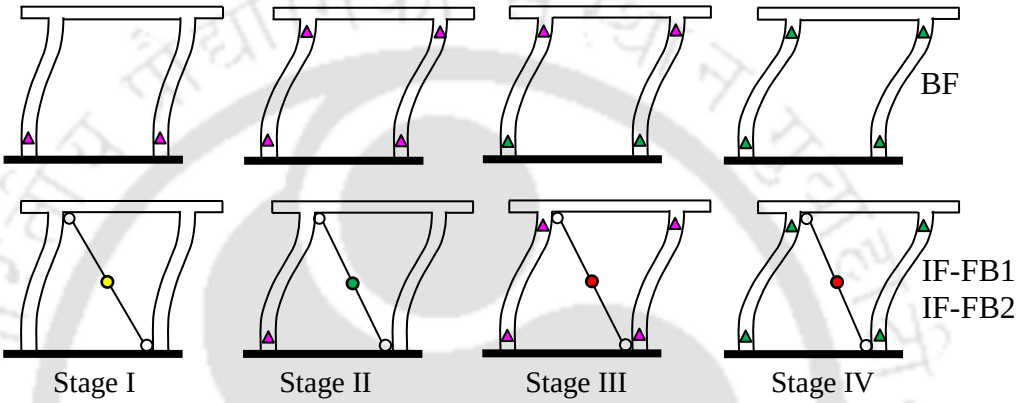

Fig. 5.5. Stages of hinge formation for bare frame (BF) and infilled frames (IF-FB1 and IF-FB2) in pushover analysis.

The same analytical model was further used to predict the response of the infilled frames by modelling infill as an equivalent diagonal strut. The comparison of experimental and analytical response along with stages of hinge formation in the infilled frames is also shown in Figs. 5.4 and 5.5, respectively. From the analytical response, it was clearly observed that the analytical strut model fittingly simulated the experimental global response of both the infilled frame specimens (IF-FB1 and IF-FB2). From the experimental study, it was observed that initially most of the lateral force was resisted by masonry infills due to their high initial stiffness. As the lateral drift increased, cracking in infill was observed followed by the attainment of capacity of the infilled frame. In case of analytical model (IF-FB1 and IF-FB2), initial yielding of axial hinges was observed followed by flexural yielding in columns (Stages I and II); prior to the attainment of the lateral load carrying capacity (Fig. 5.5). With increase in lateral drift, axial strut failed along with yielding of flexural hinges at all the plastic hinge locations (Stage III). Later on, the ultimate moment capacity (M_u) of flexure hinges (Fig. 5.2) was reached in the post peak regime after the capacity of the infilled frame ceased to about 80% of the maximum

(Stage IV). No shear hinges were formed in the analytical model, as the maximum shear force demand observed in the column was found to be far less than the shear capacity of the column. On the other hand, it was observed in the experimental study that the diagonal shear cracks were initiated in infilled frame at a lower drift level (0.77%) caused by the excessive shear demand on the column due to the frame-infill interaction. Even though the equivalent diagonal strut model was able to simulate the global response of the infilled frames, the model was unable to capture the local component failures, especially, the shear failure of the columns.

5.4 Improvement of Analytical Strut Model

From the generalized design philosophy and from the prevailing simplified strut modelling analogy, it was clearly understood that the shear force and bending moment in columns follow constant and linear variation profiles, respectively, under lateral loads (Fig. 5.6). But the past and current experimental investigations revealed that the infill exerted concentrated forces along the compression zones near the loaded corners leading to linear shear and parabolic bending moment variations in the compression zones. It was also deduced that stronger the infill, larger is the magnitude of shear forces, and higher is the likelihood of column shear failure [Fig. 5.6(d)].

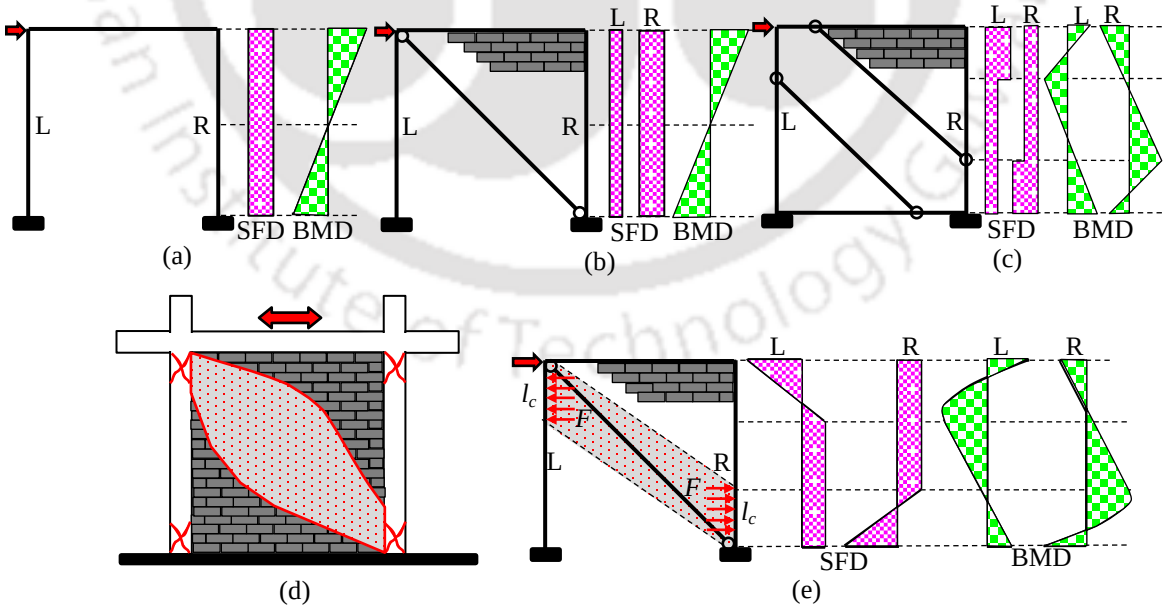

Fig. 5.6. Variation of internal force resultants for different analytical models: (a) Bare frame; (b) Infilled frame with single-strut model; (c) Infilled frame with double-strut model; (d) Shear failure of columns due to the effect of infill; and (e) Infilled frame modelled using the proposed improvement. (SFD-shear force diagram; BMD-bending moment diagram).

Similarly, it was observed that shorter the contact zone of the frame-infill interaction, higher the shear demand on the columns where it becomes difficult to verify the columns in shear. Therefore, to predict the seismic shear vulnerability of columns due to the local adverse effect of infill, the existing modelling analogy needs to be improved. This was achieved in the current study by simulating the effect of infill by applying additional shear forces incrementally along the contact length of the column as shown in Fig. 5.6(e). Initially the nonlinear analysis of the equivalent strut frame was carried out to evaluate the global response and it was calibrated with the experimental response. Then additional shear forces, F [Fig. 5.6(e)] were applied along the contact length of the column. The nonlinear pushover analysis was repeated and the response evaluation was carried out by verifying the formation of shear hinges and global response.

In the current study, it was assumed that the shear failure of the column due to the effect of infill (F) occurs only when the infill exerts maximum force onto the column. In order to evaluate this maximum force exerted by the infill on to the columns, the maximum strength of masonry infill against two failure modes (crushing and shear) calculated using Eqs. (5.3) and (5.4) was considered. Both ASCE 41 (2013) and Al-chaar (2002) recommend considering the strength of infill to be the minimum of that corresponding to crushing and shear mode, but according to Flanagan and Bennett (19991, 2001) and Maidiawati and Sanada (2016), the final failure mode of infill is crushing even though other modes of failure were observed during lateral loading. Therefore, the obtained horizontal component of the infill force (F) was applied as uniformly distributed load along the contact length (l_c) of the column.

5.4.1 Application of the Improved Strut Model

Previously tested infilled frame specimens IF-FB1 and IF-FB2 were considered to evaluate the effectiveness of the improved analytical modelling technique in predicting the global as well as local behavior of such frames. Pushover analysis of both frames was carried out and the comparative experimental and analytical envelope response of both the infilled frame specimens (IF-FB1 and IF-FB2) are plotted [Fig. 5.7(a)]. From the analytical response and various stages of plastic hinge formation [Fig. 5.7(b)], it was clearly observed that initial yielding of axial hinges was followed by flexural yielding of the frame members (Stage I). Prior to the attainment of the capacity of axial hinge in the

strut, formation of shear hinges was also observed in the columns (Stage II). This was due to the fact that the shear demand on the column due to the effect of infill was significantly higher than the shear capacity of the columns near the compression zone corners. From the experimental investigation, it was observed that the diagonal shear cracks were developed at 0.77% drift level corresponding to a lateral load of 70 kN and 95 kN in case of IF-FB1 and IF-FB2, respectively. Whereas, from the analytical response it was observed that the shear hinges near the column ends were formed at 0.66% and 0.72% drift in case of IF-FB1 and IF-FB2, respectively. Therefore, the improved analytical strut model successfully predicted the initiation of shear failure in the columns due to the effect of infill. From the analytical and experimental response, it was clearly affirmed that the columns of infilled frames designed in accordance with the current codal provisions were susceptible to shear failure due to the detrimental effect of infill.

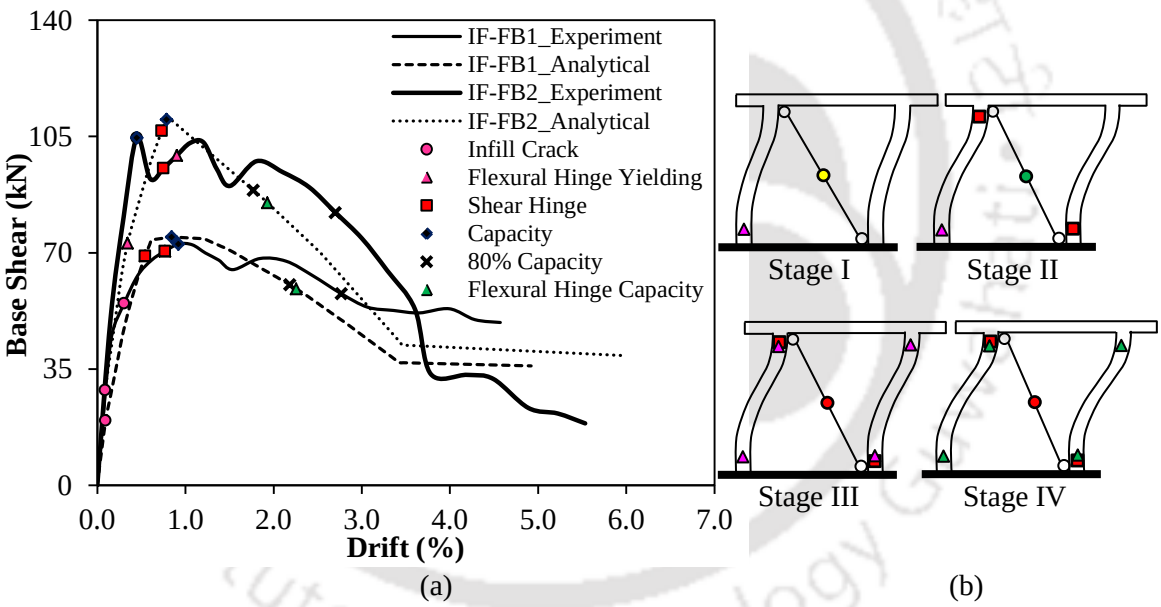

Fig. 5.7. Comparison of: (a) analytical and experimental results; and (b) stages of plastic hinge formation using the improved analytical model for infilled frames IF-FB1 and IF-FB2.

The shear failure of the columns could not be prevented even though the shear capacity of the column sections was increased significantly as in case of IF-FB2 in which high strength bars were used as reinforcement in RC members. Results of the improved analytical model showed that after the formation of shear hinges in the columns with increasing monitored drift, axial capacity of the diagonal strut was reached followed by the capacity of the infilled frame in case of IF-FB1 (Stage III). On the other hand, both axial hinge and lateral load capacity reached simultaneously in case of IF-FB2. With

further increase in drift, ultimate moment capacity (M_u) of the flexural hinges was reached after the capacity of the infilled frame was reduced to about 80% of its maximum (Stage IV). Similar observation were made in the experimental investigation where widening of the shear flexural cracks and spalling of cover concrete were noticeable. From the analytical response, it was clearly perceived that the improved analytical model not only predicted the shear failure of columns but also successfully traced the peak and post-peak response of the infilled frames. Further, the verification of the improved modelling technique is discussed in the following section.

5.4.2 Verification of Improved Analytical Model

Three frames (IF-CT, IF-CM1 and IF-CM2) from the past experimental studies, in which shear failure of columns was reported to be the primary mode of failure, were considered for the verification of the improved modelling technique. Since the nonlinear material property of masonry used in the study were not provided in these studies, the axial hinge definition for the masonry strut was developed using the nonlinear stress-strain model proposed by Kaushik et al. (2007) as shown in Fig. 5.8. As already discussed with the previously tested specimens (IF-FB1and IF-FB2), the prevalent single-strut model was not able to predict the shear failure in any of the considered frames. Therefore, the improved analytical model was used to predict the lateral load response of these frames.

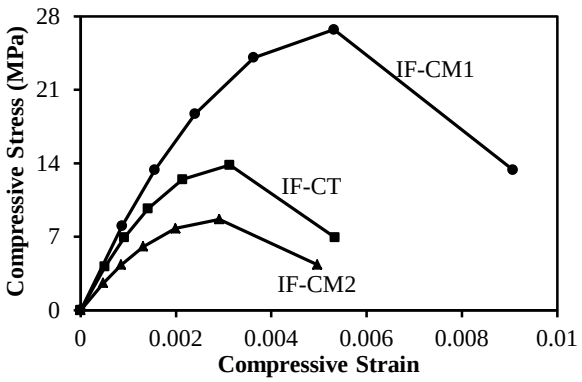

Fig. 5.8. Compressive stress-strain curve for the axial hinge in masonry infill of the three frames (Kaushik et al. 2007).

Comparison of the pushover curves obtained using the improved analytical model and experimental response of the selected infilled frames is shown in Fig. 5.9. It was observed that the global response was aptly simulated by the analytical model. Formation of hinges near the specified locations was found to be quite similar to that observed in the

experiments. In case of IF-CM1 (Al-chaar et al. 2002) and IF-CM2 (Cavaleri and Di Trapani 2014), it was observed that initially masonry strut yielded followed by the yielding of flexural hinges, and shear hinges were developed with further increase in the monitored drift. On the other hand, in case of IF-CT (Mehrabi et al. 1996) model, shear hinges reached their capacity after the yielding of axial strut but prior to the yielding of flexural hinges. The reason for IF-CT to exhibit formation of shear hinges at a lower drift level was that the section had the lowest shear capacity and shear demand was higher due to the frame-infill interaction.

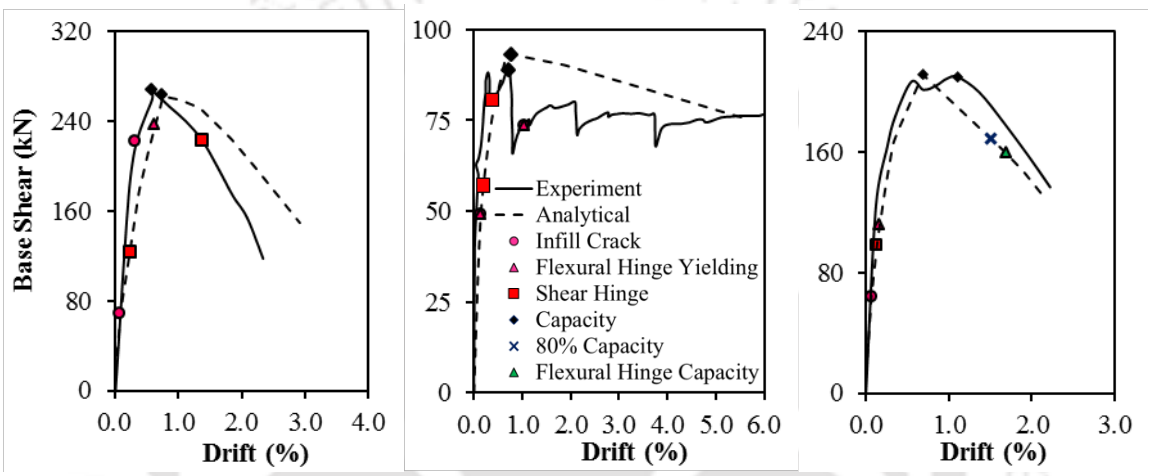

Fig. 5.9. Comparison of analytical and experimental curves using the improved analytical model for: (a) IF-CT; (b) IF-CM1; and (c) IF-CM2.

In case of IF-CT, the improved analytical model exhibited formation of shear hinge at 0.23% drift (124 kN), whereas, in experimental investigation major shear crack formation was reported at 1.37% drift (224 kN) [Fig. 5.10(a)]. In case of IF-CM1 analytical model, it was observed that the shear hinge was developed at a drift level of 0.20% corresponding to a lateral load of 57 kN; whereas the first major shear crack was reported in the experimental study at 0.4% drift (81 kN) [Fig. 5.10(b)]. No details on the initiation of the shear cracks in the columns were provided in the study. In case of IF-CM2 experimental study, it was reported that initially diagonal cracks were formed at the upper joints of the columns [Fig. 5.10(c)] but the drift corresponding to the initiation of shear cracks was not mentioned, whereas, shear hinge reached its capacity at a drift level 0.13% (98 kN) in the analytical model. From the analytical investigation carried out by D'Ayala et al. (2009) to predict the shear failure of columns, it was also observed that the

shear capacity of the sections in the analytical model was reached at a lower drift level compared to the experimental observation of major shear crack.

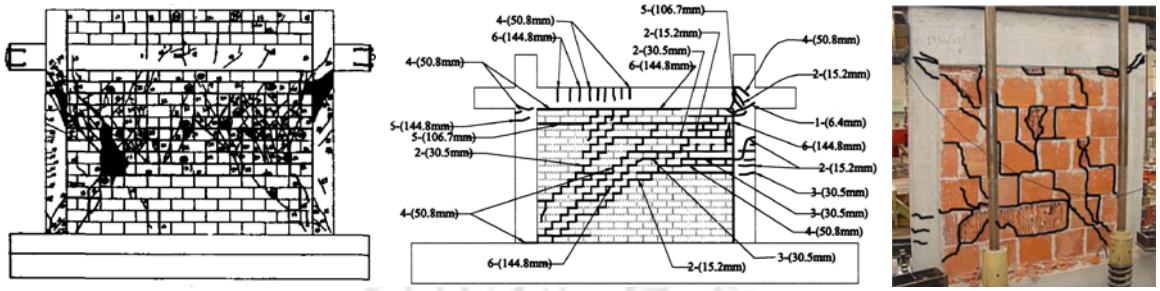

(a) (b) (c)

Fig. 5.10. Failure mechanism observed experimentally in: (a) IF-CT (Mehrabi et al. 1996); (b) IF-CM1 (Al-chaar et al. 2002); and (c) IF-CM2 (Cavaleri and Di Trapani 2014).

After the formation of shear hinges and yielding of flexural hinges, capacity of the infill as well the capacity of the infilled frame reached almost simultaneously with further increase in monitored drift. Therefore, from the comparison of the experimental results with the analytical response it can be verified that the global response as well as the local failure mechanism can be captured satisfactorily with the improved analytical model. The nonlinear masonry material model in the analysis of all three frames was developed based on the nonlinear stress-strain model proposed by Kaushik et al. (2007), and it was observed that the results are sensitive to material model as properties of masonry are region specific. A more generic masonry material model needs to be established for accurate estimation of shear demand on the columns.

5.5 SUMMARY

An attempt was made in this chapter to understand the applicability of the current recommendations of some commonly used seismic codes to estimate the shear demand on the columns. The existing equivalent strut macromodelling analogy in estimating the global response of the infilled frame was evaluated and its limiting ability of capturing the internal forces in frame members was highlighted. The existing strut modelling analogy was improved by simulating the effect of infill along the contact length of the column to account for the increased shear demand on the column due to the frame-infill interaction. The analytical response clearly showed that the improved model was able to capture the local shear failure of columns by forming shear hinges in the column, in addition to

accurately predicting the global response (lateral strength and stiffness) of the frames. The improved modelling technique was further verified using other past experimental results, and it was observed that the improved modelling technique successfully captured both the global response as well as the local component (shear) failure in infilled frames.

The shear failure of the columns could not be prevented even though the shear capacity of the column sections was enhanced significantly as per the current codes of practice. Therefore, it becomes utmost important to accurately predict the shear failure of columns in such frames so that their design can be improved. By utilizing the improved analytical macromodel, some design methodologies will be developed in the next chapter to improve the shear behavior of columns for counteracting the local adverse effect of infill.

Chapter 6
IMPROVEMENT IN SHEAR BEHAVIOR OF INFILLED FRAMES: DESIGN ENHANCEMENTS

CONTENTS

6.1 OVERVIEW

From the preliminary experimental and analytical study it was found that the columns of masonry infilled RC frames failed in shear due to the infill-frame interaction. To counteract the adverse effect of infill, i.e., to prevent or delay the shear failure in columns, three approaches were put-forward in the current study. Evaluation of the influence of the first two methodologies (enhancing the shear capacity of the column sections by considering the effect of infill, and reducing the effect of infill using weaker and softer masonry as infill) has been elaborately discussed in the current chapter. Initially, the effectiveness was evaluated numerically and analytically by carrying out a parametric study using the improved analytical model. Later, the best performing models were verified by carrying out experimental investigations on the half-scale masonry infilled RC frames.

6.2 METHODOLOGIES

The columns of the masonry infilled RC frames failed in shear due to the one-sided imbalanced contact (local adverse effect of infill). In order to prevent or delay the shear failure in columns, three approaches are followed in the current study: (i) consider the effect of infill and increase the design forces on the columns; (ii) decrease the capacity of the infill without compromising the functional requirements so that the shear demand on the column is reduced; (iii) diffuse/limit the effect of infill-frame interaction. Therefore, three methodologies (Fig. 6.1) were designed in the current study: Methodology I: increase the shear capacity of the column by considering the effect of infill in the design of frames; Methodology II: using very weak and softer masonry as infill to reduce the shear demand on the column; and Methodology III: provision of sliding mechanism along the predefined failure planes so as to limit the infill-frame interaction.

The local adverse effect of infill generally acts along the compressive loaded corners of the column over a certain contact length. To safeguard the column due to the adverse effect, the design shear capacity of the columns has to be enhanced either by increasing the shear reinforcement of the column section or by increasing the dimensions of the column section. If the contact length of the column over which the diagonal strut force (effect of infill) acts is small, the shear demand will be higher. Then, it becomes difficult to design the column for the increased shear demand as the shear resistance is governed by the shear compression failure of concrete without any yielding (failure) of transverse reinforcement. In such cases, the transverse reinforcement cannot be increased further, and therefore, the dimensions of the columns are proportioned to enhance the shear capacity of the column to avoid the shear compression failure.

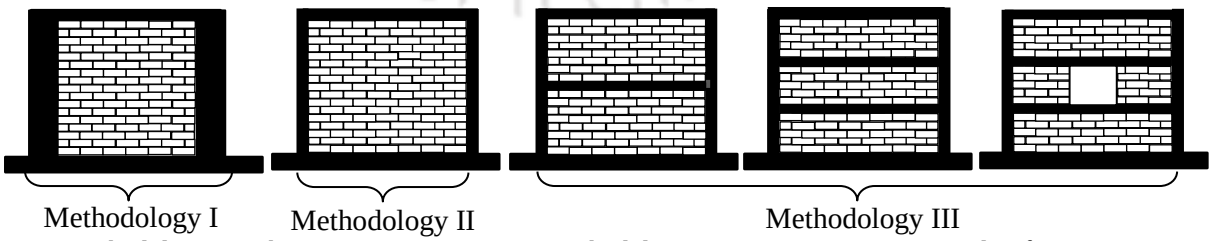

Methodology I: Enhancing Column Section; Methodology II: Using Low-strength and Soft Masonry; Methodology III: Adding Collector Beams in Infills

Fig. 6.1. Schematic representation of methodologies to improve shear behavior of columns in masonry infilled RC frames.

Enhancing the shear capacity of the column section may not be possible many a times, as the designed sections may become unrealistic and uneconomical. In the past literature (Magenes and Calvi 1997; Kaushik et al. 2007), it was observed that the use of weaker and softer masonry ensured weak and ductile mechanism for ordinary masonry walls. This induces large deformation mechanism and energy dissipation to masonry walls. To allow for this kind of mechanism in ordinary masonry, low shear strength and low vertical confining action on the mortar joints are required (Mann et al. 1988). It was understood that the use of weaker and softer mortar joint in masonry may reduce the effect of infill by allowing the masonry to fail along the bed joints rather than in brick crushing failure. Similarly, in the past studies (Preti et al. 2012; Markulak et al. 2013) low-strength masonry such as adobe bricks were employed in order to reduce the effect of infill. Therefore, in the second methodology, very weak and softer bricks were used as masonry infill to reduce the shear demand on the columns (Fig. 6.1).

Due to brittle nature of the infill, it is difficult to vary or alter the strength of the infill significantly. Therefore an improved methodology for the design of the masonry infilled RC frames is to limit or diffuse the effect of infill on the columns. This can be achieved by forcing the frame into ductile failure mechanism by providing sliding mechanism in infill along the predefined planes by which the energy absorption capacity of the infill can be enhanced. The application of sliding planes by dividing infill into various sub-panels to ensure ductile response has already been implemented previously in various building typologies by different names (Dhajji-Dewari, Fachwerk, Colombage, Casa Baraccata, Half -timber) as reported by Langenbach (2008).

Very recently, this technique has been adopted in various research projects (Langenbach 2008; Mohammadi and Akrami 2010; Preti et al. 2012, 2015; Rai et al. 2014). Most of the studies employed wood elements (Preti et al. 2012, 2015), steel plates with roller bearings (Mohammadi and Akrami 2010), and precast RC elements (Rai et al. 2014) as sliding devices. At the same time, most of the past studies were carried out on steel frames with predefined plastic hinges and lightly reinforced elements with much emphasis on the behavior of the infill rather than the RC columns. Hence, in the current study, sliding planes in the infill panels were introduced by providing cast-in-place RC collector beams (similar to lintel beam) provided at different levels along the height of infill.

Evaluation of the above mentioned three methodologies has been carried out by the verifying the columns of the infilled frames for shear failure using the improved analytical macromodel proposed in chapter 5. If the columns were found to be shear deficient, then based on the feasibility and affordability, a design methodology was selected. Initially, the effectiveness of the selected methodology was evaluated using the improved analytical macromodel by considering the effect of infill. Based on the response from the nonlinear pushover analysis, the best performing scheme of different methodology was experimentally tested under displacement controlled loading. Performance evaluation of the infilled frames was reported in terms of hysteretic response and failure mechanisms perceived under various stages of the lateral loading. The detailed evaluation of methodologies I and II is discussed in the following sections.

6.3 Analytical Evaluation of Methodology I

Enhancement of the shear capacity of the column section can be achieved either by increasing the transverse reinforcement or by increasing the dimensions of the columns. To achieve the same, previously tested infilled frame with fly ash bricks (IF-FB2) was considered to evaluate the effectiveness of the design methodology. As ascertained from the analytical and experimental investigations discussed in the previous chapters, the columns of the infilled frame IF-FB2 failed in shear. In order to prevent the brittle shear failure of columns, the design shear capacity of the column section needs to be enhanced. To achieve this, two cases were considered. In the first case, only the transverse reinforcement in the column section was enhanced; and in the second case, the dimensions of the column sections were proportionately increased by limiting the percentage transverse reinforcement.

6.3.1 Case I: Enhancement of Transverse Reinforcement

The shear capacity of IF-FB2 was found to be about 95 kN, and the provided transverse reinforcement ($\rho_{sh} = 100A_{sv}/bs$) was about 0.82%, where A_{sv} is the total cross-sectional area of transverse reinforcement within a spacing s, and b is the width of the column section. It is a well-known fact that yielding of the shear reinforcement at the ultimate limit state is essential to ensure ductile failure. However, such a failure may not be possible if excessive shear reinforcement is provided. If A_{sv} exceeds a certain limit, it is likely that the section becomes stronger in diagonal tension compared to diagonal

compression. Hence, shear-compression failure may occur even before the shear reinforcement yields. Such a situation is undesirable due to the brittle nature of the failure. Moreover, it also turns out to be uneconomical, in much the same way as over-reinforced beams.

In order to avoid the shear compression failure of members, IS 456 (BIS 2000) limits the maximum shear that can be resisted by a section to $\tau_{cmax}bd$, where τ_{cmax} represents the maximum shear stress in concrete with shear reinforcement, b and d are the width and effective depth of the cross section, respectively. Similarly, ACI 318 (2008) limits the maximum shear to be resisted by transverse reinforcement to $0.66\sqrt{f_c'}bd$, where f_c' is the compressive strength of concrete cylinder. Lee and Hwang (2010) from their study on high strength concrete beams reported that the maximum shear reinforcement should not be more than $0.2\, f_c'/f_y$. The calculation of limiting shear resistance by the column section using various standards is given in Table 6.1. It is observed that the provided transverse reinforcement of column (ρ_{sh}) designed in accordance with the Indian ductile detailing code (BIS 1993) for IF-FB2 is found to be more than the maximum limiting shear. At the same time, the current Indian standards (BIS 2000; BIS 1993) do not provide any specific recommendations for maximum percentage shear reinforcement in seismic design, especially for high strength bars. To enhance the shear capacity of the column section so as to meet the shear demand due to the effect of infill, ρ_{sh} was found to be far higher than the maximum limit reinforcement criteria. Hence, it was found that increasing the transverse reinforcement only to meet the shear demand is not a viable option as it may lead to shear compression failure of columns.

Table 6.1. Calculation of shear reinforcement for trial sections

					Maximum Limiting Shear		
Section	V_c	V_s	Shear Capacity	ρ_{sh}	IS 456 (BIS 2000)	ACI 318 (2008)	L&H*
mm×mm	kN	kN	kN	%	%	%	%
115×175	22	73	95	0.82	0.46	0.53	0.64
115×175	22	127	149	1.49	0.46	0.53	0.64
115×175	22	138	160	1.60	0.46	0.53	0.64

* L&H represent Lee and Hwang (2010).

6.3.2 Case II: Increasing Dimensions of Column Sections

In the second case, shear capacity of the column section was enhanced by designing the section such that the dimensions of the columns are increased and limiting the percentage shear reinforcement. A parametric analysis was carried out and the details of enhanced trial column sections are provided in Table 6.2. The compressive strength of concrete cubes for trial sections was assumed to be 25 MPa. The trial column section 150×250 mm was found to be a feasible option in accordance with Lee and Hwang (2010), only if the provided transverse reinforcement also increased. Similarly, 175×275 mm column section was found to be an acceptable section if the limiting shear reinforcement was considered in accordance with IS 456 (BIS 2000) and ACI 318 (2008). It is clear from the analysis that the shear capacity of the column sections can be enhanced by increasing the dimensions of the column and by limiting the shear reinforcement to avoid shear compression failure.

Table 6.2. Calculation of shear capacity for enhanced column section

			Maximum Limiting Shear		
Section	V_{cap}	ρ_{sh}	IS 456 (BIS 2000)	ACI 318 (2008)	L&H
mm×mm	kN	%	%	%	%
115X175	95	0.82	0.46	0.53	0.64
150X250	165	0.75	0.54	0.60	0.80
175X275	160	0.54	0.55	0.60	0.80

* L&H represent Lee and Hwang (2010).

Later, the infilled frames with enhanced trial column sections were evaluated analytically using the proposed improved analytical model. The details of the analytical modelling were discussed elaborately for previously tested infilled frames in chapter 5. The major difference for the trial column model was the increased dimensions of the column sections and their nonlinear properties. Nonlinear pushover analysis of the enhanced column section was carried out by applying the effect of infill along the contact length of the column. Fig. 6.2 shows the lateral load response and stages of plastic hinge formation in case of the infilled frame with enhanced trial column sections. From the analysis, it was clearly observed that initial yielding of axial hinges was followed by flexural yielding of the frame members (Stage I and II). With increase in monitored drift, failure of axial strut and flexural hinge yielding at all column locations was observed (Stage III). This was followed by capacity of the flexural hinges at all column locations

(Stage IV). There was no formation of shear hinges and the lateral load capacity of both the frames with larger dimensions increased drastically compared to that of IF-FB2. This was due to the fact that the shear demand on the column due to the effect of infill was found to be less than the shear capacity of the columns near the compression zone corners (Table 6.2). Out of the two trial sections, infilled frame with 175×275 mm column section was chosen to verify the improved methodology experimentally. The enhanced column trial section was chosen when compared to other trial sections based on the limiting reinforcement criteria in accordance with IS 456 and ACI 318.

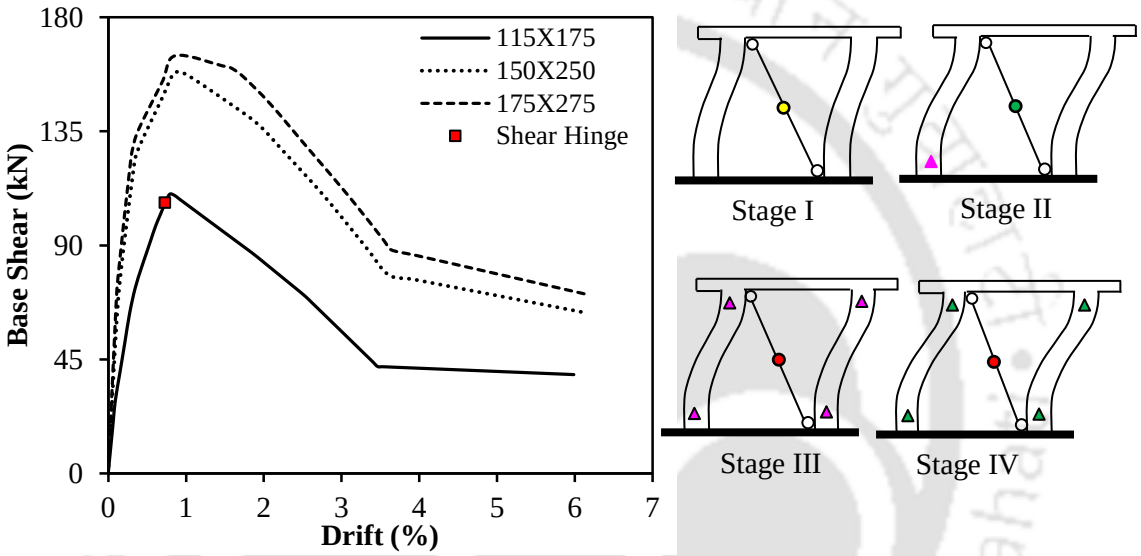

Fig. 6.2. Comparison of lateral load response obtained analytically and stages of plastic hinge formation in infilled frame with enhanced column trial sections.

6.4 Experimental Investigation of Methodology I

From the parametric analysis using the improved analytical model, it was found that the frames with enhanced column trial sections were able to prevent the shear failure due to the adverse effect of infill. Further, the effectiveness of the enhanced column sections was experimentally investigated and the results are discussed in this section.

6.4.1 Description of the Test

The design and construction of the RC frame was similar to that of the frames tested previously in the preliminary investigation (chapter 4), with the only difference being the sectional dimensions of the columns and bottom beam. The sizes of the columns have been increased from 115×175 mm to 175×275 mm and were constructed on a RC bottom

beam of size 400×420 mm. The size of the bottom beam was chosen based on cracked moment analysis, and the increased size of the base beam was found to be safe to provide proper fixity to the enhanced column section. The reinforcement detailing of the RC frame with increased column section is shown in Fig. 6.3.

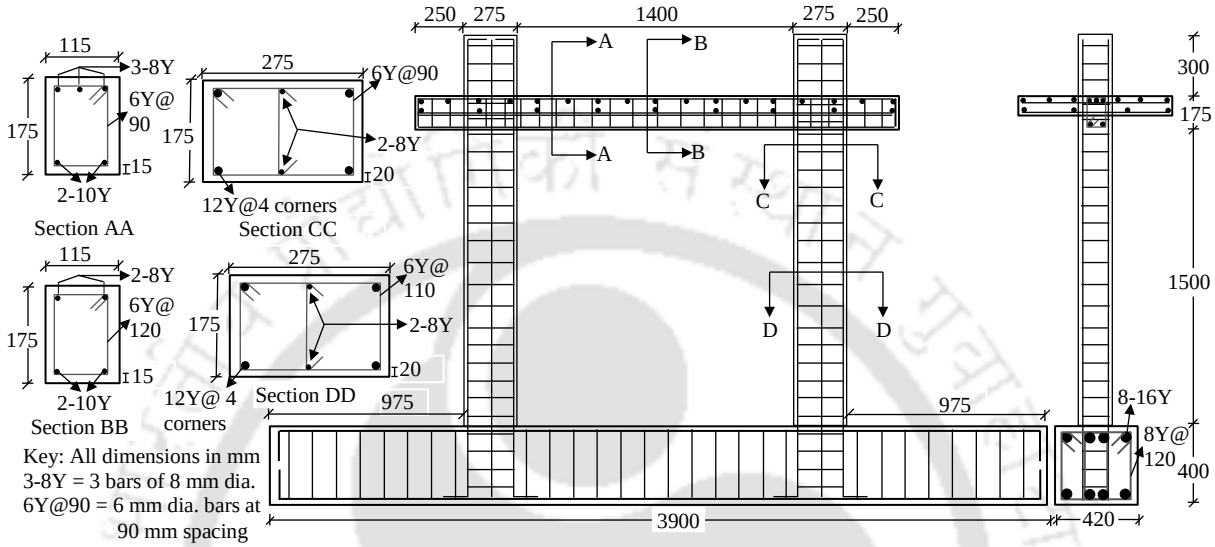

Fig. 6.3. Reinforcement detailing of infilled frame with enhanced column section (IF-EC).

The detailing of the column sections was similar to that of the original column sections consisting of 4-12 mm diameter bars and 2-8 mm diameter bars as longitudinal reinforcement. The shear reinforcement consisted of 6 mm diameter 3-legged stirrups at a spacing of 90 mm in critical regions (upto 500 mm from the face of top and bottom beams) and rest at 110 mm. The sectional dimensions and reinforcement details of beam and slab remained similar to that of the previously tested infilled frames. The aspect ratio ($h/l \approx 1$) of the frame was maintained similar to that of the original half scaled frame specimen.

The frame was constructed by casting in the horizontal position to facilitate easy placing of mixed in-place concrete. The formwork was constructed to the desired dimension and was laterally supported by placing wooden buttresses at regular intervals so as to decrease the lateral pressure on the formwork. After seven days of casting, the frame was lifted and placed in vertical position. Infill wall was constructed using full-scale fly ash bricks with 10-12 mm thick, 1:4 (cement:sand) mix mortar under skilled supervision with a water cement ratio of 0.6. After the construction of infill wall, the

infilled frame was cured for 28 days. Summary of material properties of RC frame and fly ash brick masonry are presented in the Table 6.3. Detailed material characterisation of fly ash brick masonry was discussed in chapter 3.

Table 6.3. Material properties of IF-EC

Material	Characteristics	Units	Properties
Concrete	Compressive strength	MPa	f_{ck} = 32, E_c = 28,284
	Split tensile strength	MPa	f_{ct} = 2.7
Longitudinal steel (12Y)	Tensile strength	MPa	f_y = 530, E_s = 2×10^5
Longitudinal steel (10Y)	Tensile strength	MPa	f_y = 546, E_s = 2×10^5
Longitudinal steel (8Y)	Tensile strength	MPa	f_y = 562, E_s = 2×10^5
Stirrups (6Y)	Tensile strength	MPa	f_y = 569, E_s = 2×10^5
Fly ash Brick	Dimensions	mm	230×110×75
	Compressive strength	MPa	f_b = 5.7, E_b = 3900
	Split tensile strength	MPa	f_{bt} = 0.54
Mortar	Compressive strength	MPa	f_j = 17.3, E_j = 7400
	Split tensile strength	MPa	f_{jt} = 1.2
Masonry prism	Compressive strength	MPa	f'_m = 3.9, E_m = 2667
Masonry wallette	Shear strength	MPa	f'_v = 0.14, G_m = 727

From the analytical study, it was observed that the lateral load capacity of the infilled frame with enhanced column section was higher than the previously tested infilled frames (preliminary study) but the capacity was less than the capacity (250 kN) of the servo-controlled hydraulic actuator employed. Therefore, the infilled frame with enhanced column section was tested under slow-cyclic displacement controlled loading (Fig. 6.4) applied at the slab level using the same servo-controlled hydraulic actuator of 250 kN load capacity with a stroke length of ± 125 mm (Fig. 6.4).

Experimental results were recorded continuously using load cell and displacement transducer located in the actuator arm, external *LVDT*s (linear varying displacement transducers), and strain gauges. Three cycles of each displacement level was applied and the response was recorded using a data acquisition system (Fig. 4.4). *LVDT*s were used at different locations on the columns and base beam to record the lateral displacements. Base beam was restricted from sliding by bolting it to the strong floor. Quarter-bridge, four wired, linear strain gauges (*HBM* made) were used to record the strains in the reinforcement. Strain gauges were bonded to the longitudinal reinforcement at the most likely locations of formation of plastic hinges in beam and columns (Fig. 6.4). Maximum lateral load resistance of the specimens is reported in both push (-) and pull (+) directions.

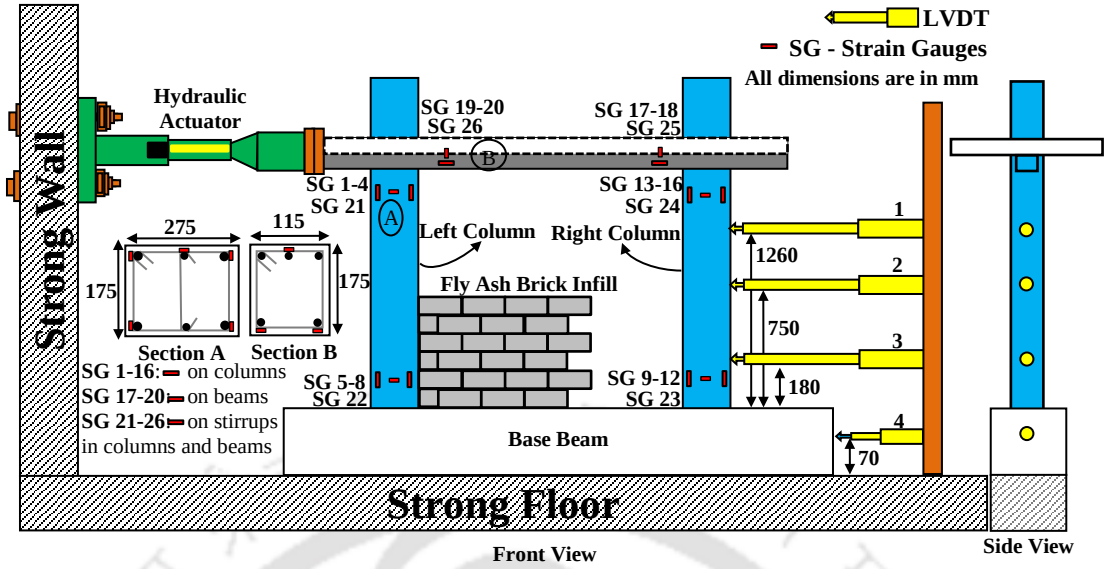

Fig. 6.4. Details of test setup and instrumentation (strain gauges and *LVDTs*) in IF-EC.

6.5 Results and Discussion of Methodology I

Experimental results of infilled frame with enhanced column section (IF-EC) was reported in terms of hysteretic curves (lateral load resistance vs applied drift at the actuator level), and the envelope curves obtained from the primary cyclic response of the specimens. In order to accurately understand the structural behavior of the infilled frames, the influencing parameters (lateral strength, stiffness, energy dissipation, deformation characteristics, and failure mechanisms) were also estimated. The results pertaining to the influencing parameters and their variation at different drift levels with respect to the previously tested infilled frame specimens are discussed in detail in the following sections.

6.5.1 Hysteretic Response

The hysteretic response of IF-EC is shown in Fig. 6.5. From the hysteretic response it was observed that the loops were closely spaced and symmetrical in both push and pull directions in the initial displacement levels, whereas the loops were distorted or unsymmetrical in case of previously tested IF-FB2. At the same time, the amount of pinching observed in case of IF-EC, was found to be significantly less than the original infilled frame as the resistance provided by the enhanced columns was higher. From the hysteretic response, it was clearly observed that the IF-EC observed significantly better performance in terms of lateral load resistance, stiffness and energy dissipation.

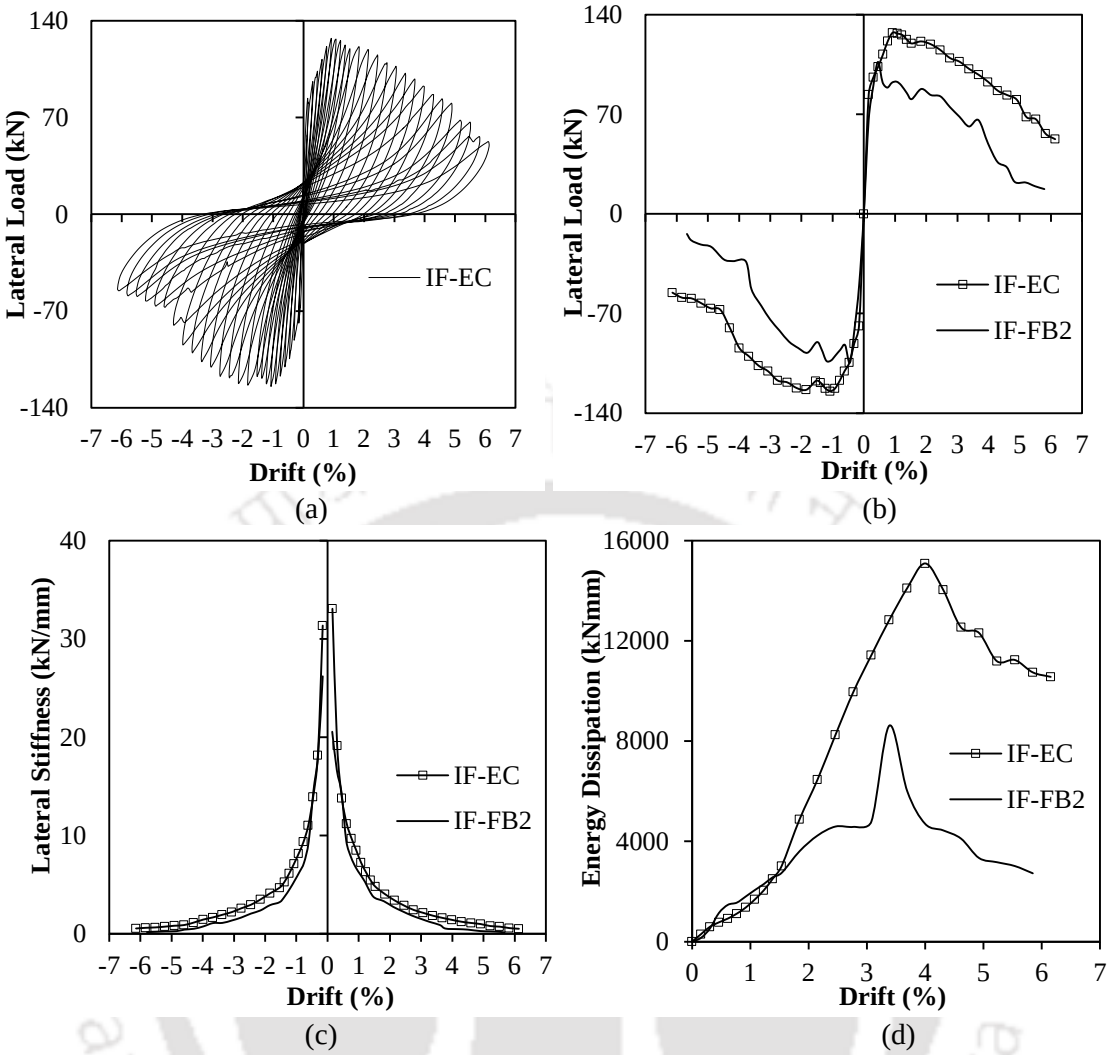

Fig. 6.5. Lateral load behavior of IF-EC: (a) hysteretic response; (b) envelope curves showing force vs. drift at actuator level; (c) variation of stiffness; and (d) energy dissipation at different drift levels.

6.5.2 Evaluation of Influencing Parameters

The results of quasi-static tests, described in terms of lateral strength, stiffness and energy dissipation and are shown in Table 6.4 and Fig. 6.5. Initial stiffness of the infilled frame with enhanced column section (IF-EC) was found to be slightly higher than the previously tested IF-FB2. The lateral load resistance observed in case of IF-EC in the initial drift level (0.15%) was found to be about 1.4 times than that of the lateral load resistance offered by the IF-FB2 in the initial drift level [Fig. 6.5(b)]. Variation of secant stiffness for the IF-EC is shown in Fig. 6.5(c). Secant stiffness of IF-EC was higher in the initial drift levels, and at the same time, it was also inferred that the rate of degradation was slightly gradual in both push and pull directions when compared to the degradation in

case of IF-FB2. The lateral load capacity of IF-EC was found to be approximately 1.2 times that of the capacity of IF-FB2 (Table 6.4). At the same time, capacity of IF-EC was reached at a higher drift level (1.07%) when compared to IF-FB2 (0.45%). The reason for the frame to observe higher initial stiffness and lateral strength was mainly due to the contribution of enhanced column section, and the increased confinement effect on the infill due to the higher sectional dimensions of the columns. It was also observed that the rate of dropdown in capacity was very gradual, whereas the dropdown was very arbitrary due to the contribution of infill in case of IF-FB2. Until 1.5% drift level, the energy dissipated by the IF-EC was found to be similar to that of IF-FB2 [Fig. 6.5(d)]. With increase in drift level, the energy dissipation capacity of the IF-EC increased, whereas the IF-FB2 observed sudden degradation due to the failure of infill. Energy dissipated by IF-EC was found to be higher when compared to other infilled frames and was about approximately 2.3 times that of IF-FB2. The main reason for this was that the frame observed lesser amount of pinching in hysteresis loops due to the contribution of both frame and infill even at higher drift levels.

Table 6.4. Influencing parameters of test specimens

S. No	Type of Frame	K_i (kN/mm)	ED (kNmm)	F_u (kN)	δ_u (mm)
1	Bare frame (BF)	4	45,201	-42, 34	100
2	Infilled frame (IF-FB2)	36	78,200	-105, +107	95
	Methodology I				
3	Infilled frame with enhanced column section (IF-EC)	55	1,79,931	-125, +127	100
	Methodology II				
4	Infilled frame with class I clay bricks (IF-CC1)	58	1,08,764	-112, +104	85
5	Infilled frame with class III clay bricks (IF-CC2)	46	1,45,442	-81, +76	100

6.5.3 Crack Pattern and Failure Mechanisms

In case of IF-EC, cracking in infill was initiated as diagonal stepped cracks along with bed joint sliding cracks propagating (three layers above and below the middle of the infill panel) at a drift level of 0.15% (-79 kN, +84 kN) as shown in Fig. 6.6(a). In the subsequent drift levels (0.46% to 0.92%) bed joint sliding cracks were formed in the different layers in central-middle-third infill panel, two layers below the soffit of the beam and three layers above the bottom beam. A slight hair line crack (diagonal tension crack) was marked near the top of the left column at a drift level of 0.46% (105 kN), similar to that observed in the previously tested infilled frame specimens, but was not prominent. No major cracks were marked in columns till 0.76% drift level, as most of the

cracks were observed in infill as bed joint sliding cracks and diagonal stepped cracks and formation of diagonal strut was clearly marked. At 0.92% drift (-123 kN, +127 kN), flexural cracks were observed near the left column bottom and right column top corners. With further increase in drift levels, similar flexural cracks were marked along the height of the columns. It was observed that most of the cracks marked were flexural in nature and the propagation of cracks was limited as the depth of the section was higher when compared to previously tested infilled frame specimens.

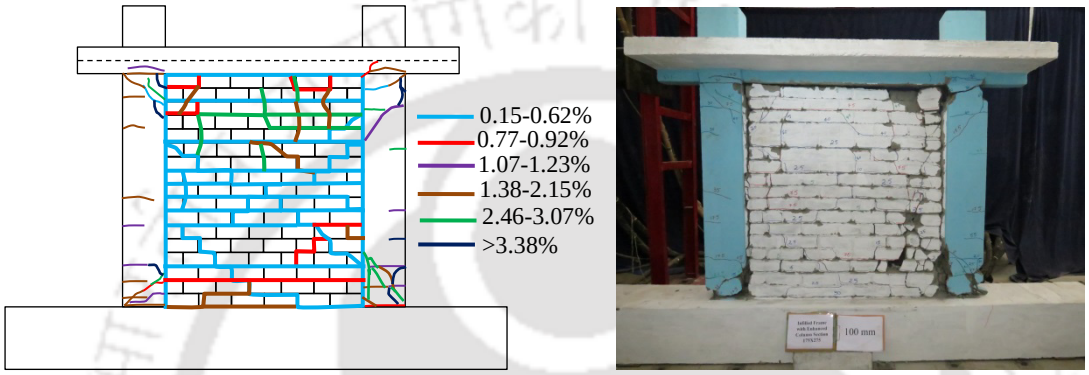

(a) (b)

Fig. 6.6. IF-EC: (a) crack pattern; and (b) failure mechanism.

At 1.07% drift (127 kN), diagonal shear cracks were marked near the right column top. The lateral load capacity of the infilled frame was also reached at the same drift level. In case of previously tested infilled frames, diagonal shear cracks were formed at a drift level ranging from 0.46% to 0.92% prior to the capacity of the infilled frames was reached. Whereas, in case of IF-EC, formation of shear cracks was delayed as well as the capacity of the infilled frame was reached at a higher drift level. With increase in drift levels, crushing of mortar bed joints and vertical splitting cracks in bricks were marked. It was also observed that in case of IF-EC the amount of cracking, especially diagonal shear cracks, near the corners was less when compared to that of flexural cracks.

Crushing and spalling of cover concrete near the left column bottom corner was observed at a drift level of 3.69% (100 kN). In the subsequent drift levels, buckling of longitudinal reinforcement followed by its tensile failure was observed at 4.30% (86 kN). Corner crushing of infill and the out-of-plane failure of infill was observed at a drift level of 4.92% (-66 kN, +80 kN). The test was terminated at 6.15% drift when most of the longitudinal reinforcement in columns failed [Fig. 6.6(b)]. From the observed crack

pattern, failure of IF-EC can be characterised as corner crushing and out-of-plane failure of infill followed by failure of longitudinal reinforcement prior to opening of hooks in shear reinforcement and crushing of core concrete. It was observed that there was no widening of shear cracks and crushing of core concrete, as it was observed in case of previously tested infilled frame specimens. The amount of diagonal shear cracks was found to be very less when compared to the previously tested infilled frame specimens. From the observed failure mechanisms, it can be apprehended that the shear failure of the infilled frame can be delayed or can be prevented if the shear capacity of the column section can be enhanced by increasing the dimensions of the columns by limiting the percentage of shear reinforcement.

6.5.4 Lateral Load-Strain Response

To evaluate the performance of cross sections under lateral loading, especially the inelastic (nonlinear) response, determination of the state-of-strain across the cross sections is a pre-requisite. In the current study, this has been done using the strain data recorded at the most likely plastic hinge regions (critical regions) of columns and beams as shown in Fig. 6.4. To understand the nonlinear behavior of the cross-sections, variation of strain in rebars in IF-EC at different drift levels was determined in this section.

Fig. 6.7 shows the lateral load-rebar strain (hysteretic) response of columns in IF-EC and Table 6.5 shows the typical strain values recorded in the strain gauges at various column locations. The strain gauge recordings of rebars on the outer face of the column were opposite in nature to that of the strain gauges fixed on the inner face rebars of the column near the infill (Fig. 6.7). The maximum strain values at different storey drifts at various column locations are shown in Fig. 6.8(a). Strain gauges SG 12 and SG 16 were found to be not operational and were not considered for further analysis. The strain recorded in tension was found to be higher when compared to compressive strain at all the locations. It was observed that the rebars located on the inner face of the left column (SG 4 and SG 7) yielded at a slightly lower drift level (0.62% and 0.77%) compared to the outer rebars. Yielding of rebars and the maximum strain was recorded at a lower drift level near the left and right column bottom locations when compared top locations with few exceptions. The rebar containing SG 15 near the right column top did not yield as the maximum strain recorded was found to be about 2448 μm/m at 3.69% drift.

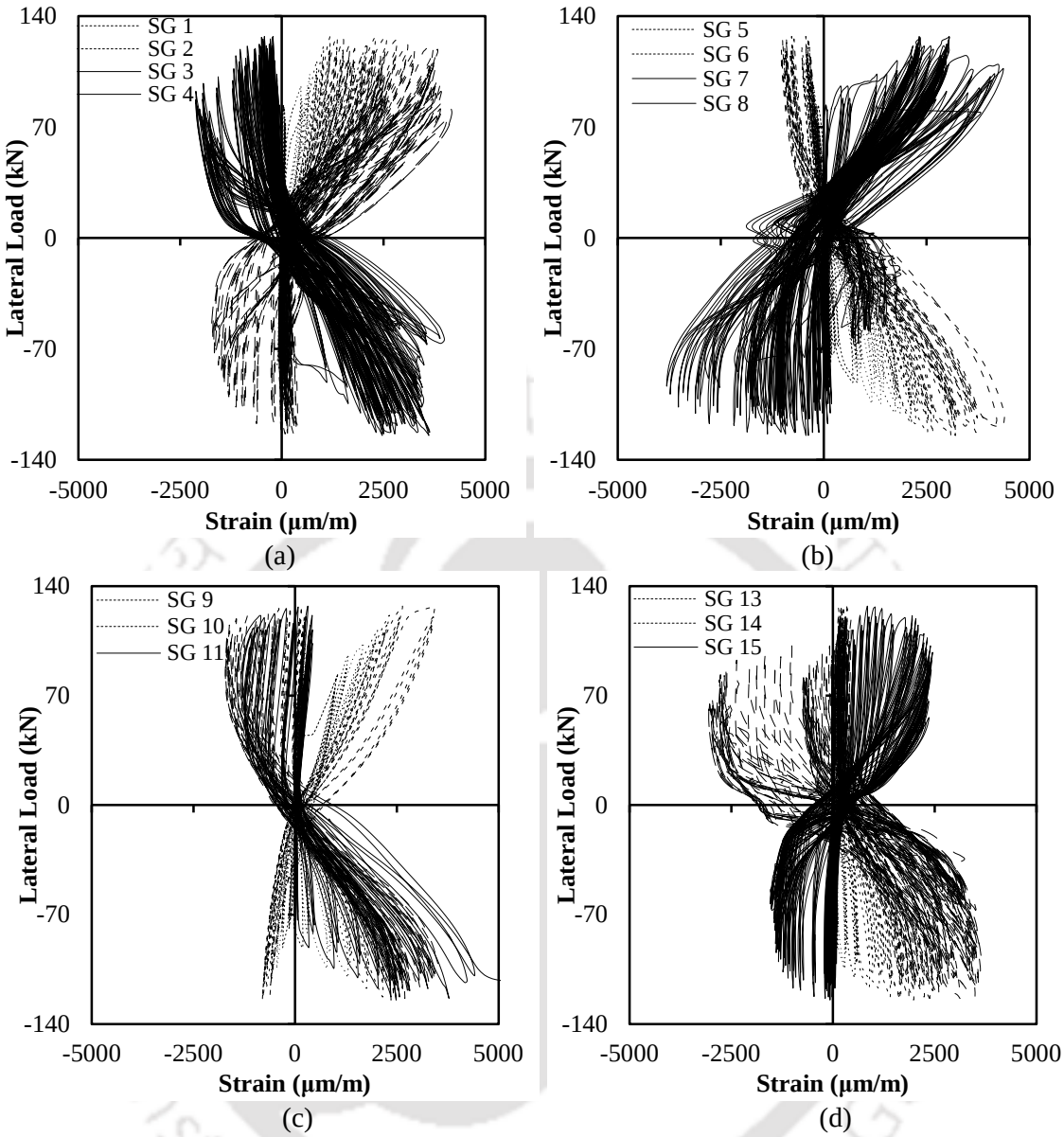

Fig. 6.7. Lateral load-rebar strain response in IF-EC: (a) near left column top (SG 1-4); (b) near left column bottom (SG 5-8); (c) near right column bottom (SG 9-12); and (d) near right column top (SG 13-16).

The strain values recorded in beams were too low and the yielding was not observed during testing. This was mainly due to the stiffening T-beam action provided by the slab. It is a well-known fact that the ductile responses of cross sections of structural members subjected to bending moments are generally measured by the curvature ductility. The detailing requirements of the potential plastic hinge regions are based on the curvature ductility demand. In the current study, curvature (φ) was calculated using the peak strain values at different storey drifts on both faces of the column at various locations.

Table 6.5. Typical strain values recorded at various column locations in IF-EC

Strain Gauges	Peak Strain				Yield		Yield Curvature /m
	Tension (+)	Compression (-)	Drift (+) %	Drift (-) %	Strain	Drift %	
			Left Column Top				
SG 1	6148	-238	5.85	-5.85	2638	3.38	0.0209
SG 2	5250	-1730	4.92	-4.92	2832	1.23	0.0140
SG 3	3467	-1134	2.77	-2.46	2684	1.23	0.0126
SG 4	3634	-2120	1.23	-4.00	2708	0.62	0.0121
			Left Column Bottom				
SG 5	4454	-915	1.54	-1.38	2541	0.92	0.0130
SG 6	5205	-1034	1.38	-1.23	2676	0.92	0.0143
SG 7	4367	-3812	3.08	-3.38	2607	0.77	0.0134
SG 8	3808	-2885	4.62	-4.00	2672	2.15	0.0186
			Right Column Bottom				
SG 9	3561	-1717	3.08	-2.46	2619	1.23	0.0247
SG 10	4416	-1432	1.85	-1.85	2633	1.23	
SG 11	3430	-807	1.08	-1.08	2638	0.92	0.0111
SG 12			Not operational				
			Right Column Top				
SG 13	3643	-752	3.69	-4.31	2647	1.54	0.0127
SG 14	3253	-2999	4.92	-4.92	2602	2.15	
SG 15	2448	-1543	3.69	-5.23	2448	3.69	
SG 16			Not Operational				

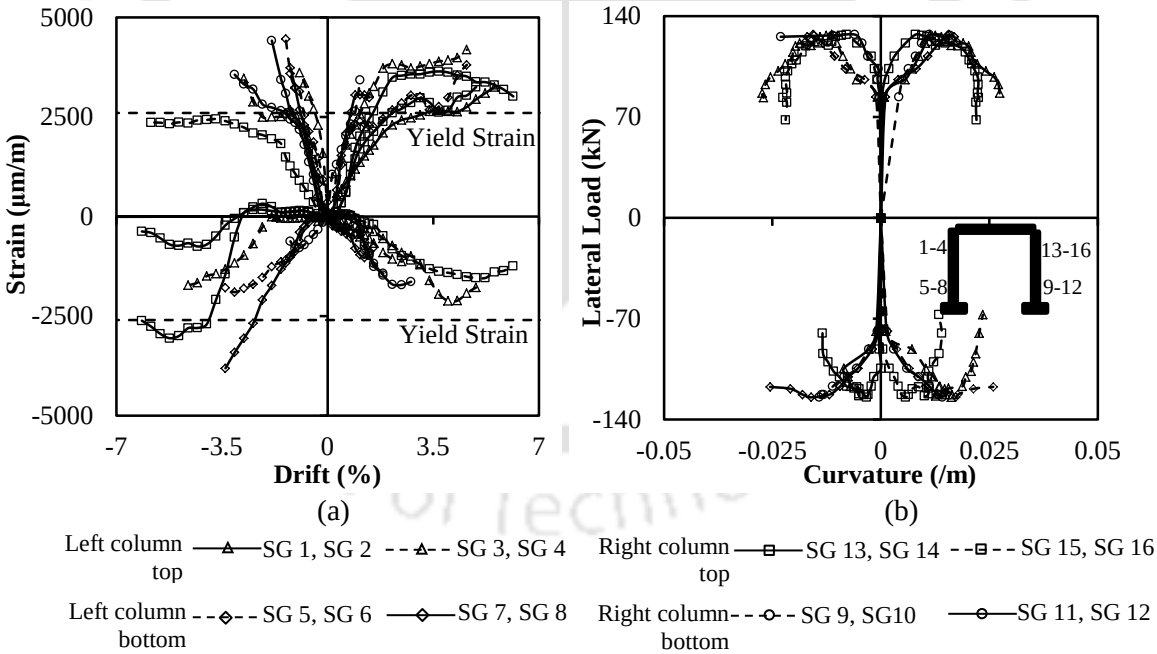

Fig. 6.8. (a) Envelope curves showing strain vs. lateral drift; and (b) lateral load-curvature response in IF-EC at various column locations.

Curvature (φ) was calculated as the ratio of strains at a particular drift level to the distance between the rebars on the opposite faces of the columns. Variation of curvature with respect to lateral load at various locations of columns is shown in Fig. 6.8(b). Based

on the first yielding of rebars (Table 6.5), the curvature corresponding to the yielding of rebar containing SG 4, SG 7 was calculated as 0.0121 /m and 0.0134 /m, respectively. No major damage events such as initiation of flexural crack (0.92%), and shear cracks (1.07%) were observed prior to yielding of rebars near the left column top (0.62%). The yielding of rebars near the left column top (0.62%) and bottom (0.77%) was observed before the lateral load carrying capacity of the infilled frame (1.08%) was reached. The capacity was reduced to 80% of maximum at 3.67% drift level. Therefore, from the drifts corresponding to the yielding of rebars and the reduction of capacity to 80% of maximum, it was affirmed that the increased column sections enhanced the ductile behavior of the infilled frame system.

6.6 Analytical Evaluation of Methodology II

To reduce the detrimental effect of infill on columns, the second alternative considered in the current study was to reduce the strength and stiffness of infill, so as to decrease the effect of infill on columns without compromising other functional requirements. The effectiveness of the methodology was evaluated by carrying out a parametric nonlinear analysis using the improved analytical macromodel by varying the strength and stiffness of infill. The geometric property (width) of the strut was calculated using the Mainstone (1971) equation. Variation of shear demand with respect to strength of infill is shown in Table 6.6. From the results, it was observed that with decrease in strength of infill, the shear demand on the column decreased even though the width of strut was increased due to frame-infill interaction.

Table 6.6. Calculation of shear demand on column due to low strength masonry

Type of Frame	f'_m	w_s	Shear Capacity	Base Shear	Shear Demand	Type of Failure
	MPa	mm	kN	kN	kN	
IF-FB2	3.9	234	95	110	97	Shear and axial failure
Trial 1	3.1	249	95	99	90	Axial failure of infill and flexural failure of column
Trial 2	2.5	251	95	88	78	
Trial 3	2	256	95	79	69	
Trial 4	1.5	265	95	70	59	
Trial 5	1	275	95	61	48	
Trial 6	0.5	295	95	51	38	

Fig. 6.9 shows the global lateral load response of the frame infilled with different strengths of masonry. It was observed that the lateral load capacity of the infilled frame

decreased with strength of masonry. Other than infilled frame with fly ash bricks (IF-FB2), all the trial sections observed axial hinges in infill followed by flexural plastic hinges in columns. From the analysis, it was ascertained that very low strength masonry may be used as infill to avoid the detrimental effects of infill. From the preliminary study (Chapter 4), it was found that even though fly ash masonry infill was weak, but the effect of infill was quite sufficient to cause shear failure of columns. Therefore, to avoid the shear failure of columns, significantly weaker and softer masonry needs to be selected to reduce the effect of infill on the columns. Therefore, from the nonlinear pushover analysis, infill with very low masonry prism strength of 1.5 MPa was considered for the experimental investigation. The detailed experimental evaluation of the methodology II has been discussed in the following sections.

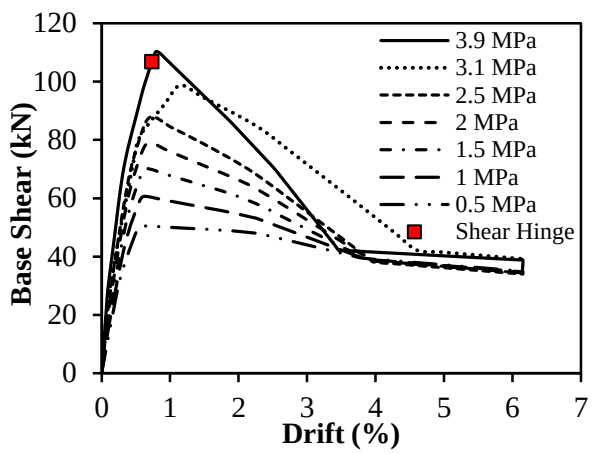

Fig. 6.9. Comparison of lateral load response of infilled frame for low strength infills.

6.7 Experimental Investigation of Methodology II

From the analytical study it was inferred that using very weak and soft masonry will decrease the shear demand on the columns and in turn delay the shear failure of columns. There needs to be a compromise between the type of the infill to be used, so as to delay the shear failure of columns without affecting the major functional requirements of infill. Various types of low-strength and soft bricks are commercially available. Past studies (Kakaletsis and Karayannis 2009; Preti et al. 2012; Markulak et al. 2013) used low-strength masonry such as adobe bricks to decrease the effect of infill. Adobe bricks are found to be advantageous in providing good deformation capacity, good thermal hygrometric performance especially in tropical countries, and cut down green-house gases as the manufacturing process does not involve burning in kilns. Inspite of many

advantages of adobe bricks, most of the modern-day construction practices have not opted for adobe bricks due to the inherited shrinkage problems, labour intensive construction and the regular maintenance.

In the current study, in lieu of the above constraints, very weak and soft burnt clay bricks, which are referred as Class III according to the current Indian specifications, were chosen. Generally, three kinds of clay bricks are available in India depending upon their mode of manufacturing: country bricks, table-moulded bricks and wire-cut bricks. Country bricks are mostly ground moulded and burned in clamps without proper temperature control. Table-moulded bricks are manufactured in semi-urban areas using intermittent or continuous kilns for burning. In the manufacturing process of table moulded bricks, moulds are lubricated with sand so that the plasticized clay will not stick to the sides of the mould. Wire-cut bricks are produced in factories by extrusion process and the quality of the bricks is superior when compared to both country and table-moulded bricks. In developing countries, including India, table-moulded bricks were very widely used due to the semi-mechanized skill requirement and cost effectiveness in the manufacturing of bricks. The other major beneficial influence of table-moulded bricks is low-compressive strength and low-elastic modulus when compared to the commonly used cement mortar in the construction of infill wall.

In the current study, to obtain weak and soft masonry, not only low-strength and soft bricks were chosen but also low strength mortar was selected, such that, a more deformable failure mechanism was observed in infill under lateral loading. Two frames were tested in the current study: frame infilled with class I burnt clay bricks (IF-CC1) and frame infilled with class III burnt clay bricks (IF-CC2). The following section describes in detail the construction of the frame using the adopted methodology.

6.7.1 Description of the Test

The design, detailing and construction of the RC frames were similar to that of the frame considered previously in preliminary study (IF-FB2). Two half-scale models (IF-CC1 and IF-CC2) were constructed and the detailing of RC frame members is shown in Fig. 6.10. Construction sequence and procedure was similar to that of the previously tested specimens. In case of IF-CC1, class I burnt clay bricks were used to construct the infill wall; such bricks are commonly used in infill in many places in India. The main reason

behind testing of RC frame with higher strength infill was to use the frame as a reference for validating the performance of frame with low-strength infill. In case of IF-CC2, class III burnt clay bricks were used in the construction of infill wall. The reason to choose class III burnt clay bricks was mainly the low-strength and soft nature (low-elastic modulus) of class III bricks compared to class I burnt clay bricks and fly ash bricks. The other major advantage of class III burnt clay bricks was their low shrinkage compared to adobe bricks. The infill wall was constructed with 1:8 (cement:sand) mortar grade so as to obtain low strength masonry. Detailed material characterisation of class I and class III brick masonry was discussed in chapter 3.

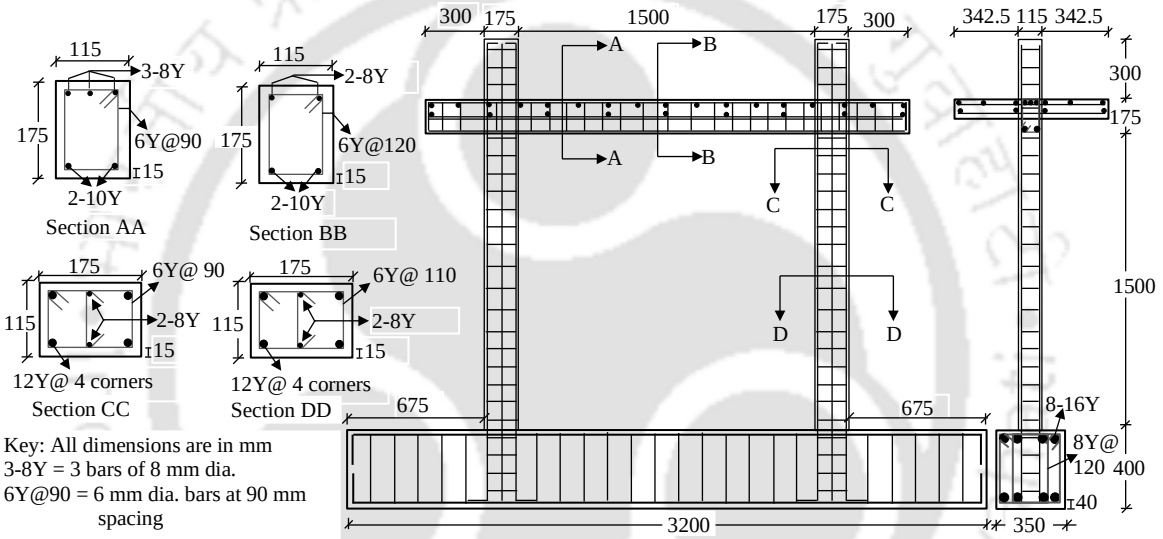

Fig. 6.10. Reinforcement detailing of infilled frames IF-CC1 and IF-CC2.

Summary of material properties of both class I and class III brick masonry are presented in the Table 6.7 along with frame material characteristics. From the material characterisation of class I and class III bricks, it was observed that class III bricks were low-strength and soft (low elastic modulus) when compared to class I burnt clay bricks. At the same time, it was also observed that the average compressive strength and modulus of elasticity of considered class III brick masonry with 1:8 cement mortar was found to be very low compared to class I burnt clay and fly ash brick masonry. Both the infilled frame specimens (IF-CC1 and IF-CC2) were tested under slow-cyclic displacement loading applied at the slab level using servo-controlled hydraulic actuator of 250 kN load capacity and a stroke length of ± 125 mm (Fig. 6.11). Three cycles of each displacement level were applied and the response was recorded using a data acquisition system. Similar

instrumentation and data acquisition was employed as that of methodology I. Experimental results were recorded continuously using load cell and displacement transducer located in the actuator arm, external *LVDT*s, and strain gauges as discussed in methodology I.

Table 6.7. Material properties of infilled frame with class I and class III clay bricks

Material	Characteristics	Units	Class I Bricks	Class III Bricks
Concrete	Compressive strength	MPa	f_{ck} = 37, E_c = 30414	
	Split tensile strength	MPa	f_{ct} = 2.8	
Longitudinal steel (12Y)	Tensile strength	MPa	f_y = 530, E_s = 2×10^5	
Longitudinal steel (10Y)	Tensile strength	MPa	f_y = 546, E_s = 2×10^5	
Longitudinal steel (8Y)	Tensile strength	MPa	f_y = 562, E_s = 2×10^5	
Stirrups (6Y)	Tensile strength	MPa	f_y = 569, E_s = 2×10^5	
Brick	Dimensions	mm	230×110×75	230×110×75
	Compressive strength	MPa	f_b = 19.2, E_b = 2061	f_b = 6.3, E_b = 516
	Split tensile strength	MPa	f_{bt} = 1.03	f_{bt} = 0.44
Mortar	Compressive strength	MPa	f_j = 17.3, E_j = 7403	f_j = 3.2, E_j = 3795
	Split tensile strength	MPa	f_{jt} = 1.2	f_{jt} = 0.4
Masonry prism	Compressive strength	MPa	f'_m = 4.4, E_m = 1744	f'_m = 1.5, E_m = 608
Masonry wallette	Shear strength	MPa	f'_v = 0.2	f'_v = 0.1

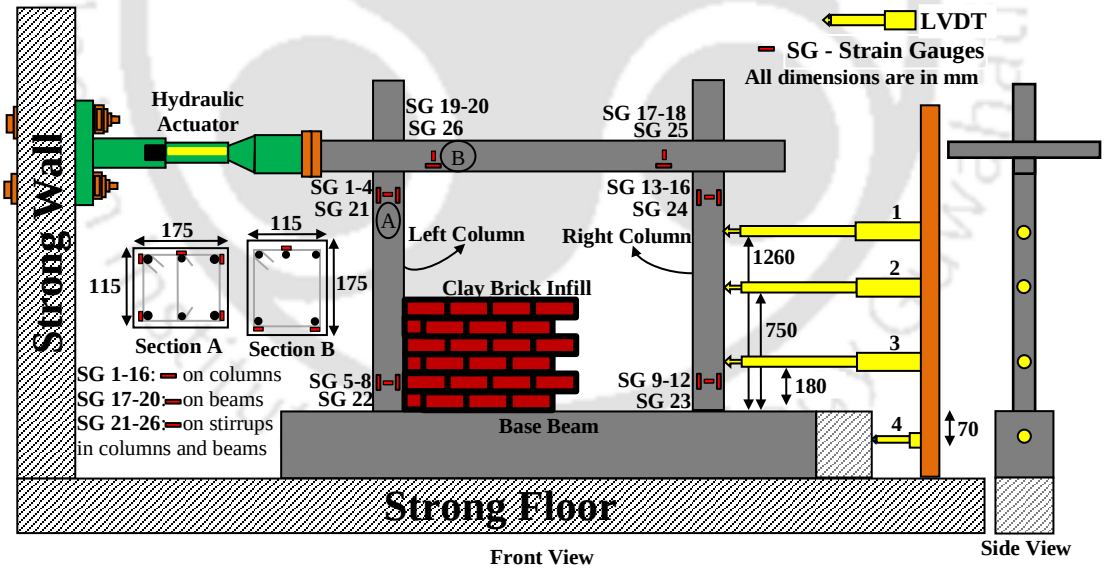

Fig. 6.11. Details of experimental setup and instrumentation of IF-CC1 and IF-CC2.

6.8 Results and Discussion of Methodology II

Experimental results of IF-CC1 and IF-CC2 specimens are reported in terms of hysteretic curves (lateral load resistance vs applied drift at the actuator level), and the envelope curves. Influencing parameters (lateral strength, stiffness, energy dissipation, deformation

characteristics, and failure mechanisms) and their variation with respect to previously tested infilled frame specimens with fly ash bricks are discussed in the following sections.

6.8.1 Hysteretic Response

Hysteretic response of infilled frames IF-CC1 and IF-CC2 is shown in Fig. 6.12. It was observed that the loops were closely spaced in the initial drift level. The lateral load resistance of IF-CC1 with class I clay bricks in the initial drift levels was comparatively higher compared to that of the IF-CC2 with class III clay bricks. It was clearly observed that the increment of lateral load resistance of IF-CC2 was very gradual both in push and pull directions, whereas, the increase was very non-uniform in case of IF-FB2 and IF-CC1 as the interlocking of the infill wall units (bricks) was re-organised with increase in drift levels. Pinching was significantly higher in case of class I brick specimen (IF-CC1) in the post peak region when compared to class III brick specimen (IF-CC2), as the resistance provided by class I masonry infill decreased due to extensive cracking and brittle nature of masonry infill. Whereas, the amount of pinching was nominal in case of IF-CC2 as the masonry provided resistance at higher drift levels by forming bed joint sliding cracks along several courses.

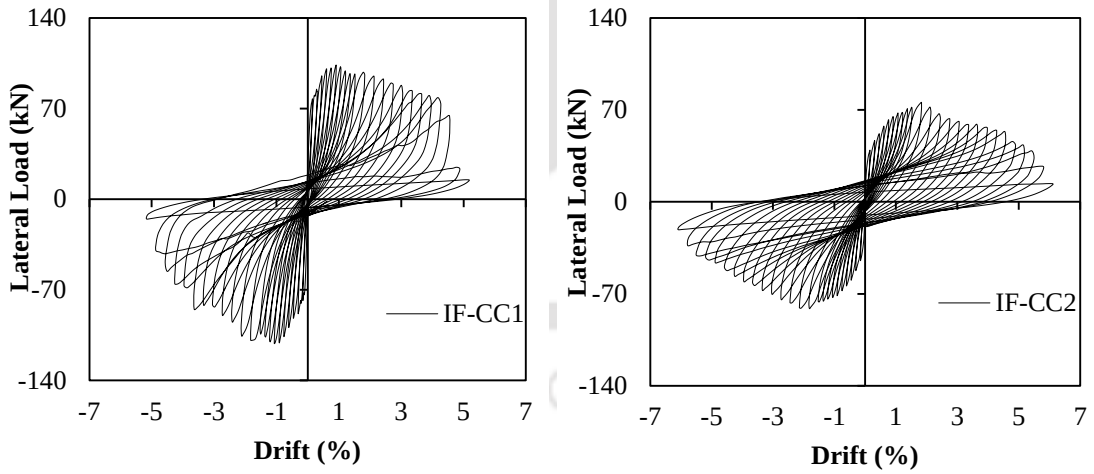

(a) (b)

Fig. 6.12. Hysteretic response of infilled frame specimens: (a) IF-CC1; and (b) IF-CC2.

6.8.2 Evaluation of Influencing Parameters

Initial stiffness of IF-CC2 was found to be lesser compared to that of IF-CC1. It was mainly due to the comparatively stronger and stiffer masonry used in IF-CC1. The

contribution of infill with regard to initial stiffness and strength was significantly higher in the initial drift levels, specifically until the lateral load capacity of the frame was reached. IF-CC2 observed slightly higher initial stiffness when compared to IF-FB2 primarily due to the higher load resistance in the initial drift level (0.15%). Variation of secant stiffness in IF-CC1 and IF-CC2 is shown in Fig. 6.13.

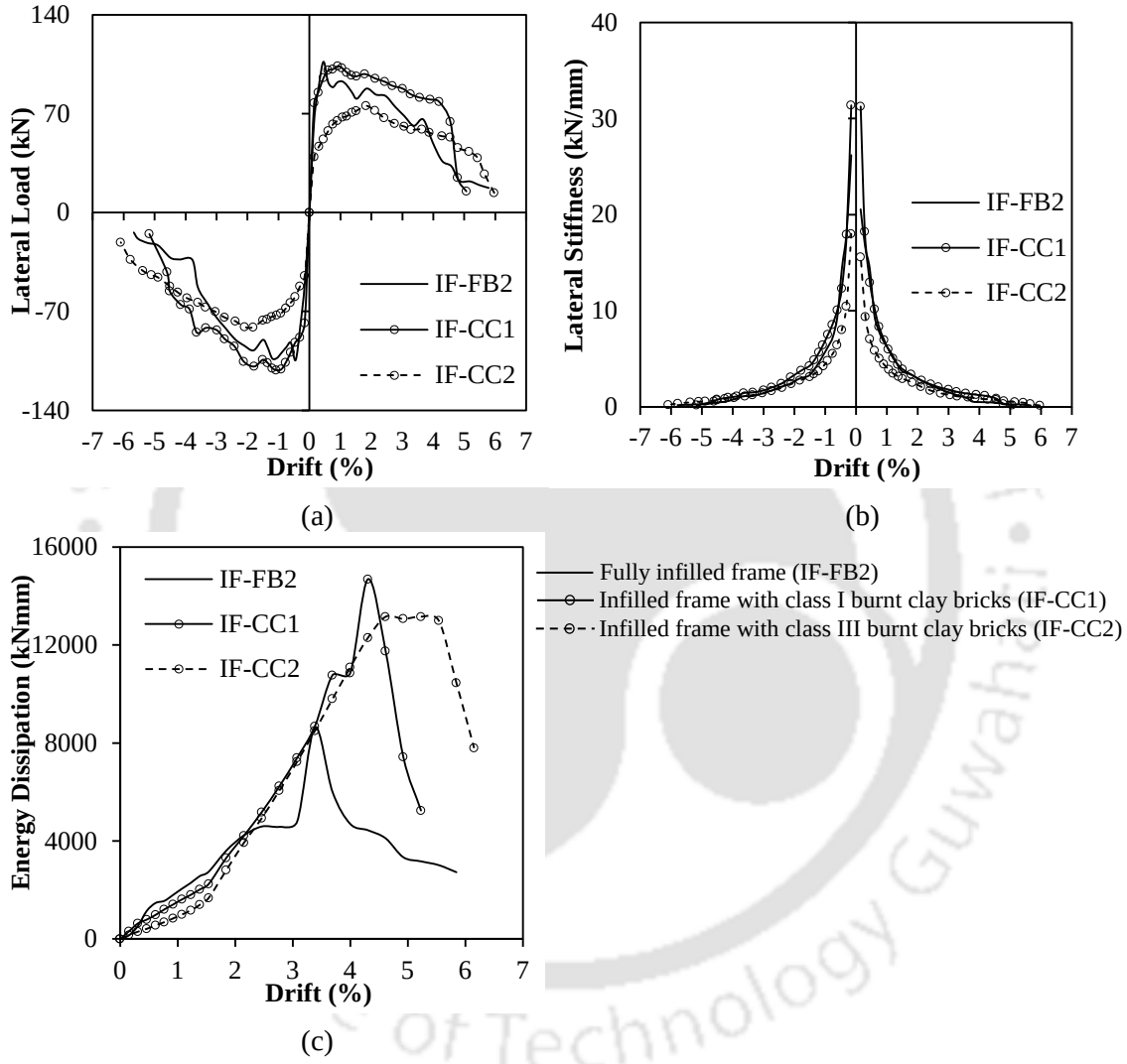

Fig. 6.13. Lateral load behavior of infilled frames IF-CC1 and IF-CC2: (a) envelope curves showing force vs. drift at actuator level; (b) variation of stiffness; and (c) energy dissipation at different drift levels.

Secant stiffness of IF-CC1 was found to be higher in the initial drift levels when compared to IF-CC2 and IF-FB2. The rate of degradation of stiffness in case of IF-CC1 and IF-FB2 was found to be higher when compared to IF-CC2 in both push and pull directions. No significant variation in secant stiffness was observed for all the tested specimens at higher drift levels (>3%). IF-CC1 attracted higher amount of lateral load

resistance in the initial drift levels, which led the specimen to observe higher initial stiffness and strength, and at the same time the capacity of the infilled frame was reached at a lower drift level (0.92%). As the soft masonry was used in IF-CC2 specimen, the lateral load carrying capacity and its degradation in the post peak regime was attained very gradually [Fig. 6.13(a)]. Contribution of infill in case of IF-CC2 in the post peak was significantly higher compared to that of the IF-CC1. The lateral load carrying capacity of IF-CC2 was found to be about 0.75 times that of the IF-FB2, whereas, the load carrying capacity of IF-CC1 was similar to that of the IF-FB2 (Table 6.4). It was observed that most of the cracks in case of IF-CC2 were bed joint sliding cracks in different courses along the height of infill wall with increase in drift levels, whereas diagonal cracking leading to the formation of diagonal strut was the major source of cracking in case of IF-CC1. Due to this reason, IF-CC1 observed higher lateral load resistance at lower drift level until infill reached its capacity.

The cumulative energy dissipated by the IF-CC2 was found to be higher compared to that of the IF-CC1 (Table 6.4). Till 3.7% drift level, it was observed that the energy dissipated by the IF-CC1 was higher compared to IF-CC2 [Fig. 6.13(c)]. As soon as the infill reached the capacity in case of IF-CC1, lateral load carrying capacity of the infill dropped suddenly due to their inherent brittle nature, which led to the transfer of the whole lateral load on to the RC frame for which it was not designed. The frame failed due to sudden transfer of lateral load, leading to the sudden drop in energy dissipation and consequently the test was terminated at a comparatively lower drift level (5.23%) compared to that of the IF-CC2 (6.15%). In case of IF-CC2, it was observed that the energy dissipation increased till 4.3% drift and remained constant till 5.8% drift and the resistance provided by the infill was laid off at 6% drift, which clearly shows the influence of weaker and softer masonry at higher drift levels, in addition to the ductile behavior of the frame. The infill was intact with the frame and no corner crushing was observed till 4.92% drift level and the sliding friction mechanism was the major source of energy dissipation due to low-strength mortar used in masonry.

6.8.3 Crack Pattern and Failure Mechanisms

Cracks in IF-CC1 initiated at a drift level of 0.15% (78 kN) as diagonal stepped cracks in infill from the loading end to the compression corner, with a bed joint sliding crack

formed one course below the middle of the panel. Multiple diagonal stepped cracks were also observed below the middle panel in both directions at the same drift level [Fig. 6.14(a)]. In case of IF-CC2 cracks in infill were initiated at a drift level of 0.15% (-45 kN, +39 kN) as bed joint sliding cracks one course above and below the mid-height of the infill panel along with interface cracking. In the subsequent drift level (0.31%), similar bed joint sliding cracks were formed two courses below the soffit of the top beam along with diagonal stepped cracking in the middle third panel near the corners [Fig. 6.14(c)].

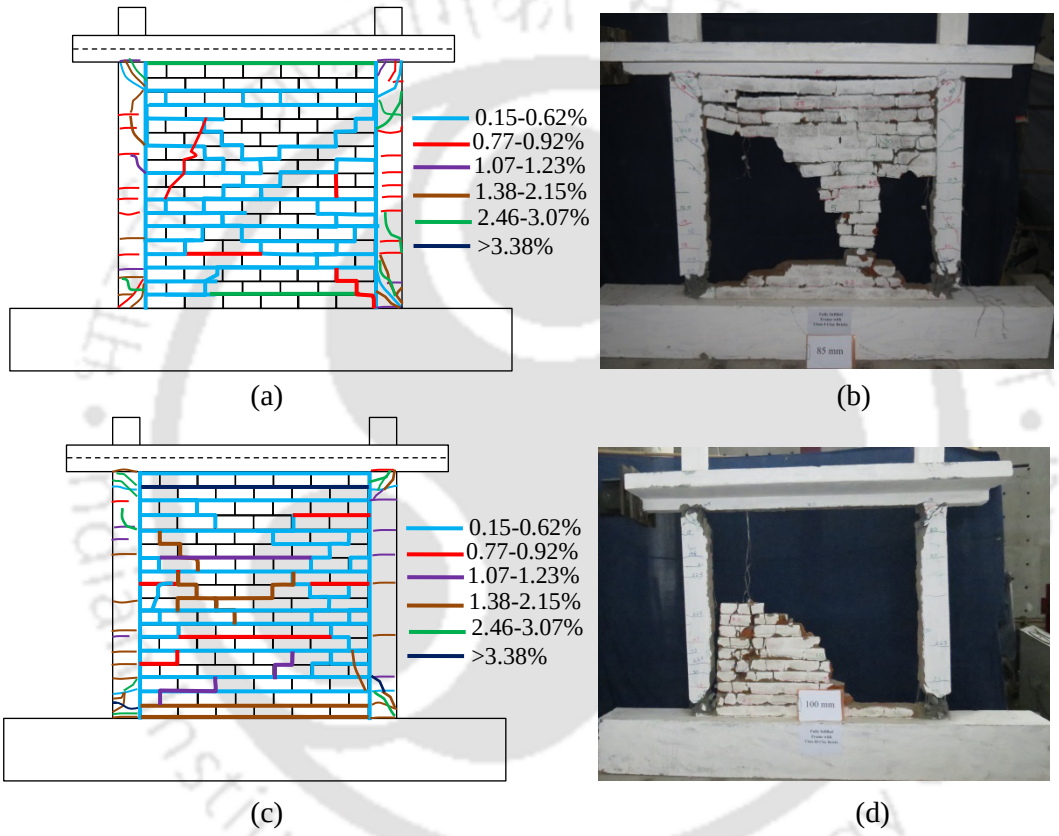

Fig. 6.14. Crack pattern and failure mechanism of: (a) and (b) IF-CC1; (c) and (d) IF-CC2.

Due to the formation of diagonal stepped cracks in IF-CC1, interface connection weakened near the corners of column and wall junctions, which lead to formation of the bed joint sliding cracks two courses below the soffit of the top beam and three courses above the bottom beam at 0.46% (-92 kN, +95 kN) drift level. Due to the weakened interface connection, columns observed initiation of shear cracks (diagonal tensile cracks) near the column ends at a smaller drift level of 0.46% (-92 kN, +95 kN). In the subsequent drift level of 0.62%, clear diagonal strut formation was observed in both push and pull directions as shown in Fig. 6.14(a). In case of IF-CC2 until 0.62% drift, most of

the cracks in infill were bed joint sliding cracks in infill panel. At 0.62% (-64 kN, +58 kN) drift, slight hair line flexural cracks parallel to the direction of loading was marked in columns in case of IF-CC2. Until 1.07% drift, similar flexural cracks were formed along the length of the columns. From the observed crack pattern, it is clearly highlighted that there is a clear shift in cracking in columns from shear to flexure in the initial drift levels when compared to the previously tested infilled frame specimens in the preliminary study (chapter 4). In case of IF-CC1, flexural cracks were initiated at a drift level of 0.76% (-106 kN, +101 kN) along the length of the column and in the subsequent drift level at 0.92% (-112 kN, +104 kN) capacity of the infilled frame was reached. Due to the weak and soft nature of the infill in case of IF-CC2, shear cracks near the column corners were marked at a higher drift of 1.85% (-81 kN, +76 kN), when compared to IF-CC1 (0.46%) and IF-FB2 (0.77%).

The capacity of the IF-CC2 also reached along with the initiation of shear cracks near the column corners at a higher drift level. As the drift levels further increased, intense bed joint sliding and crushing of mortar joints were marked in case of both IF-CC1 and IF-CC2. It was also observed that the flexural cracks developed near the column ends propagated and converted into flexural-shear cracks with increase in drift levels in case of IF-CC1, and cover concrete spalled at 2.15% drift. Widening of shear cracks near the column corners was noticed at a drift level of 3.1% and 4.6% drift, in case of IF-CC1 and IF-CC2, respectively.

In case of IF-CC1, it was observed that flexural shear cracks were marked at various locations along the length of the column, which was not observed in the previously tested infilled frame specimens. Crushing of concrete between the widened shear cracks was observed near the column corners at 4% drift. The test was terminated at 5.23% drift when out-plane failure of infill, buckling of longitudinal reinforcement and opening of shear reinforcement hooks was observed [Fig. 6.14(b)]. In case of IF-CC2, the test was terminated at 6.15% drift when out-of-plane failure of infill, crushing of concrete, tension failure of longitudinal reinforcement and opening of shear reinforcement hooks was observed [Fig. 6.14(d)]. From the observed crack pattern, it was inferred that the use of low-strength and soft masonry in case of IF-CC2 clearly delayed the initiation of shear cracks in columns without compromising other influencing parameters (lateral strength, stiffness and energy dissipation) of infilled frame.

6.8.4 Lateral Load-Strain Response

Nonlinear behavior of cross-sections in terms of variation of strain in rebars at different drift levels in case of IF-CC1 and IF-CC2 is determined using the strain data obtained from the slow-cyclic tests. Tables 6.8 and 6.9 shows the typical strain values recorded in columns of infilled frames IF-CC1 and IF-CC2. The maximum strain values at different storey drifts at various column locations are shown in Fig. 6.15 for the two clay brick specimens. All the strain gauges in columns of IF-CC1 were found to be operational during the test initiation, whereas, SG 11 of IF-CC2 was dysfunctional and therefore not considered in the analysis. It was found that in case of IF-CC2, the rebars near the left column and right column bottom yielded at a lower drift level (1.23% and 0.92%, respectively), whereas, yielding of rebars at all the locations was recorded at a higher drift level (1.38%) in case of IF-CC1.

Table 6.8. Typical strain values recorded at various column locations in IF-CC1

Strain Gauges	Peak Strain				Yield		Yield Curvature /m
	Tension (+)	Compression (-)	Drift (+) %	Drift (-) %	Strain	Drift %	
			Left Column Top				
SG 1	1873	-1289	1.85	-1.85	1873	-1.85	0.0115
SG 2	3657	-2112	4.62	-4.00	2726	-2.15	0.0213
SG 3	6501	-225	3.69	-1.08	2703	-1.38	0.0268
SG 4	2800	-920	3.08	-5.23	2602	-2.15	0.0313
			Left Column Bottom				
SG 5	4791	-1002	3.69	-2.77	2659	-3.08	0.0064
SG 6	3479	-2094	2.77	-2.77	2782	-2.46	0.0401
SG 7	4431	-1636	2.15	-2.15	2703	-1.54	0.0207
SG 8	3493	-623	1.85	-1.85	2630	-1.54	0.0237
			Right Column Bottom				
SG 9	4880	-642	1.85	-1.54	2876	1.38	0.0211
SG 10	3832	-690	1.85	-1.54	2782	1.54	0.0248
SG 11	4013	-5636	5.23	-5.23	-2724	4.00	
SG 12	1858	-4059	1.85	-3.69			
			Right Column Top				
SG 13	2887	-1707	3.69	-4.92	2701	1.85	0.0276
SG 14	4453	-629	2.15	-4.92	2566	1.38	0.0243
SG 15	2149	-1762	2.15	-4.31	2149	2.15	
SG 16	2459	-1776	2.15	-3.08	2459	2.15	

In case of IF-CC1, the rebars near the left column top, bottom and top of right column observed yielding at the same drift level (1.38%), and the rebars near the left column bottom observed yielding at a slightly higher drift level (1.54%). The curvature corresponding to yielding in case of IF-CC1 was found to vary from 0.0207 /m to 0.0268 /m. Yielding of rebars was observed at the same drift level (1.85%) near the right and left

column top locations in case of IF-CC2 and the corresponding curvature was found to be about 0.0209 to 0.0263 /m (Fig. 6.16).

Table 6.9. Typical strain values recorded at various column locations in IF-CC2

Strain Gauges	Peak Strain				Yield		Yield Curvature /m
	Tension (+)	Compression (-)	Drift (+) %	Drift (-) %	Strain	Drift %	
			Left Column Top				
SG 1	2783	-1328	2.15	-6.15	2650	1.85	0.0247
SG 2	3144	-1328	3.69	-6.15	2854	1.85	0.0263
SG 3	2522	-2081	1.85	-4.62	2522	1.85	0.0209
SG 4	1549	-1210	1.85	-3.69	1549	1.85	
			Left Column Bottom				
SG 5	4170	-1384	3.08	-4.00	2606	1.23	
SG 6	5193	-1392	5.23	-4.31	2622	1.38	0.0320
SG 7	1406	-1797	4.92	-4.92	1406	4.92	
SG 8	3417	-2983	4.62	-1.54	2654	2.77	0.0271
			Right Column Bottom				
SG 9	3853	-246	1.54	-1.54	2738	0.92	0.0239
SG 10	2026	-642	1.23	-1.23	2026	1.23	
SG 11			Not Operational				
SG 12	4490	-1778	4.31	-4.31	2627	1.54	0.0262
			Right Column Top				
SG 13	2471	-1240	2.15	-2.15	2471	2.15	
SG 14	2521	-1911	3.08	-3.08	2521	3.08	0.0213
SG 15	2783	-1389	3.08	-4.62	2642	1.85	0.0250
SG 16	2613	-741	3.08	-5.23	2613	3.08	0.0334

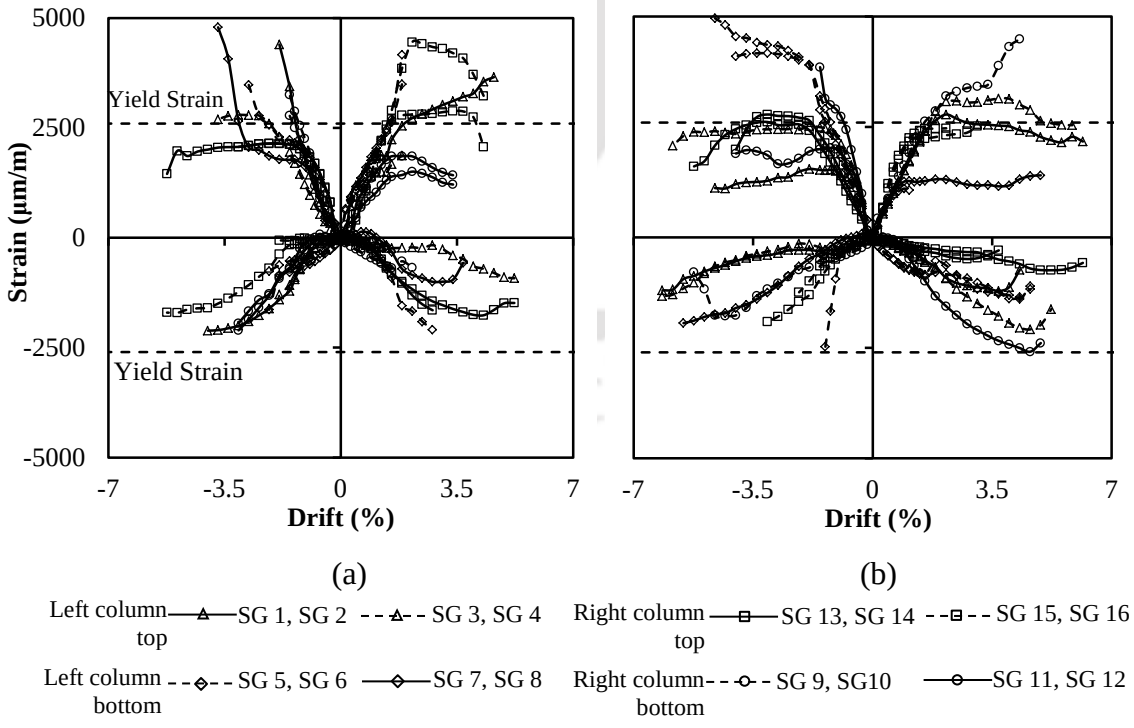

Fig. 6.15. Envelope curves showing strain vs. lateral drift for: (a) IF-CC1; and (b) IF-CC2.

From the lateral load-strain response of IF-CC1, it was affirmed that the yielding of rebars initiated in the post-peak regime at 1.38% drift after the initiation of major damage events (flexural and shear cracks). Whereas, in case of IF-CC2, it was observed that the yielding of rebars was initiated prior to the lateral load capacity of the infilled frame. The curvature corresponding to the yield drift was not considered for the strain gauges SG 1, SG 12, and SG 15 in case of IF-CC1, and SG 4, SG 7, SG 10, and SG 13 in case of IF-CC2. This is due to the maximum strain recorded being lesser than the yield strain before their disconnection. The curvature calculation corresponding to SG 11 in case of IF-CC1 was also not considered as the rebar yielded at a very higher drift level (4.0%) and the rebar on the opposite face yielded at a lower drift level. Moreover the strain gauge bonded to the reinforcement was found to be disconnected.

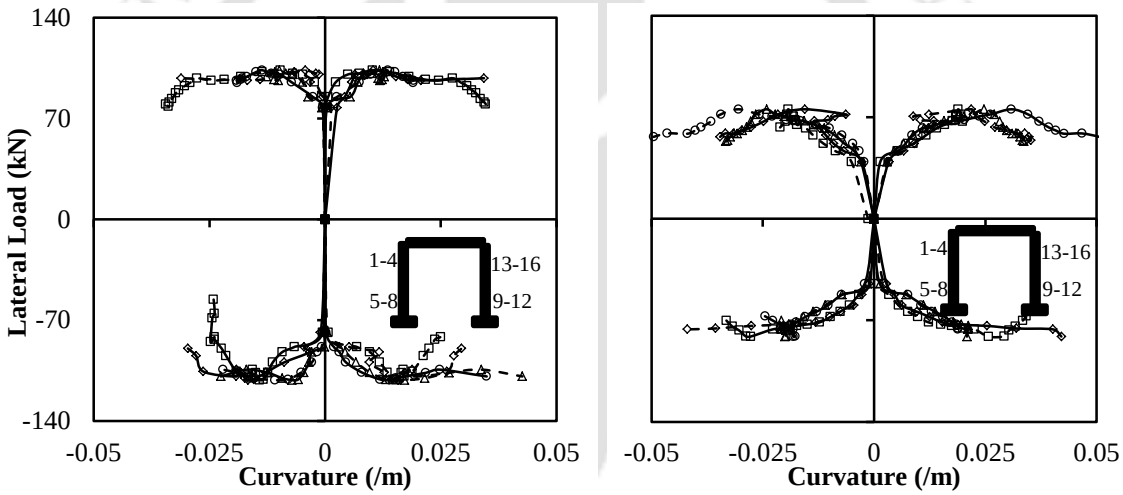

Fig. 6.16. Lateral load-curvature response of: (a) IF-CC1; and (b) IF-CC2.

It was also observed in IF-CC2 that the shear cracks developed after the yielding of rebars, whereas, the flexural cracks initiation was observed slightly before the yielding of rebars. From the analysis of strain gauge data, it was affirmed that using low-strength and soft masonry forced the infill frame system IF-CC2 in to ductile mode, which was substantiated by the yielding of rebars at a lower drift level (0.92%) and the reduction of lateral load response to 80% of maximum at a higher drift level (3.38%). Similar ductile response was not observed in case of infilled frame with high strength masonry (IF-CC1), where the difference between yielding of rebars and 80% of lateral load capacity was significantly less as the rebars yielded in the post-peak regime (1.38%) and the capacity

was reduced to 80% at 2.77% drift. This can be understood by the fact that infill contributed to lateral load capacity of the infilled frame IF-CC1 in the initial stages, and as soon as the capacity of the infill was reached, there was a sudden transfer of force from infill to frame members for which they were not designed. This led to the sudden yielding of frame members and reduction of lateral load capacity at a lower drift level in post peak regime of lateral load response.

6.9 SUMMARY

Two methodologies were proposed in this chapter for improving the lateral load response of masonry infilled RC frames, which were observed to fail due to shear failure of columns. In the first method, columns were redesigned such that the shear capacity of column becomes more than the demand, without increasing the shear reinforcement beyond a limit corresponding to the shear compression failure. In the second method, weaker and softer masonry was used to reduce the influence of masonry on the RC frame. The methodologies were evaluated analytically and experimentally. From the experimental investigation of both the methodologies, it was found that the shear failure of columns was delayed to a larger extent in addition to enhancing the influencing parameters of the infilled frames. The nonlinear response of the cross-sections of the columns was also evaluated using the data recorded from the reinforcing bars in various column sections. The third methodology in which the effect of infill on RC frame was diffused by dividing the infill into sub-panels will be discussed in the next chapter.

Chapter 7
IMPROVEMENT IN SHEAR BEHAVIOR OF INFILLED FRAMES: DECREASING FRAME-INFILL INTERACTION

CONTENTS

7.1 OVERVIEW

In the previous chapter, effectiveness of the first two methodologies (increasing the design shear capacity of the column sections, and using low-strength and soft masonry as infill) to improve the shear behavior of columns were investigated both analytically and experimentally. In the current chapter, the third methodology based on decreasing the frame-infill interaction by diffusing the effect of infill on the columns is discussed. This can be achieved by providing sliding mechanism to infill along the predefined failure planes. Sliding planes in the infill panels were introduced by dividing the infill wall into sub-panels by using RC collector beams, as partition elements. Initially, the effectiveness of the methodology was evaluated analytically by carrying out a parametric analysis for various collector beam configurations using the improved analytical macromodel. Subsequently, the best performing models were verified by carrying out experimental investigations on half-scale masonry infilled RC frames.

7.2 DESCRIPTION OF METHODOLOGY III

The main intention behind proposing the methodology is to fulfill the need to control the frame-infill interaction and minimize the building damage. It is achieved by imposing a weak deformation mechanism to the masonry infill by means of sliding joints. Creation of sliding mechanism by dividing the masonry walls into sub-panels has been traditionally adopted in various building typologies (Dhajji-Dewari, Fachwerk, Colombage, Casa Baraccata, Half-timber). This mechanism is very effective for earthquake resistance, especially, in load bearing structures and the timber frame constructions. In these types of constructions, the whole masonry panel is sub-divided into many parts with the inclusion of horizontal, vertical and diagonal elements. The presence of these elements in masonry walls under lateral loading, resists the propagation of cracking, increases progressive damage of the wall, and also increases the friction along the interfaces of masonry and the sliding elements enhancing the energy dissipation capacity. However, this methodology has never been adopted in the modern-day masonry infill RC framed constructions. This methodology has been selected and adopted in the current study with suitable modifications to evaluate the shear behavior of the columns under lateral loading (Fig. 7.1). Both analytical and experimental investigations were carried out for various collector beam configurations to evaluate the effectiveness of the methodology and are discussed in the following sections.

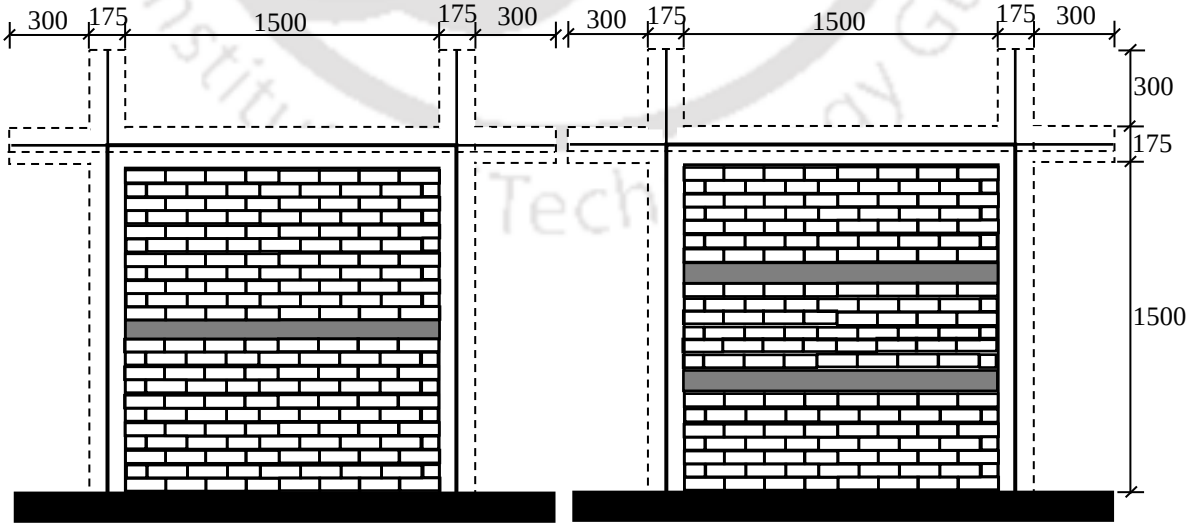

Fig. 7.1. Schematic representation of masonry infilled frame with RC collector beams.

7.3 Analytical Evaluation of Methodology III

A preliminary linear parametric analysis was carried out on infilled frames with various configurations of collector beams. This was done to check whether the diagonal compressive strut analogy is valid when collector beams are used in infills. Initially, the entire infill panel was modelled as a shell element and subsequently the panel was divided into sub-panels using collector beams. If the compression flow of principal stresses was observed along the loaded diagonal corners (compressive strut analogy), the shear demand in the column was evaluated using the improved analytical model proposed in the previous chapter. If not, micromodelling techniques were opted so as to predict shear failure on the columns due to the introduction of collector beams.

7.3.1 Linear Parametric Analysis

A linear lateral load parametric analysis was carried out to check whether the diagonal compressive strut analogy is valid or not after the introduction of collector beams. The material properties of the linear shell element were similar to that of the infill wall. The flow of principal compressive stresses in case of fully infilled frame was verified by applying a lateral load of 100 kN at the left column top. It was observed that the compressive stresses were flowing from left column top to right column bottom in case of fully infilled frame as shown in Fig. 7.2(a). The infill wall was divided into two panels by introducing central horizontal collector beam and the analysis was repeated. It was observed that the infill panel present above the central collector beam exhibited flow of compressive stresses, whereas, the bottom panel observed slightly higher amount of tensile stresses.

Similar analysis was carried out by dividing the infill shell element into three equal parts by providing two collector beams as partitions. Although flow of tensile stresses was found to be higher in the middle panel (Fig. 7.2), still compressive flow of stresses was observed. A third configuration was evaluated in which the infill was sub-divided into four panels and it was found that the compressive stresses were less in the middle panels when compared to top and bottom infill panels. From the linear parametric analysis, it was confirmed that the compressive flow of stresses took place along the loaded diagonals of the sub-panels after the introduction of collector beams. A note-of-caution is required that the number of partitions specified was a compromise between the

structural efficiency and the cost effectiveness. In fact, Preti et al. (2012) from the nonlinear finite element analysis showed that for limiting the infill damage, a minimum number of partitions are necessary so as to ensure the deformation compatibility between the frame and the infill. Such a minimum number depends on several parameters, the most important being the infill material stiffness and friction resistance at the joints.

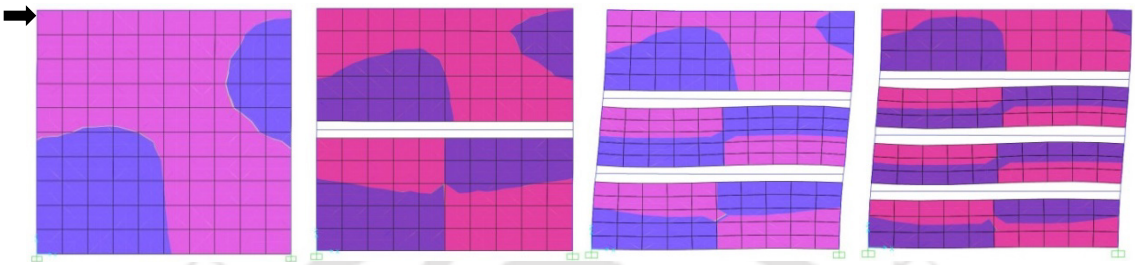

(a) (b) (c) (d)

Fig. 7.2. Comparison of flow of compressive stresses in infilled frames for various collector beam configurations: (a) no collector beam; (b) one central collector beam; (c) two collector beams; and (d) three collector beams.

7.3.2 Nonlinear Analysis using Improved Analytical Model

It was observed from the parametric analysis that for the considered collector beam configurations the compressive flow of stresses was observed from the loaded corner to the opposite diagonal end. The improved analytical macromodel strut analogy was therefore employed to evaluate the effectiveness of the methodology (sub-paneling of infill using collector beams) in diffusing the shear demand on columns. Six types of collector beam configurations were considered: (1) central horizontal collector beam; (2) two horizontal collector beams; (3) three horizontal collector beams; (4) central vertical collector beam; (5) central horizontal and vertical collector beams; and (6) two horizontal and one vertical collector beams. The details of the analytical model have been discussed elaborately in chapter 5. The major difference for the model with collector beams is the inclusion of RC collector beams at various heights of the columns. Collector beam elements were modelled as two-noded frame elements connected to the columns.

To start with, section of RC collector beam was taken as 110×110 mm, by considering the width of the beam similar to that of the infill panel thickness. Details of the design of collector beams are provided in the next section. Masonry infill was modelled as equivalent diagonal strut with the width calculated as one tenth of the

diagonal length of the infill. Nonlinear pushover analysis was carried out by applying the effect of infill along the contact length of the column. Fig. 7.3 shows the lateral load response and plastic hinge formation of the infilled frames with collector beams. In case of infilled frame with central horizontal collector beam, the base shear capacity was found to be slightly higher than that of the fully infilled frame (Table 7.1 and Fig. 7.3). There was no formation of shear hinges as the shear demand was about 13% lesser than that of the shear capacity of the column.

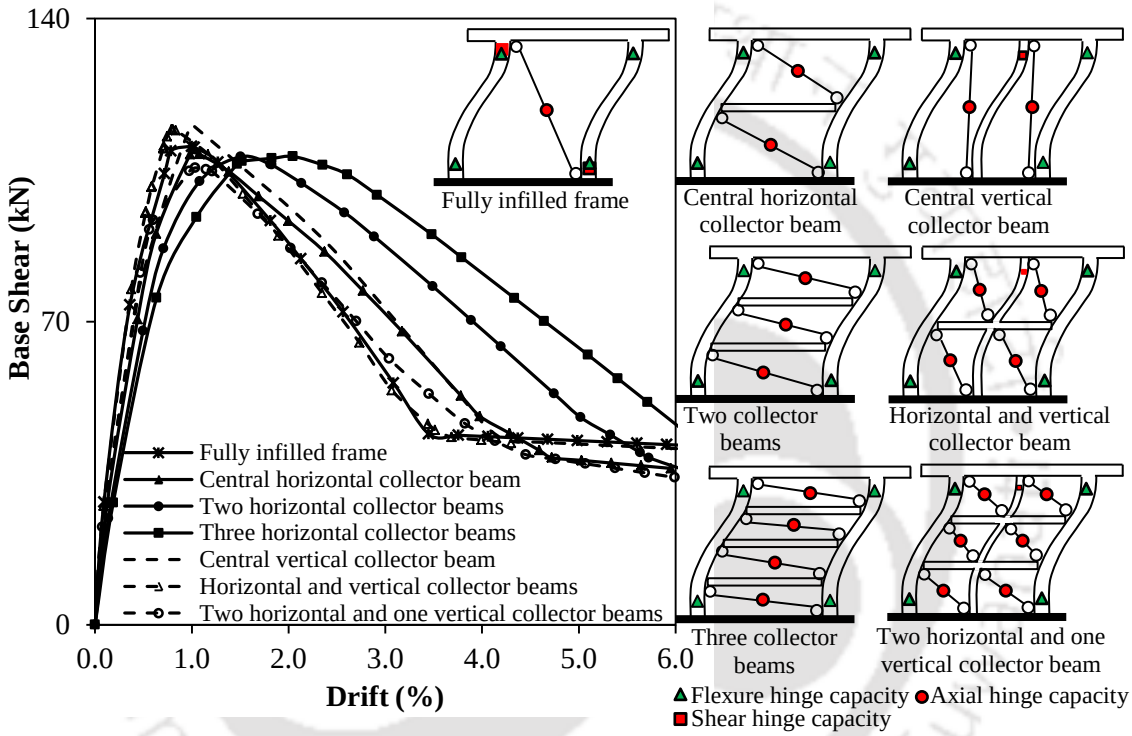

Fig. 7.3. Comparison of lateral load response and hinge formation of infilled frames with different collector beam configurations using the improved analytical model.

Table 7.1. Parametric analysis of infilled frames with collector beams

Type of Frame	w_s mm	Base Shear kN	Type of Hinges Formation
Fully Infilled frame (IF-FB2)	234	111	Axial hinges in infill, shear, and flexural in columns
Infilled frame with central horizontal collector beam	187	123	Axial hinges in infill and flexural hinges in columns
Infilled frame with two horizontal collector beams	177	116	
Infilled frame with three horizontal collector beams	173	115	
Infilled frame with central vertical collector beam	181	130	Axial hinges in infill, shear hinges in vertical collector beams and flexural hinges in columns
Infilled frame with central horizontal and vertical collector beams	117	118	
Infilled frame with two horizontal and one vertical collector beams	100	108	

In the case of infilled frame with two and three horizontal collector beams, it was observed that the base shear capacity was similar to that of the fully infilled frame. The shear demand on the column due to the effect of infill was found to be significantly reduced. In all the three horizontal collector beam configurations of infilled frames considered, similar stages of hinge formation was observed, i.e., axial hinges in infills and flexural hinge in column elements (Fig. 7.3). There was no shear hinge formation observed in columns.

In the current study, influence of vertical collector beams, in addition to horizontal collector beams, was also investigated. Provision of vertical collector beams decreased the shear demand on the column by about 50%. It may be due to the fact that vertical collector beams act as additional vertical frame elements, which significantly reduced the shear demand on the columns. Moreover, provision of both horizontal and vertical collector beams reduced the shear demand on the column significantly. It was also observed that the presence of vertical collector beams as partitions increased the base shear capacity of the frame. From the analysis, it was observed that the vertical collector beams acted as fuses by failing in shear mode in the analysed frames, thereby decreasing the shear demand on the columns. Providing both horizontal and vertical collector beams were found to be viable options in decreasing the frame-infill interaction without altering the behavior of the infilled frame. However, due to the construction difficulties provision of vertical collector beams may not be a practical feasibility especially in case of solid brick masonry construction.

An experimental study was carried out by considering the horizontal collector beams to verify the effectiveness of the third methodology. A further refined micromodelling may be carried out to evaluate the interaction and sliding effects of collector beams and infill panel. Prior to the experimental investigation, design of collector beams was carried out by considering various connectivity conditions with the columns and is discussed in the following section.

7.4 Design of Collector Beam

Generally, the concept of collector beams (lintel beams) is used in masonry structures is to support wall weight and other loads over an opening and transfer these loads to the adjacent masonry. In the current study, collector beams were employed to introduce

horizontal partitions in infill walls. These construction practices were termed as laced masonry with wood elements to break the continuity of infill wall (Langenbach 2007). Most of the past studies utilized wood elements and steel plates as partition elements. The major difficulty with the wood elements was the shrinkage and deterioration in contact with water. Whereas, the major issues with the steel foils were thermal insulation, additional cost and skilled supervision. The most feasible and affordable partition elements may be either precast concrete collector beams or concrete beams constructed simultaneously along with the construction of infill. In the current study, the latter was employed, i.e., construction of collector beams simultaneously with the construction of infill wall.

It may be emphasised that the design of collector beams was dependant on the type of connectivity with the columns. Collector beams may be connected to the RC column elements either monolithically or non-monolithically. The design details of collector beams considering the different critical loading based on various connectivity conditions are shown in Table 7.2. In case of monolithic construction, collector beams may be designed to carry moment, shear, and axial tension from the columns. Considering the maximum shear force acting on the column as the ultimate axial tensile force, and the moment evaluated using the analytical improved model, the design reinforcement was found to be higher. This is because the entire tensile force needs to be resisted by the steel reinforcement in the collector beam.

Table 7.2. Design details of collector beam

Design Parameters	Non-monolithic Collector Beam	Monolithic Collector Beam			
	Force Resultants				
Critical moment (kNm)	-	1.5	3	5.3	3
Critical shear force (kN)	-	2.4	-	-	5
Critical tensile force (kN)	95	-	58	95	-
Main reinforcement	4-8Y	4- 6Y	2-12Y 2-10Y	4-12Y	4-8Y
Transverse reinforcement	Minimum reinforcement: 6Y @ 150 mm c/c				
Section (mm)	110×210	110×110	110×110	110×150	110×150
Concrete cube strength (MPa)	20	20	20	20	20
Yield strength of steel bars (MPa)	500	500	500	500	500

If the collector beams are constructed non-monolithically, then they need to be designed for the tensile force, provided that the collector beams are not separated from the column; else design to carry masonry weight only if the beam is separated from the

column. Indian standard (BIS 2000) recommend the design of tension members in accordance with the working stress method. The entire tensile force needs to be resisted by the steel reinforcement satisfying both the serviceability and strength criteria. The concrete section should be capable of resisting tensile forces without cracking. From the table, it can be observed that, the area of concrete section required to resist tensile forces without cracking was found to be very conservative and were not considered in the current study.

If the collector beam is well separated from the column, it can be designed to resist only the masonry infill weight acting over the beam. Design of collector beam is similar to that of the lintel design in masonry construction where the effect of arching action may be considered. In the current study, the critical load case is the whole weight of masonry acting on the collector beam. No arching action will be developed in the infill, as the apex of the equilateral triangle just cuts the beam and slab. The collector beam was designed to resist the entire weight of the infill. The stiffening action provided by the RC beam-slab was quite high, and moreover, infill wall was constructed after the construction of RC frames. This type of construction practice apparently leaves gap between the soffit of the beam and the infill wall. Therefore, the vertical loads applied over the slab were not transferred to the infill wall. Considering the whole masonry weight, the area of concrete section works out to be about 110×70 mm, in which the width of the collector beam is same as that of the single-wythe infill wall. Based on the various design considerations and different connectivity conditions, it was decided to design the collector beam to resist the weight of the masonry infill and the construction will be carried out non-monolithically. The adopted design of collector beam was with 110×110 mm section consisting of 4-8 diameter bars as main reinforcement and 6 mm diameter bars @ 150 mm c/c as transverse reinforcement.

7.5 Experimental Investigation of Methodology III

The third methodology of diffusing the frame-infill interaction was verified experimentally by conducting tests on four frames comprising of: bare frame with collector beam (BF-CB) at lintel level; infilled frame with central collector beam (IF-CB1), infilled frame with two collector beams (IF-CB2), and infilled frame with two collector beams with central window opening (IF-CB3). The first test (BF-CB) was

carried out in a different study (Surendran 2012). Initially, bare frame with collector beam at lintel level (BF-CB) was constructed so as to serve as a reference specimen for the considered methodology. Infilled frame with central window opening (IF-CB3) of size 10% of overall area of infill was also tested to evaluate the influence of collector beams in case of infill walls with openings. The following section describes in detail the design, detailing, and construction of the frames.

7.5.1 Description of the Test

The design, detailing and construction of the RC frame was similar to that of the frames considered previously in methodology I and II. The major difference in case of frames with collector beams is the embedment of reinforcement at different levels along column height for different collector beam configurations. In case of reference frame BF-CB, three 8 mm diameter bars were embedded in both the columns and extended to a distance of 220 mm from the inner face of both the columns to support the RC collector beam [Fig. 7.4(a)]. The main intention behind the construction of BF-CB was to evaluate the influence of collector beam on the lateral load behavior of bare frame. The reinforcement was placed at a distance of 275 mm below the soffit of the top beam of the frame. This location of the collector beam simulates the conditions of a lintel beam in case of an infilled frame with 50% opening.

In case of infilled frames (IF-CB1, IF-CB2, IF-CB3), two different collector beam configurations were considered. In case of IF-CB1, during the reinforcement detailing schedule of RC frame, 12 mm diameter bar was embedded in both the columns near their mid-height (i.e., 750 mm above the base beam) as shown in Fig. 7.4(b). In case of IF-CB2 and IF-CB3, 12 mm diameter bars were placed at 500 mm and 1000 mm along the height of the column above the base beam in both the columns as shown in Fig. 7.4(c). Formwork was fabricated to the desired dimension and was laterally supported by placing wooden buttresses at regular intervals so as to support the lateral pressure on the formwork (Fig. 7.5). To facilitate easy placing of mixed-in-place concrete, casting of the frame was carried out in the horizontal position. After seven days of casting, formwork was removed and the frame was lifted and placed in vertical position. This was followed by the construction of both infill wall and collector beams.

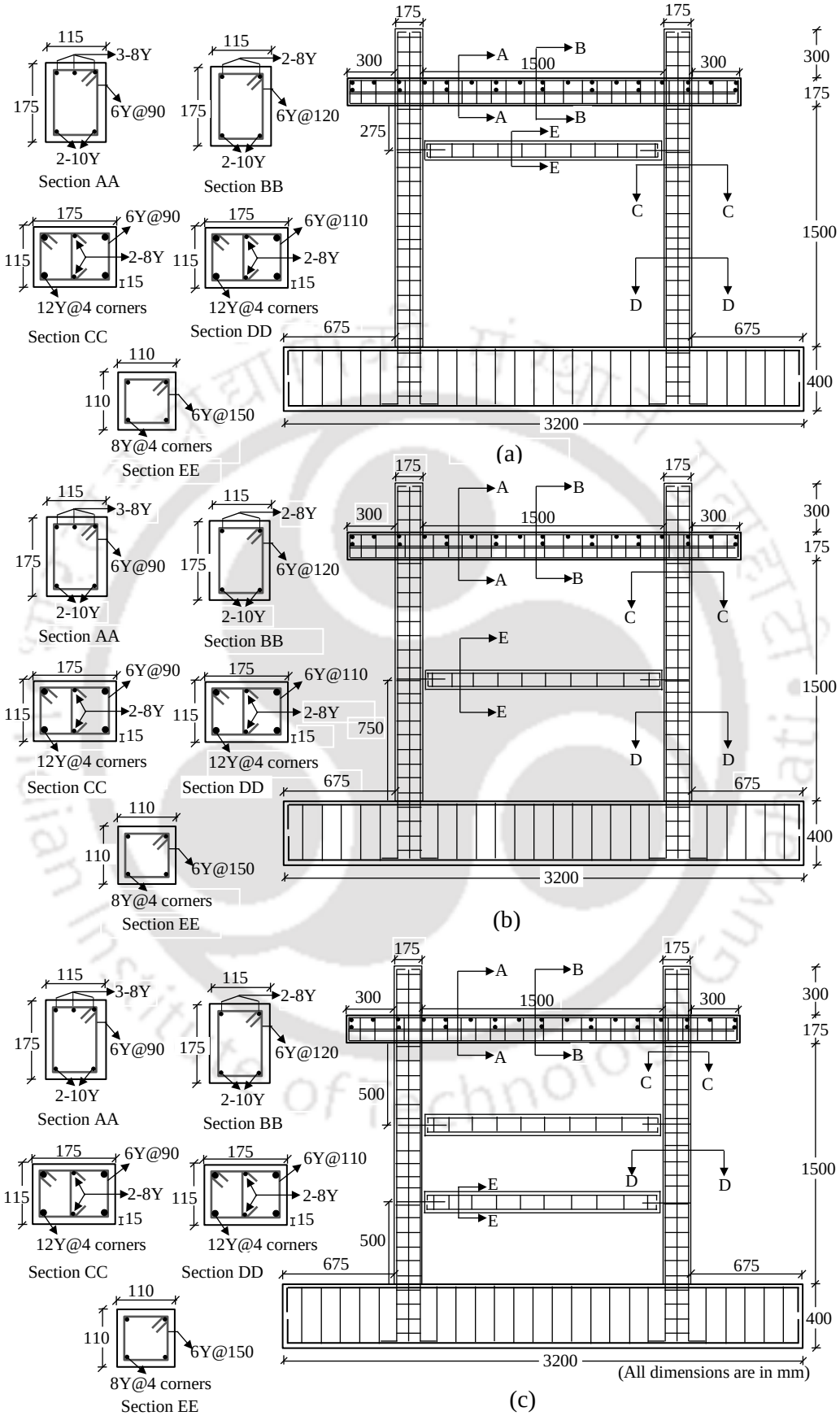

Fig. 7.4. Reinforcement detailing of: (a) BF-CB; (b) IF-CB1; and (c) IF-CB2 & IF-CB3.

In case of BF-CB, RC collector beam of size 110×110 mm was casted after erection of the frame and cured for 28 days (Fig. 7.6). In case of IF-CB1, infill wall was constructed up to 700 mm above the base beam, followed by the collector beam construction in the following day as shown in Fig. 7.6(b). The 12 mm diameter bar in both the columns was extended into the collector beam before casting in order to provide a non-monolithic connection between the RC columns and the collector beams. In order, to diffuse the friction between the mortar bed joints and concrete, polythene sheets of approximately 0.5 mm thickness were placed above and below the collector beams. Polythene sheets were mainly provided to clearly define the sliding failure planes in infill, so that the effect of infill on the columns is reduced which may inhibit the damage of columns.

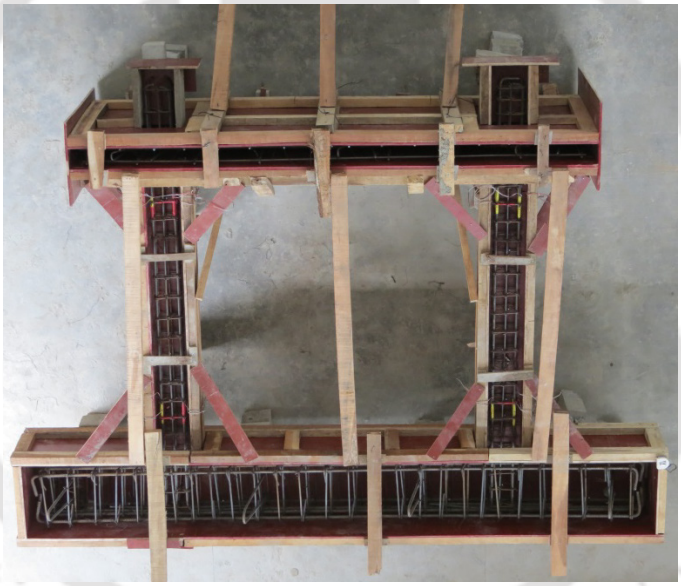

Fig. 7.5. Fabrication of formwork in the construction of RC frame.

In case of IF-CB2, infill wall construction was carried out in three parts. Initially, infill wall was constructed upto 450 mm above the base beam followed by the construction of collector beam in the following day and was allowed for curing [Fig. 7.6(c)]. Later infill wall in the middle panel was constructed followed by the construction of top collector beam on the subsequent day. The remaining wall was constructed in the following day. Construction of infill wall in case of IF-CB3 was similar to that of IF-CB2, with the only difference being the opening in the middle panel. An opening of size 475×110×475 mm was provided in the middle panel by constructing two masonry piers of size 512×110×475 mm near both the columns.

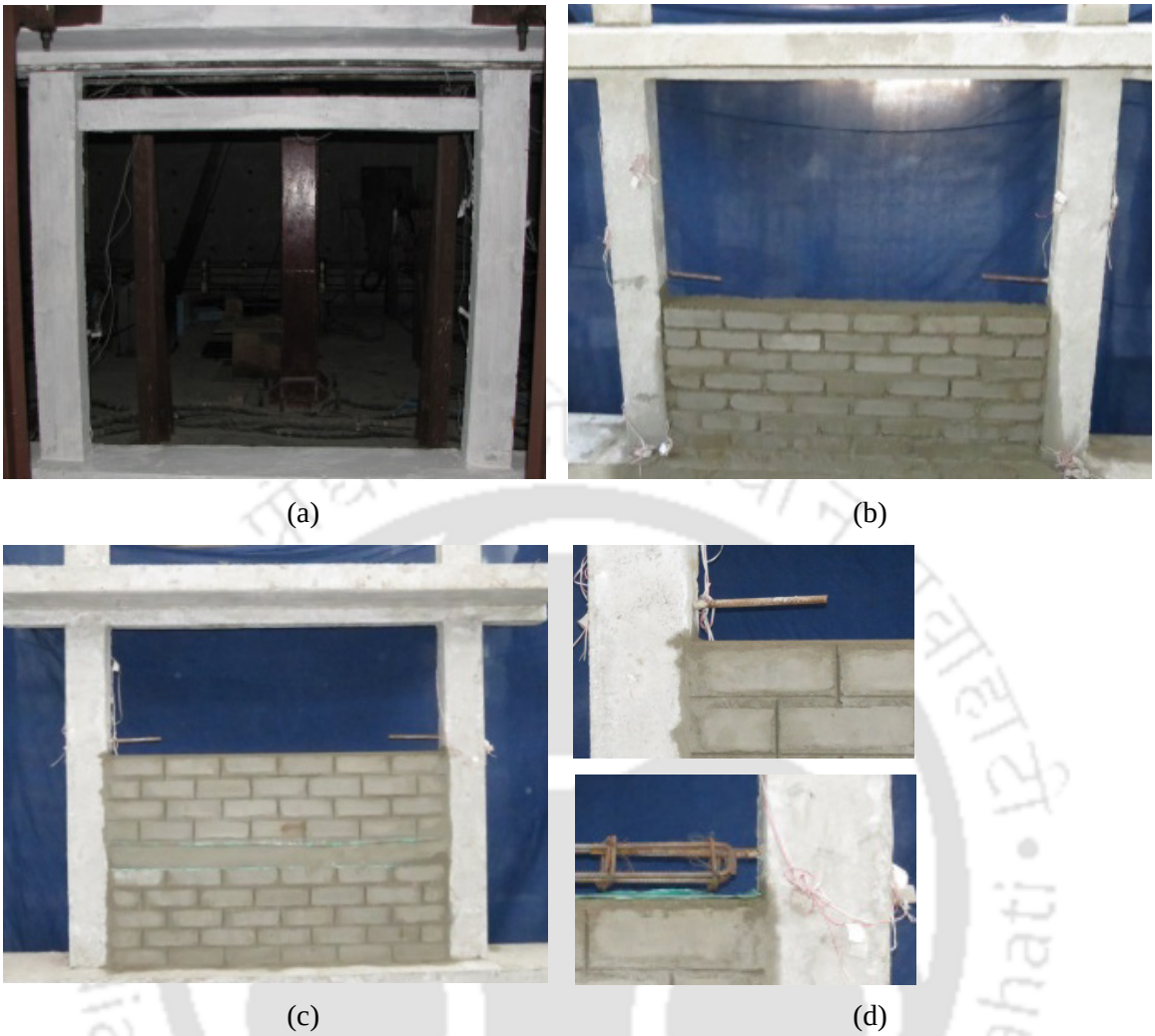

(a) (b)

(c) (d)

Fig. 7.6. Construction of frames with collector beams: (a) BF-CB; (b) IF-CB1; (c) and (d) IF-CB2.

Summary of material properties of fly ash brick masonry and frame material characteristics for the four frames with different collector beam configurations are presented in the Table 7.3. The average compressive cube strength of concrete (f_{ck}) was found to be 36 MPa with modulus of elasticity (E_c) of about 29,580 MPa and the average split tensile strength of concrete cylinder (f_{ct}) was 2.9 MPa. The frame specimens were tested under slow-cyclic displacement controlled loading as applied in case of previous specimens using servo-controlled hydraulic actuator of 250 kN load capacity and a stroke length of ± 125 mm (Fig. 7.7). The instrumentation and data acquisition remained similar as that of methodologies I and II. Experimental results were recorded continuously using load cell and displacement transducer located in the actuator arm, external *LVDT*s (linear varying displacement transducers), and strain gauges.

Table 7.3. Material properties of frame with collector beam specimens

Material	Characteristics	Units	Properties
Concrete	Compressive strength	MPa	f_{ck} = 36, E_c = 29,580
	Split tensile strength	MPa	f_{ct} = 2.9
Longitudinal steel (12Y)	Tensile strength	MPa	f_y = 530, E_s = 2×10^5
Longitudinal steel (10Y)	Tensile strength	MPa	f_y = 546, E_s = 2×10^5
Longitudinal steel (8Y)	Tensile strength	MPa	f_y = 562, E_s = 2×10^5
Stirrups (6Y)	Tensile strength	MPa	f_y = 569, E_s = 2×10^5
Fly ash brick	Dimensions	mm	230×110×75
	Compressive strength	MPa	f_b = 5.7, E_b = 3900
	Split tensile strength	MPa	f_{bt} = 0.54
Mortar	Compressive strength	MPa	f_j = 17.3, E_j = 7400
	Flexural strength	MPa	3.78
	Split tensile strength	MPa	f_{jt} = 1.2
Masonry prism	Compressive strength	MPa	f'_m = 3.9, E_m = 2700
Masonry wallette	Shear strength	MPa	f'_v = 0.14, G_m = 730

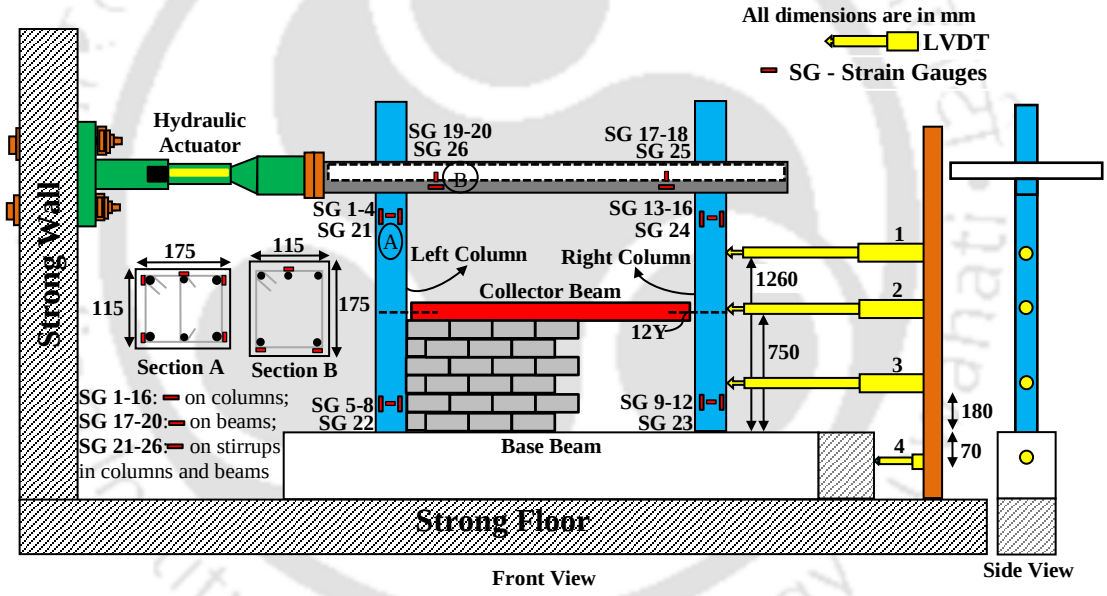

Fig. 7.7. Details of test setup and instrumentation in infilled frames with collector beams.

7.6 Results and Discussion of Methodology III

Experimental results of the frames constructed with various collector beam configurations were reported in terms of hysteretic response and envelope curves. The results pertaining to influencing parameters (lateral strength, stiffness, energy dissipation, deformation characteristics, and failure mechanisms) and their variation with respect to previously tested infilled frames are discussed in detail in the following sections. Infilled frame with 10% central window opening (IF-FB3) tested in the previous experimental study

(Surendran 2012) was considered to compare the results of infilled frame with two collector beams with 10% central opening (IF-CB3).

7.6.1 Hysteretic Response

Hysteretic responses of the bare frame with collector beam (BF-CB) and infilled frames with collector beams (IF-CB1, IF-CB2, and IF-CB3) are shown in Fig. 7.8. The hysteretic behavior of the BF-CB was similar to that of the previously tested bare frame BF. Hysteretic loops were found to be symmetric and evenly spaced in both push and pull directions. The amount of pinching in case of BF-CB was found to be slightly lesser than that of bare frame which led to slightly higher energy dissipation.

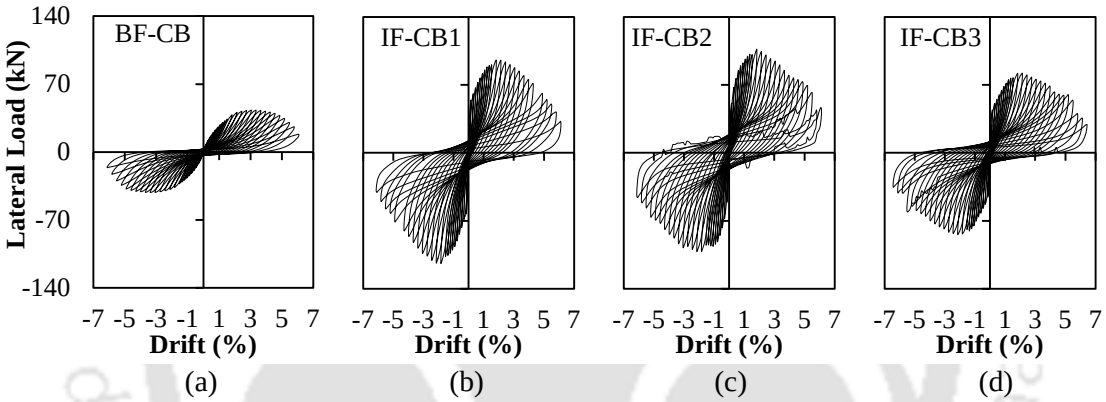

Fig. 7.8. Hysteretic response of frames with collector beams: (a) BF-CB; (b) IF-CB1; (c) IF-CB2; and (d) IF-CB3.

In case of infilled frames with collector beams, it was observed that the loops were closely spaced in the initial displacement levels, similar to that of the fully infilled frame without collector beam (IF-FB2). It was clearly observed that the increment of the lateral load resistance of IF-CB1 was gradual both in push and pull directions, whereas, the increase was very non-uniform in case of IF-FB2, as the interlocking of the infill wall units (bricks) was re-organised with increase in drift levels. In case of IF-CB2 and IF-CB3, increase in lateral load was symmetrical in both push and pull directions when compared to IF-CB1. The hysteretic loops of infilled frames with collector beams observed lesser amount of pinching compared to that observed in case of fully infilled frames. The amount of pinching observed in IF-CB2 and IF-CB3 was found to be significantly lesser compared to that of the IF-CB1. The amount of participation of infills to resist lateral load increased with number of collector beams, as the number of sliding

planes in IF-CB2 were higher compared to that of IF-CB1. The degradation of lateral load carrying capacity of infilled frames with collector beams in post peak regime was similar and found to be gradual when compared to the fully infilled frame. The reason for the frame to observe gradual increase and gradual dropdown in lateral load resistance was the distributed failure of infill along the horizontal bed joints. It was also observed that the partitions offered a sliding zone in infill, preventing the risk of brittle failure.

Kinks were observed in the hysteretic response of IF-CB2 and IF-CB3 in the post peak regime at larger drift levels prior to the termination of the test. It was due to the tensile failure of longitudinal reinforcement near the column ends. Even though longitudinal reinforcement failed, dropdown in capacity was gradual due to the presence of collector beams, which contributed to the lateral load resistance by not only preventing crushing in infill but also extensive damage in columns.

7.6.2 Evaluation of Influencing Parameters

The results of slow-cyclic tests are discussed in terms of lateral strength, stiffness and energy dissipation and are shown in Table 7.4 and Fig. 7.9. It was observed that the lateral stiffness and strength of the BF-CB was found to be similar to that of previously tested bare frames. The initial stiffness of the infilled frames with various collector beam configurations was found to be about 10 to 14 times that of BF-CB. Stiffness of the infilled frame with collector beams was found to be higher when compared to IF-FB2 in the first cycle of initial drift level (0.15%). In the second cycle of the first drift level (0.15%), IF-FB2 observed slightly higher stiffness compared to the infilled frames with collector beams (IF-CB1, IF-CB2). In the subsequent drift level (0.31%), the stiffness of IF-FB2 was found to be higher when compared to other infilled frames with collector beams. This is because the lateral load resistance of IF-FB2 (89 kN) in the second drift level was significantly higher compared to the infilled frames with collector beams (69 kN to 53 kN).

Out of the three infilled frames with collector beams, initial stiffness of IF-CB1 was found to be higher when compared to IF-CB2 and IF-CB3. The reason was primarily the increase in number of collector beams decreased the entire contribution of infill at the same drift level resulting in less lateral load resistance. Variation of secant stiffness for the infilled frames with collector beams is shown in Fig. 7.9(b). As it is expected, secant

stiffness of IF-FB2 was higher in the initial drift levels. At the same time, it was also inferred that the rate of degradation was higher in both push and pull directions when compared to infilled frames with collector beams.

Table 7.4. Influencing parameters of test specimens

S. No	Type of Frame	K_i (kN/mm)	ED (kNmm)	F_u (kN)	δ_u (mm)
1	Bare frame (BF)	4	45,201	-42, +34	100
2	Bare frame with collector beam at lintel level (BF-CB)	4	48,300	-42, +43	100
3	Infilled frame (IF-FB2)	36	78,200	-105, +107	95
4	Infilled frame with 10% opening (IF-FB3)	32	1,10,474	-74, +73	100
5	Infilled frame with central collector beam (IF-CB1)	54	1,49,550	-114, +96	100
6	Infilled frame with two collector beams (IF-CB2)	46	1,60,908	-102, +107	100
7	Infilled frame with two collector beams with 10% opening (IF-CB3)	42	1,30,499	-84, +82	105

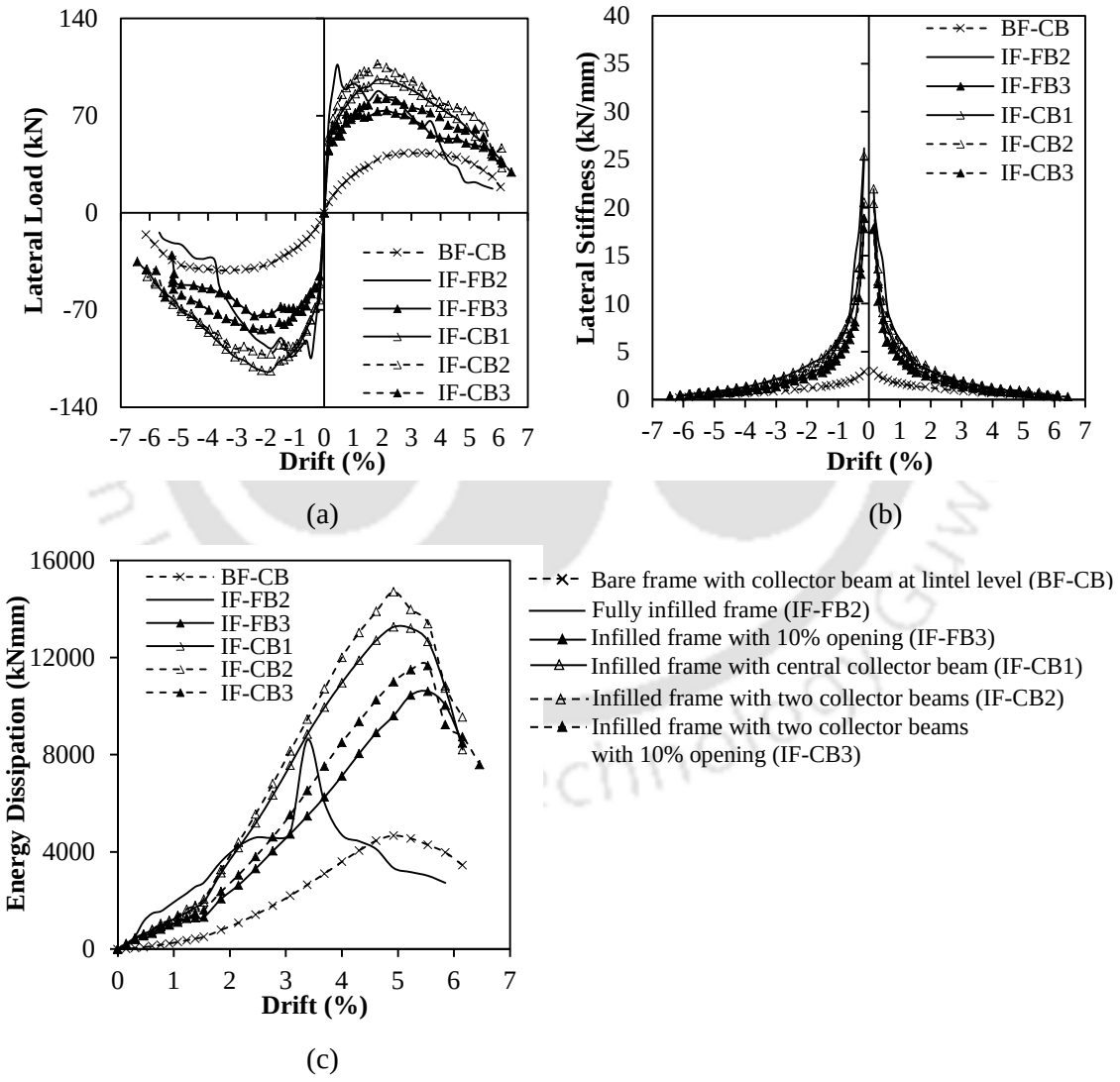

Fig. 7.9. Lateral load behavior of frames with collector beams: (a) envelope curves showing force vs. drift at actuator level; (b) variation of stiffness; and (c) energy dissipation at different drift levels.

The rate of reduction of secant stiffness decreased at higher drift levels. It was observed that the stiffness remained same for all the infilled frames at higher drift levels (>2%). The average lateral load capacity of infilled frame with collector beams without opening (IF-CB1 and IF-CB2) was found to be similar to that of the IF-FB2 (Table 7.4). The only distinction being the capacity in frames with collector beams reached at a higher drift level (1.83% - 2.15%), when compared to IF-FB2 (0.45%) as shown in Fig. 7.9(a). Further, it was observed that the participation of infills was gradual in imparting lateral load resistance due to the inclusion of collector beams. Whereas, entire infill participated in fully infilled frames by observing diagonal crack in the initial drift levels which led the frame to reach its capacity at a lower drift level. Capacity of infilled frame with two collector beams with 10% opening IF-CB3 (83 kN) was found to be slightly higher when compared to infill frame with 10% opening IF-FB3 (74 kN). In both the infilled frames with openings, with or without collector beams, capacity reached at the same drift level (2.15%). From the envelope response, it was deduced that the infilled frames with collector beams showed stable behavior in reaching peak and in the post peak regimes as discussed in hysteretic response. It was observed that the fully infilled frame attracted higher lateral loads in the initial drift level due to full participation of infill and the frame was not able to accommodate the forces at that drift level which lead to the formation of diagonal shear cracks in columns. In case of infilled frames with collector beams, column elements do not attract higher forces in the initial drift levels as the interaction of infill with columns was reduced by the provision of collector beams. This leads to a decrease in the effect of infill on the columns.

Energy dissipated under lateral loading in case of infilled frames with collector beams was about 1.9 times (IF-CB1) and 2 times (IF-CB2) that of IF-FB2, and for IF-CB3, it was about 1.2 times that of IF-FB3 (Table 7.4). IF-CB2 dissipated higher energy followed by IF-CB1 and IF-CB3 [Fig. 7.9(c)]. Infilled frames with collector beams exhibited higher energy dissipation due to the stable and ductile behavior under lateral loading. The amount of pinching in hysteresis was less as the sliding and frictional resistance provided by the infill was constant as discussed in hysteretic response. This in-turn, can be inferred as the continuous or sequential contribution of infill in imparting lateral load resistance to system with increase in drift levels. In case of IF-FB2, global diagonal strut mechanism was formed by multiple diagonal stepped cracks passing

through bed and head joints, often through brick units from the loading end to the opposite compression end. Whereas, in case of infilled frames with collector beams, the global strut mechanism was not observed as the collector beams restricted the crack propagation and acted as crack inhibitors. Local diagonal struts were formed in infill sandwiched between the collector beams, and most of the diagonal cracks were concentrated near the inner-face of columns and collector beams around the brick units. The other beneficial influence of providing collector beams was restricting the crushing of infill within a localized region near the corners.

7.6.3 Crack Pattern and Failure Mechanisms

The crack pattern observed in case of BF-CB was similar to that of the bare frame [Fig. 7.10(a)]. Till a drift of 0.6% (19.9 kN), no cracks were observed in the columns. Later, hair-line flexural cracks were observed near the right column corners at a drift level of 0.77% (22.9 kN). Minor diagonal shear cracks were initiated at a slightly higher drift level of 2.15% (-38.3 kN, +40.8 kN) near the right column end. With increase in drift levels, flexural cracks developed along the length of the columns and near the beam-column junctions. At a drift level of 3.38%, the lateral load capacity (-42 kN, +43 kN) of the BF-CB was attained. Crushing and spalling of cover concrete near the column bottom corners was initiated at a drift level of 4.61% (39.8 kN). Finally, the test was terminated at 6.15% drift (-15.8 kN, +18.3 kN) when significant crushing of core-concrete and buckling of longitudinal reinforcement was observed near the bottom of columns [Fig. 7.10(b)]. From the observed crack pattern, it was ascertained that there was no significant cracking in columns and crushing of concrete near the connection of collector beam because of non-monolithic construction. At the same time, no significant damage was observed in the columns at the location where collector beams were connected. The connection between the columns and the collector beam remained intact until the termination of the test. From the analysis of crack pattern, it was affirmed that the presence of non-monolithic collector beam did not alter the behavior of the bare frame.

In case of infilled frames with collector beams, cracks initiated in infill as bed joint sliding cracks above and below the collector beams due to the weak frictional resistance provided by the interface connection (polythene sheets). Later, the cracks were connected by minor diagonal cracks near collector beams and column corners (Fig. 7.10).

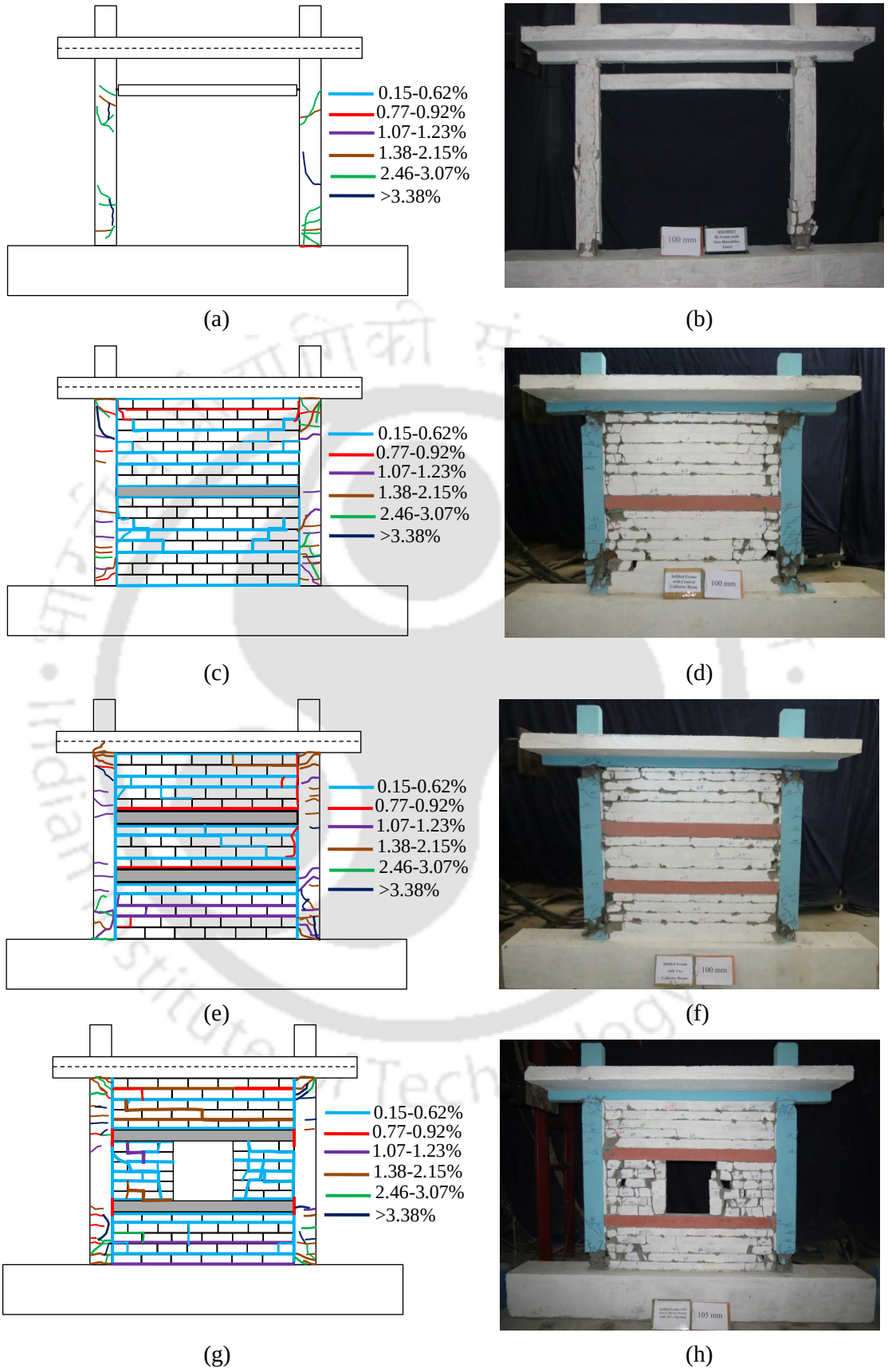

Fig. 7.10. Crack pattern and failure mechanisms of: (a) and (b) BF-CB; (c) and (d) IF-CB1; (e) and (f) IF-CB2; (g) and (h) IF-CB3.

In case of IF-CB1, cracking was initiated at 0.15% drift (-63 kN, +55 kN) as bed joint sliding cracks along the collector beam-wall interface, column-wall interface and two courses above the collector beam in infill panel. In the subsequent drift level (0.31%), diagonal stepped cracks were formed in the lower infill panel originating near the corners of the collector beam and connected by horizontal sliding cracks three courses above the bottom beam. With increase in drift levels (0.46% to 0.62%), bed joint sliding cracks were developed along the height of the infill in different courses below the soffit of the top beam and central collector beam as shown in Fig. 7.10(c).

In case of IF-CB2, cracking in infill initiated at a drift level of 0.15% (51 kN), as bed joint sliding cracks two courses below the soffit of the top beam and one course below the top collector beam connected by the diagonal cracks near the corners. It was observed that most of the cracking in infill took place in the middle infill panel, which may be due to the flow of tensile stresses as observed in the linear analysis (Fig. 7.2). Cracking in infill in the bottom infill panel was very less as most of the stresses were compressive in nature and the strength of the considered fly ash brick masonry was found to be higher compared to the applied stresses [Fig. 7.10(e)]. Only one horizontal bed joint sliding crack was observed in the lower infill panel, i.e., one course below the bottom collector beam at 0.61% drift. No major cracks were formed in columns as most of the energy dissipation was due to the friction mechanism generated by horizontal bed joint sliding cracks in infill until 0.92% drift was reached.

In case of IF-CB3, cracking in infill was initiated at 0.15% (45 kN) drift level. The cracks were concentrated in masonry piers of the middle panel as sliding cracks through mortar bed and head joints and often passed through brick units [Fig. 7.10(g)]. With increase in drift levels, bed joint sliding cracks were observed two courses below the soffit of the top beam and one course below the bottom collector beam. It was observed that most of the cracks were formed in masonry piers with only two bed joint sliding cracks in the top and bottom infill panel at 0.61% drift.

With increase in drift levels, flexural cracks and diagonal tension cracks (shear cracks) were initiated in columns. It was observed that flexural cracking in columns initiated prior to diagonal tension cracks slightly away from the plastic hinge regions at a drift level of 1.08% (97 kN) and 0.92% (70 kN) in case of IF-CB2 and IF-CB3,

respectively. Whereas, IF-CB1 observed slight diagonal shear cracks prior to flexural cracks at a drift level of 0.77% (-91 kN, +77 kN), but the cracking pattern was not as severe as observed in case of IF-FB2. The main reason for IF-CB2 to observe flexural cracking prior to shear cracking was due to the influence of collector beams in diffusing the frame-infill interaction on the column. Even though bed joint sliding cracks were formed two courses below the soffit of the top beam, diagonal tension cracks were not observed. This may be due to the lesser resistance offered by the infill near the corners. Even though the infill was in contact over a partial height, the chord rotation demand on the column was not high as the column was able to accommodate entire storey drift demand without much resistance from the infill. It can also be visualised as even though the shear span length was small, the moment resistance provided by the column was found to be higher than the shear demand. This lead to higher shear-span ratio (moment to shear ratio) and delayed the formation of diagonal tension cracks (diagonal shear cracks) in columns at a smaller drift level. At the same time, it can also be inferred that the shear-span ratio increased due to the influence of the collector beams, as the force required to develop diagonal tensile cracks was found to be less.

In case of IF-CB1, with increase in drift levels (0.92% to 1.53%), flexural cracks were formed along the height of the column parallel to the direction of loading. Whereas, in case of IF-CB2 and IF-CB3 minor diagonal shear cracks were formed near the column ends at a drift level of 1.23% (-96 kN, +100 kN) and 1.38% (-81 kN, +77 kN), respectively, along with flexural cracks. From the initiation of flexural and shear cracks in case of IF-CB1, IF-CB2 and IF-CB3, it can be inferred that the performance of the infilled frame specimens with collector beams was much better than those without collector beams, as the formation of the shear cracks in columns was greatly delayed due to the presence of collector beams.

Lateral load capacity of IF-CB1 (-114 kN, +96 kN) and IF-CB2 (-102 kN, +107 kN), was reached at a same drift level (1.85%), whereas, IF-CB3 reached its capacity (-84 kN, +82 kN) at a higher drift level (2.15%). In case of IF-FB2, capacity (-105 kN, +107 kN) was reached in the initial drift level (0.45%) when infill observed diagonal stepped cracking leading to the formation of global diagonal strut. From the drift levels corresponding to lateral load capacity, it was clearly observed that both infill and frame elements in case of infilled frames with collector beams contributed in imparting lateral

load resistance at a higher drift level unlike the fully infilled frame. Minor cracks developed near the beam-column junction highlighting the stiffening (T-beam) action provided by the RC slab, as observed in case of previously tested infilled frame specimens.

With further increase in drift levels, crushing of mortar bed joints and bricks near the inner face along the length of the column was observed. Later on, widening of diagonal flexural and shear cracks was observed followed by buckling of longitudinal reinforcement. In case of IF-CB1, crushing of mortar bed joints and bricks along column-wall interface was observed at 4%, whereas, for IF-CB2 and IF-CB3, crushing was observed at a lower drift level of 2.76%, and continued until the termination of the test. Spalling of cover concrete on the outer face of the column ends was observed at a drift level (4% – 4.3%) in all the three specimens. This was followed by widening of diagonal shear and flexural cracks leading to opening of shear reinforcement hooks and crushing of core concrete [Figs. 7.10(d, f and h)]. Buckling of longitudinal reinforcement was observed at 5.84%, 5.23%, and 5.84%, respectively, in all the three tested specimens. Finally the test was terminated when the longitudinal reinforcement failed near the column ends at a drift level of 6.15% (IF-CB1 and IF-CB2) and 6.46% (IF-CB3). It was observed in case of IF-CB2 and IF-CB3, even after the longitudinal bars were failed, there was no sudden dropdown in the lateral load resistance. This is attributed to the stability imparted by the collector beams to the frame system. There was no out-of-plane collapse of infill as the slenderness ratio of infill was reduced which inhibited the catastrophic damage to the infill under earthquake loading.

7.6.4 Lateral Load-Strain Response

Variation of strain in rebars at different drift levels in case of frames with collector beams (BF-CB, IF-CB1, IF-CB2 and IF-CB3) is shown in Fig. 7.11. Typical strain values recorded at various column locations are reported in Tables 7.5, 7.6, 7.7, and 7.8 for BF-CB, IF-CB1, IF-CB2 and IF-CB3, respectively. Only two strain gauges were bonded near the plastic regions on either face of the columns in case of BF-CB, whereas, four strain gauges were bonded in case of the infilled collector beam specimens as shown in Fig. 7.7. From the strain gauge data recordings of BF-CB, it was observed that the strain gauge readings were symmetrical in nature in both push and pull directions. The strain gauges

near the right column bottom and top in case of BF-CB very not fully operational and were not considered for further analysis.

In case of BF-CB, initiation of yielding of rebars near the left column bottom and top was observed at 0.62% and 2.15% drift, respectively (Table 7.5). The curvature corresponding to yield drift was found to be about 0.0229 /m (left column bottom) and 0.0280 /m (left column top). Some strain gauges (SG2 and SG15 in case of IF-CB1, SG13 in case of IF-CB2, and SG 12 in case of IF-CB3) malfunctioned in the beginning of the test, and were not considered for further analysis.

Table 7.5. Typical strain values recorded at various column locations in BF-CB

Strain Gauges	Peak Strain				Yield		Yield Curvature /m
	Tension (+)	Compression (-)	Drift (+) %	Drift (-) %	Strain	Drift %	
			Left Column Top				
SG 1	2752	-1267	3.69	-3.69	2685	2.08	0.0282
SG 2	3812	-692	2.77	-2.15	2648	1.82	0.0280
			Left Column Bottom				
SG 5	3600	-882	0.77	-0.65	2607	0.62	0.0229
SG 6	4061	-1964	2.46	-2.46			

Table 7.6. Typical strain values recorded at various column locations in IF-CB1

Strain Gauges	Peak Strain				Yield		Yield Curvature \m
	Tension (+)	Compression (-)	Drift (+) %	Drift (-) %	Strain	Drift %	
			Left Column Top				
SG 1	3874	-5337	5.54	-5.23	2699	1.54	0.0272
SG 2			Not Operational				
SG 3	3128	-1900	2.77	-4.31	2852	2.15	0.0244
SG 4	3099	-2108	2.77	-5.23	2806	2.15	
			Left Column Bottom				
SG 5	4413	-1685	2.46	-2.46	2693	1.23	0.0186
SG 6	4525	-1773	2.15	-2.15	2785	1.23	0.0196
SG 7	2744	-1960	3.08	-3.08	2649	2.77	0.0313
SG 8	4378	-1988	4.00	-3.69	2618	2.77	0.0442
			Right Column Bottom				
SG 9	4509	-1764	3.38	-3.38	2925	1.54	0.0298
SG 10	4174	-3950	4.00	-4.00	2654	1.23	0.0270
SG 11	3115	-1653	1.85	-1.85	2711	1.38	0.0201
SG 12	3372	-1354	1.85	-1.85	2885	1.23	0.0227
			Right Column Top				
SG 13	3841	-3042	4.31	-4.31	2778	1.38	-
SG 14	4321	-948	1.85	-1.85	2770	0.92	0.0227
SG 15			Not Operational				
SG 16	4718	-741	2.77	-2.15	2733	1.23	0.0258

Table 7.7. Typical strain values recorded at various column locations in IF-CB2

Strain Gauges	Peak Strain				Yield		Yield Curvature \m
	Tension (+)	Compression (-)	Drift (+) %	Drift (-) %	Strain	Drift %	
Left Column Top							
SG 1	5844	-909	2.46	-2.46	2886	-1.85	0.0281
SG 2	4863	-2593	4.92	-4.92	2964	-1.85	0.0268
SG 3	3286	-2362	4.92	-4.62	2654	-1.38	0.0230
SG 4	2737	-2559	3.38	-4.31	2656	-1.08	0.0222
Left Column Bottom							
SG 5	5060	-709	1.54	-1.54	2715	0.92	0.0195
SG 6	4919	-838	1.38	-1.38	2628	0.77	0.0182
SG 7	3515	-1485	3.08	-3.08	2684	1.38	0.0273
SG 8	4542	-2548	2.77	-2.77	2687	1.23	0.0269
Right Column Bottom							
SG 9	2655	-1614	3.08	-4.31	2647	2.15	0.0358
SG 10	2614	-1272	3.08	-4.31	2614	3.08	0.0384
SG 11	3782	-2117	1.54	-2.15	2789	1.08	0.0218
SG 12	3801	-1166	1.38	-1.54	2683	0.92	0.0194
Right Column Top							
SG 13	Not Operational						
SG 14	2887	-1935	2.15	-4.92	2797	1.38	0.0236
SG 15	3365	-2506	3.08	-4.92	2750	1.85	
SG 16	3412	-2184	2.46	-4.62	3005	1.85	0.0285

Table 7.8. Typical strain values recorded at various column locations in IF-CB3

Strain Gauges	Peak Strain				Yield		Yield Curvature \m
	Tension (+)	Compression (-)	Drift (+) %	Drift (-) %	Strain	Drift %	
Left Column Top							
SG 1	3823	-1763	4.31	-4.31	2995	1.85	0.0276
SG 2	3628	-2129	5.23	-5.54	2833	2.46	0.0292
SG 3	2184	-1532	3.69	-5.23	2184	3.69	0.0267
SG 4	2586	-1800	5.85	-4.92	2586	5.85	0.0321
Left Column Bottom							
SG 5	4910	-2613	3.38	-3.38	2744	1.23	0.0237
SG 6	5093	-1112	2.46	-2.46	2617	1.23	0.0196
SG 7	3921	-2901	3.69	-4.00	2786	1.85	0.0355
SG 8	3571	-356	2.15	-1.54	2810	1.85	0.0269
Right Column Bottom							
SG 9	3695	-3385	3.38	-3.69	2736	2.15	0.0324
SG 10	2868	-2085	2.46	-3.38	2610	1.85	
SG 11	4086	-2229	2.77	-2.77	2733	1.54	0.0241
SG 12	Not Operational						
Right Column Top							
SG 13	2696	-2164	2.46	-5.23	2629	1.85	0.0231
SG 14	2481	-2239	2.46	-4.92	2481	2.46	0.0219
SG 15	3383	-1352	4.31	-5.85	2713	1.85	0.0279
SG 16	3968	-1202	4.31	-6.46	2655	1.38	0.0242

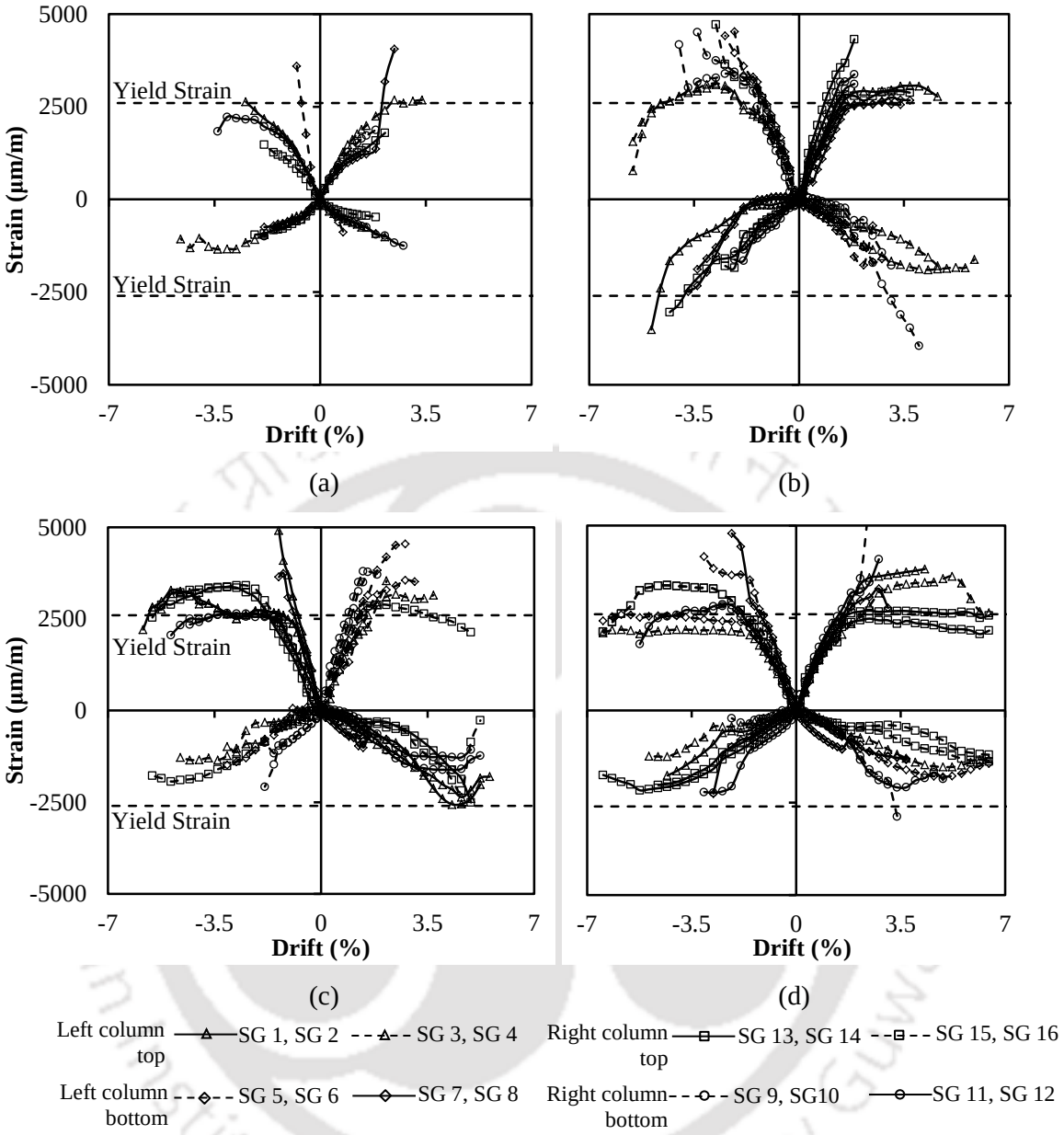

Fig. 7.11. Envelope curves showing strain vs. lateral drift in: (a) BF-CB; (b) IF-CB1; (c) IF-CB2; and (d) IF-CB3.

From the maximum strain recordings at different drift levels (Fig. 7.11), it was found that the yielding of rebars was initiated at 0.92% (right column top), 0.77% (left column bottom) and 1.23% (near left column bottom) in case of IF-CB1, IF-CB2 and IF-CB3, respectively. The range of drift levels (0.92%-1.85%) corresponding to the yielding of rebars was found to be similar in all the three collector beam specimens. The curvature corresponding to the yield drift (Fig. 7.12) was found to be in the range of 0.0186 /m - 0.0442 /m (left column bottom), 0.0194 /m - 0.0384 /m (right column bottom) and 0.0196 /m - 0.0355 /m (left column bottom) in case of IF-CB1, IF-CB2, and IF-CB3,

respectively. It was observed that the curvature corresponding to the first yield of rebars was found near the bottom of columns.

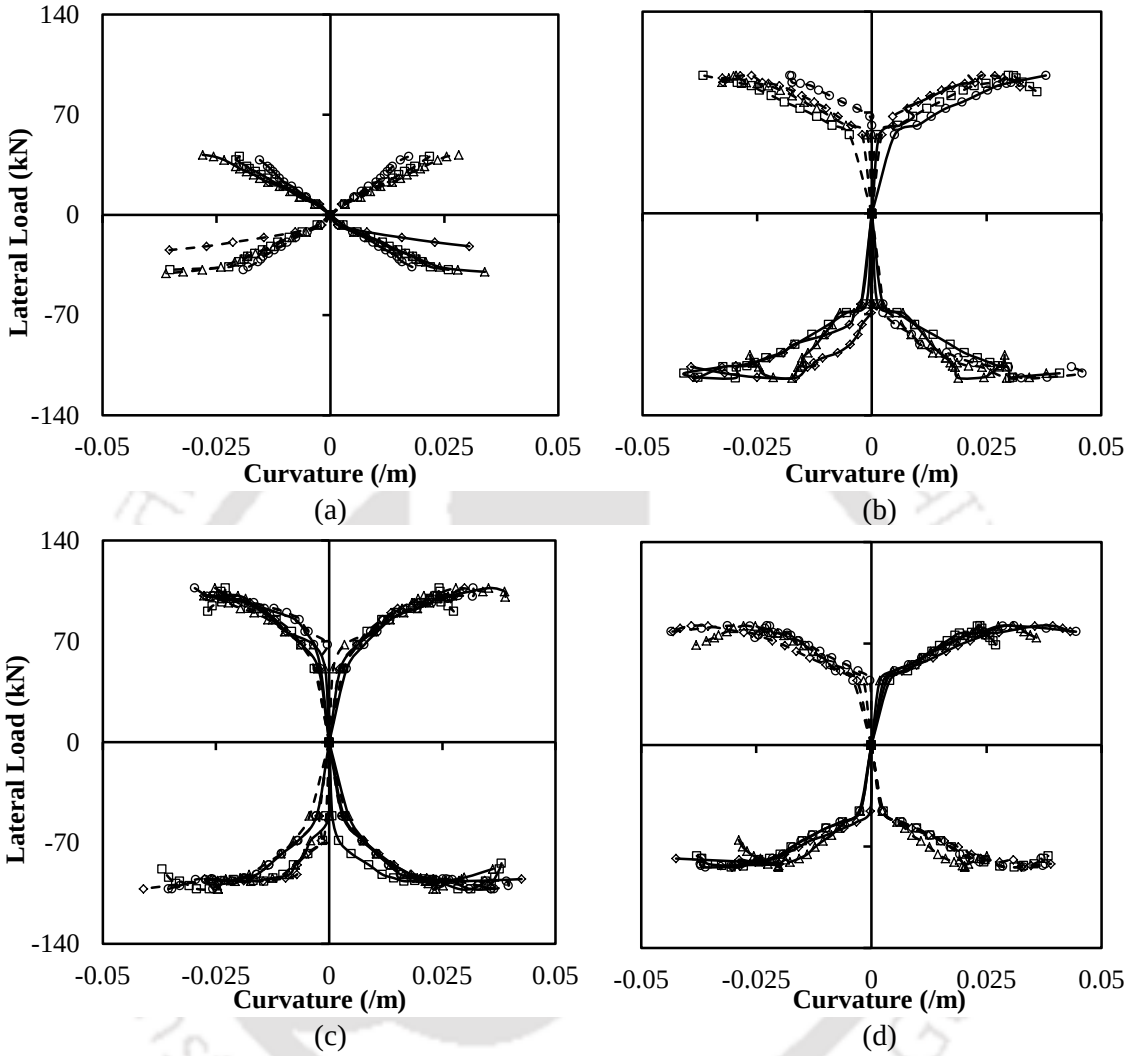

Fig. 7.12. Lateral load-curvature response of: (a) BF-CB; (b) IF-CB1; (c) IF-CB2; and (d) IF-CB3.

From the analysis of strain gauge data, it was affirmed that the introduction of collector beams helped in pushing the infill frame system to ductile response. The ductile behavior of infilled frames with collector beams can be understood from the difference of drift levels corresponding to yielding of rebars (0.77% to1.23%) in the pre-peak regime and the reduction of the capacity to 80% of its maximum in the post peak regime at higher drift levels (3.69% to 4.31%). It was also noted that the initiation of major events especially formation of shear cracks was observed after the yielding of the rebars except in case of infilled frame with central collector beam (IF-CB1). Similar observation was

made in chapter 6 in case of infilled frame with class III burnt clay bricks (IF-CC2). Therefore, from the strain gauge analysis of the infilled frames with collector beams, it was ascertained that dividing the infill into sub-panels helped the infill frame system to fail in ductile mode by reducing the frame-infill interaction.

7.7 SUMMARY

The third methodology, in which the infill wall was divided into sub-panels using RC collector beams to delay the shear failure of columns of infilled frames, was evaluated both analytically and experimentally. Four specimens were experimentally investigated under displacement controlled slow-cyclic loading. From the experimental study, it was found that the inclusion of collector beams in infill panels not only enhanced the lateral load behavior of the infilled frames in terms of strength, stiffness and energy dissipation, but also delayed the shear failure of the columns to larger drift levels. Additionally, the collector beams helped the frame to observe more ductile response when compared to the generally observed brittle behavior of the infilled frames. Similar observation was made from the analysis of strain data where the difference in yielding of rebars and the reduction of lateral load capacity to 80% was significantly higher when collector beams were used. Comparison of the three methodologies will be carried out in the next chapter, so as to assess their feasibility and affordability.

This Page is Intentionally Left Blank

Chapter 8
COMPARISON OF METHODOLOGIES AND ANALYTICAL VALIDATION

CONTENTS

8.1 OVERVIEW

Methodologies were proposed to account for the effect of infill on RC frames, and were investigated both analytically and experimentally as discussed in the previous chapters (6 and 7). A comparison of the adopted methodologies is required to be done so as to assess their effectiveness. Therefore, analytical and experimental results of the three methodologies along with the frames tested in the preliminary study are compared in this chapter. Additionally, the experimental lateral load response of the infilled frames designed and constructed as per the suggested methodologies is verified using the improved analytical model. An application of the strain gauge data obtained in the tests is also discussed.

8.2 COMPARISON OF INFLUENCING PARAMETERS

The effectiveness of the three methodologies in modifying the lateral load behavior of the infilled frames with respect to each other in terms of lateral stiffness, lateral strength and energy dissipation capacity is discussed in detail in this section.

8.2.1 Lateral Stiffness

The initial stiffness of the infilled frames adopting the three methodologies was found to be higher when compared to the previously tested infilled frames (preliminary study). It was found to be about 1.2 to 1.6 times that of the IF-FB2 specimen and about 10.5 to 14.5 times that of the bare frame (Table 8.1). It was observed that the infilled frame with class I burnt clay bricks (IF-CC1) observed the highest initial stiffness followed by the infilled frame with enhanced column section (IF-EC) as shown in Fig. 8.1. Infilled frame with two collector beams with 10% opening (IF-CB3) observed lowest initial stiffness due to the presence of the opening, in addition to the collector beams. But the initial stiffness of IF-CB3 was found to be about 1.3 times than that of the infilled frame with 10% opening (previously tested). Among the solid infilled frame specimens without openings, both IF-CB2 and IF-CC2 observed lowest initial stiffness. This was mainly due to the weak and soft masonry used in the construction of IF-CC2, whereas, IF-CB2 observed lower initial stiffness due to the presence of greater number of predefined sliding planes, inspite of the fact that the strength of masonry was quite high. From the initial stiffness calculation, it is clearly observed that employing collector beams to create sliding failure planes leads to a substantial decrease in the stiffness of the infilled frames irrespective of the strength of masonry.

Table 8.1. Influencing parameters of tested specimens

S. No	Type of Frame	K_i (kN/mm)	ED (kNmm)	F_u (kN)	δ_u (mm)
1	Bare frame (BF)	4	45,201	-42, +34	100
2	Bare frame with collector beam at lintel level (BF-CB)	4	48,300	-42, +43	100
3	Infilled frame (IF-FB2)	36	78,200	-105, +107	95
4	Infilled frame with 10% opening (IF-FB3)	32	1,10,474	-74, +73	100
	Methodology I				
5	Infilled frame with enhanced column section (IF-EC)	55	1,79,931	-125, +127	100
	Methodology II				
6	Infilled frame with class I clay bricks (IF-CC1)	58	1,08,764	-112, +104	85
7	Infilled frame with class III clay bricks (IF-CC2)	46	1,45,442	-81, +76	100
	Methodology III				
8	Infilled frame with central collector beam (IF-CB1)	54	1,49,550	-114, +96	100
9	Infilled frame with two collector beams (IF-CB2)	46	1,60,908	-102, +107	100
10	Infilled frame with two collector beams with 10% opening (IF-CB3)	42	1,30,499	-84, +82	105

From Fig. 8.1(b), it can be seen that the degradation of secant stiffness from the first drift level to the subsequent drift level was found to be in the range of 33% to 46% in all the adopted methodologies. The degradation was found to be very rapid from the first drift level to the subsequent drift level. At the same time, it was also observed that the

secant stiffness has been reduced to 85%-90% of its initial stiffness at drift level ranging from 2.15% to 2.5% in both push and pull directions.

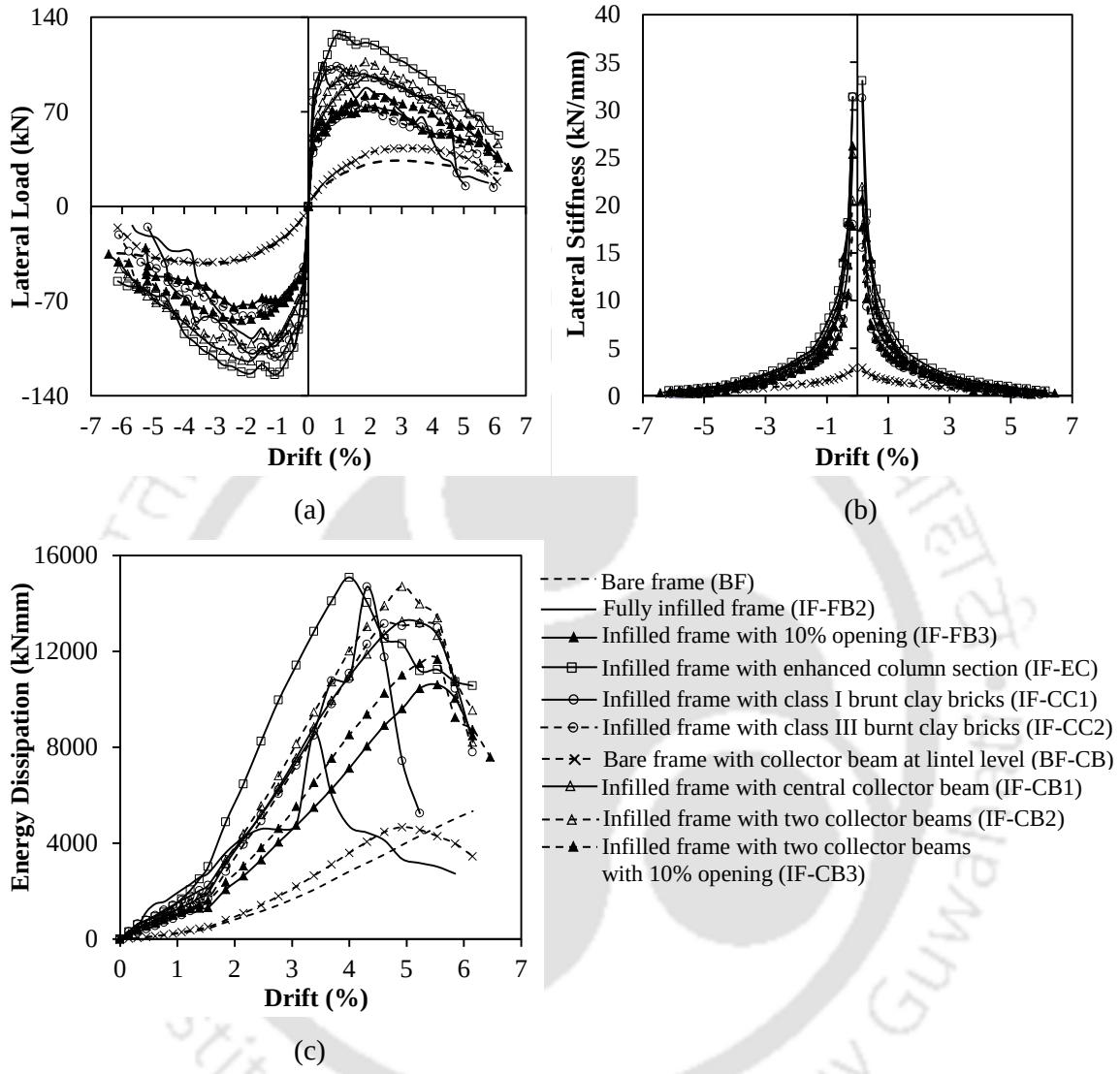

Fig. 8.1. Comparison of lateral load behavior of tested specimens: (a) envelope curves showing force vs. drift at actuator level; (b) variation of stiffness; and (c) energy dissipation at different drift levels.

8.2.2 Lateral Strength

The lateral load capacity of the infilled frames adopting the three methodologies was found to be similar to that of the previously tested infilled frames (preliminary study). The lateral load capacity was found to be about 0.7 to 1.2 times that of IF-FB2 and was about 2.1 to 3.3 times that of the bare frame (Table 8.1). Taking the advantage of the enhanced dimensions of the column, IF-EC observed highest lateral load capacity followed by frame infilled with stronger masonry (IF-CC1). The lateral load carrying

capacity of the IF-CC2 was found to be slightly lower, i.e., approximately 0.7 times that of the previously tested IF-FB2. Low lateral strength exhibited by the IF-CC2 was mainly due to the low-strength contribution of the masonry infill as described earlier.

The major beneficial influence of the three methodologies was the gradual increase and degradation of the lateral load capacity. It was observed that the lateral load carrying capacity of the infilled frames using the methodologies was reached at a drift level ranging from 0.92% to 2.15%. Infilled frames with collector beams (IF-CB1 to IF-CB3) attained similar lateral load capacity as that of the IF-FB2 but at a higher drift level (1.85%-2.15%) as shown in Fig. 8.1(a). Due to the presence of collector beams, lateral load resistance provided by the infill was very sequential and the contribution of the infill was observed at larger drift levels also. IF-CC2 attained slightly lower lateral load resistance (about 0.7 times), but at a higher drift level of 1.85% compared to the infilled frames tested in the preliminary study. It was also observed that the lateral load capacity was reduced to 80% of its maximum at a drift level ranging from 3.39% to 4.31% across the three methodologies. Whereas, the drift corresponding to 80% lateral strength was in the range of 1.9% to 3.8% for the preliminary specimens. From the current study, it was ascertained that the degradation behavior of the infilled frames can be enhanced by employing the methodologies, specifically dividing the infill wall into sub-panels using the collector beam configurations.

8.2.3 Energy Dissipation

Infilled frames designed using the three methodologies showed enhanced energy dissipation and it was found to be about 1.4 to 2.3 times that of the IF-FB2, and about 2.4 to 4.0 times that of the bare frame. Among all the specimens, IF-EC observed highest energy dissipation followed by IF-CC2 [Fig. 8.1(c)]. The reason for the infilled frame with enhanced column section (IF-EC) to show highest energy dissipation was mainly due to the confinement effect provided by the surrounding frame to the infill and the resistance imparted by the infill even at larger drift levels (2.46% drift). The reason for the infilled frames with collector beams to observe higher energy dissipation capacity compared to previously tested infilled frames was mainly due to the sequential or continuous contribution of infill in imparting lateral load resistance to system with increase in drift levels. The energy dissipation potential of IF-CC2 was found to be quite

similar to that of IF-CB1. The reason for IF-CC2 to depict better energy dissipation was mainly due to the inherent sliding mechanism created by the application of low-strength mortar and the contribution of infill even at higher drift levels. The degradation of energy dissipation capacity was observed at higher drift level (5.23%-5.84%) in case of collector beam specimens and class III clay brick specimen. Whereas, frames with enhanced column section and class I burnt clay bricks observed the degradation at a slightly lower drift level of 4.6%.

8.2.4 Calculation of Equivalent Viscous Damping

Another way of representing energy dissipation capacity is in terms of equivalent viscous damping. The equivalent viscous damping (β_{eq}) was calculated as per the guidelines of FEMA 368 (2001) and ATC 40 (1996), using Eqs. (8.1) and (8.2). The variation of equivalent viscous damping at various drift levels is shown in Fig. 8.2.

$$K_{eq} = \frac{F^{+} - F^{-}}{\Delta^{+} - \Delta^{-}} \tag{8.1}$$

$$\beta_{eq} = \frac{2}{\pi} \frac{E_{cycle}}{K_{eq}\left(\Delta^{+} - \Delta^{-}\right)^{2}} \tag{8.2}$$

where K_{eq} is the effective stiffness, Δ^{+} and Δ^{-} are the peak lateral displacements corresponding to peak lateral forces F^{+} and F^{-} in both pull and push directions, respectively, and E_{cycle} represent the energy dissipated per displacement cycle.

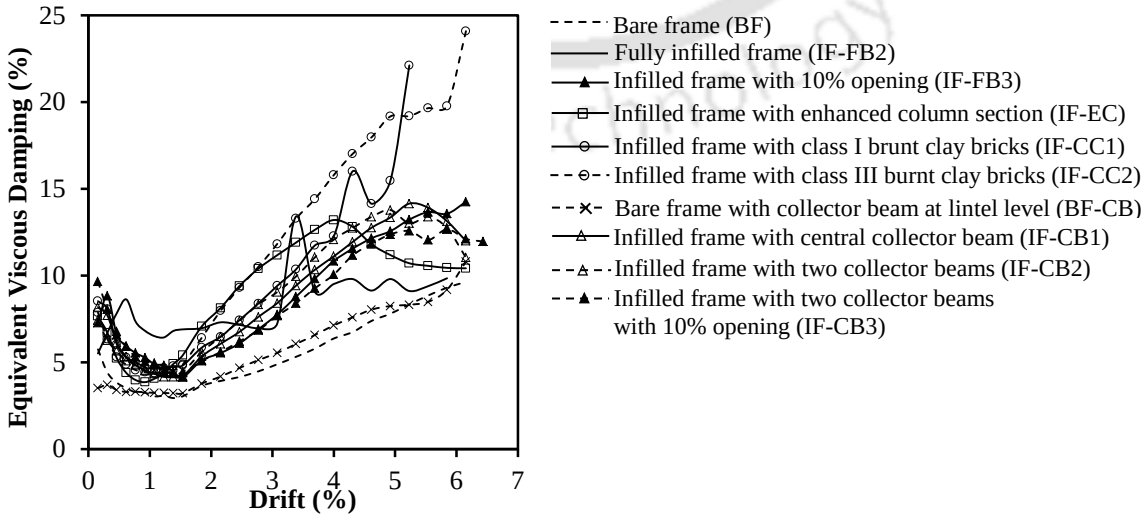

Fig. 8.2. Comparison of equivalent viscous damping of the tested specimens.

The equivalent viscous damping ratio was found to decrease in the initial drift levels until various energy dissipating mechanisms were activated, and later the ratio increased more or less linearly with increase in drift levels. All the specimens exhibited similar behavior, among which IF-CC2 showed highest equivalent damping ratio. Till 1.5% drift, equivalent damping ratio was found to be very uneven due to the contribution of infill, and later the ratio increased linearly with increase in drift levels as the damage in RC members was initiated. The equivalent viscous damping ratio of infilled frames with collector beams followed similar trend.

8.3 Crack Pattern and Failure Mechanisms

One of the primary objectives of the current study was to delay or prevent the shear failure of columns of infilled frames due to frame-infill interaction. From the experimental study, it was observed that the proposed methodologies showed better performance in terms of lateral strength, stiffness and energy dissipation as discussed earlier. The failure mechanism, which is one of the major parameter in performance evaluation, has been compared in this section.

It was observed that in almost all the investigated specimens (Table 8.2), cracking in infill was initiated at a similar drift level (about 0.15%) as: bed joint sliding cracks along the height of the infill (IF-CB1, IF-CB2, IF-CB3, and IF-CC2); and combination of both bed joint sliding and diagonal stepped cracking (IF-EC and IF-CC1). With increase in drift levels, flexural cracks developed in most of the specimens (drift level 0.62% to 1.08%) except in case of IF-CB1 where hair line diagonal shear cracks initiated prior to flexural cracks. In case of previously tested infilled frames (preliminary study), diagonal shear cracks developed at an average drift level of 0.58% and flexural cracks at 0.88% drift. In case of IF-CB2 and IF-CB3, flexural cracks developed at a drift level of 1.08% and 0.92% respectively. In case of IF-CC2 and IF-EC flexural cracks initiated at a slightly lower drift level of 0.62% and 0.92%, respectively. Later at drift levels ranging from 1.08% to 1.38%, hair line diagonal shear cracks initiated in all the tested infilled frames with the adopted methodologies. The reason for the infilled frames to exhibit much delayed shear cracking was mainly due to the diffusion of frame-infill interaction in case IF-CB2 and IF-CB3, whereas, using low-strength and soft masonry was the main reason in case of IF-CC2.

Table 8.2. Drift levels corresponding to major events

S. No	Type of Frame	DR_i	Dr_f	Dr_s	DR_{max}	DR_{80}	DR_u
					%		
1	Bare frame	-	0.77	1.84	3.38	-6.15, +5.23	6.15
2	Bare frame with collector beam at lintel level	-	0.77	2.15	3.38	-5.23, +5.23	6.15
3	Infilled frame	0.46	0.92	0.77	0.46	-2.77, +2.15	5.85
4	Infilled frame with 10% opening	0.15	0.92	0.77	2.15	-3.38, +3.69	6.15
5	Infilled frame with enhanced column section	0.15	0.92	1.08	1.08	-3.39, +3.67	6.15
6	Infilled frame with class I clay bricks	0.15	0.77	0.46	0.92	-2.77, +3.38	5.23
7	Infilled frame with class III clay bricks	0.15	0.62	1.23	1.85	-3.69, +3.08	6.15
8	Infilled frame with central collector beam	0.15	1.08	0.77	1.85	-3.69,+4.00	6.15
9	Infilled frame with two collector beams	0.15	1.08	1.23	1.85	-4.31,+3.69	6.15
10	Infilled frame with two collector beams with 10% opening	0.15	0.92	1.38	2.15	-4.31, +4.31	6.46

In case of IF-EC, the columns were designed to counteract the adverse effect of infill and the methodology was found to be effective in delaying the shear cracks in columns. In case of infilled frame with collector beams, the effect of infill reduced to a large extent due to the presence of collector beams, and the columns were able to accommodate the entire storey drift demand without much resistance from the infill. Similar observation was made in case of IF-CC2. IF-CC1 observed shear cracks at a lower drift level of 0.46%, followed by flexural cracking (0.77%) similar to previously tested IF-FB2. The lateral load carrying capacity and the reduction of capacity to 80% of its maximum has been observed at a comparatively higher drift levels in case of all the infilled frames using the methodologies. Stable hysteretic behavior was observed in case of IF-CB1 to IF-CB3 which was mainly due to the presence of collector beams, whereas, kinks were observed due to reorganization of bricks in case of IF-CC1 and IF-EC at higher drift levels.

With further increase in drift levels, crushing of mortar joints and bricks along the column-wall interface was observed in case of specimens with collector beams, whereas, corner crushing of infill was observed in case of IF-EC. In case of infilled frames with burnt clay bricks and enhanced column section, out-of-plane failure of infill was observed. No out-of-plane movement of infill was observed in case of infilled frames with collector beams as the slenderness ratio of infill was reduced due to the presence of collector beams. The tests were terminated when crushing of core concrete was observed in the widened shear cracks, and buckling and/or tensile failure of longitudinal reinforcement was observed in case of infilled frames with collector beams and burnt clay bricks. In case of specimen with enhanced column section, there was no crushing of core

concrete and opening of shear reinforcement, but the frame failed due to the tensile failure of longitudinal reinforcement only.

From the observed crack pattern, it was ascertained that the amount of shear cracks was found to be very less and the formation has been delayed to a greater extent in all the specimens without compromising other functional requirements. From the observed failure mechanism, it can be inferred that the adopted methodologies were found to be viable options in delaying the shear failure of columns.

8.4 ANALYTICAL VALIDATION

The experimentally evaluated lateral load responses of the three methodologies were analytically verified using the improved macromodel. Modelling of RC members, infill and the plastic hinge definitions were similar to the analytical model described in chapter 5. Using the nonlinear material characteristics reported in chapter 6 and chapter 7 for the three methodologies, plastic hinge definitions (flexural, shear and axial) of the infilled frames were evaluated. Schematic representation of the analytical models along with hinge definitions is shown in Fig. 8.3.

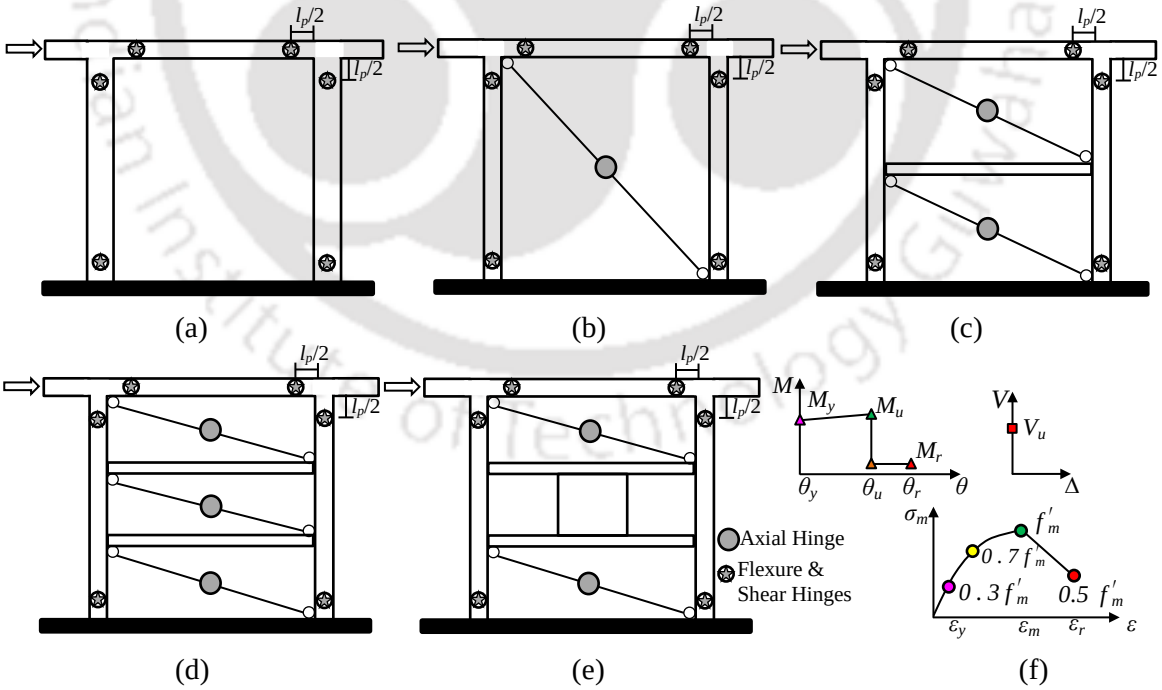

Fig. 8.3. Schematic representation of the analytical model and plastic hinge definitions for: (a) IF-EC; (b) IF-CC1 and IF-CC2; (c) IF-CB1; (d) IF-CB2; (e) IF-CB3; and (f) definitions of flexure hinge (M-θ), shear hinge (V-Δ), and axial hinge (σ_m-ε) relation.

The width of the strut was taken as one-tenth the diagonal length of the infill wall. In case of IF-CB3, the infill wall was neglected in the middle panel as the size of the opening was about 32% of the middle panel area [Fig. 8.3(e)]. The effect of infill was calculated and the additional shear forces were applied as uniformly distributed load along the contact length of the column and the analysis was carried out. The comparison of the analytical and experimental envelope responses of the infilled frames is shown in Figs. 8.4 and 8.5. It was observed that the global response was appropriately simulated by the analytical model. Formation of hinges near the specified locations was found to be quite similar to that observed in the experiments.

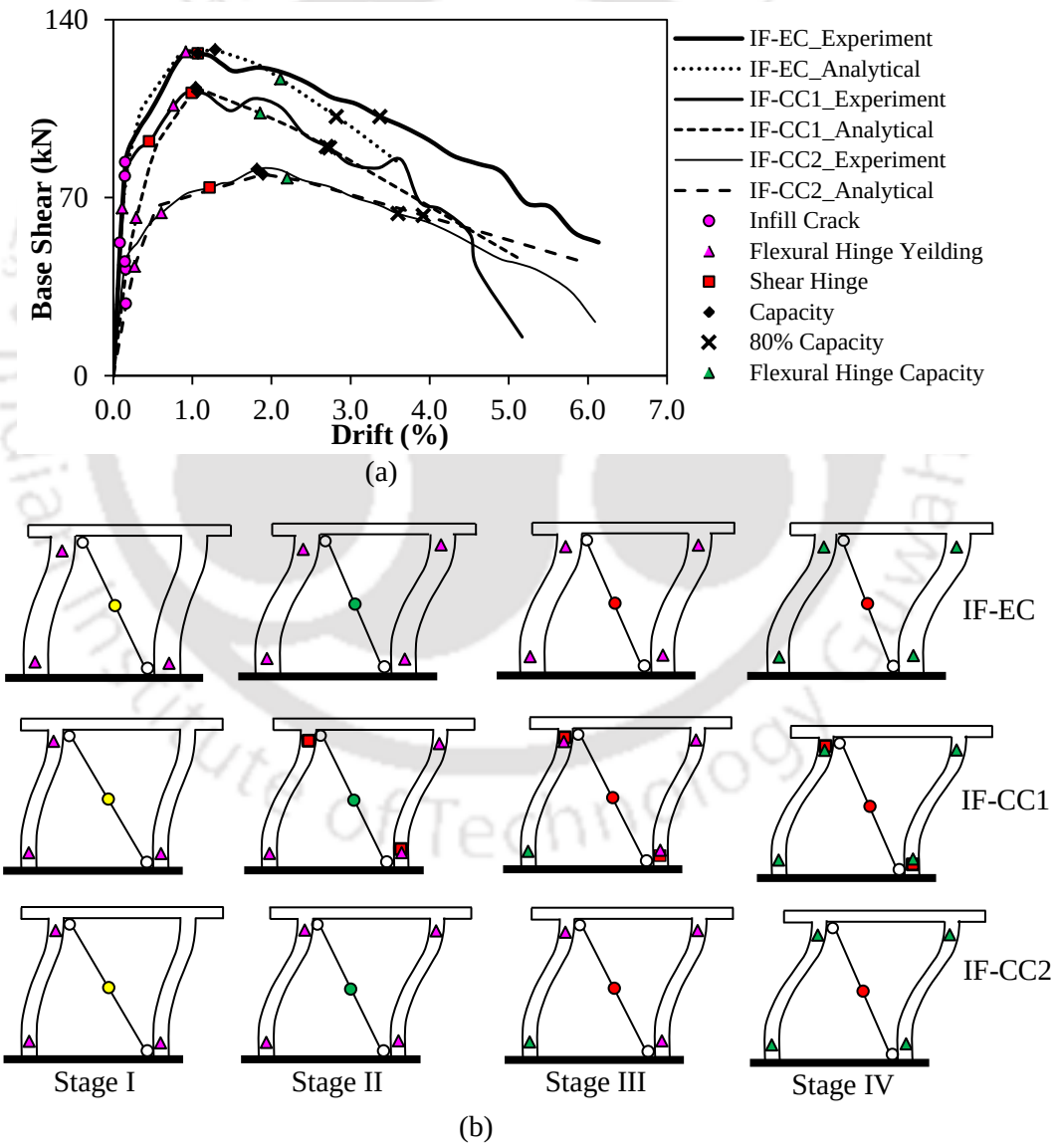

Fig. 8.4. (a) Comparison of experimental and analytical lateral load response; and (b) stages of hinge formation using improved analytical model for methodology I (IF-EC) and methodology II (IF-CC1 and IF-CC2).

From the analytical response and the various stages of plastic hinge formation (Fig. 8.4), it was clearly observed that initial yielding of axial hinges was followed by flexural yielding of the frame members (Stage I). With increase in monitored drift, the axial hinge capacity reached along with yielding of flexural hinges (Stage II) in case of methodology I and II. This was followed by failure of axial strut in Stage III. With further increase in drift, flexure hinges at all locations reached their capacity. Slightly different type of hinge formation was observed in specimens of methodology III. Yielding of axial and flexural hinges (Stage I) was observed simultaneously, followed by 70% of axial hinge capacity (Stage II).

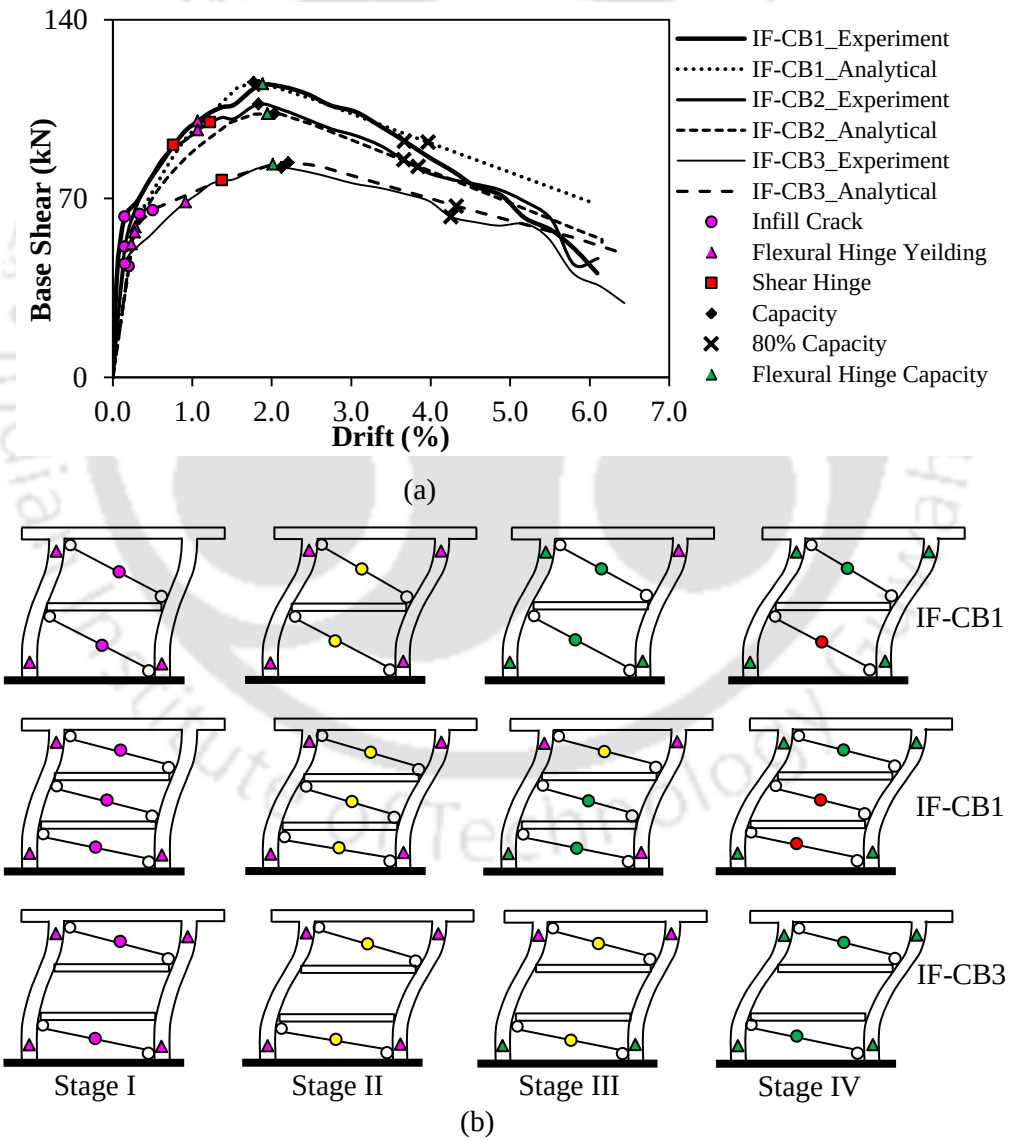

Fig. 8.5. (a) Comparison of experimental and analytical lateral load response; and (b) stages of hinge formation using improved analytical model for methodology III (IF-CB1, IF-CB2, and IF-CB3).

Subsequently, with increase in monitored drift, capacity of both axial and flexural hinges reached in stage III [Fig. 8.5(b)]. Due to the presence of multiple struts in methodology III, infill did not observe failure in the top panels even though the capacity of flexure hinges reached at all locations (Stage IV). Analytically, no shear hinges were formed in column members of all the tested specimens using the three methodologies except in case of IF-CC1 [Fig. 8.4(b)]. In case of IF-CC1, the shear hinge was formed in stage II, as the shear force demand due to the high strength infill was found to be higher than the shear capacity of the column section near the compression zone corners. From the analytical response, it was observed that there is a slight over-estimation of the maximum lateral load capacity in case IF-EC, IF-CC1, and IF-CC2. But the drift corresponding to the lateral load capacity remained same in both the analytical and experimental models. From Figs. 8.4 and 8.5, it was also observed that the post-peak response can also be appropriately simulated by the analytical model. No hinges were formed in beams in the analytical model as observed during the experimental investigation. Therefore, from the analytical response, it was clearly found that the global behavior as well the prediction of shear failure of the infilled frames can be evaluated using the improved equivalent diagonal strut model.

8.5 Evaluation of Moment-Curvature Response

It is a well-known fact that the earthquake response of the reinforced concrete members in the inelastic range can be easily predicted using the moment (M) - curvature (φ) relationship. In the current study, M-φ relationship was evaluated for the tested specimens and is shown in Fig. 8.6. Curvature was calculated as the gradient of the strain profile at the member ends using the strain recorded in the strain gauges attached on the longitudinal reinforcement. Moment demand on the column sections was calculated from the lateral load resistance of the tested specimens. The equivalent moment demand was calculated by assuming plastic hinges to be formed at both ends of the columns. The moment at each end of the column was calculated as $\frac{V_f (h - l_p)}{4}$, where V_F represents the combined lateral load resistance of the frame and infill including the axial load effects, h, and l_p represents the length of the column and plastic hinge, respectively. Both the curvature and moment was calculated at various drift levels and an average moment curvature curve was plotted.

Four control points were identified in the average *M-φ* curve:

i) In most of the infilled frames, 50%-70% of the lateral load resistance was achieved at about 0.15% drift level and it is a valuable point in defining the initial lateral load behavior of the frame system. Hence, the first point was selected corresponding to curvature and moment at 0.15% drift level.

ii) The second point corresponds to the first yielding of longitudinal rebars.

iii) The third point corresponds to the maximum moment demand on the column.

iv) The fourth point corresponds to 80% of moment demand in the post peak regime or the maximum curvature recorded before malfunctioning of strain gauges, whichever occurred first.

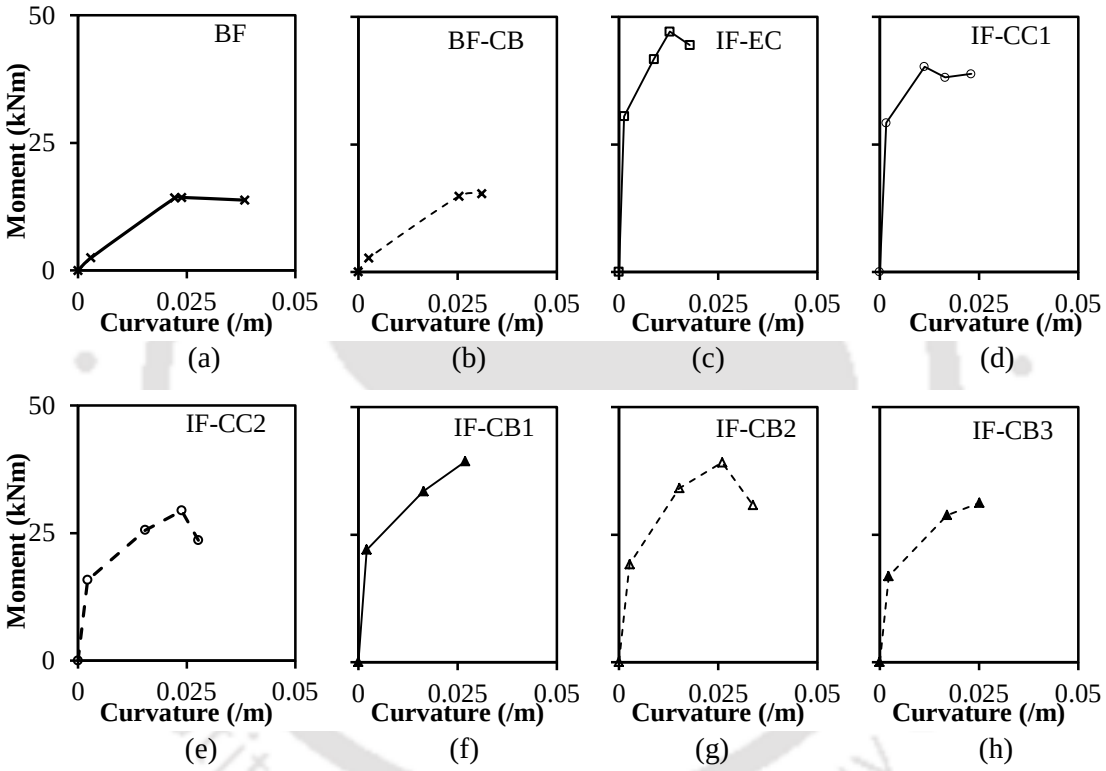

Fig. 8.6. Moment-curvature response of the tested specimens: (a) BF; (b) BF-CB; (c) IF-EC; (d) IF-CC1; (e) IF-CC2; (f) IF-CB1; (g) IF-CB2; and (h) IF-CB3.

In the current study, it was observed that the average curvature corresponding to first yielding of rebars was about 0.0223 /m and 0.0253 /m for bare frames without and with collector beam, respectively; 0.0155-0.0170 /m in case of infilled frames with collector beams and with clay bricks; and about 0.0088 /m in case of infilled frame with enhanced column section. In case of IF-EC, the curvature corresponding to yielding of rebars (0.0088 /m) and maximum moment (0.013 /m) was found to be lower when compared to other infilled frame specimens (Fig. 8.6). In case of IF-CC1 and IF-CC2, the maximum moment was reached at a curvature of 0.0113 /m and 0.0239 /m, respectively.

It was observed that the moment of resistance of IF-CC1 reached prior to yielding of longitudinal reinforcement (0.0165 /m) as shown in Fig. 8.6(d). In case of infilled frames with collector beams the maximum moment was reached at a curvature level ranging from 0.0251-0.0269 /m. In some of the specimens (IF-CB1 and IF-CB3), fourth control point is not shown as most of the strain gauges malfunctioned after the moment capacity of the sections was attained [Figs. 8.6(f and h)].

8.6 Application of Moment-Curvature Response

In the current study, the global response of the infilled frames was evaluated using the moment-curvature (M-φ) curves developed in the previous section. Generally, the global response of the infilled frame was evaluated by modelling column and beams as 2-noded frame elements and infill as equivalent diagonal strut. The nonlinearity in the frame sections was modelled using lumped plasticity approach at specified hinge locations as discussed in detail in analytical modelling (Chapter 5). The major difficulty in modelling of the infilled frames is the determination of the geometrical, mechanical properties of the infill and their interaction with the frame members. Therefore, in the current study an attempt has been made to evaluate the lateral load response of the bare and infilled frames using the equivalent moment-curvature response developed using the strain gauge data. The lateral load response of the infilled frames was evaluated without modelling the infill as equivalent diagonal strut. In the analytical model, the effect of infill was considered in the equivalent moment capacity calculations. Flexural hinges in columns were defined using the equivalent moment-curvature curves.

Nonlinear static pushover analysis was carried out using SAP2000 (CSI 2015). The analytical models were calibrated by modifying the stiffness of the frame elements so as to take into account the initial stiffness provided by the infill. Comparison of both analytical and experimental lateral load response of the tested specimens is shown in Fig. 8.7. From the figure, it is clearly observed that the analytical response of the infilled frames matched quite well with experimental envelope response. The lateral load capacity of the infilled frames was found to be comparable with the experimental capacity. Therefore, it can be said that the global response of the infilled frames can be easily evaluated using the equivalent moment-curvature relation of the frame elements without modelling infill.

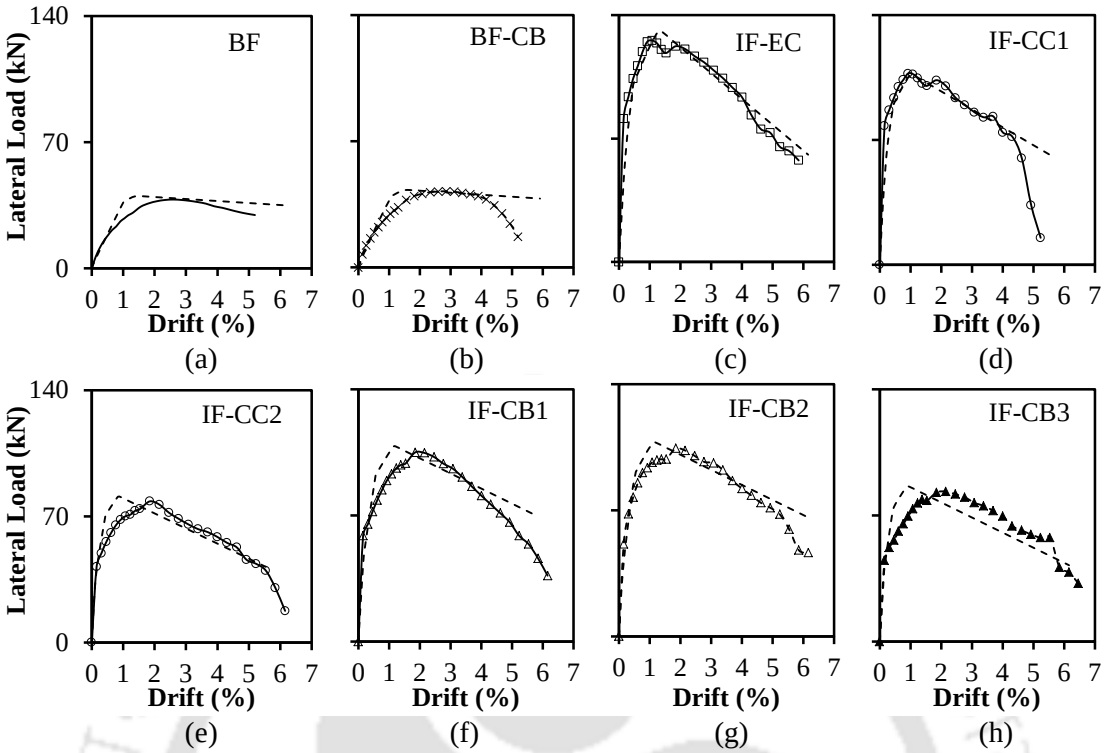

Fig. 8.7. Comparison of lateral load behavior using moment-curvature response: (a) BF; (b) BF-CB; (c) IF-EC; (d) IF-CC1; (e) IF-CC2; (f) IF-CB1; (g) IF-CB2; and (h) IF-CB3.

8.7 SUMMARY

In this chapter, the experimental results of the three developed methodologies for improving the lateral load behavior of the masonry infilled RC frames (enhancing the column section, using low-strength and soft masonry, and providing collector beams) were compared with each other. From the comparison of the experimental results, it was observed that the infilled frame with collector beams provided better and stable lateral load response in comparison with the other two design methodologies. The analytical lateral load response obtained from the upgraded analytical model matched quite well with the experimental results. The equivalent moment curvature relationship derived from the strain response of the longitudinal rebars can be applied to evaluate the global response of bare and infilled frames.

Chapter 9
SUMMARY, CONCLUSIONS AND RECOMMENDATIONS FOR FUTURE WORK

CONTENTS

9.1 OVERVIEW

Even though masonry infilled RC frames are some of the most common building typologies, masonry infills are not considered in the design, but rather regarded as non-structural elements. The major detrimental effect of infill is that its interacts with the RC frame and alters the failure mode of columns from flexure to shear. Most of the past studies dealt with the global adverse effects of infills, i.e., the effect of irregular distribution of infills in plan and elevation on the behavior of RC frames. Recommendations were made in terms of design and strengthening strategies. A very few studies addressed the local adverse effect of infill, especially for the frames with one-sided imbalanced contact with infill in the ground storey. Therefore, it is of primary importance to understand the local detrimental effect of infill in causing shear failure of columns for proper design that results in ductile flexural failure.

The current study deals with the evaluation of reasons for shear failure of columns due to the local adverse effect of infill, and methodologies were proposed to protect the columns from the detrimental effect of masonry infill. From the review of the past literature, it was clearly noted that the applicability of the current requirements for the seismic design of masonry infilled RC frames were not understood clearly. Therefore, a preliminary experimental study was carried out to understand the design

recommendations of some commonly used national standards including the Indian seismic standards. The shear demand on the columns due to the effect of infill was estimated both analytically and numerically. As the available simplified analytical models were not able to capture the shear failure of columns, the existing macromodel was improved by considering the effect of infill. In the current study, fly ash bricks were used for masonry infill walls. An extensive experimental material characterisation of fly ash brick masonry was carried out.

Seismic design codes of many countries neglect the contribution of masonry infills in lateral load resistance and design the RC frames as bare frames. On the other hand, a few national standards (IS 13920, Eurocode 8, and ASCE 41) have specific provisions for columns of such frames, and recommend enhancing their shear capacity by increasing the transverse reinforcement. Merely increasing the shear capacity by increasing the transverse reinforcement ratio may lead to shear compression failure of the columns. In order to prevent or delay the shear failure of columns, improved design and construction methodologies were proposed in the current study: (i) considering the effect of infill in the design and proportionately increasing the dimensions of the column sections; (ii) reducing the effect of infill on the columns by using weak and soft masonry; and (iii) diffusing the effect of infill on the columns by dividing the infill into sub-panels using collector beams. It was observed from the analytical and experimental study that the adopted methodologies were viable options in delaying or preventing the shear failure of columns, without abating the other influencing parameters of the infilled frames.

9.2 SUMMARY

The study can be summarized into four parts: material characterisation; preliminary experimental study to evaluate the current codal recommendations; estimation of shear demand on columns and improvement of the existing analytical macromodel; and proposal and evaluation of the methodologies to improve the shear behavior of columns.

9.2.1 Material Characterisation

In the current study, sun-dried fly ash bricks were used as infill to examine their suitability as infill material. Engineering properties, especially the nonlinear stress-strain characteristics of fly ash brick masonry, need to be determined in order to consider them

in analysis and design of masonry infilled RC frames. More than hundred and fifty specimens consisting of fly ash bricks, mortar cubes, masonry prisms, Z-shaped masonry specimens, masonry triplets and masonry wallettes for three different grades of mortar were tested under monotonic compression, tension and diagonal compressive loading using servo controlled hydraulic actuator. It was observed that due to the intricate soft and weak nature of fly ash bricks, masonry prisms exhibited an unusual behavior with lower strength and stiffness compared to that of fly ash bricks as well as mortar. Modulus of elasticity of fly ash brick units, mortars and masonry prisms was found to be about 680, 400 and 600 times their corresponding compressive strengths, respectively. From the diagonal compression test, the average shear strength of the full scale masonry wallettes was found to be about 0.14 MPa and the shear modulus was found to be about 0.27 times the elastic modulus of the corresponding masonry prisms.

To understand the reasons for the weaker and softer compressive behavior of fly ash bricks, internal structure of fly ash bricks was studied by finding out their mineralogical and chemical composition. Three different techniques (X-Ray Fluorescence analysis, Scanning Electron Microscope associated with Energy Dispersive Spectrometer and powder X-Ray Diffraction) were used. Presence of CH (Portlandite) in the material composite showed incomplete pozzolanic reaction leading to porous matrix responsible for weaker and softer nature of fly ash bricks. The material properties determined experimentally were used in the analysis and design of masonry infilled RC frames.

9.2.2 Preliminary Study to Evaluate Codal Recommendations

A preliminary experimental study was conducted to evaluate the recommendations of the national standards on the design of masonry infilled RC frames. Eleven half-scale ductile and non-ductile RC frames infilled with full-scale and half scale bricks were investigated under slow-cyclic lateral loading in two stages. In the first stage, eight frames were designed as per the prevalent practice where infills were treated as non-structural elements. In the second stage, three ductile frames designed and detailed for improved performance as per provisions of current seismic standards were tested. From the first stage testing, it was deduced that the columns of infilled frames failed in shear mode even though the masonry used in the frame was quite weak. The brittle behavior of columns was primarily attributed to weakening of interface connection between column and infill

with increasing load that resulted in decreasing the effective length of column in contact with infill. This further increases the chord rotation demand leading to smaller shear span ratio and excessive shear demand on columns for which they were not designed. From the results of the second stage, it was observed that the frames with improved shear capacity using special confining reinforcement showed improvement in the post-peak load behavior, energy dissipation, and ultimate deformation capacity. However, shear failure of columns could not be prevented, even though the initiation of shear cracks was delayed and the amount of shear cracks was lesser in the improved specimens. No significant damage was observed in beams of all the tested specimens due to stiffening (T-beam) action provided by the RC slab.

Based on the major damage events observed during the tests (initiation of infill cracks, shear cracks, flexural cracks, maximum capacity, and 80% of the capacity in the post-peak regime), an idealized load-displacement relationship was proposed for masonry infilled RC frames. This may serve as a guideline in the design of similar frames for required performance levels. It was also understood that due care has to be taken while designing RC frames infilled even with weak masonry, as they may alter the failure mechanism of RC frame system.

9.2.3 Numerical and Analytical Estimation of Shear Demand

As the columns of masonry infilled RC frames are prone to shear failure due to the detrimental effect of infill, estimation of actual shear demand on columns due to the infill-frame interaction is of primary importance for design of columns that results in ductile flexural failure. The current earthquake design codes provide limited guidelines to estimate the local adverse effect of infill, but their applicability requires verification. In the current study, shear demand on the columns was estimated both numerically based on codal recommendations, and analytically using an improved analytical model. In case of numerical estimation, it was observed that as per the recommendations of Eurocode 8 (CEN 2004b), ASCE 41 (2013), and MSJC (2013), the shear demand on the column was very high, and difficult to implement as the design requirements were conservative.

In case of analytical modelling, the available simplified macromodel was not able to estimate the realistic shear forces and bending moments in the frame members. Therefore, the macromodel was improved in the current study by simulating the effect of

infill on RC columns by applying additional shear forces incrementally along the contact length of the column. Applicability of the improved macromodel was also verified using other past experimental studies. From the analysis, it was observed that the proposed improved modelling technique successfully predicted both the global response and local component (shear) failure in columns of infilled frames.

9.2.4 Methodologies to Improve Shear Behavior of Columns

From the preliminary experimental and analytical study it was found that the columns of masonry infilled RC frames fail in shear due to the infill-frame interaction. To counteract the adverse effect of infill, i.e., to prevent or delay the shear failure in columns, three approaches were followed in the current study. Methodology I: increase the shear capacity of the column by considering the effect of infill in the design of frames; Methodology II: using weaker and softer masonry as infill to reduce the shear demand on the column; and Methodology III: provision of sliding mechanism along the predefined failure planes so as to limit the infill-frame interaction. Initially, the effectiveness of the adopted methodologies in preventing the shear failure of columns was evaluated analytically by carrying out a parametric study using the improved analytical model. Based on the nonlinear responses, the best methodologies were validated experimentally.

In case of Methodology I, the column sections were redesigned to account for the shear demand due to the effect of the infill, and by limiting the maximum shear reinforcement to avoid shear compression failure. From the parametric analysis, a column section of size 175×275 mm was found to be able to counteract the effect of infill. The strength and stiffness of the masonry infill was reduced in case of Methodology II, so as to decrease the detrimental effect of the infill on columns without affecting the functional requirements of the infills. In order to evaluate the effectiveness of the methodology II, low-strength and soft burnt clay bricks (referred as Class III bricks according to the current Indian specifications) were chosen. Two frames were tested: frame infilled with low strength and soft class III burnt clay bricks, and frame infilled with high strength and stiff class I burnt clay bricks. The third methodology considered in the current study was to limit the frame-infill interaction by dividing infill wall into sub-panels using RC collector beams as partition elements. Four specimens were tested: bare frame with collector beam at lintel level; infilled frame with central collector beam, infilled frame

with two collector beams, and infilled frame with two collector beams with 10% opening in infill wall. The RC collector beams were non-monolithically connected to the RC columns using reinforcing bars as dowels.

From the results of the experimental study, it was found that the influencing parameters (lateral stiffness, lateral strength, and energy dissipation) of the improved frames were significantly better. Further the adopted methodologies were successful in either preventing or delaying the shear failure of RC columns. The major beneficial influence of the three methodologies was the gradual increase and dropdown in the lateral load capacity of the infilled frames in the pre- and post- peak regimes, which is not generally observed phenomenon in case of infilled frames. From the observed crack pattern, it was ascertained that the amount of shear cracks was very less and the formation of shear cracks was delayed to a greater extent in all the improved specimens without compromising other functional requirements of infilled frames. In case of infilled frames with enhanced column section (Methodology I), and with weaker and softer masonry infill (Methodology II), out-of-plane failure of infill was observed during the tests. Whereas, out-of-plane failure of infill was not observed in case of infilled frames with collector beams (Methodology III), as the slenderness ratio of infill was reduced.

Further, the experimental lateral load responses of the infilled frames redesigned using the adopted methodologies were verified using the improved analytical model. From the analytical response, it was clearly observed that the global lateral load behavior (strength and stiffness) as well the shear failure of columns were successfully predicted by the improved analytical model. Additionally, the inelastic response of cross sections of columns (moment- curvature relationship) was determined using the strain data recorded at the plastic hinge regions of the columns. The obtained equivalent moment curvature relations were used in defining the plastic hinges in columns without modelling the infill walls. From the analytical results, it was found that the lateral load capacity of the infilled frames can be successfully predicted using the analytical model with equivalent plastic hinges considered only in columns without modelling the masonry infills. However, the failure modes and internal force distribution in the frame elements cannot be predicted using the equivalent model.

9.3 CONCLUSIONS

Following major conclusions can be drawn from the current study:

- Nonlinear material characterisation of fly ash brick masonry was carried out by extensive experimental study. Simple empirical relations were proposed to estimate the strength, and elastic and shear modulus of fly ash brick masonry.
- Fly ash bricks were found to be highly water absorbant, weak, and soft in comparison with the mortars used. Masonry infilled RC frames constructed using such bricks also need special attention during design and construction, since the behavior of such frames may be altered.
- From the preliminary study of masonry infilled RC frames, it was deduced that even though the influencing parameters, i.e., strength, stiffness and energy dissipation, were enhanced due to the presence of infill, the current codal recommendations were deficient in preventing shear failure of columns.
- An idealized lateral load-displacement relationship was proposed based on the major damage events (performance levels) observed during the experimental study. This may serve as a guideline in the design of similar infilled frames for required performance levels.
- The improved analytical model in which the frame-infill interaction was accounted for, was found to be a useful tool in predicting the shear failure of columns and can be used for practical engineering purposes.
- The three developed methodologies were found to be effective in delaying the shear failure in columns in addition to enhancing the lateral load behavior of infilled frames.
- Methodology-I (enhancing the column sections) and Methodology-II (using low strength and soft masonry) may be employed in existing and new construction projects if the strength of the infill is known apriori.
- On the other hand, Methodology-III (dividing infill into sub-panels using RC collector beams) was found to be a feasible and affordable option even if the strength of the infill is not known, as the effect of infill was diffused by introducing sliding mechanism along predefined failure planes. Methodology-III can also be effectively used if the other two methods cannot be worked out, for example, if the column section cannot be increased or if the low strength bricks are not available.

- In most of the specimens designed as per the three methodologies, flexural cracking commenced prior to shear cracking with minor shear cracks forming at higher drift levels, highlighting the influence of the design methodologies in delaying shear failure of columns. Out-of-plane collapse of the infill was fully avoided by providing the collector beams, as the slenderness ratio of the infill was reduced.
- It is recommended to provide two non-monolithic collector beams, one each at sill and lintel level, in masonry infilled RC frames in order to improve their shear behavior. Since no damage was observed in the collector beams in any tests, minimum reinforcement can be provided in these sections in the form of four bars of 8 mm diameter with minimum shear reinforcement. Width of the beam should be equal to thickness of the infill wall and thickness can be kept as 75-100 mm.

9.4 RECOMMENDATIONS FOR FUTURE WORK

Some recommendations for the future work are discussed below.

- An idealised numerical model for estimation of capacity of masonry infilled RC frames considering various strengths of fly ash brick masonry may be developed by carrying out tests on different combinations of bricks and mortar grades.
- The current set of experimental investigations was carried out on single bay-single storey half-scale models of low-rise masonry infilled RC frame buildings for low axial load ratios. The study may be extended to multi-bay multi-storey for higher axial load ratios.
- Similarly, the improved analytical macromodel can be extended to multi-storey masonry infilled RC frames.
- A more refined finite element analysis may be carried out to accurately simulate the influence of collector beams on the behavior of infilled frames.
- In the present study, the influence of openings was evaluated for single central opening with two collector beams. As the presence of openings significantly influence the lateral load behavior of infilled frames including failure mechanisms, various positions of window and door openings may be considered to verify the performance of different collector beam configurations.

LIST OF PUBLICATIONS

REFEREED INTERNATIONAL JOURNALS

- Basha, S. H., and Kaushik, H. B. (2016). "Behavior and failure mechanisms of masonry-infilled RC frames (in low-rise buildings) subject to lateral loading." *Engineering Structures*, Elsevier, 111, 233–245.
- Basha, S. H., and Kaushik, H. B. (2016). "Suitability of fly ash brick masonry as infill in reinforced concrete frames." *Materials and Structures*, Springer Publications, Co-published with RILEM, 49(9), 3831–3845.
- Basha, S. H., and Kaushik, H. B. (2015). "Evaluation of non-linear material properties of fly ash brick masonry under compression and shear." *Journal of Materials in Civil Engineering*, ASCE, 27(8), 04014227.
- Basha, S. H., and Kaushik, H. B. "Macromodel for the assessment of the shear failure in columns of masonry infilled RC frames." *Journal of Structural Engineering*, ASCE, (under review).
- Basha, S. H., and Kaushik, H. B. "Improving the shear behavior of columns in masonry infilled RC frames under lateral loads." *Journal of Structural Engineering*, ASCE, (under review).

INTERNATIONAL CONFERENCES

- Basha, S. H., and Kaushik, H. B. (2017). "Predicting shear failure in columns of masonry infilled RC frames using macro-modeling approach." *16th World Conference on Earthquake Engineering*, Santiago Chile, Paper No. 3168.
- Basha, S. H., and Kaushik, H. B. (2015). "Influence of collector beams on lateral load response of RC frames with masonry infills." *12th International Conference on Vibration Problems (ICOVP)*, Indian Institute of Technology Guwahati, India, Paper No. O0272.
- Basha, S. H., and Kaushik, H. B. (2015). "Non-linear behavior of weak brick-strong mortar masonry in compression." in Advances in Structural Engineering: Materials, Vol. Three, Matsagar, V. (Editor), Springer.
- Basha, S. H., and Kaushik, H. B. (2013). "Influence of masonry properties on lateral load response of reinforced concrete frames." *International Conference on Structural Engineering and Mechanics (ICSEM-2013)*, National Institute of Technology Rourkela, India, Paper No. 031.
- Basha, S. H., and Kaushik, H. B. (2012). "Evaluation of shear demand on columns of masonry infilled reinforced concrete frames." *15th World Conference on Earthquake Engineering*, Lisbon, Portugal, Paper No. 601.

This Page is Intentionally Left Blank

REFERENCES

ACI. (2008). "Building code requirements for structural concrete." American Concrete Institute, *ACI 318*, Farmington Hills, MI.

ACI. (2012). "Guide for design of slab-column connections in monolithic concrete structures." American Concrete Institute, *ACI 352.1R-11*, Farmington Hills, MI.

Aimin, X., and Sarkar, S. L. (1991). "Microstructural study of gypsum activated fly ash hydration in cement paste." *Cement and Concrete Research*, 21, 1137–1147.

Al-Chaar, G. (2002). *Evaluating strength and stiffness of unreinforced masonry infill structures*. Construction Engineering Research Laboratory, Engineering Research and Development Center, US Army Corps of Engineers, ERDC/CERL TR-02-01.

Al-Chaar, G., Issa, M., and Sweeney, S. (2002). "Behavior of masonry–infilled nonductile reinforced concrete frames." *Journal of Structural Engineering*, 128(8), 1055–1063.

Alecci, V., Fagone, M., Rotunno, T., and Stefano, M.D. (2013). "Shear strength of brick masonry walls assembled with different types of mortar." *Construction and Building Materials*, 40, 1038–1045.

Anil, Ö., and Altin, S. (2007). "An experimental study on reinforced concrete partially infilled frames." *Engineering Structures*, 29(3), 449–460.

Applied Technology Council (ATC). (1996). "Seismic evaluation and retrofit of concrete buildings." *ATC-40*, California Seismic Safety Commission, California, Volume 1.

ASCE. (2013). "Seismic evaluation and retrofit of existing buildings." *ASCE/SEI 41-13*, Reston, Virginia, USA.

Asteris, P. G., and Cotsovos, D. M. (2012). "Numerical investigation of the effect of infill walls on the structural response of RC frames." *Open Construction and Building Technology Journal*, Bentham Science Publishers, 6, 164–181.

Asteris, P. G., Antoniou, S. T., Sophianopoulos, D. S., and Chrysostomou C. Z. (2011). "Mathematical macromodeling of infilled frames: State of the Art." *Journal of Structural Engineering*, 137(12), 1508–1517.

Asteris, P. G., Cavaleri, L., Di Trapani, F., and Sarhosis, V. (2016). "A macro-modelling approach for the analysis of infilled frame structures considering the effects of

openings and vertical loads." *Structure and Infrastructure Engineering*, 12(5), 551–566.

Asteris, P. G., Cotsovos, D. M., Chrysostomou, C. Z., Mohebkhah, A., and Al-Chaar, G. K. (2013). "Mathematical micromodeling of infilled frames: State of the Art." *Engineering Structures*, 56, 1905-1921.

Asteris, P. G., Kakaletsis, D. J., Chrysostomou, C. Z., and Smyrou, E. E. (2011). "Failure modes of in-filled frames." *Electronic Journal of Structural Engineering* 11, 11-20.

ASTM. (2007). "Standard test methods for splitting tensile strength of masonry units." *ASTM C1006-07*, ASTM International, USA.

ASTM. (2008). "Standard test methods for Flexural Strength of Hydraulic-Cement Mortars.", *ASTM C348-08*, ASTM International, USA.

ASTM. (2010). "Standard test method for diagonal tension (shear) in masonry assemblages." *ASTM E 519/E519M-10*, ASTM International, USA.

ASTM. (2011). "Standard Test Method for Splitting Tensile Strength of Cylindrical Concrete Specimens." *ASTM C496/C496M- 11*, ASTM International, USA.

ASTM. (2012). "Standard test method for compressive strength of masonry prisms." *ASTM C1314-12*, ASTM International, USA.

ASTM. (2013a). "Standard test methods for sampling and testing brick and structural clay tile." *ASTM C67-13*, ASTM International, USA.

ASTM. (2013b). "Standard test method for compressive strength of hydraulic cement mortars using 2-in or 50-mm cube specimens." *ASTM C109/C109M-13*, ASTM International, USA.

Atkinson, R. H., and Noland, J. L. (1983). "A proposed failure theory for brick masonry in compression." *Proceedings of 3rd Canadian Masonry Symposium*, Edmonton, Alta., Canada, 5.1–5.17.

Basha, S. H. (2011). *Evaluation of ductility provisions in seismic codes for masonry infilled RC frame buildings*. M.Tech thesis, Department of Civil Engineering, Indian Institute of Technology Guwahati, India.

Benjamin, J. R., and Williams, H. A. (1958). "The behavior of one-storey shear walls." *Proceedings of American Society for Civil Engineers*, ST4, 1723.

Bennett, R. M., Boyd, K. A., and Flanagan, R. D. (1997). "Compressive properties of structural clay tile prisms." *Journal of Structural Engineering*, 123(7), 920–926.

Bertero, V. V., and Brokken, S. T. (1983). "Infills in seismic resistant building." *Journal of Structural Engineering*, 109(6), 1337–1361.

Blackard, B., William, K., and Mettupalayam, S. (2009). "Experimental observations of masonry infilled reinforced concrete frames with openings." *ACI Special Publication*, SP-265-9, 199–222.

Borri, A., Castori, G. M., and Corradi, M. (2011). "Shear behavior of masonry panels strengthened by high strength steel cords." *Construction and Building Materials*, 25, 494–503.

Bose, S., and Rai, D. C. (2016). "Lateral load behavior of an open-ground-story RC building with AAC infills in upper stories." *Earthquake Spectra*, 32(3), 1653–1674.

Bosiljkov, V. (2006). "Micro vs. macro reinforcement of brickwork masonry." *Materials and Structures*, 39, 235–245.

Brignola, A., Frumento, S., Lagomarsino, S., and Podestà, S. (2009). "Identification of shear parameters of masonry panels through the in-situ diagonal compression." *International Journal of Architectural Heritage*, 3, 52–73.

Brokken, S. T., and Bertero, V. V. (1981). *Studies on effects of infills in seismic resistant RC construction. Earthquake Engineering Research Center*, Report No. UCB/EERC-81/12, University of California, Berkeley, California.

Bureau Indian Standards (BIS). (1987). "Indian standard code of practice for structural use of unreinforced masonry." *IS 1905*, 2nd Revision, New Delhi, India.

Bureau of Indian Standards (BIS). (1992a). "Indian standard methods of test of burn clay building bricks–Part 1: Determination of compressive strength." *IS 3495*, 3rd Revision, New Delhi, India.

Bureau of Indian Standards (BIS). (1992b). "Indian standard methods of test of burn clay building bricks–Part 2: Determination of water absorption." *IS 3495*, 3rd Revision, New Delhi, India.

Bureau of Indian Standards (BIS). (1993). "Indian standard ductile detailing of reinforced concrete structures subjected to seismic forces–Code of practice." *IS 13920*, New Delhi, India.

Bureau of Indian Standards (BIS). (2000). "Indian standard plain and reinforced concrete–Code of practice." *IS 456*, 4th Revision, New Delhi, India.

Bureau of Indian Standards (BIS). (2002b). "Indian standard criteria for earthquake resistant design of structures–Part 1: General provisions and buildings." *IS 1893*, New Delhi, India.

Bureau of Indian Standards (BIS). (1981). "Indian standard code of practice for preparation and use of masonry mortars." *IS 2250*, 5th Revision, New Delhi, India.

Bureau of Indian Standards (BIS). (1999). "Indian standard code splitting tensile strength of concrete- method of test." *IS 5816*, 1st Revision, New Delhi, India.

Bureau of Indian Standards (BIS). (2002a). "Indian standard pulverized fuel ash – lime bricks–specification." *IS 12894*, 1st Revision, New Delhi, India.

Campione, G., Cavaleri, L., Macaluso, G., Amato, G., and Di Trapani, F. (2015). "Evaluation of infilled frames: an updated in-plane-stiffness macro-model considering the effects of vertical loads." *Bulletin of Earthquake Engineering*, 13(8), 2265–2281.

Cavaleri, L., and Di Trapani, F. (2014). "Cyclic response of masonry infilled RC frames: experimental results and simplified modeling." *Soil Dynamics and Earthquake Engineering*, 65, 224–242.

Cavaleri, L., and Di Trapani, F. (2015). "Prediction of the additional shear action on frame members due to infills." *Bulletin of Earthquake Engineering*, 13(5), 1425–1454.

Cavaleri, L., Fossetti, M., and Papia, M. (2004). "Effect of vertical loads on lateral response of infilled frames." *13th World Conference on Earthquake Engineering*, 2931.

Celarec, D., and Dolšek, M. (2013). "Practice-oriented probabilistic seismic performance assessment of infilled frames with consideration of shear failure of columns." *Earthquake Engineering and Structural Dynamics*, 42(9), 1339–1360.

Chiou, T. C., and Hwang, S. J. (2015). "Tests on cyclic behavior of reinforced concrete frames with brick infill." *Earthquake Engineering and Structural Dynamics*, 44(12), 1939–1958.

Christy, C. F., and Tensing, D. (2011). "Greener building material with fly ash." *Asian Journal of Civil Engineering* (*Building and Housing*), 12(1), 87–105.

Christy, C. F., Tensing, D., and Shanthi, R. M. (2013). "Experimental study on compressive strength and elastic modulus of clay and fly ash brick masonry." *Journal of Civil Engineering and Construction Technology*, 4(4), 134–141.

Chrysostomou, C. Z., Gergely, P., and Abel, J. F. (2002). "A six-strut model for nonlinear dynamic analysis of steel infilled frames." *International Journal of Structural Stability and Dynamics*, 2(3), 335–353.

Colangelo, F. (2005). "Pseudo-dynamic seismic response of reinforced concrete frames infilled with non-structural brick masonry." *Earthquake Engineering and Structural Dynamics*, 34(10), 1219–1241.

Comite Euro-International Du Beton (CEB). (1996). *RC frames under earthquake loading: State of the Art Report*. Thomas Telford, London.

Crisafulli, F. J. (1997). *Seismic behaviour of reinforced concrete structures with masonry infills*. PhD thesis, Department of Civil Engineering, University of Canterbury, New Zealand.

Crisafulli, F. J., and Carr, A. J. (2007). "Proposed macro-model for the analysis of infilled frame structures." *Bulletin of New Zealand Society for Earthquake Engineering*, 40(2), 69–77.

Crisafulli, F. J., Carr, A. J., and Park, R. (2000). "Capacity design of infilled frame structures." *Proceedings of 12th World Conference on Earthquake Engineering*, Auckland, New Zealand, 0221.

CSI. (2015). Structural Analysis Program (SAP2000)–Advanced, Static and Dynamic Finite Element Analysis of Structures. Computers and Structures, Inc., Berkeley, USA.

Cultrone, G., Sebastiàn, E., and de la Torre, M. J. (2005). "Mineralogical and physical behavior of solid bricks with additives." *Construction and Building Materials*, 19, 39–48.

D'Ayala, D., Worth, J., and Riddle, O. (2009). "Realistic shear capacity assessment of infill frames: Comparison of two numerical procedures." *Engineering Structures*, 31(8), 1745–1761.

Dawe, J. I., and Young, T. C. (1985). "An investigation of factors influencing the behavior of masonry infills in steel frames subjected to in-plane shear." *Proceedings of 7th International conference on brick masonry*, Melbourne.

Dawe, J. L., and Seah, C. K. (1989). "Behaviour of masonry infilled steel frames." *Canadian Journal of Civil Engineering*, 16(6), 865–876.

Dayaratnam, P. (1987). *Brick and reinforced brick structures*, Oxford and IBH, New Delhi, India.

Decanini, L. D., and Fantin, G. E. (1987). "Modelos simplificados de la mampostería incluida en porticos. Características de rigidez y Resistencia lateral en astado límite." *Jornadas Argentinas de Ingeniería Estructural III*, Asociacion de Ingenieros Estructurales, Buenos Aires, Argentina, 2, 817–836 (in Spanish).

Dehghani, A., Fischer, G., and Alahi, F. N. (2015). "Strengthening of masonry infills using engineered cementitious composites." *Materials and structures*, 48(1), 185–204.

Di Trapani, F., Macaluso, G., Cavaleri, L., and Papia, M. (2015). "Masonry infills and RC frames interaction: literature overview and state of the art of macromodeling approach." *European Journal of Environmental and Civil Engineering*, 19(9), 1059–1095.

Dizhur, D., and Ingham, J. M. (2013). " Diagonal tension strength of vintage unreinforced clay brick masonry wall panels." *Construction and Building materials*, 43, 418–427.

Drysdale, R. G., Hamid, A. A., and Baker, L. R. (1994). *Masonry structures: Behavior and design*, Prentice-Hall, Englewood Cliffs, USA.

El-Dakhakhni, W. W., Elgaaly, M., and Hamid, A. A. (2003). "Three-Strut Model for Concrete Masonry-Infilled Steel Frames." *Journal of Structural Engineering*, 129(2), 177–185.

El-Dakhakhni, W. W., Hamid, A. A., Hakam, Z. H. R., and Elgaaly, M. (2006). " Hazard mitigation and strengthening of unreinforced masonry wall using composites." *Computers and Structures*, 73, 458–477.

Ellul, F., and D'Ayala, D. (2012). "Realistic FE models to enable push-over non linear analysis of masonry infilled frames." *The open Construction and Building Technology Journal*, 6, (Suppl 1-M14), 213–235.

European Committee for Standardization (CEN). (2002). "Method of test for masonry – part 3 determination of initial shear strength." *BS EN 1052-3*, Brussels, Belgium.

European Committee for Standardization (CEN). (2004a). "Design of concrete structures - Part 1-1: General rules and rules for buildings." *BS EN 1992-1-1*, Eurocode 2, Brussels, Belgium.

European Committee for Standardization (CEN). (2004b). "Design of structures for Earthquake Resistance–Part 1: General rules, seismic actions and rules for buildings." *BS EN 1998-1*, Eurocode 8, Brussels, Belgium.

European Committee for Standardization (CEN). (2005a). "Design of masonry structures. Part 1-1: General rules for buildings—Reinforced and unreinforced masonry." *BS EN 1996-1-1, Eurocode 6*, Brussels, Belgium.

European Committee for Standardization (CEN). (2005b). "Design of structures for earthquake resistance Part 3: Assessment and retrofitting of buildings." *BS EN 1998-3, Eurocode 8*, Brussels, Belgium.

European Committee for Standardization (CEN). (2007). "Methods of test for mortar for masonry. Part 11 Determination of flexural and compressive strength of hardened mortar." *BS EN 1015-11*, Brussels, Belgium.

Fardis, M. N. (2009). *Seismic design, assessment and retrofitting of concrete buildings, based on EN-Eurocode 8. Series: geotechnical, geological and earthquake engineering 8*, Springer, New York.

Fardis, M. N., and Panagiotakos, T. B. (1997). "Seismic design and response of bare and infilled reinforced concrete buildings–Part II: Infilled structures." *Journal of Earthquake Engineering*, 1(3), 473–503.

FEMA. (2000). "Prestandard and commentary for the seismic rehabilitation of buildings." *FEMA-356*, Prepared by American Society of Civil Engineers for Federal Management Agency, Washington, DC.

FEMA. (2001). "The 2000 NEHRP recommended provisions for seismic regulations for new buildings and old structures." *FEMA-368*, Prepared by American Society of Civil Engineers for Federal Management Agency, Washington, DC.

Fiore, A., Netti, A., and Monaco, P. (2012). "The influence of masonry infill on the seismic behaviour of RC frame buildings." *Engineering Structures*, 44, 133–145.

Fiore, A., Spagnoletti, G., and Greco, R. (2016). "On the prediction of shear brittle collapse mechanisms due to the infill-frame interaction in RC buildings under pushover analysis." *Engineering Structures*, 121, 147–159.

Flanagan, R. D., and Bennett, R. M. (1999). "In-plane behaviour of structural clay tile infilled frames." *Journal of Structural Engineering*, 125(6), 590–599.

Flanagan, R. D., and Bennett, R. M. (2001). "In-plane analysis of masonry infill materials." *Practice Periodical on Structural Design and Construction* 6(4), 176–182.

Ghosh, A. K., and Amde, A. M. (2002). "Finite element analysis of infilled frames." *Journal of Structural Engineering*, 128(7), 881–889.

Gumaste, K. S., Nanjunda Rao, K. S., Venkatarama Reddy, B. V., and Jagadish, K. S. (2007). "Strength and elasticity of brick masonry prisms and wallets under compression." *Materials and Structures*, 40, 241–253.

Haldar, P., Singh, Y., and Paul, D. K. (2013). "Identification of seismic failure modes of URM infilled RC frame buildings." *Engineering Failure Analysis*, 33, 97–118.

Hendry, A.W. (1998). *Structural Masonry*. Macmillan Press, 2nd edition, London.

Holmes, M. (1961). "Steel frames with brickwork and concrete infilling." *Proceedings of the Institution of Civil Engineers*, 19(4), 473–478.

Ismail, N., Petersen, R. B., Masia, M. J., and Ingham, J. M. (2011). " Diagonal shear behaviour of unreinforced masonry wallettes strengthened using twisted steel bars." *Construction and Building materials*, 25, 4386–4393.

Jaiswal, K., Sinha, R., and Goyal, A. (2002). "Reinforced Concrete Frame Building with Masonry Infill Walls designed for Gravity Loads". World Housing Encyclopedia. Earthquake Engineering Research Institute and International Association for Earthquake Engineering, India/Report-19.

Jurina, L. (1977). Pareti in muratura soggette ad azionic sismiche. Rivista Costuire, 100.

Kakaletsis, D. J., and Karayannis, C. G. (2008). "Influence of masonry strength and openings on infilled R/C frames under cycling loading." *Journal of Earthquake Engineering*, 12(2), 197–221.

Kakaletsis, D. J., and Karayannis, C. G. (2009). "Experimental investigation of infilled reinforced concrete frames with openings." *ACI Structural Journal*, 106(2), 132–141.

Kakaletsis, D. J., Karayannis, C. G., and Panagopoulos, G. K. (2011). "Effectiveness of rectangular spiral shear reinforcement on infilled RC frames under cyclic loading." *Journal of Earthquake Engineering*, 15(8), 1178–1193.

Kaushik, H. B., Rai, D. C., and Jain, S. K. (2006). "Code approaches to seismic design of masonry-infilled reinforced concrete frames: A state-of-the-art review." *Earthquake Spectra*, 22(4), 961–983.

Kaushik, H. B., Rai, D. C., and Jain, S. K. (2007). "Stress-strain characteristics of clay brick masonry under uniaxial compression." *Journal of Materials in Civil Engineering*, 19(9), 728–739.

Kaushik, H. B., Rai, D. C., and Jain, S. K. (2009). "Effectiveness of some strengthening options for masonry-infilled RC frames with open first story." *Journal of Structural Engineering*, 135(8), 925–937.

Keshava, M., Vijayendra, K.V., and Raghunath, S. (2013). "Strength efficiency of commonly used block work masonry." *International Journal of Earth Sciences and Engineering*, 3(4), 586–598.

Khalaf, F. M. (2005). "New test for determination of masonry tensile bond strength." *Journal of Materials in Civil Engineering*, 17(6), 725–732.

Klingner, R. E., and Bertero, V. V. (1976). *Infilled Frames in Earthquake- Resistant Construction*. Report No. EERC 76-32, University of California, Berkeley, CA.

Kumar, S. (2002). "A perspective study on fly ash–lime–gypsum bricks and hollow blocks for low cost housing development." *Construction and Building Materials*, 16, 519– 525.

Langenbach, R. (2007). "From 'Opus Craticium' to the 'Chicago Frame': Earthquake-resistant traditional construction." *International Journal of Architectural Heritage*, 1(1), 29–59.

Langenbach, R. (2008). "Learning from the past to protect the future: Armature Crosswalls." *Engineering Structures*, 30(8), 2096–2100.

Lee, C. Y., Lee, H. K., and Lee, K. M. (2003). "Strength and microstructural characteristics of chemically activated fly ash–cement systems." *Cement and Concrete Research*, 33, 425–431.

Lee, J. Y., and Hwang, H. B. (2010). "Maximum shear reinforcement of reinforced concrete beams." *ACI Structural Journal*, 107(5), 580–588.

Liauw, T. C., and Kwan, K. H. (1984). "Nonlinear behaviour of nonintegral infilled frames." *Computers and Structures*, 18, 551–560.

Liauw, T. C., and Kwan, K. H. (1985). "Unified plastic analysis for infilled frames." *Journal of Structural Engineering*, 111(7), 1427–1448.

Liauw, T. C., and Kwan, K. H. (1992). "Experimental study of shear wall and infilled frame on shake table." *Proceedings of 10th World Conference on Earthquake Engineering*, Madrid, 2659–2663.

Liauw, T. C., and Lee, S. W. (1977). "On the behavior and the analysis of multistorey infilled frames subjected to lateral loading." *Proceedings of the Institution of Civil Engineering*, Part 2, 63, 641–656.

Magenes, G., and Calvi G. M. (1997). "In–plane seismic response of brick masonry walls." *Earthquake Engineering and Structural Dynamics*, 26, 1091–1112.

Magenes, G., Penna, A., Galasco, A., and Rota, M. (2010). "Experimental characterisation of stone masonry mechanical properties." *Proceedings of 8th international masonry conference*, Dresden, 247–256.

Mahmood, H., and Ingham, J. M. (2011). "Diagonal compression testing of FRP-retrofitted unreinforced clay brick masonry wallettes." *Journal of Composites for Construction*, 15(5), 810–820.

Maidiawati, and Sanada, Y. (2016). "R/C frame–infill interaction model and its application to Indonesian buildings." *Earthquake Engineering and Structural Dynamics*. DOI: 10.1002/eqe.2787.

Mainstone, R. J. (1971). "On the stiffness and strength of infilled frames." *Proceedings of the Institution of Civil Engineering*, 49(2), 57–90.

Mainstone, R. J. (1974). Supplementary note on the stiffness and strengths of infilled frames, Building Research Station, Garston, UK.

Malaviya, S. K., Chatterjee, B., and Singh, K. K. (1999). "Fly ash - an emerging alternative building material." *Proceedings of the National Seminar on Fly Ash Utilization*, February 26-27, 1999, National Metallurgical Laboratory, Jamshedpur, India, 59–67.

Mallick, D. V., and Garg, R. P. (1971). "Effects of openings on the lateral stiffness of infilled frames." *Proceedings of the Institution of Civil Engineering*, 49, paper 7371, 193–210.``

Mallick, D. V., and Severn, R. T. (1967). "The behaviour of infilled frames under static loading." *Proceedings of the Institution of Civil Engineering*, 39, 639–656.

Mander, J. B., Priestley, M. J. N., and Park, R. (1988). "Theoretical stress-strain model for confined concrete." *Journal of Structural Engineering*, 114, 1804–1826.

Mann, W., König, G., and Ötes, A. (1988). "Tests of masonry walls subjected to seismic forces." *Proceedings of Brick and Block Masonry (8th IBMAC)*, London, Elsevier Applied Science, 2, 764–773.

Mansouri A, Marefat, M. S., and Khanmohammadi, M. (2014). "Experimental evaluation of seismic performance of low-shear strength masonry infills with openings in reinforced concrete frames with deficient seismic details." *The Structural Design of Tall and Special Buildings*, 23(15), 1190–1210.

Markulak, D., Radić, I., and Sigmund, V. (2013). "Cyclic testing of single bay steel frames with various types of masonry infill." *Engineering Structures*, 51, 267–277.

Marshall, O. S. Jr., Sweeney, S. C., and Trovillion, J. C. (2000). "Performance testing of fiber-reinforced polymer composite overlays for seismic rehabilitation of unreinforced masonry walls." ERDC/CERL TR-00-18, Construction Engineering Research Laboratory (CERL), Engineer Research and Development Center, U.S. Army Corps of Engineers, Champaign, IL.

Masonry Standards Joint Committee (MSJC). (2013). "Building code requirements and specifications for masonry structures." Farmington Hills, MI.

McNary, W. S., and Abrams, D. P. (1985). "Mechanics of masonry in compression." *Journal of Structural Engineering*, 111(4), 857–870.

Mehrabi, A. B., and Shing, P. B. (1997). "Finite element modelling of masonry-infilled RC frames." *Journal of Structural Engineering*, 123(5), 604–613.

Mehrabi, A. B., Shing, P. B., Schuller, M. P., and Noland, J. L. (1996). "Experimental evaluation of masonry-infilled RC frames." *Journal of Structural Engineering*, 122(3), 228–237.

Mehta, P. K., and Monteiro, P. J. M. (2006). *Concrete microstructure, properties, and materials*. Tata McGraw-Hill, New Delhi.

Misir, I. S., Ozcelik, O., Girgin, S. C., and Kahraman, S. (2012). "Experimental work on seismic behavior of various types of masonry infilled RC frames." *Structural Engineering and Mechanics*, 44(6), 763–774.

Moghaddam, H. A., and Dowling, P. J. (1987). *The state of the art in infilled frames*, ESEE Research Report No 87–2, Civil Engineering Department, Imperial College of Science and Technology, London.

Mohammadi, M., and Akrami, V. (2010). "An engineered infilled frame: Behavior and calibration." *Journal of Constructional Steel Research*, 66(6), 842–849.

Mohammed, A., and Hughes, T.G. (2011). "Prototype and model masonry behavior under different loading conditions." *Materials and Structures*, 44, 53–65.

Moretti, M. L., Papatheocharis, T., and Perdikaris, P. C. (2014). "Design of reinforced concrete infilled frames." *Journal of Structural Engineering*, 140(9), 04014062(10).

Mosalam, K., White, R., and Gergely, P. (1997). "Static Response of Infilled Frames Using Quasi-Static Experimentation." *Journal of Structural Engineering*, 123(11), 1462–1469.

Murty, C. V. R., and Jain, S. K. (2000). "Beneficial influence of masonry infill walls on seismic performance of RC frame buildings." *Proceedings of 12th World Conference on Earthquake Engineering*, Auckland, New Zealand, 1790.

Nazief, M. A. (2014). *Finite element characterization of the behaviour of masonry infill shear walls with and without openings*. PhD thesis, Department of Civil and Environmental Engineering, University of Alberta.

NBC. (1994). "Nepal national building code for mandatory rules of thumb for reinforced concrete buildings with masonry infill." *NBC 201*, Ministry of Housing and Physical Planning, Department of Buildings, Nepal.

Paulay, T., and Priestley, M. J. N. (1992). Seismic design of reinforced concrete and masonry buildings. Wiley, New York.

Polyakov, S. V. (1960). "On the interaction between masonry filler walls and enclosing frame when loading in the plane of the wall." Translation in earthquake engineering, *Earthquake Engineering Research Institute (EERI)*, San Francisco, 36–42.

Preti, M., Bettini, N., and Plizzari, G. (2012). "Infill walls with sliding joints to limit infill-frame seismic interaction: Large-scale experimental test." *Journal of Earthquake Engineering*, 16(1), 125–141.

Preti, M., Migliorati, L., and Giuriani, E. (2015). "Experimental testing of engineered masonry infill walls for post-earthquake structural damage control." *Bulletin of Earthquake Engineering*, 13(7), 2029–2049.

Priestley, M. J. N., and Calvi, G. M. (1991). "Towards a capacity-design assessment procedure for reinforced concrete frames." *Earthquake Spectra*, 7(3), 413–437.

Puglisi, M., Uzcategui, M., and Flórez-López, J. (2009). "Modeling of masonry of infilled frames, Part I: The plastic concentrator." *Engineering Structures*, 31, 113–118.

Rai, D. C., and Dhanapal, S. (2013). "Bricks and mortars in Lucknow monuments of c.17–18 century." *Current Science*, 104(2), 238–244.

Rai, D. C., Singhal, V., Paikara, S., and Mukherjee, D. (2014). "Sub-paneling of masonry walls using precast reinforced concrete elements for earthquake resistance." *Earthquake Spectra*, 30(2), 913–937.

Ravichandran, S. S., and Klingner, R. E. (2012). "Behavior of steel moment frames with AAC infills." *ACI Structural Journal*, 109(1), 83–90.

RILEM (1994). "LUM B6 Diagonal tensile strength of small wall specimens, 1991." *RILEM Technical Recommendations for the Testing and Use of Constructions Materials*, E & FN SPON, London, 488–489.

Rodrigues, H., Varum, H., and Costa, A. (2010). "Simplified macro-model for infill masonry panels." *Journal of Earthquake Engineering*, 14(3), 390–416.

Sahoo, D. R. (2008). "Seismic strengthening of open-ground storey RC frame using steel-caging and Aluminium shear –yielding dampers. PhD thesis, Department of Civil Engineering, Indian Institute of Technology Kanpur, India.

Saneinejad, B. A., and Hobbs, B. (1995). "Inelastic design of infilled frames." *Journal of Structural Engineering*, 121(4), 634–650.

Sarangapani, G., Venkatarama Reddy, B. V., and Jagadish, K. S. (2002). "Structural characteristics of bricks, mortars and masonry." *Journal of Structural Engineering*, 29(2), 101–107.

Sarangapani, G., Venkatarama Reddy, B. V., and Jagadish, K. S. (2005). "Brick–mortar bond and masonry compressive strength." *Journal of Materials in Civil Engineering*, 17(2), 229–237.

Schwarz, S., Hanaor, A., and Yankelevsky, D. Z. (2015). "Experimental response of reinforced concrete frames with AAC masonry infill walls to in-plane cyclic loading." *Structures*, 3, 306–319.

Sezen, H. and Moehle, J. (2004). "Shear strength model for lightly reinforced concrete columns." *Journal of Structural Engineering*, 130(11), 1692–1703.

Shi, C. (1998). "Pozzolanic reaction and microstructure of chemical activated lime-fly ash pastes." *ACI Material Journal*, 95(5), 537–545.

Shing, P. B., and Stavridis, A. (2014). "Analysis of seismic response of masonry-infilled RC frames through collapse." *ACI Structural Journal*, SP 297-7, 1-20.

Singh, Y., and Das, D. (2006). "Effect of URM infills on seismic performance of RC frame buildings." *Proceedings of 4th International Conference on Earthquake Engineering*, Center for Urban Earthquake Engineering (CUEE), Tokyo.

Singhal, V., and Rai, D.C. (2014). "Suitability of half scale burnt clay bricks for shake table tests on masonry walls." *Journal of Materials in Civil Engineering*, 26(4), 644–657.

Smith, B. S. (1966). "Behaviour of the square infilled frames." *Journal of Structural Division, Proceedings of ASCE*, 91(ST1), 381–403.

Smith, B. S. (1967). "Methods for predicting the lateral stiffness and strength of multi-storey infilled frames." *Building Science*, Vol. 2, Pergamon Press, Oxford, U.K., 247–257.

Smith, B. S. (1968). "Model test results of vertical and horizontal loading of infilled frames." *ACI Journal*, 65, 618–624.

Smith, B. S., and Carter, C. (1969). "A method of analysis for infilled frames." *Proceedings of the Institution of Civil Engineers*, 44(1), 31–48.

Stavridis, A., and Shing, P. B. (2010). "Finite-element modelling of nonlinear behavior of masonry-infilled RC frames." *Journal of Structural Engineering*, 136(3), 285–296.

Stavridis, A., Koutromanos , I., and Shing, P. B. (2012). "Shake-table tests of a three-story reinforced concrete frame with masonry infill walls." *Earthquake Engineering and Structural Dynamics*, 41(6), 1089–1108.

Stylianidis, K. C. (2012). "Experimental investigation of masonry infilled R/C frames." *The Open Construction and Building Technology Journal*, 6 (Suppl 1-M13), 194–212.

Sucuoğlu, H., and Siddiqui, U. A. (2014). "Pseudo-dynamic testing and analytical modeling of AAC infilled RC frames." *Journal of Earthquake Engineering*, 18(8), 1281–1301.

Surendran, S. (2012). *Lateral load behavior of masonry infilled RC frames with central opening*. Mtech thesis, Department of Civil Engineering, Indian Institute of Technology Guwahati, India.

Tasnimi, A. A., and Mohebkhah, A. (2011). "Investigation on the behavior of brick-infilled steel frames with openings, experimental and analytical approaches." *Engineering Structures*, 33(3), 968–980.

Thiruvengadam, V. (1985). "On the natural frequencies of infilled frames." *Earthquake Engineering and Structural Dynamics*, 13(3), 401–419.

Turgut, P. (2010). "Masonry composite material made of limestone powder and fly ash." *Powder Technology*, 204, 42–47.

Turgut, P. (2012). "Manufacturing of building bricks without Portland cement." *Journal of Cleaner Production*, 37, 361–367.

Uva, G., Raffaele, D., Porco, F., and Fiore, a. (2012). "On the role of equivalent strut models in the seismic assessment of infilled RC buildings." *Engineering Structures*, 42, 83–94.

Valiasis, T., and Stylianidis, K. (1989). "Masonry infilled R/C frames under horizontal loading. Experimental results." *European Earthquake Engineering*, III, 3, 10–20.

Wood, R. H. (1978). "Plasticity, composite action and collapse design of unreinforced shear wall panels in frames." *ICE Proceedings*, 65, 381–411.

Zarnic, R., and Tomazevic, M. (1985). *Study of the behaviour of masonry infilled reinforced concrete frames subjected to seismic loading-Part II*. Research Report ZRMK/IKPI-85/02, Institute for Testing and Research in Materials and Structures, Ljubljana.

Zarnic, R., and Tomazevic, M. (1988). "An experimentally obtained method for evaluation of the behaviour of masonry infilled RC frames." *Proceedings of 9th World Conference on Earthquake Engineering*, Tokyo-Kyoto, Japan, 6, 163-168.

Zovkic, J., Sigmund, V., and Guljas, I. (2013). "Cyclic testing of a single bay reinforced concrete frames with various types of masonry infill." *Earthquake Engineering and Structural Dynamics*, 42(8), 1131–1149.